

**Design, Synthesis and Photophysical Studies of Diketopyrrolopyrrole-
Based Small Molecules and their Application in Bulk Heterojunction
Solar Cell**

**Thesis Submitted to AcSIR for the Award of the Degree of
DOCTOR OF PHILOSOPHY
in Chemical Sciences**



By

LAKSHMYKANTH T.M.

Registration No: 10CC11J39013

Under the guidance of

Dr. K. R. Gopidas



**CSIR-NATIONAL INSTITUTE FOR INTERDISCIPLINARY
SCIENCE AND TECHNOLOGY (CSIR-NIIST)
THIRUVANANTHAPURAM-695 019, KERALA, INDIA**

2017

Dedicated

to

My family & friends

DECLARATION

I hereby declare that the matter embodied in the Ph. D. thesis entitled: **“Design, Synthesis and Photophysical Studies of Diketopyrrolopyrrole-Based Small Molecules and their Application in Bulk Heterojunction Solar Cell”** is the result of an independent work carried out by me at the Photosciences and Photonics, Chemical Sciences and Technology Division of the CSIR-National Institute for Interdisciplinary Science and Technology (CSIR-NIIST), Thiruvananthapuram, under the supervision of Dr. K. R. Gopidas and the same has not been submitted elsewhere for other degree or diploma.

In keeping with the general practice of reporting scientific observations, research material obtained from other investigations has been duly cited and acknowledged in the thesis.

Lakshmykanth T.M.

Thiruvananthapuram

August 2017



सीएसआईआर- राष्ट्रीय अंतर्विषयी विज्ञान तथा प्रौद्योगिकी संस्थान
CSIR-NATIONAL INSTITUTE FOR INTERDISCIPLINARY SCIENCE &
TECHNOLOGY

इंडस्ट्रियल इस्टेट पी.ओ., तिरुवनंतपुरम - 695 019, केरल, भारत
Industrial Estate P.O., Thiruvananthapuram - 695 019, Kerala, INDIA.

डॉ. के.आर. गोपिदास, एफ.ए.एससी

Dr. K. R. Gopidas F.A.Sc.

मुख्य वैज्ञानिक

Chief Scientist

रसायन विज्ञान तथा प्रौद्योगिकी प्रभाग

Chemical Sciences and Technology Division

August 7, 2017

CERTIFICATE

This is to certify that the work incorporated in this Ph.D. thesis entitled ***“Design, Synthesis and Photophysical Studies of Diketopyrrolopyrrole-Based Small Molecules and their Application in Bulk Heterojunction Solar Cell”*** submitted by Mr. *Lakshmykanth T. M.* to Academy of Scientific and Innovative Research (AcSIR) in fulfillment of the requirements for the award of the Degree of *Doctor Of Philosophy in Chemical Sciences*, embodies original research work under my supervision/guidance. I further certify that this work has not been submitted to any other University or Institution in part or full for the award of any degree or diploma. Research material obtained from other sources has been duly acknowledged in the thesis. Any text, illustration, table etc., used in the thesis from other sources, have been duly cited and acknowledged.

Lakshmykanth T. M.

Dr.K.R.Gopidas

(Thesis Supervisor)

टेलीफोन /Telephone: 91-471-2515390(O), 9446520537(M)
फैक्स /Fax : +91-471-2491712, ई-मेल /E-mail: gopidaskr@niist.res.in, gopidaskr@gmail.com

ACKNOWLEDGEMENTS

I have great pleasure in placing on record my deep sense of gratitude to Dr. K. R. Gopidas, my thesis supervisor, for suggesting the research problem and for his guidance, support, and encouragement throughout my research career which leads to the successful completion of this work.

I would like to express my sincere thanks to Professor M. V. George for being a real motivation and his support during the tenure of this work.

I wish to thank Dr. A. Ajayaghosh, Dr. Suresh Das and Dr. Gangan Prathap, present and former Directors of the CSIR-National Institute for Interdisciplinary Science and Technology, Thiruvananthapuram, for providing me the necessary facilities for carrying out this work.

Dr. D. Ramaiah, Dr. Joshy Joseph, Dr. N. Unni, Dr. K. Yoosaf, Dr. C. Vijayakumar, Dr. B. P. Deb and Dr. V. Karunakaran, Scientists of the Photosciences and Photonics, Chemical Sciences and Technology Division, are greatly acknowledged for the scientific discussions. Also, I would like to thank Dr. R. Luxmi Varma, Dr. Mangalam S. Nair and Dr. S. Ananthakumar for their help in the successful completion of my coursework.

I thank Dr. V .K. Praveen, Dr. Suraj Soman, Dr. Rakesh Mishra for their fruitful discussion.

I thank Prof. Mukundan Thelakkat, University of Bayreuth, Germany, for teaching the fabrication of dye sensitized solar cells.

I would like to thank Prof Rene Janssen for his support, care and fruitful discussion during my stay at Eindhoven technical university. I also like to thank Dr. Martijn Wienk and Dr. Stefen Meskers for their discussion. Very special thanks go to Dr. Weiwei for teaching me the fabrication of BHJ solar cells during my first visit to Eindhoven Technical University in 2014 for two months. I also sincerely thank my Chinese friend Mike Wang for helping me for the last two years of my Ph.D life. During my stay at Eindhoven university I really enjoyed working in the synthesis lab 1, device lab and in the office STO 4.25. Mike Wang, Koen Hendriks, Ruurd Heuvel and Duan Chunhui for their nice discussion, support and help

during the synthesis of molecules in the chapter 3 and chapter 4. When I fabricated organic solar cell devices, I worked together with colleagues in the device lab: Serkan Esiner, Gaël Heintges, Dario Dicarolo Rasi, Bardo Brujnaers for their help when I encountered problems in evaporation or EQE measurement. G.W.P. van Pruissen and Robin willems for helping me for fixing the problems during cyclic voltammetry measurements. Fallon Colberts for the all the TEM images that I kept in my Thesis. Also I would like to Thank Mr.Ralf for MALDI-TOF spectral analysis for my samples. I really enjoyed the discussion with Dr. X. Lou during late hours in the device lab. M.Sc project students Pieter Leenaers, Junke wang and Kunal Datta working in the Rene's group are acknowledge for their nice discussion with me. I happy to acknowledge all my Indian friends Dr. Karthik Gnanasekaran, Dr.Hitesh Khandelwal, Mrs Monali Moirangthem, Dr.Chidambar Kulkarni, Dr. Gayatri Kumari, Dr. Anindita Das, Dr. Balu Thota, Mrs. Rathna Kumari for their love and care during my stay at Eindhove .

I would like to thank Dr. V. K. Retheesh Kumar, Dr. K. Retheesh, Dr. A. M. Rakhi, Dr. Tony George Thomas, Dr. M. V. Vinayak, Dr. K. Sreedevi, Dr.Prakash S. P. , Dr. Nagaraj Nayak and Mr. K. Sumesh Babu for their valuable suggestions, advice and constructive critics. Also, I wish to thank Mr. M. Yoosuf, Ms. K. J. Athira and Mrs. K. B. Daisymol for their care and support. I would like to thank the MSc Project students Ms. Deepthi Rajan for helping me in the synthesis of DPP derivatives.

I sincerely thank Dr. J. D. Sudha for her support and care during my stay at Ph.D NIIST.

Mr. P. Robert and Mr. M. Kiran for TEM analysis , Mrs. Saumini, Mr. Saran for NMR analysis, Mrs. Viji and Ms. Athira for HRMS data.

I sincerely thank all my teachers for their encouragement at different stages of my academic career.

I am deeply grateful to my family for their support, love, and wishes.

I am grateful to Dr. Manoj A. G. Namboothiry and Dr. Giribabu L for being part of my external examination committee.

Finally, I take this opportunity to sincerely thank Council of Scientific and Industrial Research (CSIR), Department of Science and Technology (DST), Government of India, Indo-

European collaborative Large Cells Project, and Eindhoven Technical University for financial assistance.

Lakshmykanth T.M.

CONTENTS

	Page
Declaration	i
Certificate	ii
Acknowledgements	iii
Contents	v
Preface	ix
List of Figures	xi
List of Tables	xiv
List of Schemes	xiv
List of Abbreviations	xv
Chapter 1. Diketopyrrolopyrrole Based Small Molecules for Bulk Heterojunction Solar Cells: An Overview	
1.1. Abstract	1
1.2. Introduction	2
1.3. History of solar cell	2
1.4. Bulk heterojunction solar cell	5
1.4.1. Device structure	5
1.4.2. Working principle	6
1.5. Diketopyrrolopyrrole (DPP) based small molecules	14
1.5.1. Mono-diketopyrrolopyrrole	16
1.5.2. Bis-diketopyrrolopyrrole	32
1.6. Outline of the thesis	45
1.7. References	46

Chapter 2. Design, Synthesis and Photovoltaic Properties of Small Molecules Based on Tetraphenylethylene and Diketopyrrolopyrrole

2.1.	Abstract	55
2.2.	Introduction	56
2.3.	Results and discussion	59
2.3.1.	Synthesis	59
2.3.2.	Optical properties	61
2.3.3.	Electrochemical properties	63
2.3.4.	Thermal properties	65
2.3.5.	Photovoltaic properties	66
2.3.6.	Morphological studies	71
2.4.	Conclusion	73
2.5.	Experimental section	73
2.5.1.	General methods	73
2.5.2.	Fabrication of bulk heterojunction solar cell	74
2.5.3.	Experimental procedures	75
2.6.	References	85

Chapter 3. Exploring the Effect of Donor Substituents in Pyridine Capped Diketopyrrolopyrrole Based Small Molecules in Photovoltaics

3.1.	Abstract	89
3.2.	Introduction	90
3.3.	Results and discussion	95
3.3.1.	Synthesis	95
3.3.2.	Optical properties	98
3.3.3.	Electrochemical properties	100

3.3.4.	Thermal properties	102
3.3.5.	Photovoltaic properties	104
3.3.5.1	Effect of MoO ₃ hole transporting layer and total concentration	112
3.3.6.	Morphological studies	117
3.4	Conclusion	120
3.5.	Experimental section	120
3.5.1.	General methods	120
3.5.2.	Fabrication of bulk heterojunction solar cell	121
3.5.3.	Experimental procedures	123
3.6.	References	140
Chapter 4.	D-A-D and D-A-D-A-D Small Molecules Based on Pyridine Capped Diketopyrrolopyrrole for Bulk Heterojunction Solar Cell	
4.1.	Abstract	143
4.2.	Introduction	144
4.3.	Results and discussion	145
4.3.1.	Synthesis	145
4.3.2.	Optical properties	148
4.3.3.	Electrochemical properties	149
4.3.4.	Photovoltaic properties	152
4.3.5.	Morphological studies	157
4.4.	Conclusion	160
4.5.	Experimental section	160
4.5.1	General methods	160
4.5.2	Fabrication of bulk heterojunction solar cell	161
4.5.3.	Experimental procedures	161
4.6.	References	172

List of Publications	175
Curriculum Vitae	177

PREFACE

Renewable energies are considered as the energies of the future because of their small impact on the environment. Among them, solar energy is probably the most promising one because it can be directly converted into electricity using photovoltaic modules. Organic photovoltaics, that are solar cells with an organic small molecule or polymer as photoactive layer, represent an attractive future technology as large-scale and low-cost green energy source. In organic solar cells, donor and acceptor materials are combined in the active layer to convert light into electrical power. The search for a cheaper and an efficient material for harvesting sunlight into electricity has been received much attention for more than two decades. Organic solar cell with polymer and small molecules have dominated in the research and achieved more than 11% efficiency in the laboratory scale.

This thesis deals with the synthesis, photophysical and electrochemical studies and solar cell characterization of diketopyrrolopyrrole (DPP) based small molecules in the bulk heterojunction solar cell. As presented above, the first chapter gives an introduction to the advent and history of solar cells, particularly bulk heterojunction solar cells, the working principle of bulk heterojunction (BHJ) solar cells, and literature review focusing mainly on DPP based solution processable small molecule BHJ solar cells.

In the second chapter, we present the design and synthesis of two D-A-D small molecules TDPPC₁₀(TPE)₂ and TDPPEH(TPE)₂, having alkyl-substituted (decyl or ethylhexyl) DPP as acceptor core and two tetraphenylethylene groups as donor units attached to the DPP through a thiophene linker. Preliminary studies such as absorption spectra of the molecules in solution and film state were studied. Energy levels were evaluated from the

electrochemical studies. BHJ solar cells with PC₆₁BM acceptor were fabricated and the results are presented here.

In the next chapter, we explored the effect of donor substituents in pyridine capped DPP in BHJ solar cells with PC₆₁BM as an acceptor. A series of five pyridine capped DPP-based small molecules have been synthesized. Preliminary absorption studies, electrochemical studies, film forming capabilities, morphology studies, and device performance are presented and discussed. The role of MoO₃ hole transporting layers in the device efficiency was also investigated and the results are presented in this chapter.

In the fourth chapter, synthesis, characterization and detailed photovoltaic studies of mono pyridine capped DPP with 5'-hexyl-2,2'-bithiophene end group and bis pyridine capped DPP based small molecules with 5'-hexyl-2,2'-bithiophene as an end group and dithienopyrrole as central core are discussed. The molecules were coded as PyDPPBO(bithiohexyl)₂, 'PyDPPHD(bithiohexyl)₂', and 'DTP(PyDPPHD(bithiohexyl)₂', exhibited PCEs of 1.36 %, 0.52 % and 0.67 % in BHJs with PC₆₁BM as acceptor. The detailed synthesis, characterization, energy level evaluation, device performance and morphological results are given. The relationship between total concentration of the solution, spin casted speed and device performance, were explored and the morphology of the best device are presented.

List of Figures

		Page
1.	Figure 1.1	5
2.	Figure 1.2	7
3.	Figure 1.3	10
4.	Figure 1.4	14
5.	Figure 1.5	19
6.	Figure 1.6	21
7.	Figure 1.7	24
8.	Figure 1.8	27
9.	Figure 1.9	28
10.	Figure 1.10	31
11.	Figure 1.11	33
12.	Figure 1.12	35
13.	Figure 1.13	37
14.	Figure 1.14	39
15.	Figure 2.1	57
16.	Figure 2.2	58
17.	Figure 2.3	59
18.	Figure 2.4	61

19.	Figure 2.5	62
20.	Figure 2.6	64
21.	Figure 2.7	65
22.	Figure 2.8	66
23.	Figure 2.9	68
24.	Figure 2.10	70
25.	Figure 2.11	70
26.	Figure 2.12	72
27.	Figure 2.13	72
28.	Figure 2.14	72
29.	Figure 2.15	82
30.	Figure 2.16	82
31.	Figure 2.17	84
32.	Figure 2.18	84
33.	Figure 3.1	91
34.	Figure 3.2	93
35.	Figure 3.3	95
36.	Figure 3.4	99
37.	Figure 3.5	101
38.	Figure 3.6	102
39.	Figure 3.7	103

40.	Figure 3.8	104
41.	Figure 3.9	106
42.	Figure 3.10	107
43.	Figure 3.11	108
44.	Figure 3.12	110
45.	Figure 3.13	110
46.	Figure 3.14	112
47.	Figure 3.15	114
48.	Figure 3.16	115
49.	Figure 3.17	116
50.	Figure 3.18	118
51.	Figure 3.19	119
52.	Figure 3.20	119
53.	Figure 3.21	130
54.	Figure 3.22	131
55.	Figure 3.23	132
56.	Figure 3.24	133
57.	Figure 3.25	134
58.	Figure 3.26	135
59.	Figure 3.27	136
60.	Figure 3.28	137

61.	Figure 3.29	138
62.	Figure 3.30	139
63.	Figure 4.1	145
64.	Figure 4.2	149
65.	Figure 4.3	151
66.	Figure 4.4	152
67.	Figure 4.5	154
68.	Figure 4.6	156
69.	Figure 4.7	157
70.	Figure 4.8	158
71.	Figure 4.9	158
72.	Figure 4.10	159
73.	Figure 4.11	159
74.	Figure 4.12	162
75.	Figure 4.13	163
76.	Figure 4.14	165
77.	Figure 4.15	165
78.	Figure 4.16	167
79.	Figure 4.17	168
80.	Figure 4.18	170
81.	Figure 4.19	171

List of Tables

1.	Table 1.1	29-31
2.	Table 1.2	42-44
3.	Table 2.1	64
4.	Table 2.2	64
5.	Table 2.3	67
6.	Table 2.4	69
7.	Table 2.5	71
8.	Table 3.1	94
9.	Table 3.2	100
10.	Table 3.3	103
11.	Table 3.4	105
12.	Table 3.5	107
13.	Table 3.6	109
14.	Table 3.7	109
15.	Table 3.8	111
16.	Table 3.9	111
17.	Table 3.10	114

18.	Table 3.11	115
19.	Table 3.12	116
20.	Table 3.13	116
21.	Table 3.14	117
22.	Table 3.15	118
23.	Table 4.1	151
24.	Table 4.2	154
25.	Table 4.3	155
26.	Table 4.4	156

List of Schemes

1.	Scheme 2.1	60
2.	Scheme 2.2	60
3.	Scheme 2.3	61
4.	Scheme 3.1	96
5.	Scheme 3.2	97
6.	Scheme 3.3	97
7.	Scheme 3.4	98
8.	Scheme 3.5	98
9.	Scheme 4.1	146
10	Scheme 4.2	147

List of Abbreviations

- 1 (n-Bu)₄NPF₆ - Tetrabutylammonium hexafluorophosphate
- 2 μJ - microjoule
- 3 μm - micrometer
- 4 μM - micromolar
- 5 ¹H - proton
- 6 A - Acceptor
- 7 A - Ampere
- 8 ACN - Acetonitrile
- 9 Ag/AgCl - Silver-Silver chloride
- 10 Ar - Argon
- 11 CDCl₃ - deuteriated chloroform
- 12 cm - centimeter
- 13 cm² - square centimetre
- 14 CN - cyano
- 15 1-CN- 1-chloronaphthalene
- 16 CT - Charge transfer
- 17 CuI - Copper iodide
- 18 DIO-1,8-diiodooctane
- 19 *o*-DCB-*ortho*-dichlorobenzene
- 20 DIPA - Diisopropylamine
- 21 DMSO - Dimethyl sulphoxide
- 22 E_F - Fermi level energy
- 23 EIS - Electrochemical Impedance Spectroscopy
- 24 EQE - External Quantum Efficiency
- 25 *et al.* - *et alia*, Latin phrase meaning 'and others'
- 26 eV - electron volt
- 27 FF - Fill Factor
- 28 fs - femtosecond
- 29 h - hours
- 30 H - Hydrogen

- 31 HCl - Hydrochloric acid
- 32 HOMO - Highest occupied molecular orbital
- 33 HRMS - High Resolution Mass Spectroscopy
- 34 HTM - Hole Transporting Material
- 35 Hz – Hertz
- 36 I⁻/I₃⁻ - iodide-triiodide
- 37 I₂ – Iodine
- 38 IPCE - Incident photon to current conversion efficiency
- 39 I_{sc} - Short Circuit Current
- 40 I-V - Current-Voltage
- 41 J_{sc} - Short circuit current density
- 42 J-V - Current density-Voltage
- 43 kHz - kilohertz
- 44 LHE - Light Harvesting Efficiency
- 45 LiF – Lithium Fluoride
- 46 LUMO - Lowest unoccupied molecular orbital
- 47 m/z - mass to charge ratio
- 48 m² - square metre
- 49 mA - milliampere
- 50 mg - milligram
- 51 MHz - Megahertz
- 52 min. - minutes
- 53 mL - millilitre
- 54 mm - millimetre
- 55 mM - millimolar
- 56 mmol - millimole
- 57 mV - millivolt
- 58 mW - milliwatt
- 59 Na - Sodium
- 60 NHE - Normal Hydrogen Elctrode
- 61 nm- nanometer
- 62 NMR - Nuclear Magnetic Resonance

- 63 NREL - National Renewable Energy Laboratory
- 64 O₃ - Ozone
- 65 o-DCB - ortho-dichlorobenzene
- 66 °C - degree celsius
- 67 OFET - Organic Field Effect Transistor
- 68 OLED - Organic Light Emitting Diode
- 69 p- TiO₂ - porous TiO₂
- 70 P3HT - Poly-3-hexylthiophene
- 71 PCE or η - Power conversion Efficiency
- 72 ppm - parts per million
- 73 ps - picosecond
- 74 R - resistance
- 75 RB - round bottom
- 76 rt - room temperature
- 77 s - second
- 78 TGA - Thermogravimetric Analysis
- 79 THF - Tetrahydrofuran
- 80 TiCl₄ - Titanium tetrachloride
- 81 TPA - Triphenylamine
- 82 UV - ultraviolet
- 83 V - Volt
- 84 V_{OC} - open circuit voltage
- 85 W - Watt

Chapter 1

Diketopyrrolopyrrole Based Small Molecules for Bulk Heterojunction Solar Cells : An Overview

1.1 Abstract

Most of the research efforts in organic photovoltaics have been devoted to solution processed organic solar cell based on bulk heterojunction (BHJ) structures, which incorporate π -conjugated molecules as donor and acceptor components. Effective absorption of solar irradiation and hence material and device properties are significantly influenced by the π -conjugated chromophore of donor materials. Among the various π -conjugated systems, diketopyrrolopyrrole (DPP) derivatives have emerged as a class of efficient materials for photovoltaic applications due to their functional versatility. In combination with appropriate electron-rich aromatic segments, electron deficient nature of DPP core has been exploited for the synthesis of extremely narrow band gap donor-acceptor type materials that are well-suited for photovoltaic applications with high power conversion efficiency (PCE). This chapter provides an overview of the recent developments on bulk heterojunction solar cell using DPP based small molecules and discussions on the structure-property relationship with respect to the photovoltaic performance. Finally, the aim and the outline of the present thesis are given.

1.2 Introduction

The International Energy Outlook 2016 predicted that the global energy-related CO₂ emission will rise from 32.2 billion metric tons in 2012 to 35.6 billion metric tons in 2020 and to 43.2 billion metric tons in 2040.¹ The fast growing industrial countries like China and India are seriously contributing to this by burning fossil fuels, which is predominantly used to meet the energy demand. The present level of CO₂ has reached beyond 400 ppm and the adverse effects of climate change are already impacting the humanity. So, the urgency of shifting towards alternative and renewable energy sources is very necessary for the world. Among these, solar energy is the primary candidate with 174 PW reaching the earth's surface, well above the global energy demand.²⁻³ Therefore, conversion of solar energy to other usable forms of energy, such as electricity, has been the prime important focus in the energy technology community.

1.3 History of solar cell

In 1839, Becquerel demonstrated the photovoltaic effect and found an electrical current when illuminating a silver chloride covered platinum electrode in a liquid electrolyte.⁴⁻⁵ Charles Fritts in 1877 fabricated a 1 % efficient solar cell by coating selenium with a thin layer of gold.⁶ Nearly 77 years later Chapin *et al.*; demonstrated silicon-based solar cell with 6 % efficiency.⁷ The first p-n junction solar cell was fabricated by doping arsenic into the silicon (n-doped silicon) and subsequent deposition of boron on the surface creating positively charged silicon (p-doped

silicon).⁸ Today the PCE has reached maximum values of 25 % on a lab scale and ~15 % in commercial modules⁹. In 2015, the photovoltaic world market grew by roughly 20 % in terms of solar cell production to about 57 GW. According to the Ministry of New and Renewable Energy (MNRE), by the end of July 2016, India achieved a total solar power capacity of 7.8 GW.¹⁰

Alternative options for the solar cell applications that have emerged during the last three decades in the laboratories are dye-sensitized solar cells, polymers/small molecules based bulk heterojunction organic solar cells and perovskite solar cells.¹¹⁻¹⁵ Although the progress has been enormous in the laboratories regarding efficiency, it needs further research to commercialize highly efficient large area modules with stability. Eventually, organic solar cells may offer the desired combination of being low cost, abundant, non-toxic materials together with high efficiencies and good stability.¹⁶ The impact on society will be gigantic if the organic materials for bulk heterojunction organic solar cells achieve an efficiency of 10 % and the lifetime of 5 years.

In 1977 Hideki Shirakawa, Alan MacDiarmid and Alan J. Heeger discovered conductivity of conjugated polymers which paved the way for organic electronics research.¹⁷ Thereafter researchers started exploring the conjugated polymers and small molecules to study the absorption, emission and charge transport for the applications in field organic photovoltaics (OPV), light-emitting diodes (OLED) and organic field effect transistors (OFET)¹⁸⁻²⁰. The light-to-electric energy conversion in organic solar cells starts from the formation of a tightly bound charge pair called an

exciton. The low dielectric constant of organic materials results in a strong coulomb interaction between the electron and the hole. The binding energy is typically around 0.3 to 0.4 eV, which is much larger than thermal energy (0.025 eV) and makes the charge separation quite difficult.²¹ The efficiency of the solar cell was only 0.3 % at earlier times due to the exciton binding energy.²² Then the interface (heterojunction) of two materials with different electron affinities was used to separate these excitons, which was realized by Tang in 1986 using a double layer structure of an electron donating (D, p-type) and an electron accepting (A, n-type) material.²³ However, efficiencies remained below 1 % due to the short lifetime of excitons which diffuse 10 to 20 nm²⁴⁻²⁵. The excitons decay before reaching the interface of a bilayer solar cell which is usually ~100 nm thickness to absorb all light. Hence, only the excitons formed close to the interface can be dissociated and contribute to the current. Sariciftci *et al.* observed fast photo induced electron transfer from conducting polymers onto buckminsterfullerene's made the turning point in the organic photovoltaic research.²⁶ He dreamed up the idea of forming an interpenetrating network by mixing the donor and acceptor which laid the foundation for the bulk heterojunction solar cell. In 1995 Halls and Yu simultaneously manufactured the first bulk heterojunction solar cells.²⁷⁻²⁸ In 2001 Shaheen *et al.*, reported the significant effect of the processing solvent in the PCE of a solar cell.²⁹ Since then the trial and error experiments for the efficient devices with new donor polymers or small molecules mixed with fullerene and non-fullerene acceptors have been made in the laboratories.

1.4 Bulk heterojunction solar cell

1.4.1 Device structure

A glass substrate covered with patterned indium tin oxide (ITO) is used as a transparent electrode with a thickness of ~ 120 nm. In the normal configuration, ~ 40 nm layer of poly(3,4-ethylenedioxythiophene):poly(styrenesulfonate) (PEDOT:PSS) is spin coated on the ITO contact. PEDOT:PSS decreases the roughness of the ITO layer, adjusts the work function, and is a real hole conducting layer.³⁰ The photoactive layer made of a donor-acceptor blend is sandwiched between the PEDOT:PSS layer and a low work function electrode lithium fluoride (1 nm) and aluminum (~ 100 nm). The device architecture of a typical bulk heterojunction solar cell is given in the Figure 1.1. The thickness of the photoactive layer is usually optimized for higher performance and varies roughly in the range from 50 to 300 nm, depending on the actual nature of the organic semiconductor.

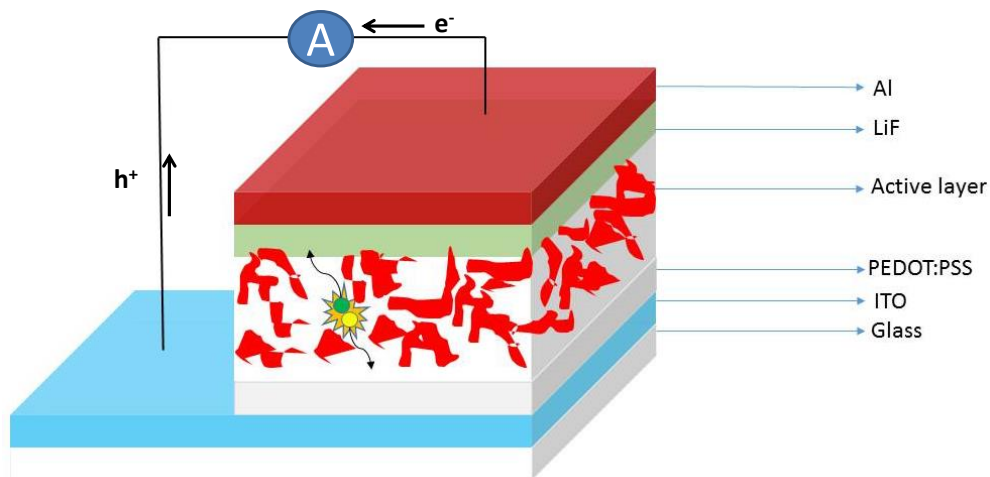


Figure 1.1 Schematic representation of bulk heterojunction solar cell device architecture

1.4.2 Working principle

The performance of a solar cell is determined by measuring a current density-voltage (J-V) curve in the dark and under illumination at 25 °C. The AM1.5G (air mass 1.5 global) solar spectrum is the light that reaches the earth's surface on a clear, cloudless day when the sun is at a 48.2 ° angle with the zenith such that the light travels through 1.5 times the thickness of the earth atmosphere.³¹ Typically the J-V curves are measured using a lamp and appropriate filters to simulate the AM1.5 G solar spectrum.

In the dark, the solar cell behaves like a diode and the current can go through the device only in forward bias. Under illumination, the curve is shifted downwards which is given in Figure 1.2. The difference between the current measured in the dark and under illumination is the photocurrent that has been generated by the solar cell. From the J-V characteristics under illumination, the maximum power point (P_{MPP}) can be found out at the point when the product of the current density and voltage is maximum. The symbols indicate the parameters, the open circuit voltage (V_{oc}), the short-circuit current density (J_{sc}), the maximum power point (P_{MPP}), the corresponding voltage (V_{MPP}), and the current density (J_{MPP}). A solar cell is characterized by three parameters: the open-circuit voltage (V_{oc}), the short-circuit current density (J_{sc}) and the fill factor (FF). The V_{oc} which is the maximum photo voltage that the device can supply is defined by the voltage where the current under illumination is zero. The fill factor (FF) defines the ratio of the maximum power density (P_{MPP}) to the product of the open circuit voltage and short circuit current

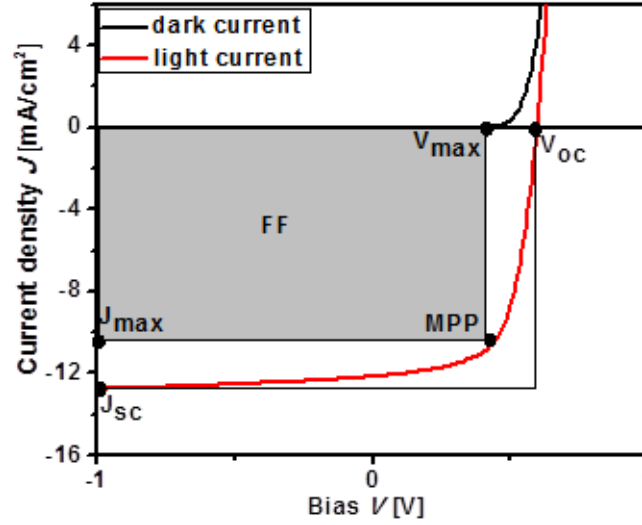


Figure 1.2 Typical J-V curves of a solar cell in dark and under illumination.

density which is given in the equation (1).

$$FF = \frac{P_{MPP}}{J_{sc} \times V_{oc}} = \frac{J_{MPP} \times V_{MPP}}{J_{sc} \times V_{oc}} \quad (1)$$

The fill factor is influenced by the leaked current and the efficiency of charge collection in the cell. The power conversion efficiency (PCE) (η) of a solar cell is defined by the ratio of P_{MPP} and the power density of the incident light (P_{in}) and is given in the equation (2).

$$\eta = \frac{P_{MPP}}{P_{in}} = \frac{J_{sc} \times V_{oc} \times FF}{P_{in}} \quad (2)$$

This equation (2) shows a linear dependence between the power conversion efficiency and the short circuit current, open circuit voltage and fill factor and increase in the efficiency involves enhancing the three parameters.

In general, both the spectrum and intensity of the incident light has a greater influence on the PCE of a solar cell. In reporting the PCE of solar cells, it is

customary to use the AM1.5G spectrum at an intensity of 1000 W/m². Usually, simulated solar light is used to obtain the J-V characteristics and to estimate the efficiency of the solar cell. The simulated spectrum obtained from a white light source and filters is not the same as the AM1.5G spectrum; hence the obtained J-V curve differs from what is expected in solar light. A more precise estimation of J_{sc} can be obtained using the spectrally resolved external quantum efficiency (EQE), which is the fraction of incident photons that is converted to electrons by the external circuit at short circuit conditions at a particular wavelength (λ). J_{sc} can be calculated by convolution of the spectrally resolved measurement with the AM1.5G spectral irradiance at 1000 W/m² is given in the equation (3).

$$J_{sc}(SR) = \int EQE(\lambda) \times E_{AM\ 1.5G}(\lambda) \times \frac{e \cdot \lambda}{h \cdot c} d\lambda \quad (3)$$

where 'e' represents the elementary charge, 'h' is the Planck constant and 'c', the speed of light. The EQE of organic solar cells is preferably determined under continuous bias illumination that enables to measure EQE at one-sun operating condition. This is necessary due to the sub-linear light intensity dependence of organic solar cells. At low light intensity carrier concentrations are low and recombination is limited which resulted in higher current comparing to the one-sun intensity. Recombination increases and carrier transport is less efficient due to space-charge build up in the solar cells, and measurements are carried out using bias illumination to prevent overestimation of the J_{sc}.³²⁻³³

The improvements of BHJ OPV solar cells are possible due to the better understanding of the basic processes involved in the generation of electricity upon

illumination. Although the area is well explored and understood for the past two decades, it is still difficult to optimize the design to maximize the PCE of an organic solar cell. Here we discuss each process which is crucial for the device performance.

Five possible processes are starting from light absorption in the bulk heterojunction solar cell which is listed below and schematically given in the Figure 1.3.

- 1) Light absorption with exciton formation and migration.
- 2) Formation of charge transfer state from exciton.
- 3) Separation of charge transfer state into free charge.
- 4) Charge transport to respective electrodes.
- 5) Charge collection.

- 1) Light absorption with exciton formation and migration.

When light falls on the active layer, both the donor and acceptor materials can be excited. In this schematization, the donor material absorbs light energy. Indeed in BHJ solar cells, the primary light absorber is the donor while using fullerene derivatives as the electron acceptor. Thanks to intense research in this area there are highly efficient light absorbing non-fullerene acceptors which also create exciton.³⁴ The material absorbs a photon that has enough energy to promote an electron from the highest occupied molecular orbital (HOMO) to the lowest unoccupied molecular orbital (LUMO). The minimum energy for excitation is called the optical band gap energy (E_g). Absorbed photons with energy larger than E_g will create a 'hot exciton' that will thermalize *via* non-radiative decay processes to the

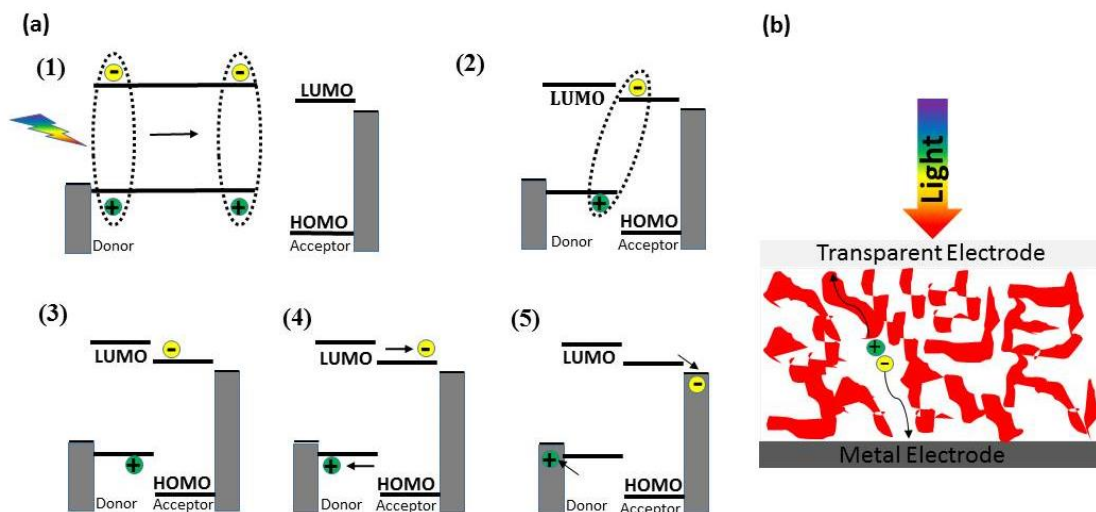


Figure 1.3 (a) Schematic band diagram of a donor-acceptor heterojunction. (1) Absorption of light in the donor, exciton formation and its diffusion to the interface. (2) Formation of charge transfer state from exciton. (3) separation of the CT state into free charges. (4) charge transport to the respective electrodes. (5) charge collection. Note that an excitation in the acceptor can very similarly lead to hole transfer to the donor, provided there is a sufficient energy offset between the HOMO energy levels. (b) Schematic representation of a bulk heterojunction.

HOMO and LUMO band edges. The optical band gap of the materials is small enough such that a large part of the solar spectrum can be absorbed.

The generation of the exciton created away from the donor/acceptor (D/A) interface, and exciton diffuses to the interface has to take place before charge dissociation. As a consequence of the small relative permittivity ($\epsilon_r = 3-4$) of these materials, the value of exciton binding energy is 0.3–0.4 eV for the organic material which is substantially higher than that of the inorganic semiconductors ($EB = \sim 10$ meV with $\epsilon_r \geq 10$).³⁵⁻³⁸ As a result, the average exciton diffusion length in the active layer is approximately between 10 to 20 nm. Thus the phase separation of the donor and acceptor domains in the active layer should not be larger than the exciton diffusion length otherwise resulted in geminate recombination. Experimental

determination of diffusion length for small molecule donor materials yield value in the range of 3-30 nm,³⁹⁻⁴¹ 20 nm for conjugated polymer Poly(3-hexylthiophene-2,5-diyl) (P3HT),⁴²⁻⁴³ and 40 nm for C₆₀.⁴⁴

2) Formation of charge transfer state from exciton.

The excitons that reach the interface between p-type and n-type material were dissociated by an electron transfer from the LUMO of the photoexcited p-type material to the n-type material. Note that the alternative process is also possible: a hole in the HOMO of the photoexcited n-type material can be transferred to the HOMO of the p-type material. In practice both processes take place. If the energy difference between the ionization potential IP_D of the electron donating material and the electron affinity EA_A of the electron acceptor material is larger than the exciton binding energy E_B , that is usually 0.3-0.4 eV⁴⁵⁻⁴⁸, exciton dissociation is energetically favored.

3) Separation of charge transfer state into free charge.

To overcome the columbic attraction between the electron-hole pair, spatially separated but still bound at the D/A interface, a built-in electric field is needed. This internal electric field is mainly determined by the different work-functions of the electrode materials at the anode and cathode sides of the device. If the electric field is too low, non-geminate recombination will occur; otherwise successful charge carrier separation resulted in the formation of free electrons and holes.

4) Charge transport to respective electrodes.

The free electrons and holes have to travel to the appropriate electrode. In the

conventional device structure, the holes reach the ITO and electrons move towards the aluminum contact. But in the case of inverted device structure, an electron reaches the ITO and holes travel towards silver or gold electrode. The first requirement is that the morphology of the material blend should allow a pathway for the charges to arrive at the electrodes. Second, the materials have to possess a rather high mobility to transport the charges efficiently. If charge transport is slow or impeded, bimolecular charge recombination may occur which reduces the performance. The charge carrier mobility of the materials may depend on device configuration, charge carrier density, temperature, electric field, morphology and time scale of the experiment. So it is not an easy task as the actual value may change and it is advisable to measure the mobility in a device structure very similar to the solar cell device. For solar cells, this is a sandwich configuration in which a thin film is placed between large area top and bottom contacts. Further, it is important to measure only one type of carrier (i.e. hole or electron) at a time. The most suitable method is space charge limited current (SCLC) ⁴⁹.

5) Charges collection.

To facilitate charge collection without energetic losses, both the hole and electron collecting electrodes should form an ohmic contact with the HOMO energy level of the donor and the LUMO of the acceptor respectively. Interlayers between the electrodes and the active layer play an important role in improving the efficiency of the solar cells. These layers are often based on metal oxides or (highly doped) organic materials and provide selectivity and enhancement of the extraction of

either holes or electrons. Typically, poly(3,4-ethylenedioxythiophene):polystyrene sulfonate (PEDOT:PSS), MoO₃, or NiO are used as hole transporting layers (HTL) and LiF, ZnO, poly[(9,9-bis(3'-(N,N-dimethylamino)propyl)-2,7-fluorene)-alt-2,7-(9,9-dioctylfluorene)] (PFN), or ethoxylatedpolyethylenimine (PEIE) can be used as electron transporting layers (ETL). The exact mechanism responsible for the enhanced extraction of electrons by materials such as LiF, PFN, or PEIE is still under debate. The most suggested mechanisms involve dipole (and mirror image dipole) formation with the metal electrode, lowering the work function and enhancing electron transfer from the organic semiconductor to the metal.⁵⁰⁻⁵³

Triphenylamine, thiophene and oligothiophene, fluorene, squaraine, benzothiadiazole and benzobisthiadiazole, bodipy, isoindigo, diketopyrrolopyrrole (DPP) are various classes of organic dyes extensively studied in the field of bulk heterojunction solar cells.⁵⁴ Among them DPP organic pigment is widely used in the applications such as paints, plastics and ink etc.⁵⁵ Due to its tunable absorption in the visible and near infrared region, high charge carrier mobility and the improvement in the solar cell efficiency in the laboratories, its incorporation promises the scope for commercialization of organic solar cell technology.

1.5 Diketopyrrolopyrrole (DPP) based small molecules

Diketopyrrolopyrrole (DPP) based organic semiconductors have several advantages such as facile synthetic modification, good photochemical stability and strong light absorption. The DPP unit is an attractive building block for organic photovoltaics (OPVs), which shows desirable optical properties and sufficient solubility in organic solvents for spin-cast devices. Especially, its strong π -electron withdrawing properties provide the possibility to control the absorption spectrum into the near - IR (NIR) region *via* conjugation with electron-rich aromatic units.⁵⁶⁻⁵⁸ This can be explained by a simple molecular orbital representation which is shown in the Figure 1.4. Hybridization of the frontier orbital levels of the donor and acceptor units

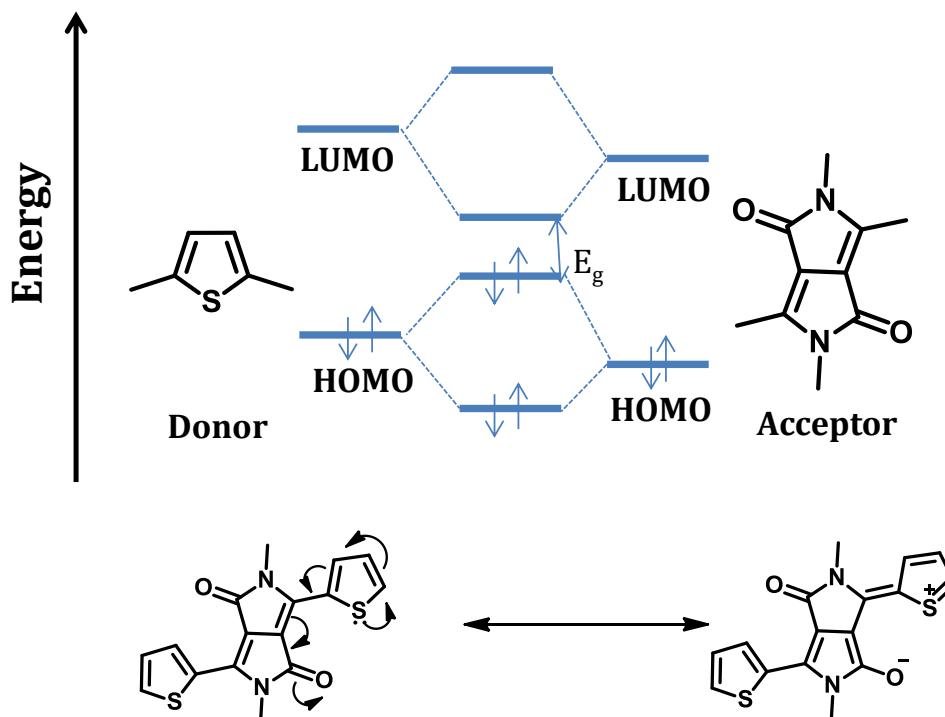


Figure 1.4 Schematic energy level diagram of the recombination of molecular orbital levels in a donor-acceptor system, creating a small band gap (E_g) in the D-A compound. Thiophene and Diketopyrrolopyrrole are shown as typical example and its resonance structures.

results in new molecular orbitals with a significant decrease of the band gap. In these push-pull systems the LUMO of the acceptor primarily determines the LUMO of the resulting small molecule whereas the HOMO is mainly determined by the HOMO of the donor. This gives easy control because individual orbital levels can now be adjusted by exchange with a stronger or weaker donor or acceptor unit. The various electron rich conjugated oligomers are benzene, thiophene, pyrrole, furan, or combinations thereof as building blocks, sometimes in fused ring configurations are often used. The rigid and planar aromatic structure helps to enhance the intermolecular packing and therefore leads to very high charge carrier mobility.

Solubility of the DPP small molecules plays an important role in the solution-processed bulk heterojunction solar cell. N -alkylated DPPs show remarkably higher solubility than the corresponding N -unsubstituted pigments, because alkyl groups present at nitrogen atoms prevent the formation of intermolecular hydrogen bonds. Alkyl groups provide steric repulsion to prevent strong π - π interactions and branching enhance solubility more than linear ones, and groups like 2-ethylhexyl, 2-butyloctyl, 2-hexyldecyl etc. are commonly used.⁵⁹⁻⁶⁰ The positioning of the alkyl chains on a molecule or polymer also has a major influence on the supramolecular packing.⁶¹ The effect of even small modifications on alkyl groups has been shown many times to have a major effect on performance due to changes in film packing.⁶² Alkyl side chains also act as significant electron donating groups due to hyperconjugation.⁶³ The process of molecular design in organic electronics requires

a great deal of trial and error, because even the various effects of alkyl chains on different properties can't be predicted with accuracy.

1.5.1 Mono-diketopyrrolopyrrole

Tamayo *et al.* synthesized a new thiophene-based DPP chromophore with *t*-Boc **1**, and ethyl hexyl **2** substituted at N, N-position or the lactam N atoms of DPP unit. The absorption extends to 720 nm in solution and 820 nm in the film. The molecule **2** has higher thermal stability than **1**. The molecule **1** with PC₆₁BM in 70:30 donor-acceptor ratio showed a PCE of 2.3 %, with a V_{oc} of 0.67 V, J_{sc} of 8.42 mA/cm² and EQE close to 30 % between 550 and 750 nm. The molecule **2** showed a PCE of 3.0 % with a large V_{oc} of 0.75 V and J_{sc} of 9.2 mA/cm² with PC₇₁BM as the acceptor.⁶⁴
⁶⁵ The chemical structures of the mono DPP from **1** to **12** are given in the Figure 1.5. In 2009, the same research group replaced bithiophene units with fused benzofuran **4a** and blended with PC₇₁BM in the ratio of 60:40 yielding a J_{sc} of 10 mA/cm², V_{oc} of 0.92 V, a FF of 0.48, and a PCE of 4.4 %.⁶⁶ The effect of change in the hetero-atom substitutions were also examined by replacing the aromatic end-groups of **4a** by benzothiophene **4d** and N-methylindole **4e**. The photovoltaic performance of **4d** and **4e** showed lesser efficiency than **4a**. The optimal device of **4d** mixing with PC₇₁BM in the ratio of 1:1 and annealing at 80 °C, gives J_{sc} of 5.70 mA/cm², V_{oc} of 0.76 V, FF of 0.33 and PCE of 1.43 %. The device fabricated from **4e** with an PC₇₁BM rich blend (30:70), annealed at 80 °C, producing a J_{sc} of 4.31 mA/cm², V_{oc} of 0.81 V, FF of 0.30 and PCE of 1.03 %.⁶⁷

Reynolds and co-workers replaced ethylhexyl chain **2** with hydrophilic

triglyme chains to the DPP core and studied the self-assembly profile of the oligomer **3** and the solar cell devices with PC₆₁BM exhibited a relatively low PCE of 0.68 %.⁶⁸ The same authors synthesized a series of molecules **4a**, **4b**, **4c**, **4d**, **4e**, **4f** and fabricated bilayer solar cell devices by spin-coating a film of a donor of typically 20 nm and C₆₀ layer were thermally deposited. The donor molecule **4a** leads to the highest efficiency, with a J_{sc} close to 8.0 mA/cm² and a PCE of 2.50 %.⁶⁹

Benzo[1,2-b;4,5-b']dithiophene (BDT), triphenylamine, pyrene substitution at C₁ and C₂ attached to both side of the DPP core were synthesized by Fréchet and co-workers and self-assembly was studied through the electron-rich π -stacking units in the BHJ solar cell with PC₇₁BM. The intermolecular connectivity promoted by C₂-pyrene allows devices containing blends of **5** and PC₇₁BM to reach a maximum PCE of 4.0 % with a FF approaching 0.6.⁵⁹ The effect of halogen atom substitution in the DPP-based small molecules was investigated by Zhang and Co-workers and Choy and co-workers. The molecule **2** in which the hexyl chains were replaced by F and Cl atoms were evaluated to investigate the effects of halogenation on the photovoltaic properties of the organic solar cell. The higher PCE of 4.32 % was obtained for the fluorine containing molecule compared to the 1.0 % efficiency for the chlorine substituted derivative.⁷⁰ Choy and co-workers synthesized derivatives having naphthalene and fluoro naphthalene end group on both sides of the DPP core. Device performance with the photovoltaic device structure (ITO/PEDOT:PSS/**12**:PC₆₁BM/Al) yielded approximately 3.0 % efficiency with high V_{oc} of 0.90 V and FF of 54 %.⁷¹ Shin *et al* achieved the liquid-crystalline organization for the DPP core

molecule **2** while replacing the oligothiophene with hexyl benzene **13** and dodecyl benzene **14**. They studied the self-assembly and photovoltaic devices with the PC₇₁BM acceptor. The efficiency of the device with **13** was 4.3 % with a high V_{oc} of 0.93 V, J_{sc} of 8.27 mA/cm² and a FF of 0.55 and that of **14** was 1.2 % with a high V_{oc} of 0.93 V but low J_{sc} of 3.73 mA/cm² and FF of 0.35.⁷² The Figure 1.6 and 1.7 contains the chemical structure of the molecules from **13** to **22** and **23** to **31** respectively. Jin and coworkers compared the solar cell efficiency of molecules **7** and **15**. The device optimization of **7** and **15** achieved an efficiency of 1.45 % and 1.75 % respectively.⁷³

Two asymmetrical push-pull small molecules have been reported, consisting of triphenylamine and DPP as a dipolar D- π -A, **16** and D- π -A-A, **17** with ethynylbenzene as the π -bridge. The molecules **17** with cyanophenyl exhibited a low optical band gap of 1.65 eV, and solution processed device based on **17** : PC₆₁BM showed a PCE of 5.94 %. Under the same experimental conditions, the PCE of BHJ device based on a blend of **16** and PC₆₁BM reached 2.06 %.⁷⁴

Zhu and coworkers designed and synthesized three small molecules **18**, **19**, and **20** based on a DPP unit featuring acetylenic linkage. The photovoltaic response of **18** showed a PCE of 4.39 % with V_{oc} of 0.77 V with the simple structure (ITO/PEDOT: PSS/**18**:PC₆₁BM/Al), without a high boiling point solvent additive or solvent vapor annealing. Thermal annealing of the active layer at 70 °C led to decreasing of the PCE, which may arise from the high crystallization tendency of **18**, yielding unfavorable morphology with large domain sizes. The photovoltaic

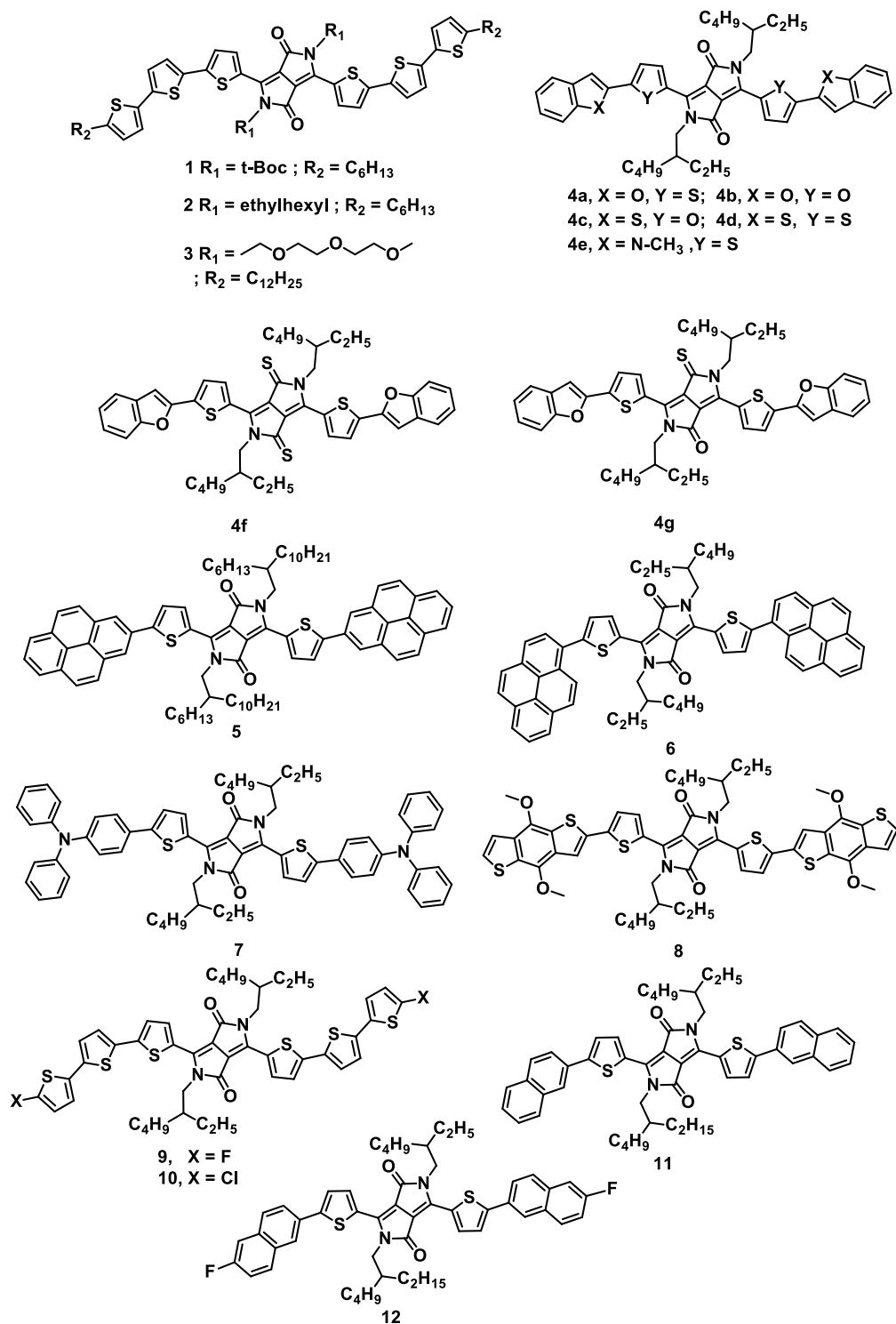


Figure 1.5 Chemical structure of mono diketopyrrolopyrrole

response of **19**, and **20** while incorporating a thin cathode interlayer Phen-NaDPO, spin-cast from isopropanol solution was seen to improve the cathode interfacial contact, and the thermal annealing of the active layer at 100 °C resulted in an efficiency of 2.01 % for compound **19** and 2.62 % for compound **20**.⁷⁵⁻⁷⁶

Li and co-workers investigated the effect of triple-bond for the D-A-D system. DPP as acceptor with alkylated carbazole and fluorene as terminal electron-donating groups, **21** and **23** and the ethynyl π -linkage between the donor and acceptor **22** and **24** respectively. The ethynyl-linkage structural design could not only lower the HOMO, but also delicately balanced the relationship between the deep-lying HOMO and narrow band gap, thus improving the photovoltaic performance. As a result, compounds **22** and **24** exhibited relatively deep-lying HOMO relative to **21** and **23**, resulting in the corresponding photovoltaic (PV) devices with an increased V_{oc} of 0.84 V and 0.98 V, with PCE of 1.99 % and 3.10 %, respectively, whereas **21** and **23** based devices showed a V_{oc} of 0.46 V and 0.89 V, and a PCE of 1.48 % and 2.23 %, respectively.⁷⁷ The same authors have investigated π -linkage effects between the donor triphenylamine and acceptor DPP **25**, **26**, **27** and **28**. The vinylene π -linkage exhibited, relatively higher PCE of 3.76 % due to better molecular coplanarity.⁷⁸ The authors also investigated the effect of the terminal donor's thiophene, thieno [3,2-b]thiophene and selenophene to the DPP core **34**, **35**, and **36** respectively and tested their performance in the solar cell devices. The best efficiency obtained in the ratio of 3 : 1 with **34**:PC₆₁BM, **35**:PC₆₁BM and **36**:PC₆₁BM were 1.90 %, 1.30 %, and 2.33 % respectively.⁷⁹

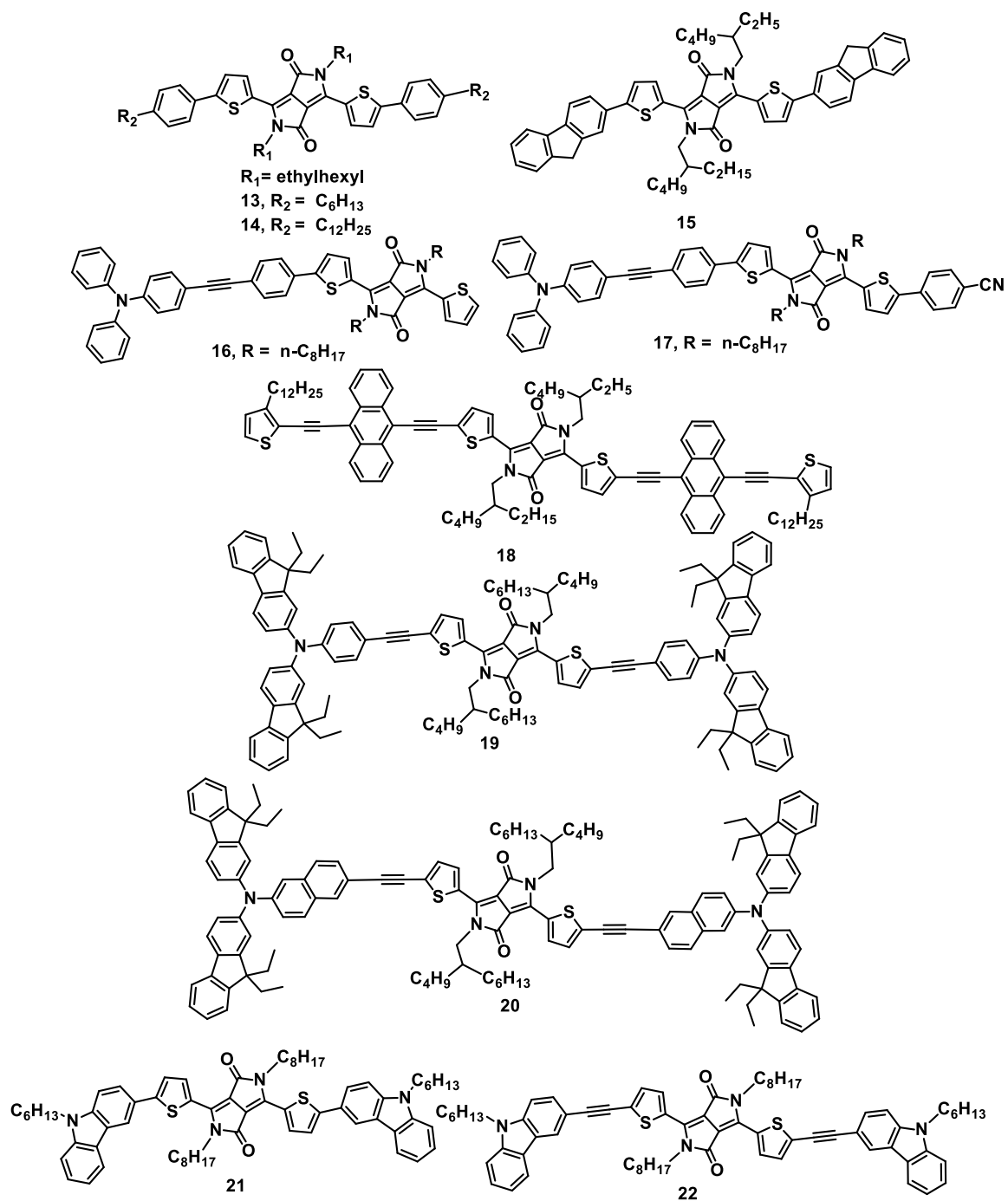


Figure 1.6 Chemical structure of mono diketopyrrolopyrrole

Lim and co-workers synthesized two π -conjugated simple DPP molecules, attached to a DPP core with thiophene and furan respectively **29** and **30**, using the Suzuki coupling reaction. Solar cell devices were fabricated with the configuration ITO/PEDOT: PSS/**29** or **30**:PC₇₁BM/LiF/Al and the **29** and **30** films were post-annealed at 80 °C and 100 °C for 10 min, respectively. The molecule **29** showed higher PCE (1.44 %) than **30** (0.85 %). The J_{sc} of **29** (4.38 mA/cm²) was nearly twice that of **30** (2.49 mA/cm²). The improved J_{sc} of **29** could be explained by the better optical properties of **29** and the surface morphology of **29**:PC₇₁BM film having a root mean square roughness of 1.37 nm, compared to **30** having lesser absorption and the surface rms roughness of 5.50 nm for a **30**:PC₇₁BM film.⁸⁰

Janssen and co-workers investigated the effect of the side chain position on the three isomeric DPP molecules **31**, **32**, and **33** that consist of DPP unit substituted by two bithiophenes (2T) of which the terminal thiophenes carry a hexyl chain in the 3, 4, or 5 position respectively. The Figure 1.8 and 1.9 contains the chemical structure of the molecules from **32** to **41** and **42** to **50** respectively. Solar cells were prepared by spin-casting PEDOT: PSS on precleaned ITO patterned glass substrates. The PEDOT:PSS layer was dried by heating at 120 °C for 20 min before deposition of the active layer. On top of the dried PEDOT: PSS the active layers were deposited by spin-casting a mixture of the donor with PC₇₁BM in a 2:1 ratio from chloroform. A back contact of 1 nm LiF and 100 nm Al was evaporated in vacuum. Annealing of the active layers was performed after evaporation of the back contact

in a nitrogen environment. The PCE of the devices **31**:PC₇₁BM, **32**:PC₇₁BM, **33**:PC₇₁BM were found to be 2.48 %, 3.30 %, 1.90 % respectively.⁶¹

In 2013, Russell and co-workers reported 'A-D-A-D-A' molecule **37** with 3,3'-dioctyl-2,2':5',2''-terthiophene as donor attached to both side of central core acceptor DPP unit with terminal group acceptor as octylcyanoacetate. BHJ solar cells were fabricated in the traditional sandwich structure ITO/PEDOT:PSS/**37**:PC₇₁BM/LiF/Al. The active layer with the thickness around 85 nm obtained by spin coating with chloroform solution in 1:1 donor - acceptor ratio providing an efficiency of 1.18 %. Detailed morphological studies were conducted by adding various volume fractions of DIO in chloroform ranging from 0.25 % to 10 %. Upon adding 3 vol % DIO to the solvent, the efficiency of the solar cell increases to 4.73 %.⁸¹ Similarly in 2016, Chen and co-workers replaced the donor parts of the molecule **37** with 3, 4'-dioctyl-2, 2'-bithiophene having lesser number of thiophene attached to both sides of central core acceptor DPP unit with two terminal group acceptor as octylcyanoacetate and 3-octylrhodanine **38** and **39** respectively. The two molecules in films exhibited broad absorption ranging from 300 to 900 nm with **39** as donors and PC₇₁BM as acceptor gave a PCE of 2.05 % and 1.09 %, respectively. The device performances were low owing to the large domain size and phase separation.⁸²

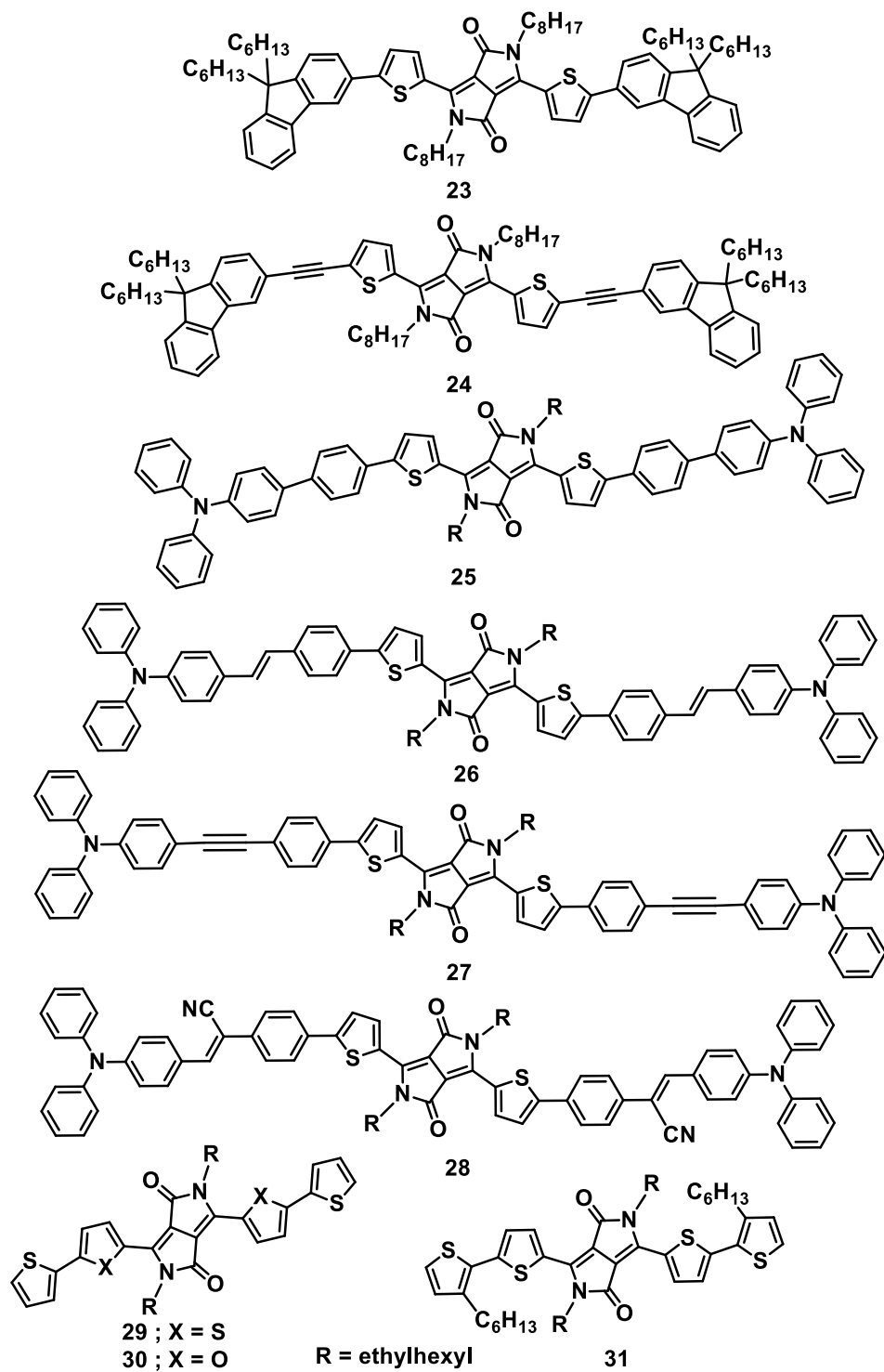


Figure 1.7 Chemical structure of mono diketopyrrolopyrrole

Skabara and co-workers synthesized two molecules based on a DPP central core and two 4, 4-difluoro-4-bora-3a,4a-diaza-s-indacene (BODIPY) units attached by thiophene rings **40**, and **41**. These molecules showed high molar extinction coefficient, and both of them were blended with PC₇₁BM as acceptor in different ratios by weight percentage and their PV properties were studied. For both the triads, a modest PV performance was observed, having an efficiency of 0.65 %.⁸³ Santos and co-workers synthesized phthalocyanine attached to both ends of the DPP core units **42** and mixed with PC₇₁BM as an active layer in the solar cell device. PV devices fabricated using the general architecture ITO/MoO₃/**42**:PC₇₁BM/Ca/Ag showed an efficiency of 1.04 %.⁸⁴

Ziessel and co-workers report dumbbell-shaped molecules with triazatruxene attached to both sides of thiophene DPP at para and meta position of the nitrogen atom of the ring **43** and **44** respectively. The molecule showed a broad absorption spectrum up to 750 nm in the film state for both isomers and devices were fabricated with PC₇₁BM. The PCE for the meta substitution was 4.4 % with a V_{oc} of 0.65 V, J_{sc} of 13.1 mA/cm² and a FF of 0.52. But the para derivative shows a higher current of 14.6 mA/cm² with an efficiency of 5.3 %.⁸⁵ Sharma and co-workers extensively studied DPP based small molecules for the application of bulk heterojunction (BHJ) solar cell in India. G. D. Sharma and co-workers synthesized thiophene capped DPP as acceptor with various donor units at the both end and the structure of the molecules from **45** to **53**. The Figure 1.10 contains the chemical structure of the molecules from **51** to **54**. Photovoltaic properties of BHJ devices

with the active layer **45** : PC₆₁BM (1:1) performs a J_{sc} of 6.83 mA/cm², V_{oc} of 0.80 V, FF of 0.44, PCE of 2.40 %.⁸⁶ The end terminal group indole **46** and 2, 4, 6-tri-isopropyl phenyl **47** showed an efficiencies of 4.96 % and 3.04 % with PC₇₁BM as acceptor annealed at 110 °C for 10 minutes.⁸⁷ 1,3 difluorobenzene and 1,3 dibutoxybenzene act as an end terminal group for the molecule **48** and **49** and the PV performance with PC₇₁BM and 0.5 % 1-chloronaphthalene (1-CN) as solvent additive in chloroform gave 3.22 % and 4.65 % respectively.⁸⁸ They studied the effect of thermal and solvent annealing on the morphology and photovoltaic performance for the compound **50** to **53**. Among these set of molecules, **52** showed efficiency of 3.55 % and solvent and thermal annealing treatment improved the efficiency upto 5.47 %.⁸⁹ A low band gap small molecule with a D- π -A- π -D molecular structure composed of a dithiafulvalene donor and a DPP acceptor **54** was synthesized and tested for organic solar cells. Using the small molecule **54** as an electron donor and PC₇₁BM as acceptor high PCE of 4.3 % was achieved.⁹⁰

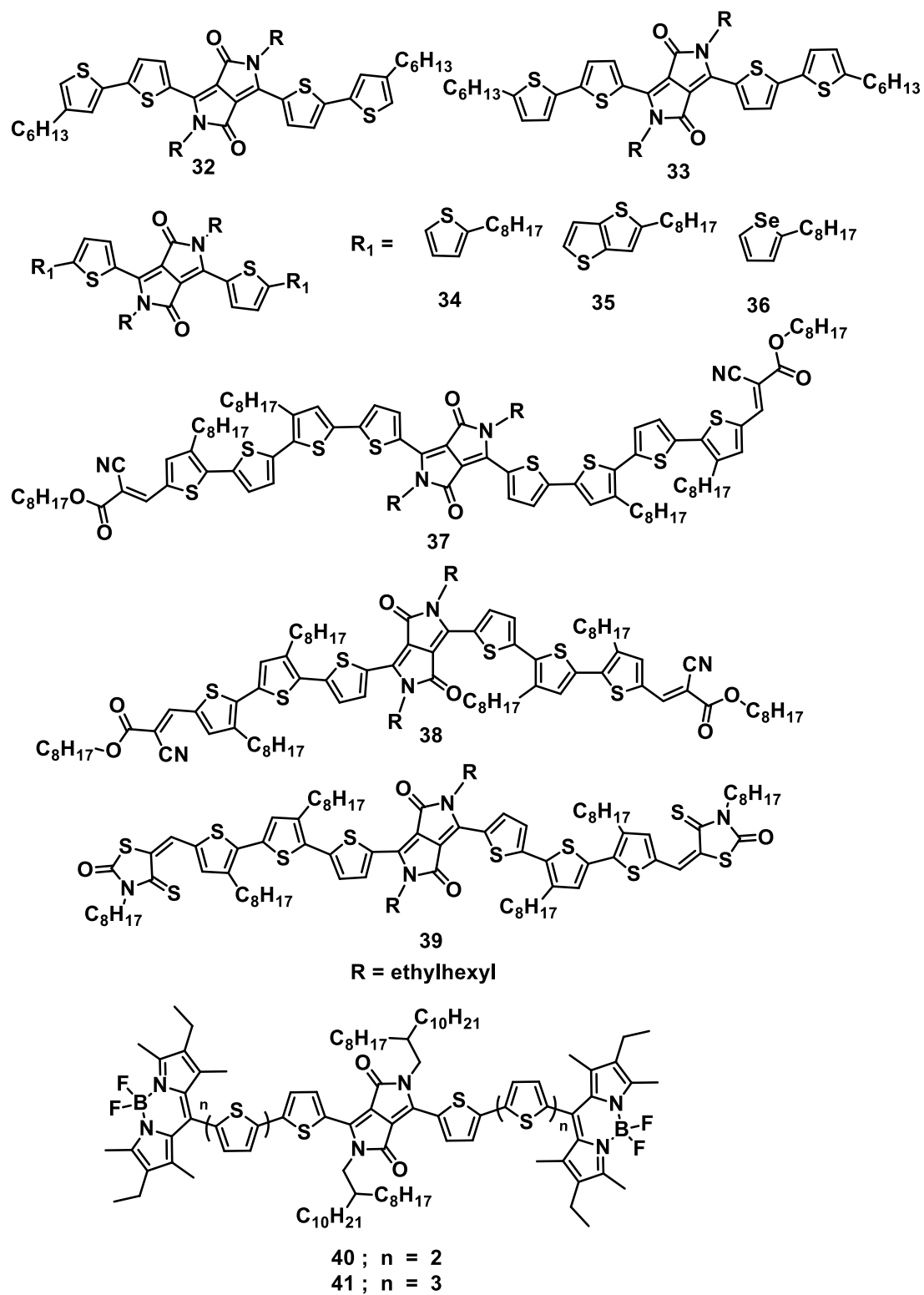


Figure 1.8 Chemical structure of mono diketopyrrolopyrrole.

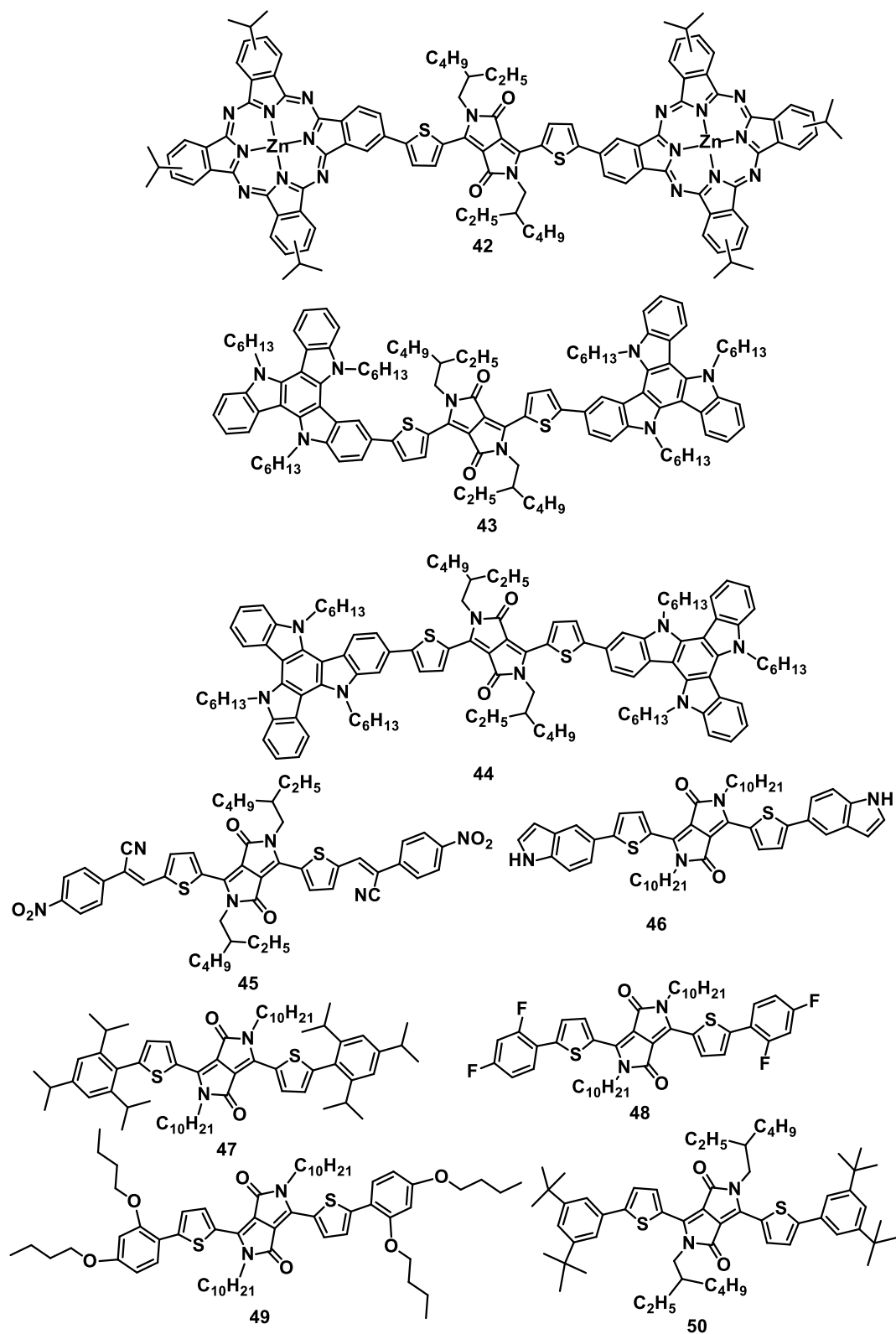


Figure 1.9 Chemical structure of mono diketopyrrolopyrrole.

Table 1.1 The photovoltaic properties of mono diketopyrrolopyrrole derivatives

SL.No	Active Layer (D:A)	Annealing	V _{oc} (V)	J _{sc} (mA/cm ²)	FF	PCE %	Ref
1)	1:PC ₇₁ BM (70:30)	rt	0.67	8.42	0.45	2.33	64-
2)	2:PC ₇₁ BM (50:50)	rt	0.75	9.20	0.44	3.00	65
3)	3:PC ₆₁ BM (1:1)	90 °C	0.55	2.41	0.55	0.68	68
4)	4a:PC ₇₁ BM(60:40)	110 °C	0.92	10.0	0.48	4.40	66
5)	4d:PC ₇₁ BM(50:50)	80 °C	0.76	5.70	0.33	1.43	67,69
6)	4e:PC ₇₁ BM(30:70)	80 °C	0.81	4.31	0.30	1.03	
7)	Bilayer 4b and C ₆₀	---	0.60	3.30	0.39	0.80	69
8)	Bilayer 4c and C ₆₀	---	0.66	3.22	0.32	0.75	
9)	Bilayer 4d and C ₆₀	rt	0.39	0.13	0.19	0.01	
10)	Bilayer 4f and C ₆₀	rt	0.09	0.003	0.25	0.001	
11)	5:PC ₇₁ BM (2:1)	130 °C	0.76	8.30	0.58	3.70	59
12)	6:PC ₇₁ BM (1:4)	100 °C	0.73	3.20	0.29	0.70	
13)	7:PC ₇₁ BM (1:4)	110 °C	0.73	4.30	0.31	1.00	
14)	8: PC ₇₁ BM (1:4)	110 °C	0.81	6.20	0.30	1.30	
15)	9:PC ₇₁ BM (3:2)	110 °C	0.67	11.17	0.55	4.32	70
16)	10:PC ₇₁ BM (3:2)	110 °C	0.67	5.29	0.28	1.00	
17)	11:PC ₇₁ BM (3:2)	110 °C	0.84	4.06	0.50	2.61	71
18)	12:PC ₇₁ BM (3:2)	110 °C	0.92	4.18	0.54	3.15	
19)	13: PC ₇₁ BM (1:1)	140 °C	0.93	8.27	0.54	4.20	72
20)	14:PC ₆₁ BM (1:2)	120 °C	0.93	3.73	0.35	1.20	73
21)	15:PC ₇₁ BM (1:1)	rt	0.87	5.03	0.39	1.73	
22)	16:PC ₆₁ BM (1:2)	rt	0.97	7.07	0.30	2.06	74
23)	17:PC ₆₁ BM(1:2)	rt	0.93	14.86	0.43	5.94	

Table 1.1 The photovoltaic properties of mono diketopyrrolopyrrole derivatives

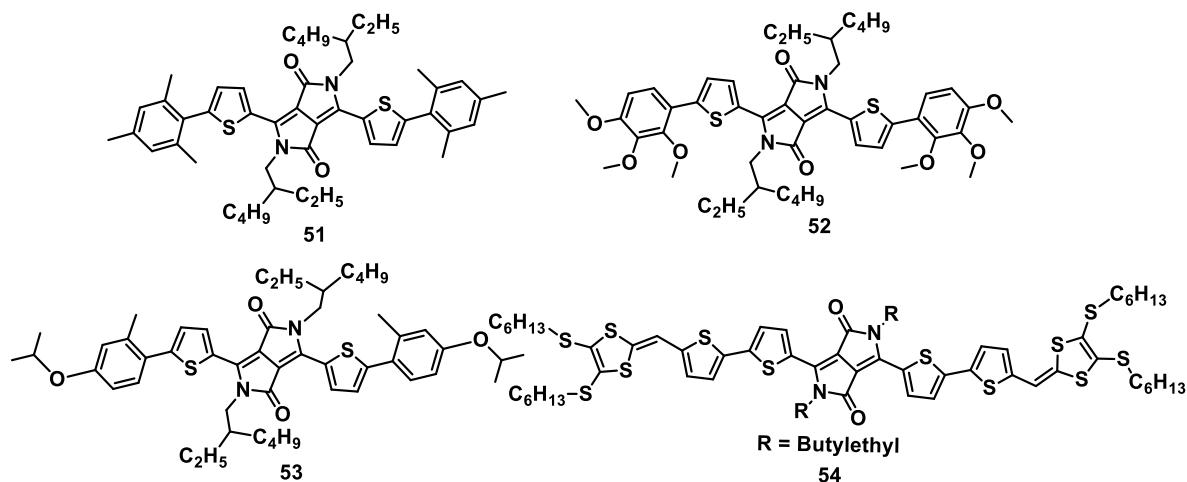
(Continuation from the previous page)

Sl.No	Active Layer (D:A)	Annealing	V _{oc} (V)	J _{sc} (mA/cm ²)	FF	PCE %	Ref
24)	18:PC ₆₁ BM	50 °C	0.77	9.28	0.61	4.39	74-76
25)	19:PC ₆₁ BM	100 °C	0.92	5.42	0.42	2.01	
26)	20:PC ₆₁ BM	100 °C	0.96	6.24	0.43	2.62	
27)	21:PC ₆₁ BM(1:2)	rt	0.49	6.60	0.49	1.48	77
28)	22:PC ₆₁ BM(1:2)	rt	0.89	7.17	0.35	2.23	
29)	23:PC ₆₁ BM(1:2)	rt	0.84	7.67	0.31	1.99	
30)	24:PC ₆₁ BM(1:2)	rt	0.98	9.04	0.35	3.10	
31)	25:PC ₆₁ BM	rt	0.88	8.62	0.36	2.74	78
32)	26:PC ₆₁ BM	rt	0.84	11.90	0.38	3.76	
33)	27:PC ₆₁ BM	rt	0.93	10.30	0.32	3.10	
34)	28:PC ₆₁ BM	rt	0.90	9.73	0.33	2.92	
35)	29:PC ₇₁ BM(2:1)	rt	0.90	4.38	0.37	1.44	80
36)	30:PC ₇₁ BM(2:1)	rt	0.83	2.49	0.41	0.85	
37)	31:PC ₇₁ BM(2:1)	100 °C	0.85	5.89	0.50	2.48	61
38)	32:PC ₇₁ BM (2:1)	100 °C	0.85	7.47	0.53	3.30	
39)	33:PC ₇₁ BM(2:1)	100 °C	0.79	5.30	0.45	1.90	
40)	34:PC ₆₁ BM(3:1)	rt	0.78	5.59	0.44	1.88	79
41)	35:PC ₆₁ BM(2:1)	rt	0.78	5.74	0.38	1.67	
42)	36:PC ₆₁ BM(3:1)	rt	0.86	5.80	0.46	2.30	
43)	37:PC ₆₁ BM(1:1)	rt	0.72	13.6	0.47	4.73	81
44)	38:PC ₇₁ BM(1:1)	rt	0.76	3.12	0.46	1.09	82
45)	39:PC ₇₁ BM(1:1)	rt	0.76	5.09	0.53	2.05	
46)	40:PC ₇₁ BM(1:1)	rt	0.71	3.39	0.27	0.65	83
47)	41:PC ₇₁ BM(1:1)	rt	0.53	4.55	0.26	0.64	

Table 1.1 The photovoltaic properties of mono diketopyrrolopyrrole derivatives

(Continuation from the previous page)

Sl.No	Active Layer (D:A)	Annealing	V _{oc} (V)	J _{sc} (mA/cm ²)	FF	PCE %	Ref
48)	42:PC ₇₁ BM(1.5:1)	rt	0.55	5.00	0.38	1.04	84
49)	43:PC ₇₁ BM(1:0.75)	110 °C	0.63	14.6	0.58	5.3	85
50)	44:PC ₇₁ BM(1:0.75)	120 °C	0.65	13.1	0.58	4.4	
51)	45 : PC ₇₁ BM (1:1)	rt	0.80	6.83	0.44	2.40	86
52)	46 : PC ₇₁ BM (1:1)	110 °C	0.82	10.82	0.56	4.96	87
53)	47 : PC ₇₁ BM (1:1)	110 °C	0.92	7.34	0.46	3.04	
54)	48: PC ₇₁ BM (1:1)	rt	0.78	8.06	0.52	3.23	88
55)	49:PC ₇₁ BM (1:1)	rt	0.72	10.68	0.60	4.65	
56)	50:PC ₇₁ BM (1:1)	rt	0.90	8.12	0.40	3.05	89
57)	51:PC ₇₁ BM(1:1)	rt	1.02	7.38	0.38	2.86	
58)	52:PC ₇₁ BM(1:1)	rt	0.88	9.18	0.44	3.55	
59)	53:PC ₇₁ BM(1:1)	rt	0.94	7.68	0.40	2.89	
60)	54:PC ₇₁ BM(1:1)	rt	0.69	12.24	0.51	4.30	90

**Figure 1.10** Chemical structure of mono diketopyrrolopyrrole

1.5.2 Bis-diketopyrrolopyrrole

Mark and co-workers synthesized a bis-DPP molecule with the central donor as 5,10-bis(2-ethylhexyloxy)naphtho[2,3-b:6,7-b']dithiophene and both side DPP as acceptor **55**. The PV device was fabricated based on the conventional architecture ITO/PEDOT:PSS/**55**:PC₆₁BM/LiF/Al. The best solar cell device was obtained at 1.5:1 ratio of **55**: PC₆₁BM with annealing at 110 °C for 10 min to yield a $V_{oc} = 0.84$ V, $J_{sc} = 11.27$ mA/cm², FF = 0.42, and PCE = 4.06 %.⁹¹ The authors synthesized the positional isomer of the central donor 4,9-bis(2-ethylhexyloxy)naphtho[1,2-b:5,6-b']dithiophene **56** and obtained a higher efficiency of 4.70 % with a FF = 0.50. The energy difference between the LUMO of the donor **55** and **56** with the LUMO of PC₆₁BM were 0.39 eV and 0.49 eV respectively. The hole mobility measured by OFET and space charge limited current for **56** (found to be $\mu_{FET} = 0.057$ cm²/Vs; $\mu_{SCLC} = 1.0 \times 10^{-4}$ cm²/Vs) is higher than **55**'s ($\mu_{FET} = 0.046$ cm²/Vs; $\mu_{SCLC} = 2.5 \times 10^{-7}$ cm²/Vs). The higher energy difference between LUMO of donor and acceptor resulting in more CT states and also the high mobility increased the J_{sc} and FF for the device **56**.⁹² The same authors synthesized benzo[1,2-b:6,5-b']dithiophene (bBDT) framework as the central donor unit with varying alkyl chain attached to the DPP on both sides as end group giving the molecule **57**, **58** and **59**. The Figure 1.11 and 1.12 contains the chemical structure of the molecules from **55** to **69** and **70** to **80** respectively.

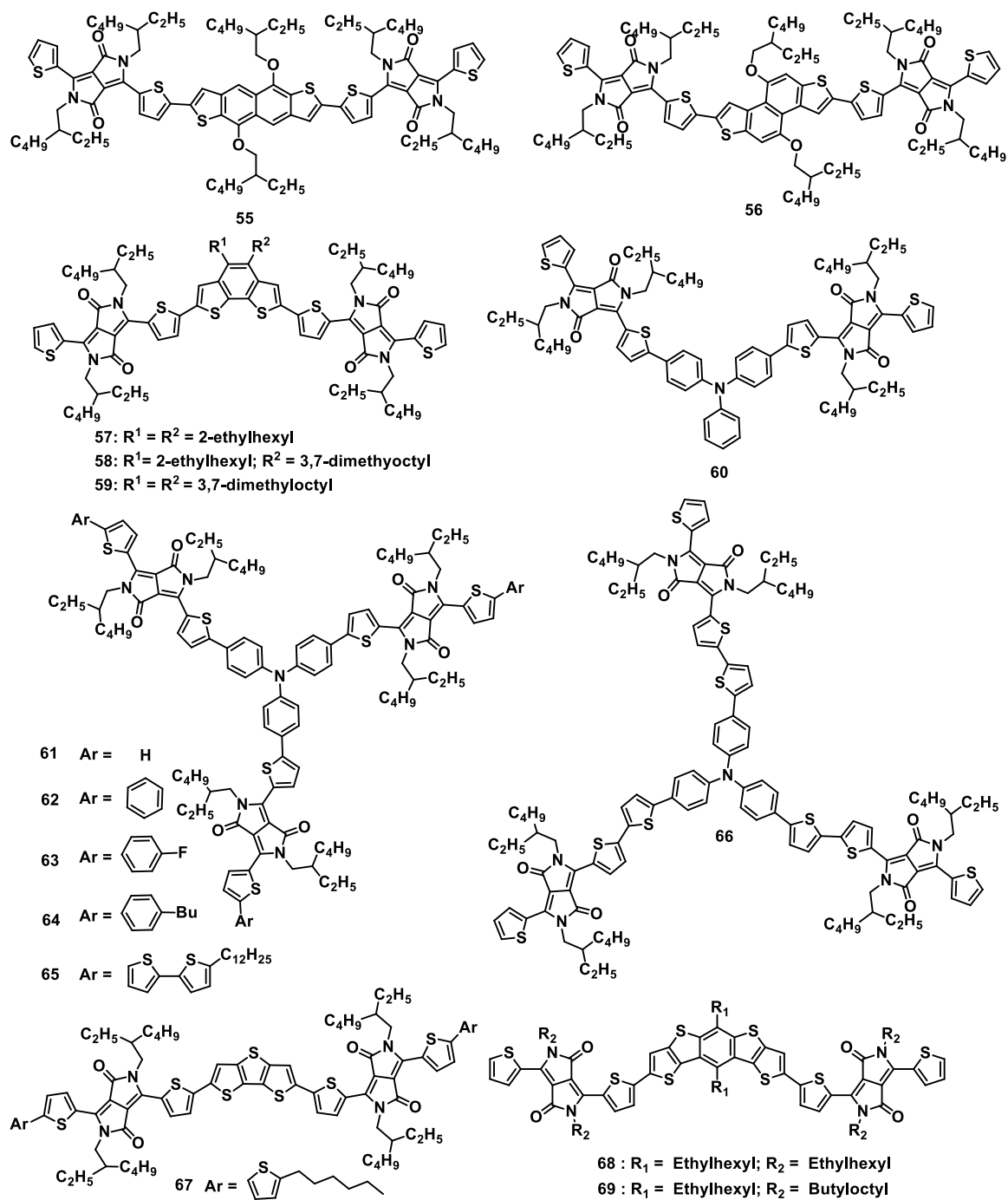


Figure 1.11 Chemical structure of bis diketopyrrolopyrrole

An inverted solar cell with a device structure of ITO/ZnO/ **57**, **58** or **59**: PC₇₁BM/MoO_x/Ag was fabricated using a solvent of 1 vol % DIO in chloroform. The best efficiencies for the devices **57** : PC₇₁BM (1:1.5), **58** : PC₇₁BM (1:1) and **59** : PC₇₁BM (1:1) were found to be 1.39 %, 5.53 % and 3.96 % respectively.⁹³ Star shaped small molecules based on triphenylamine and DPP were explored by various research groups, molecule **60** and **61** were developed by Chu and co-workers which showed red shifted absorption and a significantly higher molar absorption coefficient. They explored the application of the molecule **60** and **61** in OPVs by fabricating BHJ photovoltaic devices with the configuration ITO/PEDOT:PSS(30 nm)/**60** or **61**:PC₆₁BM blend(80 nm)/Ca(30 nm)/Al(100 nm). The PCE of **60** was found to be 0.97 % in the D:A ratio of 1:2 and that of **61** was found to be 1.22 % in 1:3 ratio.⁹⁴ Shi and co-workers synthesized three compounds **62**, **63**, and **64** mixed with PC₆₁BM as acceptor and device measurement gave performed efficiency of 2.98 %, 1.63 % and 1.98 % respectively.⁹⁵ Kirkus *et al* synthesized the star shaped compound **65** with 5-hexylbithiophene as the end group showing an efficiency of 3.25 % when mixed with PC₆₁BM.⁹⁶ The compounds **61** and **66** reported by Yao and co-workers obtained an efficiency of 1.38 % and 2.95 % with PC₇₁BM acceptor.⁹⁷

The compound dithienothiophene and DPP with an end group of hexyl thiophene **67** have been synthesized for application in organic solar cells and achieved an efficiency of 2.2 % as reported by Nguyen and co-workers.⁹⁸ The fused dithieno[2,3-d:2',3'-d']benzo[1,2-b:4,5-b']dithiophene structure was coupled with DPP to get **68** and **69**. In the presence of 0.6 vol % DIO, **68** gave the best PCE of

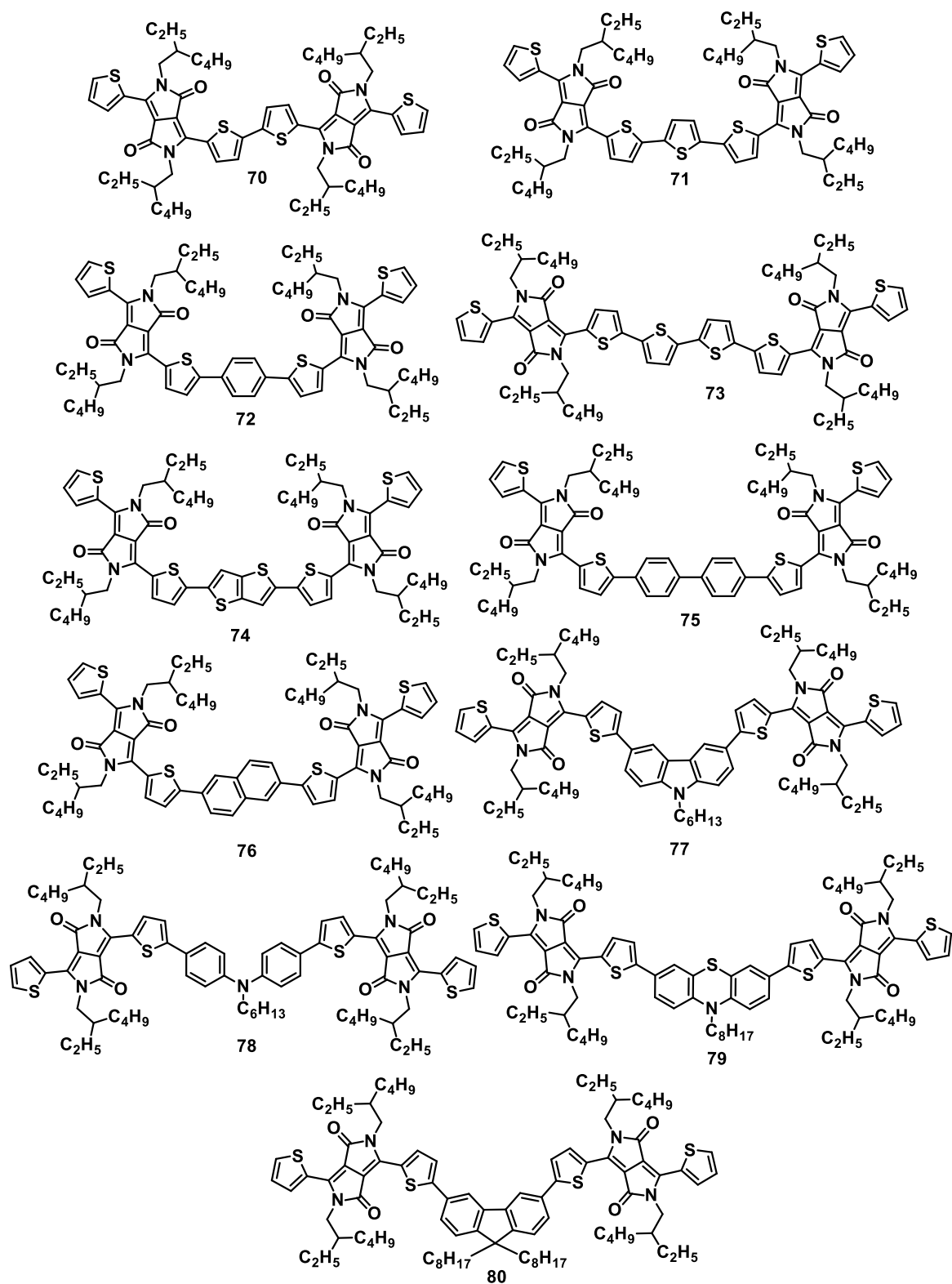


Figure 1.12 Chemical structure of bis diketopyrrolopyrrole

4.35 %. Similarly, the use of 0.4 vol % of DIO yielded the best PCE of 2.69 % for the **69**.⁹⁹ Jo and co-workers explored seven donor molecules based on bis-DPP from **70** to **77**. The compound **70**, homo coupling of two thiophene DPP units. The different central electron-donating units thiophene **71**, phenylene **72**, bithiophene **73**, thienothiophene **74**, phenylene **75**, and naphthalene **76** were introduced as a central core of bis-DPP for investigation. The different molecular planarity of thiophene vs phenylene, bithiophene vs. thienothiophene, and biphenylene vs. naphthalene and the different donating strength influences the hole mobility and the PCE of **70**, **71**, **72**, **73**, **74**, **75** and **76** are 2.31 %, 1.49 %, 4.01 %, 3.0 %, 4.0 %, 3.80 % and 4.40 % respectively.¹⁰⁰⁻¹⁰¹ Li and co-workers successfully synthesized a series of A-D-A structured small molecular donors in which the central donors have alkylated carbazole **77**, diphenylamine **78**, phenothiazine **79** and fluorene **80**. The PV properties of the donors were studied by fabricating BHJ solar cells with a typical structure of ITO/PEDOT:PSS/donors:PC₆₁BM/LiF/Al. The PCEs of the devices based on **77**, **78**, **79** and **80** were 1.50 %, 0.53 %, 0.75 % and 0.78 %, respectively.¹⁰²

The donor molecule **81** with benzodithiophene (BDT) as the central unit and DPP as acceptor was reported by two groups of scientists independently and achieved an efficiency of 5.29 % and 5.48 %.¹⁰³⁻¹⁰⁴ The Figure 1.13 and 1.14 contains the chemical structure of the molecules from **81** to **101** and **102** to **113** respectively. Researchers explored the change of the end group of the donor **81** leading to several molecules **82** to **88** and the highest efficiency of 6.0 % was shown by the trifluoromethyl benzene (CF₃) end-group-containing oligomer **84**. The device with the

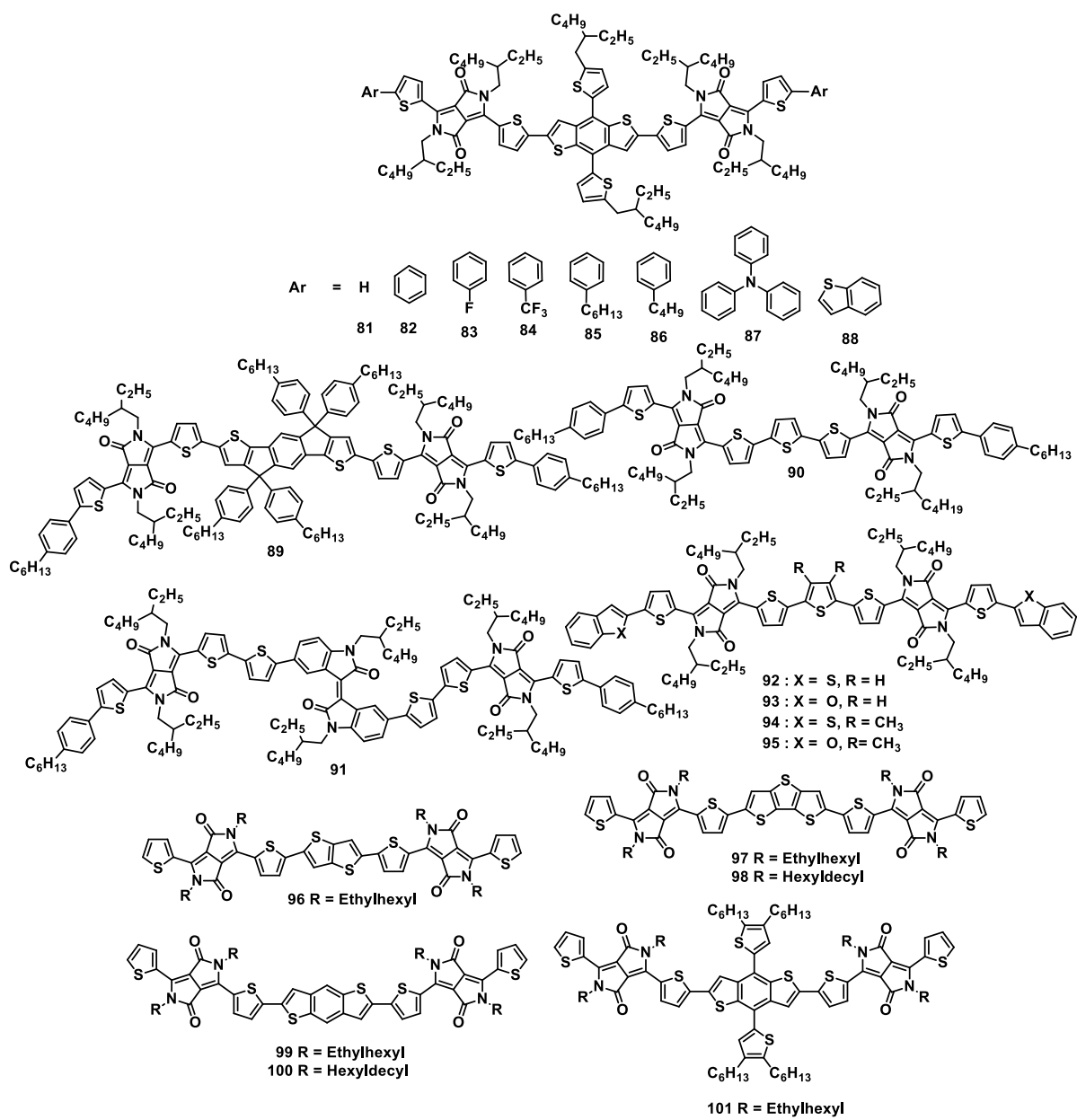


Figure 1.13 Chemical structure of bis diketopyrrolopyrrole

active layer **82**, **83**, **84**/PC₇₁BM (1:1 w/w), 15 mg/mL of donors in chloroform solvent had low PCE of 1.27 %, 1.57 %, and 1.60 %, respectively. The measured J_{sc} values of the devices fabricated using **82**, **83** and **84** were 3.88, 3.82, and 5.50 mA/cm² respectively. The addition of 2.5 vol % of 1-CN increases the PCEs to 3.65 %, 4.96 % and 6.00 % for the devices with an active layer of **82**, **83**, **84**/PC₇₁BM.¹⁰⁵ In case of n-butylbenzene and triphenylamine end group containing small molecules, **86** and **87** showed an efficiency of 3.20 % and 5.77 % in chloroform solvent with an additive of 1 % and 0.8 % respectively.¹⁰⁶ BHJ solar cells were fabricated with an inverted device structure ITO/ZnO/donor:PC₇₁BM/MoO_x/Ag for **85**, **89**, **90**, **91** and the efficiencies were found to be 5.8 %, 1.8 %, 2.3 %, and 2.1 %.¹⁰⁷

Janssen and co-workers synthesized four bis-DPP derivatives having small structural difference with identical photophysical and electrochemical properties but different solubility for the donor molecules end-capped with 2-(thiophen-2-yl)-benzo[b] thiophene **92** and **94** or 2-(thiophen-2-yl)benzofuran **93** to **95**. The authors explained about the effect of solubility, donor/acceptor ratio, total concentration, processing solvent, layer thickness, spin coating speed and use of the additive for achieving high PCE. The solar cells based on **92** and **93** with PC₇₁BM reach PCEs of 4.6 % and 4.0 % but the highly soluble donor molecules with a central 3, 4-dimethylthiophene **94** and **95** achieves an efficiency of 3.5 % and 3.8 %.¹⁰⁸

Similarly, researchers from the same group investigated a series of eight bis-DPP donor molecules **81**, **88**, **96** to **101**. The effect of central core, side chains in DPP

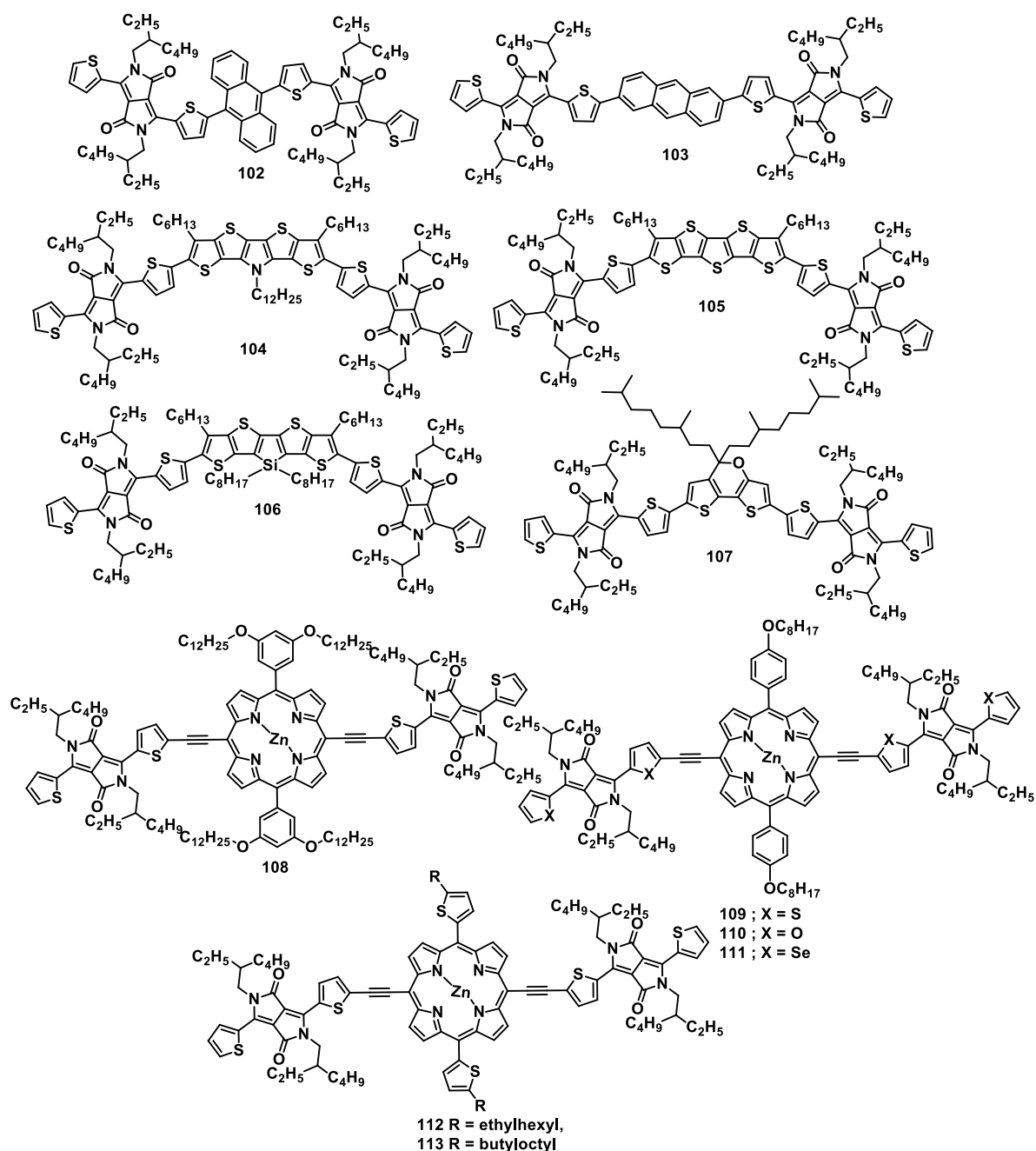


Figure 1.14 Chemical structure of bis diketopyrrolopyrrole

as well as central core and the effect of thermal annealing were well studied to establish the relation between blend morphology and PCE. These molecules showed similar optical and electrochemical properties and due to different blend

morphology with PC₆₁BM they differ in the PV properties. It was found that the molecules **81**, **88** and **96** with relatively high efficiencies around 4.4 % present similar morphology features in active layers: small but distinctive phase separation, which corresponded to their moderate tendency of aggregation as well as crystallization. In other cases, large phase separation occurs when the tendency of aggregation or crystallization of DPP molecule is relatively high. In the case of molecule **101** (PCE = 2.5 %), two linear side chains attach to the appendix thiophenes on BDT core instead of branched side chains in the case of molecule **81**, the crystallinity of the former molecule is much higher than that of the latter one. As a result, large phase separation only occurs in the case of molecule **101** after thermal annealing. As for molecules **97** (PCE = 2.3 %) and **99** (PCE = 2.7 %), having dithieno[3,2-b:2',3'-d]thiophene and benzo [1,2-b:4,5-b']dithiophene units as center core respectively, higher tendency of aggregation which can be expected compared with molecules **81** and **96** due to the different size and topology of central cores. Correspondingly, larger phase separation only occurs in the former two cases. When the ethylhexyl side chains of molecule **97** and **99** are replaced with longer hexyldecyl ones, molecule **98** (PCE = 2.8 %) and **100** (PCE = 2.7 %) show higher solubility and the feature of liquid-liquid (L-L) phase separation starts to appear in their active layers.¹⁰⁹ Zhu and co-workers investigated two isomeric anthracene based small molecules of **102** and **103**, with two acceptor arms of DPP. Solution-processed OPV cells based on **102** and **103** were made with a device configuration of ITO/PEDOT:PSS (40 nm)/photoactive layer (80 nm)/Ca(10 nm)/Al(100 nm). The

best efficiency obtained for **102** was 1.46 % and that of **103** was 5.44 %.¹¹⁰ Shi and co-worker synthesized pentathiophene based central donor with two acceptor DPP on both side **104**, **105** and **106**. The PCEs of **104** - **106**, when mixed with PC₇₁BM, were reported to be 3.69 %, 2.39 % and 2.23 % respectively.¹¹¹⁻¹¹² The molecule **107** having 5H-dithieno[3,2-b:2',3'-d]pyran acts as the strong donor due to the presence of electron rich nature of oxygen atom than the benzo[1,2-b:6,5-b']dithiophene **57** resulted in the rise of the HOMO energy level with lower bandgap. The HOMO-LUMO energy level of **107** was -5.23 eV and -3.73 eV, and the electrochemical band gap was 1.50 eV. The PCE of solar cells with PC₇₁BM as the acceptor is 6.88 %.¹¹³

Peng and co-workers synthesized a series of Zn-porphyrin as central donor attached to two DPP units by ethylene bridges from **108** to **112**. The PCE of 3, 5-di (dodecyloxy)-phenyl connected to porphyrin **108** was found to be 4.78 % but when it is replaced with 4-octyloxy-phenyl **109** the efficiency increases to 7.23 %.¹¹⁴⁻¹¹⁵ The donor molecules **109** in which thiophene is replaced with oxygen **110** and selenium **111** shows a lower PCE of 4.26 % and 5.81 %.¹¹⁶ DPP-porphyrin derivative with 2-ethylhexyl-thienyl side **112** or 2-butyloctyl-thienyl side **113** attached to the central core achieved the highest efficiency of 8.08 % and 9.06 % for DPP based small molecule bulk heterojunction solar cell.¹¹⁷⁻¹¹⁸

Table 1.2 The photovoltaic properties of bis diketopyrrolopyrrole derivatives

SL:No	Active Layer (D:A)	Annealing	V _{oc} (V)	J _{sc} (mA/cm ²)	FF	PCE %	Ref
1)	55:PC ₆₁ BM (1.5:1)	110 °C	0.84	11.27	0.42	4.06	91
2)	56 :PC ₆₁ BM(1.2:1)	140 °C	0.75	11.70	0.50	4.40	92
3)	57 : PC ₇₁ BM (1:1.5)	rt	0.78	4.57	0.38	1.39	93
4)	58 : PC ₇₁ BM (1:1)	rt	0.76	11.4	0.63	5.53	
5)	59 : PC ₇₁ BM (1:1)	rt	0.75	8.47	0.61	3.88	
6)	60 : PC ₆₁ BM (1:2)	rt	0.58	4.88	0.34	0.97	94
7)	61 : PC ₆₁ BM (1:3)	rt	0.66	7.92	0.34	1.81	
8)	61: PC ₆₁ BM (1:2)	rt	0.77	5.08	0.35	1.38	
9)	62: PC ₆₁ BM (1:1)	rt	0.72	7.94	0.52	2.98	95
10)	63: PC ₆₁ BM (1:1)	rt	0.76	5.14	0.42	1.63	
11)	64: PC ₆₁ BM (1:2)	rt	0.80	5.83	0.42	1.98	
12)	65:PC ₆₁ BM (1:2)	rt	0.75	8.20	0.53	3.25	96
13)	66:PC ₇₁ BM (1:4)	rt	0.81	10.06	0.36	2.95	97
14)	67:PC ₇₁ BM (1:1)	rt	0.81	7.67	0.50	2.19	98
15)	68:PC ₆₁ BM(6:4)	rt	0.85	9.90	0.51	4.35	99
16)	69:PC ₆₁ BM(6:4)	rt	0.82	7.30	0.45	2.69	
17)	70:PC ₇₁ BM(1:1)	120 °C	0.84	7.40	0.37	2.31	100
18)	71:PC ₇₁ BM(1:1)	120 °C	0.80	4.30	0.43	1.49	
19)	72:PC ₇₁ BM(1:1)	120 °C	0.93	9.09	0.47	4.01	
20)	73: PC ₇₁ BM(1:1)	rt	0.78	6.80	0.57	3.0	101
21)	74: PC ₇₁ M (1.5:1)	rt	0.81	9.30	0.53	4.0	

Table 1.2 The Photovoltaic properties of bis diketopyrrolopyrrole derivatives

(Continuation from the previous page)

SL:No	Active Layer (D:A)	Annealing	V _{oc} (V)	J _{sc} (mA/cm ²)	FF	PCE %	Ref
22)	75 : PC ₇₁ BM (1.5:1)	rt	0.86	8.30	0.53	3.8	100,101
23)	76 : PC ₇₁ BM (1:1)	rt	0.87	9.50	0.53	4.4	
24)	77 : PC ₆₁ BM(1:2)	rt	0.66	4.12	0.44	1.50	
25)	78:PC ₆₁ BM(1:2)	rt	0.64	1.95	0.34	0.53	
26)	79:PC ₆₁ BM(1:2)	rt	0.65	2.63	0.35	0.75	102
27)	80:PC ₆₁ BM(1:2)	rt	0.66	3.17	0.30	0.78	
28)	81:PC ₆₁ BM(1.5:1)	rt	0.94	7.40	0.34	2.37	103,104
29)	82:PC ₇₁ BM(1:1)	rt	0.70	10.21	0.51	3.30	
30)	83:PC ₇₁ BM(1:1)	rt	0.69	12.98	0.58	4.64	105
31)	84:PC ₇₁ BM(1:1)	rt	0.69	13.60	0.64	5.87	
32)	85:PC ₇₁ BM(1:1)	rt	0.76	12.2	0.62	5.80	107
33)	86:PC ₇₁ BM(1:1.5)	rt	0.67	8.35	0.57	3.20	
34)	87:PC ₇₁ BM(1:1.5)	rt	0.62	15.64	0.59	5.77	106
35)	88:PC ₆₁ BM(1:1)	110 °C	0.77	9.90	0.56	4.30	109
36)	89:PC ₇₁ BM(1:1)	rt	0.86	4.10	0.54	1.80	
37)	90:PC ₇₁ BM(1:1)	rt	0.66	8.16	0.43	2.30	107
38)	91:PC ₇₁ BM(1:1)	rt	0.66	8.47	0.40	2.10	
39)	92:PC ₇₁ BM(1:1)	rt	0.69	11.9	0.57	4.60	
40)	93:PC ₇₁ BM(1:1)	rt	0.67	10.4	0.58	4.00	
41)	94:PC ₇₁ BM(1:1)	rt	0.73	10.6	0.45	3.50	108
42)	95:PC ₇₁ BM(1:1)	rt	0.71	10.3	0.52	3.80	
43)	96:PC ₆₁ BM(1:1)	110 °C	0.81	9.46	0.56	4.30	109
44)	97:PC ₆₁ BM(1:1)	rt	0.76	6.82	0.44	2.30	

Table 1.2 The Photovoltaic properties of bis diketopyrrolopyrrole derivatives

(Continuation from the previous page)

SL:No	Active Layer (D:A)	Annealing	V _{oc} (V)	J _{sc} (mA/cm ²)	FF	PCE %	Ref
45)	98:PC ₆₁ BM(1:1)	rt	0.80	5.83	0.60	2.80	109
46)	99:PC ₆₁ BM(1:1)	rt	0.85	5.95	0.53	2.70	
47)	100:PC ₆₁ BM(1:1)	rt	0.85	5.53	0.58	2.73	
48)	101:PC ₆₁ BM(1:1)	rt	0.80	5.67	0.55	2.52	
49)	81:PC ₆₁ BM(1:1)	110 °C	0.83	9.36	0.56	4.40	
50)	102:PC ₇₁ BM(1:1.5)	rt	0.97	4.09	0.31	1.45	110
51)	103:PC ₇₁ BM(1:1)	rt	0.82	11.90	0.55	5.49	
52)	104:PC ₇₁ BM(1.5:1)	100 °C	0.71	10.69	0.48	3.69	111-
53)	105:PC ₇₁ BM(1:1)	100 °C	0.77	6.82	0.45	2.39	112
54)	106:PC ₇₁ BM(1:1.5)	rt	0.84	7.77	0.36	2.36	
55)	107:PC ₆₁ BM(1:3)	rt	0.80	14.12	0.61	6.88	113
56)	108:PC ₆₁ BM(1:1)	rt	0.80	11.88	0.50	4.78	114-
57)	109:PC ₆₁ BM(1:1.2)	rt	0.71	16.00	0.63	7.23	115
58)	110:PC ₆₁ BM(1:1)	130 °C	0.81	10.52	0.50	4.26	
59)	111:PC ₆₁ BM(1:1)	130 °C	0.71	14.93	0.54	5.81	116
60)	112:PC ₆₁ BM(1:1.2)	120 °C	0.78	16.76	0.61	8.08	117-
61)	113:PC ₆₁ BM(1:1)	100°C	0.73	19.58	0.63	9.06	118

1.6 Outline of the Thesis

As mentioned in the above sections, photovoltaic properties of π -conjugated chromophores are sensitive to functionalities and the intermolecular interactions in the solid state packing. We are interested to functionalize the DPP core with various chromophores and to study the photovoltaic properties.

In the second chapter, we report the synthesis a set of D–A–D small molecules [TDPPC₁₀(TPE)₂ and TDPPEH (TPE)₂] with broad absorption and suitable energy levels having DPP as a core acceptor with various alkyl chains (decyl and ethylhexyl) and tetraphenylethylene as an end donor units. Two small molecules as donor components along with the PC₆₁BM as an electron acceptor were used for the preparation of BHJ. The effect of nano scale phase separation of the photoactive layers on the solar cell device performance has been described in detail.

In the third chapter, we explored the effect of donor substituents in pyridine capped DPP in the BHJ solar cell with PC₆₁BM as an acceptor. A series of five pyridine capped DPP based small molecules with varying alkyl chain have been synthesized. We studied the photophysical and electrochemical properties. The photovoltaic device were fabricated using PEDOT:PSS and MoO₃ as hole transporting layer in the normal device structure. We optimized the photovoltaic performance of the solar cell by employing an additives and the total concentration in the 1:1 ratio of the donor and acceptor. The active layer morphology was studied using TEM analysis.

In the fourth chapter, mono and bis pyridine capped DPP based small molecules were synthesized and its photophysical and electrochemical were

studied. We fabricated photovoltaic devices structure ITO/MoO₃/active-layer/LiF/Al and characterizations were summarized. We also studied the morphology of the active layer using TEM images.

1.7 References

- (1) *World Energy Outlook*; IEA Publications, 2016; Vol. ISBN:9789264264946.
- (2) Fröhlich, C.; Lean, J.; *Astron. Astrophys. Rev.*, **2004**, *12*, 273-320.
- (3) Fröhlich, C.; Lean, J.; *Geophys. Res. Lett.*, **1998**, *25*, 4377-4380.
- (4) Williams, R.; *J. Chem. Phys.*, **1960**, *32*, 1505-1514.
- (5) Gauthier-Villars; Académie des sciences C. R. Acad. Sci: Paris, 1835.
- (6) Petrova-Koch, V.: Milestones of Solar Conversion and Photovoltaics. *High-Efficient Low-Cost Photovoltaics: Recent Developments*; Petrova-Koch, V., Hezel, R., Goetzberger, A., Eds.; Springer Berlin Heidelberg: Berlin, Heidelberg, 2009; pp 1-5.
- (7) Chapin, D. M.; Fuller, C. S.; Pearson, G. L.; *J. Appl. Phys.*, **1954**, *25*, 676-677.
- (8) Perlin, J.: Silicon Solar Cell Turns 50, . 2004.
- (9) Green, M. A.; Emery, K.; Hishikawa, Y.; Warta, W.; *Prog. photovolt.*, **2011**, *19*, 84-92.
- (10) PV Status Report Joint Research Centre (JRC), the European Commission's science and knowledge service: Luxembourg, 2016; Vol. doi:10.2790/682995.
- (11) Hagfeldt, A.; Boschloo, G.; Sun, L.; Kloo, L.; Pettersson, H.; *Chem. Rev.*, **2010**, *110*, 6595-6663.
- (12) Clarke, T. M.; Durrant, J. R.; *Chem. Rev.*, **2010**, *110*, 6736-6767.
- (13) Günes, S.; Neugebauer, H.; Sariciftci, N. S.; *Chem. Rev.*, **2007**, *107*, 1324-1338.
- (14) Hains, A. W.; Liang, Z.; Woodhouse, M. A.; Gregg, B. A.; *Chem. Rev.*, **2010**, *110*, 6689-6735.
- (15) Stoumpos, C. C.; Kanatzidis, M. G.; *Adv. Mater.*, **2016**, *28*, 5778-5793.

- (16) Kang, H.; Kim, G.; Kim, J.; Kwon, S.; Kim, H.; Lee, K.; *Adv. Mater.*, **2016**, *28*, 7821-7861.
- (17) Chiang, C. K.; Fincher, C. R.; Park, Y. W.; Heeger, A. J.; Shirakawa, H.; Louis, E. J.; Gau, S. C.; MacDiarmid, A. G.; *Phys. Rev. Lett.*, **1978**, *40*, 1472-1472.
- (18) Dimitrakopoulos, C. D.; Malenfant, P. R. L.; *Adv. Mater.*, **2002**, *14*, 99-117.
- (19) Horowitz, G.; *Adv. Mater.*, **1998**, *10*, 365-377.
- (20) Friend, R. H.; Gymer, R. W.; Holmes, A. B.; Burroughes, J. H.; Marks, R. N.; Taliani, C.; Bradley, D. D. C.; Santos, D. A. D.; Bredas, J. L.; Logdlund, M.; Salaneck, W. R.; *Nature*, **1999**, *397*, 121-128.
- (21) Arkhipov, V. I.; Bäessler, H.; *physica status solidi (a)*, **2004**, *201*, 1152-1187.
- (22) Chamberlain, G. A.; *Solar Cells*, **1983**, *8*, 47-83.
- (23) Tang, C. W.; *Appl. Phys. Lett.*, **1986**, *48*, 183-185.
- (24) Haugeneder, A.; Neges, M.; Kallinger, C.; Spirkl, W.; Lemmer, U.; Feldmann, J.; Scherf, U.; Harth, E.; Gügel, A.; Müllen, K.; *Phys. Rev. B*, **1999**, *59*, 15346-15351.
- (25) Markov, D. E.; Amsterdam, E.; Blom, P. W. M.; Sieval, A. B.; Hummelen, J. C.; *J. Phys. Chem. A*, **2005**, *109*, 5266-5274.
- (26) Sariciftci, N. S.; Smilowitz, L.; Heeger, A. J.; Wudl, F.; *Science*, **1992**, *258*, 1474-1476.
- (27) Halls, J. J. M.; Walsh, C. A.; Greenham, N. C.; Marseglia, E. A.; Friend, R. H.; Moratti, S. C.; Holmes, A. B.; *Nature*, **1995**, *376*, 498-500.
- (28) Yu, G.; Gao, J.; Hummelen, J. C.; Wudl, F.; Heeger, A. J.; *Science*, **1995**, *270*, 1789-1791.
- (29) Shaheen, S. E.; Brabec, C. J.; Sariciftci, N. S.; Padinger, F.; Fromherz, T.; Hummelen, J. C.; *Appl. Phys. Lett.*, **2001**, *78*, 841-843.
- (30) Tengstedt, C.; Crispin, A.; Hsu, C. H.; Zhang, C.; Parker, I. D.; Salaneck, W. R.; Fahlman, M.; *Org. Electron.*, **2005**, *6*, 21-33.
- (31) American Society for Testing and Materials (ASTM) Standard G173-03, available at: [:http://rredc.nrel.gov/solar/spectra/am1.5](http://rredc.nrel.gov/solar/spectra/am1.5).
- (32) Metzendorf, J.; *Appl. Opt.*, **1987**, *26*, 1701-1708.

- (33) Wehenkel, D. J.; Hendriks, K. H.; Wienk, M. M.; Janssen, R. A. J.; *Org. Electron.*, **2012**, *13*, 3284-3290.
- (34) Liang, N.; Jiang, W.; Hou, J.; Wang, Z.; *Mater. Chem. Front.*, **2017**.
- (35) Halls, J. J. M.; Cornil, J.; dos Santos, D. A.; Silbey, R.; Hwang, D. H.; Holmes, A. B.; Brédas, J. L.; Friend, R. H.; *Phys. Rev. B*, **1999**, *60*, 5721-5727.
- (36) Brédas, J.-L.; Beljonne, D.; Coropceanu, V.; Cornil, J.; *Chem. Rev.*, **2004**, *104*, 4971-5004.
- (37) Koster, L. J. A.; Mihailetschi, V. D.; Blom, P. W. M.; *Appl. Phys. Lett.*, **2006**, *88*, 093511.
- (38) Scharber, M. C.; Mühlbacher, D.; Koppe, M.; Denk, P.; Waldauf, C.; Heeger, A. J.; Brabec, C. J.; *Adv. Mater.*, **2006**, *18*, 789-794.
- (39) Lin, J. D. A.; Mikhnenko, O. V.; van der Poll, T. S.; Bazan, G. C.; Nguyen, T. Q.; *Adv. Mater.*, **2015**, *27*, 2528-2532.
- (40) Lin, J. D. A.; Mikhnenko, O. V.; Chen, J.; Masri, Z.; Ruseckas, A.; Mikhailovsky, A.; Raab, R. P.; Liu, J.; Blom, P. W. M.; Loi, M.; García-Cervera, C. J.; Samuel, I. D. W.; Nguyen, T.-Q.; *Mater. Horiz.*, **2014**, *1*, 280-285.
- (41) Mikhnenko, O. V.; Lin, J.; Shu, Y.; Anthony, J. E.; Blom, P. W. M.; Nguyen, T.-Q.; Loi, M.; *PCCP*, **2012**, *14*, 14196-14201.
- (42) Wang, H.; Wang, H.-Y.; Gao, B.-R.; Wang, L.; Yang, Z.-Y.; Du, X.-B.; Chen, Q.-D.; Song, J.-F.; Sun, H.-B.; *Nanoscale*, **2011**, *3*, 2280-2285.
- (43) Bruno, A.; Reynolds, L. X.; Dyer-Smith, C.; Nelson, J.; Haque, S. A.; *J. Phys. Chem. C*, **2013**, *117*, 19832-19838.
- (44) Peumans, P.; Yakimov, A.; Forrest, S. R.; *J. Appl. Phys.*, **2003**, *93*, 3693-3723.
- (45) Cornil, J.; Beljonne, D.; Brédas, J. L.; *J. Chem. Phys.*, **1995**, *103*, 834-841.
- (46) Fesser, K.; Bishop, A. R.; Campbell, D. K.; *Phys. Rev. B*, **1983**, *27*, 4804-4825.
- (47) Cornil, J.; Brédas, J.-L.; *Adv. Mater.*, **1995**, *7*, 295-297.
- (48) Barth, S.; Bäessler, H.; *Phys. Rev. Lett.*, **1997**, *79*, 4445-4448.
- (49) Murgatroyd, P. N.; *J. Phys. D: Appl. Phys.*, **1970**, *3*, 151.
- (50) Brabec, C. J.; Shaheen, S. E.; Winder, C.; Sariciftci, S. N.; Denk, P.; *Appl. Phys. Lett.*, **2002**, *80*, 1288-1290.

- (51) Zhou, Y.; Fuentes-Hernandez, C.; Shim, J.; Meyer, J.; Giordano, A. J.; Li, H.; Winget, P.; Papadopoulos, T.; Cheun, H.; Kim, J.; Fenoll, M.; Dindar, A.; Haske, W.; Najafabadi, E.; Khan, T. M.; Sojoudi, H.; Barlow, S.; Graham, S.; Brédas, J.-L.; Marder, S. R.; Kahn, A.; Kippelen, B.; *Science*, **2012**, *336*, 327-332.
- (52) van Reenen, S.; Kouijzer, S.; Janssen, R. A. J.; Wienk, M. M.; Kemerink, M.; *Adv Mater Interfaces*, **2014**, *1*, 1400189.
- (53) He, Z.; Zhong, C.; Huang, X.; Wong, W. Y.; Wu, H.; Chen, L.; Su, S.; Cao, Y.; *Adv Mater.*, **2011**, *23*, 4636-4643.
- (54) Mishra, A.; Bäuerle, P.; *Angew. Chem. Int. Ed.*, **2012**, *51*, 2020-2067.
- (55) Hao, Z.; Iqbal, A.; *Chem. Soc. Rev.*, **1997**, *26*, 203-213.
- (56) Bundgaard, E.; Krebs, F. C.; *Sol. Energy Mater. Sol. Cells*, **2007**, *91*, 954-985.
- (57) Havinga, E. E.; ten Hoeve, W.; Wynberg, H.; *Synth. Met.*, **1993**, *55*, 299-306.
- (58) Kitamura, C.; Tanaka, S.; Yamashita, Y.; *Chem. Mater.*, **1996**, *8*, 570-578.
- (59) Olivia, P. L.; Alan, T. Y.; Pierre, M. B.; Claire, H. W.; Thomas, W. H.; Jill, E. M.; Jessica, D. D.; Mark, S. C.; Jean, M. J. F.; *Adv. Mater.*, **2011**, *23*, 5359-5363.
- (60) Liu, J.; Zhang, Y.; Phan, H.; Sharenko, A.; Moonsin, P.; Walker, B.; Promarak, V.; Nguyen, T.-Q.; *Adv. Mater.*, **2013**, *25*, 3645-3650.
- (61) Veronique, S. G.; Eva, M. H.; Mindaugas, K.; Koen, H. H.; Martijn, M. W.; Jan, P.; Peter, M.-B.; René, A. J. J.; *Chem. Mater.*, **2014**, *26*, 916-926.
- (62) Más-Montoya, M.; Janssen, R. A. J.; *Adv. Funct. Mater.*, **2017**, *27*, 1605779.
- (63) Steinberger, S.; Mishra, A.; Reinold, E.; Müller, C. M.; Uhrich, C.; Pfeiffer, M.; Bäuerle, P.; *Org. Lett.*, **2011**, *13*, 90-93.
- (64) Arnold, B. T.; Bright, W.; Thuc-Quyen, N.; *J. Phys. Chem. C*, **2008**, *112*, 11545-11551.
- (65) Arnold Bernarte, T.; Xuan-Dang, D.; Bright, W.; Junghwa, S.; Tyler, K.; Thuc-Quyen, N.; *Appl. Phys. Lett.*, **2009**, *94*, 103301.
- (66) Bright, W.; Arnold, B. T.; Xuan-Dung, D.; Peter, Z.; Jung Hwa, S.; Andres, G.; Mananya, T.; Thuc-Quyen, N.; *Adv. Funct. Mater.*, **2009**, *19*, 3063-3069.
- (67) Jianhua, L.; Bright, W.; Arnold, T.; Yuan, Z.; Thuc-Quyen, N.; *Adv. Funct. Mater.*, **2013**, *23*, 47-56.

- (68) Jianguo, M.; Kenneth, R. G.; Romain, S.; Shree Prakash, T.; Hyeunseok, C.; Jaewon, S.; Masafumi, Y.; Colin, N.; Bernard, K.; Ronald, K. C.; John, R. R.; *Chem. Mater.*, **2011**, *23*, 2285-2288.
- (69) Emilie, R.; Dora, D.; Théodulf, R.; Emmanuel, B.-C.; Magali, A.; Riccardo, P.; Philippe, L.; Jean, R.; *Dyes Pigm.*, **2012**, *95*, 126-133.
- (70) Shi-Xin, S.; Yong, H.; Miao-Miao, L.; Xiaowen, H.; Hai-Jun, Z.; You-Wen, Z.; You-Dan, Z.; Xiao-Long, C.; Zi-Fa, S.; Xiong, G.; Yongsheng, C.; Hao-Li, Z.; *ACS Appl. Mater. Interfaces*, **2015**, *7*, 19914-19922.
- (71) Rui, Z.; Qing-Duan, L.; Xin-Chen, L.; Shun-Mian, L.; Li-Ping, W.; Chun-Hui, Z.; Ju, H.; Ping, C.; Feng, L.; Xu-Hui, Z.; Wallace, C. H. C.; Junbiao, P.; Yong, C.; Xiong, G.; *Dyes Pigm.*, **2014**, *101*, 51-57.
- (72) Woong, S.; Takuma, Y.; Go, W.; Yu Seok, Y.; Chihaya, A.; *Chem. Mater.*, **2013**, *25*, 2549-2556.
- (73) Sushil, S. B.; Hanok, P.; Seon-nam, Y.; Sung-Ho, J.; Soo-Hyoung, L.; *Chem. Phys. Lett.*, **2015**, *630*, 37-43.
- (74) Hang, G.; Yanqin, L.; Lihui, W.; Changyan, J.; Yue, W.; Wenjing, T.; Xichuan, Y.; Lunxiang, Y.; *Chem. Commun.*, **2014**, *50*, 10251-10254.
- (75) Yan, X.; Wan-Yi, T.; Li-Ping, W.; Chun-Hui, Z.; Ling, P.; Xu-Hui, Z.; Junbiao, P.; Yong, C.; *Dyes Pigm.*, **2016**, *126*, 96-103.
- (76) Wang, L.-P.; Xia, Y.; Luo, G.-P.; Zhang, C.-H.; Liu, Q.; Tan, W.-Y.; Zhu, X.-H.; Wu, H.-B.; Peng, J.; Cao, Y.; *Asian J. Org. Chem.*, **2015**, *4*, 470-476.
- (77) Changyan, J.; Lunxiang, Y.; Kechang, L.; Lihui, W.; Xueying, J.; Yingji, S.; Yanqin, L.; *RSC Adv.*, **2015**, *5*, 31606-31614.
- (78) Changyan, J.; Lunxiang, Y.; Lihui, W.; Tao, J.; Shixiang, M.; Yingji, S.; Yanqin, L.; *J. Mater. Chem. C*, **2014**, *2*, 4019-4026.
- (79) Jianhua, H.; Hui, J.; Liangjie, L.; Zhenhuan, L.; Wenqing, Z.; Weiwei, H.; Bo, J.; Ailing, T.; Zhan'ao, T.; Chuanlang, Z.; Yongfang, L.; Jiannian, Y.; *PCCP*, **2012**, *14*, 14238-14242.
- (80) Yujeong, K.; Chang Eun, S.; Ara, C.; Jungwoon, K.; Yoonho, E.; Jongho, A.; Sang-Jin, M.; Eunhee, L.; *Mater. Chem. Phys.*, **2014**, *143*, 825-829.

- (81) Hongyu, W.; Feng, L.; Laju, B.; Jun, G.; Cheng, W.; Wei, W.; Thomas, P. R.; *Adv. Mater.*, **2013**, *25*, 6519-6525.
- (82) Huijing, Z.; Nailiang, Q.; Wang, N.; Bin, K.; Miaomiao, L.; Qian, Z.; Xiangjian, W.; Yongsheng, C.; *Dyes Pigm.*, **2016**, *126*, 173-178.
- (83) Diego, C.-L.; Calvyn, T. H.; Upendra, K. P.; Joseph, C.; Neil, J. F.; Anto Regis, I.; Tell, T.; Peter, J. S.; Ifor, D. W. S.; *Beilstein J. Org. Chem.*, **2014**, *10*, 2683-2695.
- (84) Desiré, M.; Antonio, G.; Germà, G. B.; Fernando, F. L.; Ángela, S. S.; *Eur. J. Org. Chem.*, **2014**, *2014*, 4585-4591.
- (85) Thomas, B.; Nicolas, L.; Rony, B.; Patrick, L.; Thomas, H.; Raymond, Z.; *Adv. Energy Mater.*, **2013**, *3*, 1118-1124.
- (86) Sharma, G. D.; Mikroyannidis, J. A.; Sharma, S. S.; Roy, M. S.; Thomas, K. R. J.; *Org. Electron.*, **2012**, *13*, 652-666.
- (87) Sharma, G. D.; Reddy, M. A.; Ganesh, K.; Surya Prakash, S.; Chandrasekharam, M.; *RSC Adv.*, **2013**, *4*, 732-742.
- (88) Chandrasekharam, M.; Reddy, M. A.; Ganesh, K.; Sharma, G. D.; Surya Prakash, S.; Rao, J. L.; *Org. Electron.*, **2014**, *15*, 2116-2125.
- (89) Kumar, C. H. P.; Ganesh, K.; Suresh, T.; Abhishek, S.; Bhanuprakash, K.; Sharma, G. D.; Malapaka, C.; *RSC Adv.*, **2015**, *5*, 93579-93590.
- (90) Narayanaswamy, K.; Venkateswararao, A.; Vinay, G.; Suresh, C.; Surya Prakash, S.; *Chem. Commun.*, **2015**, *52*, 210-213.
- (91) Stephen, L.; Carson, J. B.; Hiroyuki, M.; Rocío Ponce, O.; Antonio, F.; Samuel, I. S.; Tobin, J. M.; *J. Am. Chem. Soc.*, **2011**, *133*, 8142-8145.
- (92) Stephen, L.; Hiroyuki, M.; Jonathan, W. H.; Jeremy, S.; Chun, H.; Antonio, F.; Tobin, J. M.; *Chem. Commun.*, **2012**, *48*, 8511-8513.
- (93) Tobias, H.; Nanjia, Z.; Eric, F. M.; Sylvia, J. L.; Xinge, Y.; Melanie, R. B.; Amod, T.; Riccardo, T.; Mark, A. R.; Lin, X. C.; Robert, P. H. C.; Antonio, F.; Tobin, J. M.; *Chem. Commun.*, **2014**, *50*, 4099-4101.
- (94) Duryodhan, S.; Chia-Hua, T.; Hung-Yu, W.; Kuo-Chuan, H.; Feng-Chih, C.; Chih-Wei, C.; *J. Mater. Chem.*, **2012**, *22*, 7945-7953.

- (95) Jun-Ying, P.; Li-Jian, Z.; Xiao-Lian, H.; Wei-Fei, F.; Mei-Rong, C.; Lei, F.; Xiao, G.; Hang-Qi, S.; Min-Min, S.; Han-Ying, L.; Hong-Zheng, C.; *ACS Appl. Mater. Interfaces*, **2013**, *5*, 972-980.
- (96) Kirkus, M.: Diketopyrrolopyrrole based molecular materials: Synthesis, Optical characterisation and application in photovoltaics., Eindhoven Technical University TU/e, 2013.
- (97) Ailing, T.; Liangjie, L.; Zhenhuan, L.; Jianhua, H.; Hui, J.; Chuanlang, Z.; Zhan'ao, T.; Yongfang, L.; Jiannian, Y.; *J. Mater. Chem. A*, **2013**, *1*, 5747-5757.
- (98) Jin Kuen, P.; Chunki, K.; Bright, W.; Thuc-Quyen, N.; Jung Hwa, S.; *RSC Adv.*, **2012**, *2*, 2232-2234.
- (99) Minwoo, J.; Dongkyun, S.; Kyungwon, K.; Ajeong, K.; Wonsuk, C.; Hyunjung, K.; Youngwoon, Y.; Min Jae, K.; Doh-Kwon, L.; Jin Young, K.; Hae Jung, S.; BongSoo, K.; *Dyes Pigm.*, **2015**, *115*, 23-34.
- (100) Jong Won, L.; Yoon Suk, C.; Won Ho, J.; *Org. Electron.*, **2012**, *13*, 3060-3066.
- (101) Yoon Suk, C.; Won Ho, J.; *Org. Electron.*, **2013**, *14*, 1621-1628.
- (102) Ling, Z.; Shaohang, Z.; Lunxiang, Y.; Changyan, J.; Kechang, L.; Yanqin, L.; Yue, W.; *New J. Chem.*, **2012**, *37*, 632-639.
- (103) Jianhua, H.; Chuanlang, Z.; Xin, Z.; Yan, Z.; Zhenhuan, L.; Hui, J.; Bo, J.; Jian, Y.; Shanlin, Z.; Ailing, T.; Yunqi, L.; Qibing, P.; Jiannian, Y.; *ACS Appl. Mater. Interfaces*, **2013**, *5*, 2033-2039.
- (104) Yuze, L.; Lanchao, M.; Yongfang, L.; Yunqi, L.; Daoben, Z.; Xiaowei, Z.; *Adv. Energy Mater.*, **2013**, *3*, 1166-1170.
- (105) Ji-Hoon, K.; Jong Baek, P.; Hoichang, Y.; In Hwan, J.; Sung Cheol, Y.; Dongwook, K.; Do-Hoon, H.; *ACS Appl. Mater. Interfaces*, **2015**, *7*, 23866-23875.
- (106) Ailing, T.; Chuanlang, Z.; Jiannian, Y.; *Adv. Energy Mater.*, **2015**, *5*, 1500059.
- (107) Woong, S.; Takuma, Y.; Yu, H.; Go, W.; Ryota, A.; Keiro, N.; Takahiro, Y.; Wakako, M.; Kengo, M.; Chihaya, A.; *Adv. Energy Mater.*, **2014**, *4*, 1400879.
- (108) Weiwei, L.; Mathias, K.; Martijn, M. W.; René, A. J. J.; *J. Mater. Chem. A*, **2013**, *1*, 15150-15157.

- (109) Wang, Q.; van Franeker, J. J.; Bruijnaers, B. J.; Wienk, M. M.; Janssen, R. A. J.; *J. Mater. Chem. A*, **2016**, *4*, 10532-10541.
- (110) Xiongwei, D.; Manjun, X.; Jianhua, C.; Xiangdong, W.; Wenhong, P.; Linrui, D.; Hua, T.; Gangtie, L.; Renqiang, Y.; Weiguo, Z.; *ACS Appl. Mater. Interfaces*, **2015**, *7*, 18292-18299.
- (111) Qing-Cai, Y.; Wei-Fei, F.; Jun-Hua, W.; Xiao-Feng, W.; Min-Min, S.; Hong-Zheng, C.; *ACS Appl. Mater. Interfaces*, **2014**, *6*, 5798-5809.
- (112) Qing-Cai, Y.; Wei-Fei, F.; Hong-Yu, W.; Xiao-Feng, W.; Jun-Hua, W.; Min-Min, S.; Hong-Zheng, C.; *Asian J. Org. Chem.*, **2014**, *3*, 984-993.
- (113) Jae Woong, J.; Thomas, P. R.; Won Ho, J.; *Chem. Mater.*, *27*, 4865-4870.
- (114) Lisheng, L.; Yuying, H.; Junbiao, P.; Yong, C.; Xiaobin, P.; *J. Mater. Chem. A*, **2012**, *1*, 2144-2150.
- (115) Hongmei, Q.; Lisheng, L.; Fangqing, G.; Shijian, S.; Junbiao, P.; Yong, C.; Xiaobin, P.; *Energy Environ Sci*, **2014**, *7*, 1397-1401.
- (116) Tianxiang, L.; Liangang, X.; Chang, L.; Ke, G.; Hongmei, Q.; Yong, C.; Xiaobin, P.; *Org. Electron.*, **2016**, *29*, 127-134.
- (117) Ke, G.; Lisheng, L.; Tianqi, L.; Liangang, X.; Yuan, H.; Fei, H.; Junbiao, P.; Yong, C.; Feng, L.; Thomas, P. R.; René, A. J. J.; Xiaobin, P.; *J. Am. Chem. Soc.*, *137*, 7282-7285.
- (118) Gao, K.; Miao, J.; Xiao, L.; Deng, W.; Kan, Y.; Liang, T.; Wang, C.; Huang, F.; Peng, J.; Cao, Y.; Liu, F.; Russell, T. P.; Wu, H.; Peng, X.; *Adv. Mater.*, **2016**, *28*, 4727-4733.

Chapter 2

Design, Synthesis and Photovoltaic Properties of Small Molecules Based on Tetraphenylethylene and Diketopyrrolopyrrole

2.1 Abstract

Two D–A–D small molecules based on tetraphenylethylene (TPE) and DPP coded as TDPPC₁₀(TPE)₂ and TDPPEH(TPE)₂ with decyl and ethylhexyl chain respectively. The molecules have been synthesized and their optical, thermal, electrochemical and photovoltaic properties were investigated. Two small molecules as donor components along with the PC₆₁BM as the electron acceptor were used for the preparation of bulk heterojunction (BHJ) active layer in the small molecule organic photovoltaics. The optimal power conversion efficiencies (PCE) obtained with TDPPC₁₀(TPE)₂ and TDPPEH(TPE)₂ are 0.20 % and 0.25 % when the BHJ active layers were cast from a solution with chloroform as the solvent.

2.2 Introduction

Solution-processed organic solar cells are usually obtained by mixing a suitable p-type π -conjugated polymer or small molecule with an n-type fullerene derivative in a bulk heterojunction photoactive layer.¹ The highest PCE of the polymers and the small molecules with the fullerene derivatives reaches up to 11.7 % and 10.08 % respectively.²⁻³ The performance of the polymer solar cells not only depends on the extension of absorption wavelength and the energy level but also strongly depends on the morphology of the active layer.⁴ The polymer properties like molecular weight, regioregularity and end groups of the polymer have a profound influence on the morphology of the active layer and performance of the solar cell.⁵⁻¹¹ With the existing polymerization techniques to synthesize π -conjugated polymers, it is challenging to minimize batch-to-batch variations of the performance in polymer solar cell. Although small molecules show less batch to batch variation in the clear structure, it's hard to achieve an optimum morphology for the donor and acceptor blend to yield high efficiency.¹²⁻¹⁴

TPE derivatives shows aggregation-induced emission (AIE) with high quantum yield Φ_F values in the solid state and has potential application in the area of OLEDs.¹⁵⁻²² TPE based small molecules in the solution processed bulk heterojunction solar cells have not been widely explored. In 2014, Yan and coworker reported quasi-3D molecular structure tetraphenylethylene decorated with perylenediimide **114** to replace near-spherical shaped fullerene acceptors with polymer **115** in the bulk heterojunction solar cell. The structure of non-fullerene

acceptor **114** and the donor polymer is given in Figure 2.1. The polymer **115** with PC₇₁BM achieved 10.8 % PCE.²³ Thus the spherical molecular structures capable of light harvesting and charge-transport in three dimensional networks have been expected to increase the PCE. Thus the authors demonstrated a TPE core-based small molecule acceptor, **114**, with a high PCE of 5.53 %. The reasonably high efficiency is due to the highly twisted nature of the TPE core resulted in weak molecular aggregation of perylenediimide, less

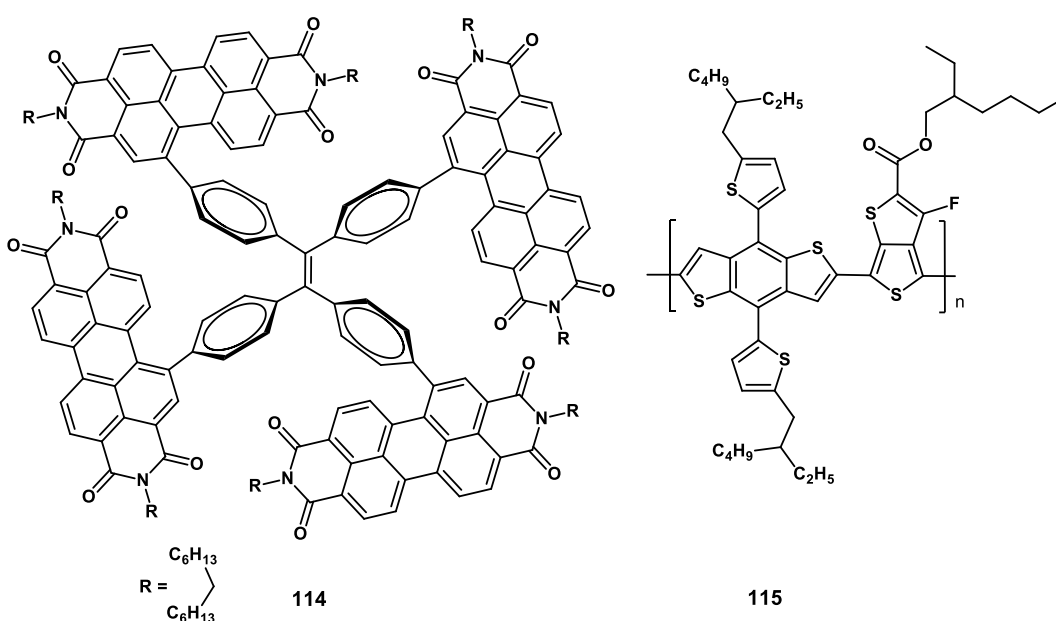


Figure 2.1 (a) Non-Fullerene acceptor based on tetraphenylethylene decorated with perylenediimide (b) structure of donor polymer **115**.

crystalline, small donor and acceptor domains. The 3D structure of **114** facilitates the formation of a 3D charge-transport network and thus enables reasonably good electron-transport ability.²⁴

Bhosale and coworkers synthesized four dimensional diketopyrrolopyrrole attached to TPE core **116** and fabricated bulk heterojunction solar cell with P3HT

donor polymer. The structure of the molecule **116** and P3HT polymer, **117** is given in the Figure. 2. 2. The solubility of **116** was 30 mg/mL in *o*-dichlorobenzene. The thermogravimetric analysis (TGA) revealed that the chromophore was thermally stable and 5% weight loss happened at 225 °C. The HOMO energy levels were estimated from the photoelectron spectroscopy in air (PESA) and LUMO was calculated from the absorption onset at 720 nm of the film state. The best BHJ devices obtained in the Donor : Acceptor weight ratio of 1 : 1.2 with V_{oc} , J_{sc} , FF, and PCE, reached 1.18 V, 5.17 mA/cm², 0.64, and 3.86 %, respectively.²⁵

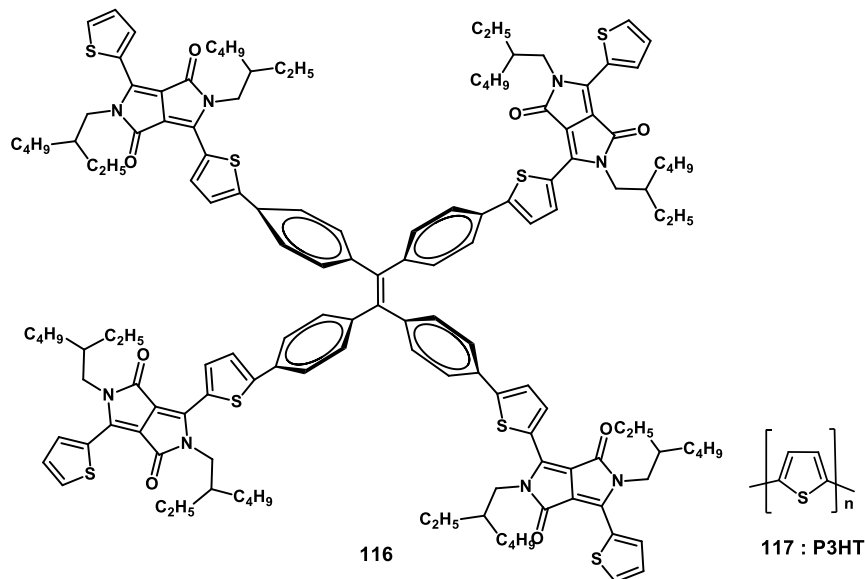


Figure 2.2 (a) Non-Fullerene acceptor based on tetraphenylethylene decorated with diketopyrrolopyrrole, **116** (b) structure of donor polymer P3HT, **117**.

We designed tetraphenylethylene attached to both ends of the diketopyrrolopyrrole with two alkyl chain n-decyl and ethylhexyl for different solubility.

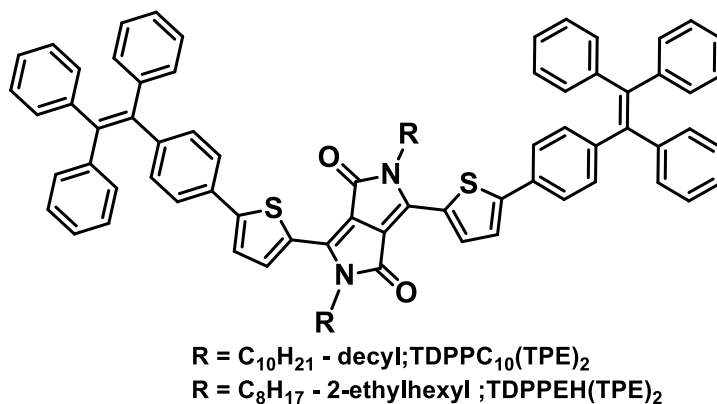
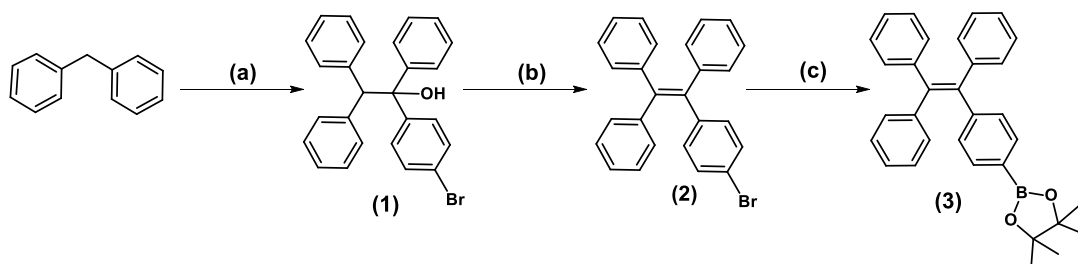


Figure 2.3 Structure of tetraphenylethylene attached to thiophene diketopyrrolopyrrole

2.3 Results and discussion

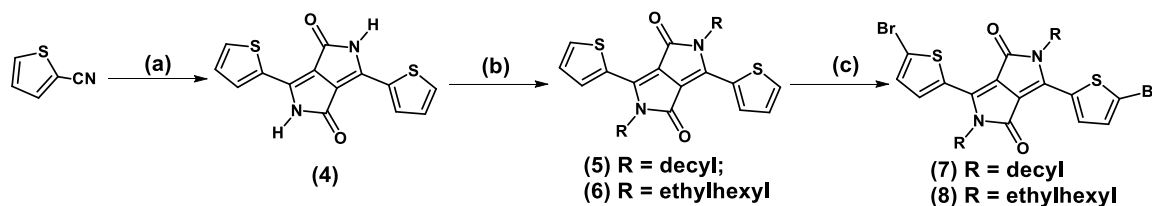
2.3.1 Synthesis

Scheme 2.1 shows the synthetic pathway for the intermediate 4,4,5,5-tetramethyl-2-(4-(1,2,2-triphenylvinyl)phenyl)-1,3,2-dioxaborolane **3**. The synthesis of **3** was according to the literature report involving three step procedures using readily available starting material diphenylmethane. The treatment of butyllithium with diphenylmethane in the dry THF resulted in an orange-red solution, and then it was transferred to the dry solution of 4-bromobenzophenone in THF at 0 °C. Then the reaction mixture was allowed to warm to room temperature and stirred for 6 hours to get the hydroxy intermediate, **1**. The compound **1** was used without further purification in the next step. The compound **2** was obtained by the dehydration reaction of **1** in the presence of the *p*-toluenesulfonic acid with an overall yield of 64 %. The borylation of **2** using palladium catalyst in the necessary condition yielded the compound **3** with 68 %.²⁶



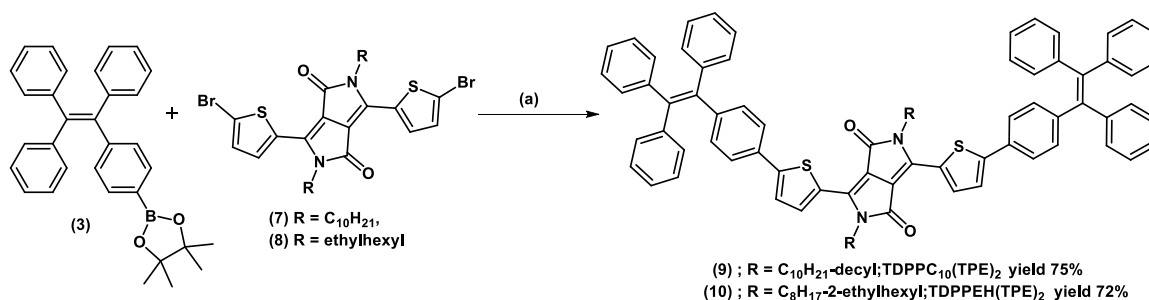
Scheme 2.1 Synthesis of 4,4,5,5-tetramethyl-2-(4-(1,2,2-triphenylvinyl)phenyl)-1,3,2-dioxaborolane : Reaction condition ; (a) *n*-BuLi, THF, 4-bromobenzophenone, 0 °C, rt, 6 h (b) *p*-toluenesulfonic acid, toluene, refluxed, 6 h, 64 %, (c) Bis(pinacolato)diboron, KOAc, PdCl₂(dppf)₂, 1,4-dioxane, 80 °C, 24 h, 68 %

The dithienyl-DPP derivative **4** was synthesized using Iqbal method of condensation of 2-thiophencarbonitrile with diisopropyl succinate in the presence of sodium which is given in the Scheme 2.2.²⁷⁻³⁰ Subsequent alkylation with decyl bromide and ethylhexyl bromide in the presence of K₂CO₃ dissolved in DMF. Finally, the bromination of the alkylated DPP **5** and **6** in dry CHCl₃ were done by using freshly recrystallized *N*-bromosuccinimide.



Scheme 2.2 Reaction condition; (a) Na, *tert*-amyl alcohol, diisopropyl succinate, 110 °C, overnight, CH₃COOH (b) DMF, K₂CO₃, R-Br, 100 °C, 12 h, 35-40 % (c) NBS, CHCl₃, 0 °C to rt, 24 h, > 90 %

The synthetic scheme of the final molecule is given in the scheme 2.3. The *N*-alkylated dibromo DPP compounds **5** and **6** were subjected to a double Suzuki-Miyaura cross-coupling with tetraphenylethylene boronic ester **3** using Pd(PPh₃)₄ as the catalyst.²⁶ The structure and purity of TDPPC₁₀ (TPE)₂ and TDPPEH(TPE)₂ were confirmed by ¹H-NMR and ¹³C-NMR spectroscopy and matrix-assisted laser desorption/ionization time-of-flight (MALDI-TOF) mass spectrometry.



Scheme 2.3 Reaction condition; (a) Pd(PPh₃)₄, K₂CO₃, Toluene : Ethanol : H₂O, 90 °C, 24 h

2.3.2 Optical properties

The normalized optical absorption spectra of the TDPPC₁₀(TPE)₂ and TDPPEH(TPE)₂ in dilute (10⁻⁶ M) chloroform solutions and thin film are shown in Figure 2.4. The solution absorption spectra of both TDPPC₁₀(TPE)₂ and TDPPEH(TPE)₂ having weak shoulder band at 577 nm and intense peak at 618 nm. The film state of both molecule shows a red-shifted absorption having a more pronounced peak at 588 nm

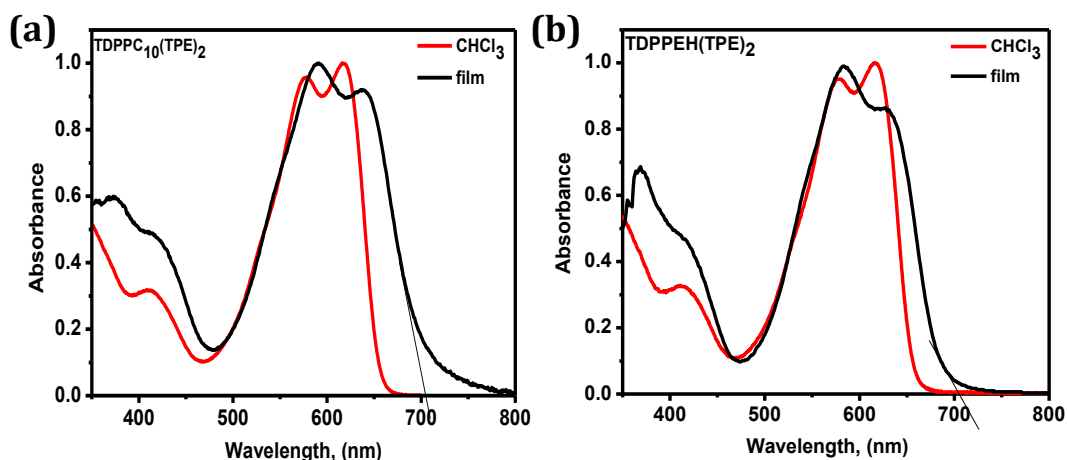


Figure 2.4 Absorption spectra of (a) TDPPC₁₀(TPE)₂ and (b) TDPPEH(TPE)₂ and a weak shoulder peak at 637 nm for TDPPC₁₀(TPE)₂, whereas TDPPEH(TPE)₂ has the prominent peak at 629 nm. The optical band gap calculated from the absorption edge for both derivatives is found to be 1.76 eV. The fluorescence spectra

of TDPPC₁₀(TPE)₂ and TDPPEH(TPE)₂ in chloroform solution and thin film is given in the Figure 2.5. The photophysical properties were summarized in the Table 2.1. The emission maximum for both of the molecules in solution is 647 nm and a shoulder peak present at 793 nm. The film state emission is weak and broad having a maximum at 790 nm. The stoke shift of 724 cm⁻¹ suggests that the chromophore doesn't have the similar ground and excited state structure. Absorption spectra of these small molecules in thin films are broadened with red-shift in comparison with the absorption spectra those of in chloroform solution, which can be described due to the molecular self-organization of π -chromophore. J-type molecular aggregation is further proved by the red shifted broad emission band of both the compounds in film state compared to solution state. The emission spectra of both the derivatives are overlapping with each other clearly denies any role of alkyl chains on the arrangement chromophores in the film state, which was quite anticipated.

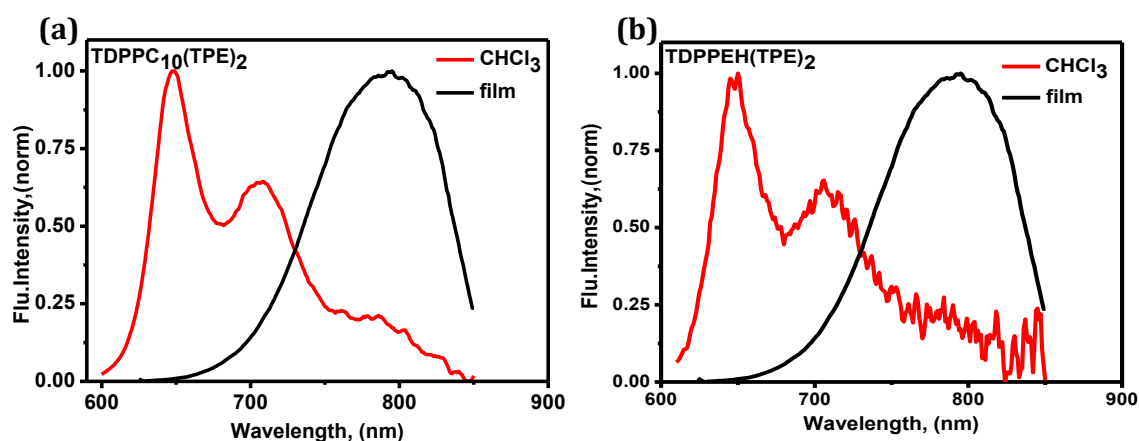


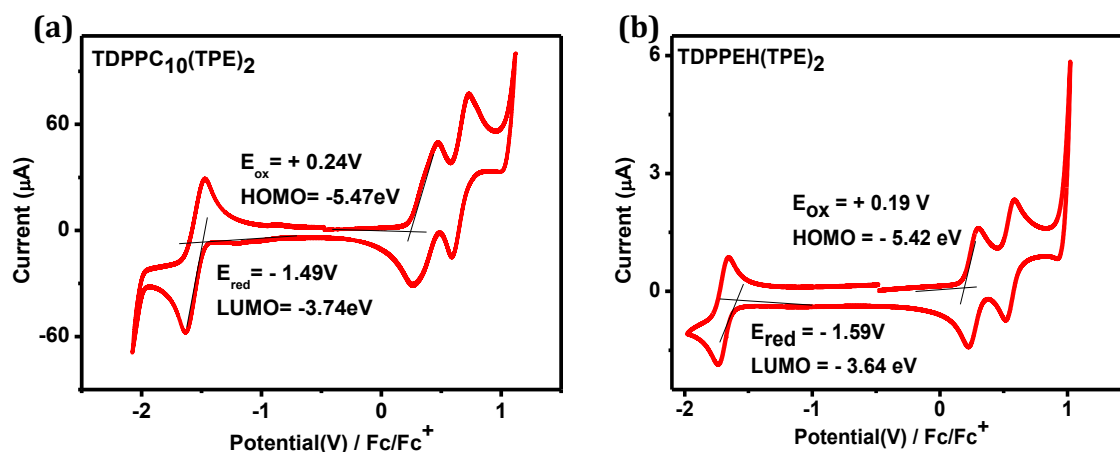
Figure 2.5 Emission spectra of (a) TDPPC₁₀(TPE)₂ and (b) TDPPEH(TPE)₂ excited at 580.

2.3.3 Electrochemical Properties

The oxidation and reduction potentials and the corresponding HOMO and LUMO levels were determined by cyclic voltammetry (Figure 2.6) in dichloromethane solution under an inert N₂ atmosphere at room temperature. The oxidation and reduction potentials of TDPPC₁₀(TPE)₂ and TDPPEH(TPE)₂ with respect to Fc/Fc⁺ shows the value near to +0.24 V, +0.19 V and -1.49 V, -1.59 V respectively. Using these redox potentials the HOMO and LUMO levels were estimated using $E = -5.23 - qE_{\text{redox}}$.³¹⁻³² The electrochemical band gaps were determined as the difference between the onset of the redox potentials, and obtained values are in proper agreement with the optical band gaps determined using the onsets of the absorption spectra in the film state.³³ The optical data, electrochemical values, and band gap are given in the Table 2.1 and 2.2 respectively. It is observed that the energy levels of the TDPP-TPE molecules are suitably placed for electron transfer to PC₆₁BM as shown in the energy level diagram in Figure. 2. 7. The LUMO level of the acceptor should be at least 0.3 eV lower than that of the donor to drive charge separation after exciton formation. The difference between HOMO of the donor and LUMO of the acceptor is 1.25 eV, which could lead to high V_{oc} of solar cell.

Table 2.1 Optical data of the TDPPC₁₀(TPE)₂ and TDPPEH(TPE)₂ in chloroform solutions, and in the thin films at room temperature. $\lambda_{exc} = 580$ nm for both.

Compound	Absorption (nm)		Emission(nm) excited at 580		τ (ns) CHCl ₃	ϵ (Mol ⁻¹ cm ⁻¹)
	λ_{max}^{sol}	λ_{max}^{film}	λ_{em}^{sol}	λ_{em}^{film}		
TDPPC ₁₀ (TPE) ₂	618	638	647	790	2.4	63000
TDPPEH(TPE) ₂	618	638	647	790	2.4	63000

**Figure 2.6** Cyclic voltammograms of (a) TDPPC₁₀(TPE)₂ and (b) TDPPEH(TPE)₂ in CH₂Cl₂ in the presence of 0.1 M of TBAPF₆ as electrolyte at 25 °C**Table 2.2** Electrochemical potentials (vs. Fc/Fc⁺) in dichloromethane containing 0.1 M TBAPF₆ (scan rate = 0.1 V/s)

Compound	λ_{0-0}^{film} (nm)	E_{0-0}^{opt} (eV)	E_{ox}^{sol} (V/Fc/Fc ⁺)	E_{red}^{sol} (V/Fc/Fc ⁺)	HOMO (eV)	LUMO (eV)	E_{0-0}^{cv} (eV)
TDPPC ₁₀ (TPE) ₂	704	1.76	+0.24	-1.49	-5.47	-3.74	1.73
TDPPEH(TPE) ₂	704	1.76	+0.19	-1.59	-5.42	-3.64	1.78

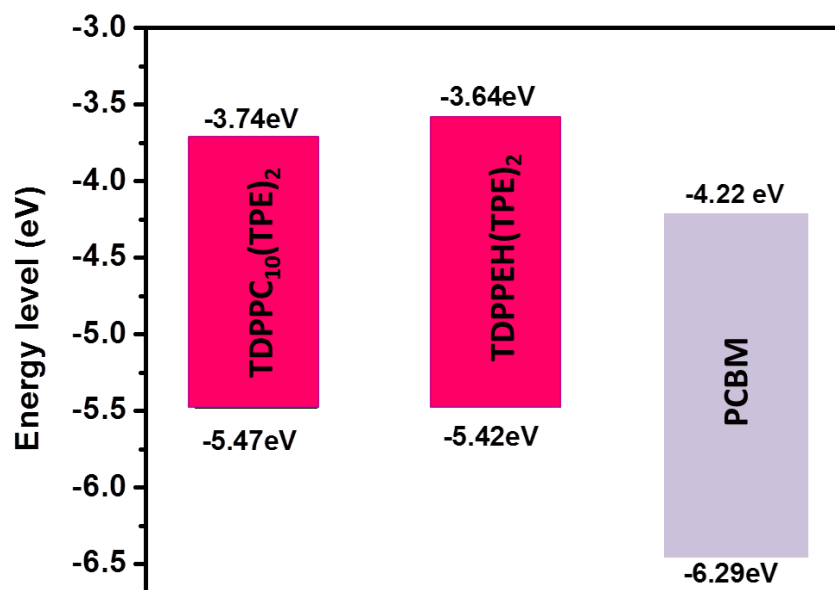


Figure 2.7 HOMO-LUMO energy level diagram of TDPPC₁₀(TPE)₂, TDPPEH(TPE)₂, and PCBM

2.3.4 Thermal Properties

To assess the thermal stability and behavior of the molecules, they were characterized by the TGA and DSC. Figure 2.8 (a) depicts DSC plots and (b) TGA of both small molecules in the solid state. TGA experiment was carried out at a heating rate of 10 °C / min under N₂ atmosphere. Irrespective of the alkyl chain nature, both derivatives exhibited a 5 % weight loss at a temperature around 370 °C, which indicate that all the two molecules are thermally stable enough for application in solar cells. Thermal behaviors of the DPP-containing molecules have been further studied by DSC (N₂ atmosphere). The melting temperature (T_m) occurs at 195 °C for TDPPC₁₀(TPE)₂ and 173 °C for TDPPEH(TPE)₂. Endothermic peaks at 77 °C and 107 °C observed for TDPPC₁₀(TPE)₂ and TDPPEH(TPE)₂ respectively, indicates the probable phase transition occurs in the solid state packing of the molecules. Difference in phase transition temperature can be ascribed due to the influence of

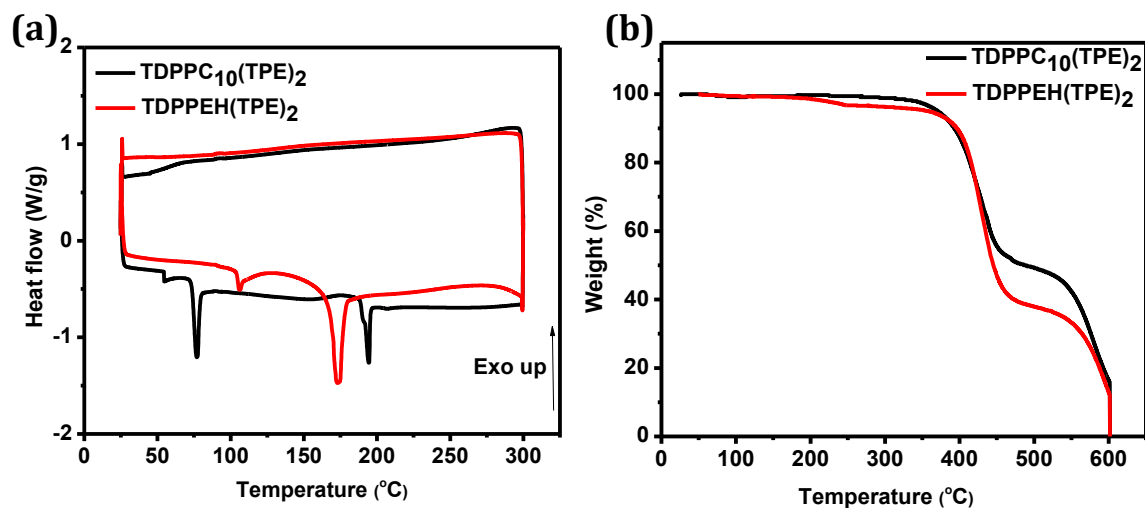


Figure 2.8 (a) DSC plots and (b) TGA of TDPPC₁₀(TPE)₂ and TDPPEH(TPE)₂.

the alkyl chain length on the molecular packing in the film state.

2.3.5 Photovoltaic properties

To investigate the photovoltaic properties of the two small molecules, BHJ solar cells with a device structure of ITO/PEDOT:PSS/DPP-donors:PC₆₁BM/LiF/Al were fabricated. Solar cell devices were prepared using a total concentration of 20 mg/mL from blends of each donor material with PC₆₁BM as the electron acceptor and optimized with respect to additives and annealing temperature. Thickness of the PEDOT:PSS, active layer, LiF, aluminum were 40 nm, 90-100 nm, 1 nm, 100 nm respectively. The additives used in this work were DIO, *o*-DCB and 1-CN. The active layers of the devices were fabricated under a donor and acceptor weight ratio of 1:1, and the thermal annealing was conducted at 110 °C. Device performance is summarized in Table.2.3. The TDPPC₁₀(TPE)₂ device with the highest performance was obtained with active layer without any additives, producing J_{sc} of 1.05 mA/cm², V_{oc} of 0.90 V, FF of 0.25 and MPP value of 0.25 mW/cm². For the blend of

TDPPC₁₀(TPE)₂ and PC₆₁BM it was observed that after annealing the solar cell performance decreases. Blend mixtures from TDPPEH(TPE)₂ and PC₆₁BM also showed similar trend except for the mixture which used DIO as the additive. Best device from TDPPEH(TPE)₂ produced a J_{sc} of 1.77 mA/cm², V_{oc} of 0.79 V, FF of 0.26 and MPP value of 0.37 mW/cm². The current density–voltage (J–V) curves for the best solar cells of TDPPC₁₀(TPE)₂ and TDPPEH(TPE)₂ are shown in Figure 2.9 and 2.10 and the device optimization results are described in the Table 2.3 and 2.4 respectively.

The efficiency of exciton dissociation and the possibility of geminate recomb-

Table 2.3 Device optimization of TDPPC₁₀(TPE)₂ : PC₆₁BM

TDPPC ₁₀ (TPE) ₂ : PC ₆₁ BM (1:1)	Spin Coating (rpm)	Thick ness (nm)	Anneal ing temp	V _{oc} (V)	FF	J _{sc} (mA/ cm ²)	MPP (mW/ cm ²)
CHCl ₃	1500	100	rt	0.86	0.25	0.88	0.20
	1800	105	rt	0.90	0.25	1.05	0.25
	1800	110	110 °C	0.58	0.26	0.77	0.12
0.2% DIO/CHCl ₃	1800	100	rt	0.51	0.26	0.78	0.11
	1800	96	110 °C	0.18	0.25	0.77	0.04
0.2 % o-DCB/CHCl ₃	1800	99	rt	0.80	0.25	0.89	0.18
	1800	98	110 °C	0.38	0.25	0.75	0.08
0.2% 1-CN/CHCl ₃	1800	100	rt	0.42	0.26	0.74	0.08
	1800	97	110 °C	0.60	0.26	0.75	0.12

*Note: The MPP was estimated from the V_{oc} , FF and J_{sc} obtained from the J-V measurements. J–V characteristics were measured with a Keithley 2400 source meter under ~100 mW/cm² white light illumination from a tungsten-halogen lamp filtered by a Schott GG385 UV filter and a Hoya LB120 daylight filter that provides illumination conditions within ~10 % of 100 mW/cm² AM1.5G for most cells.

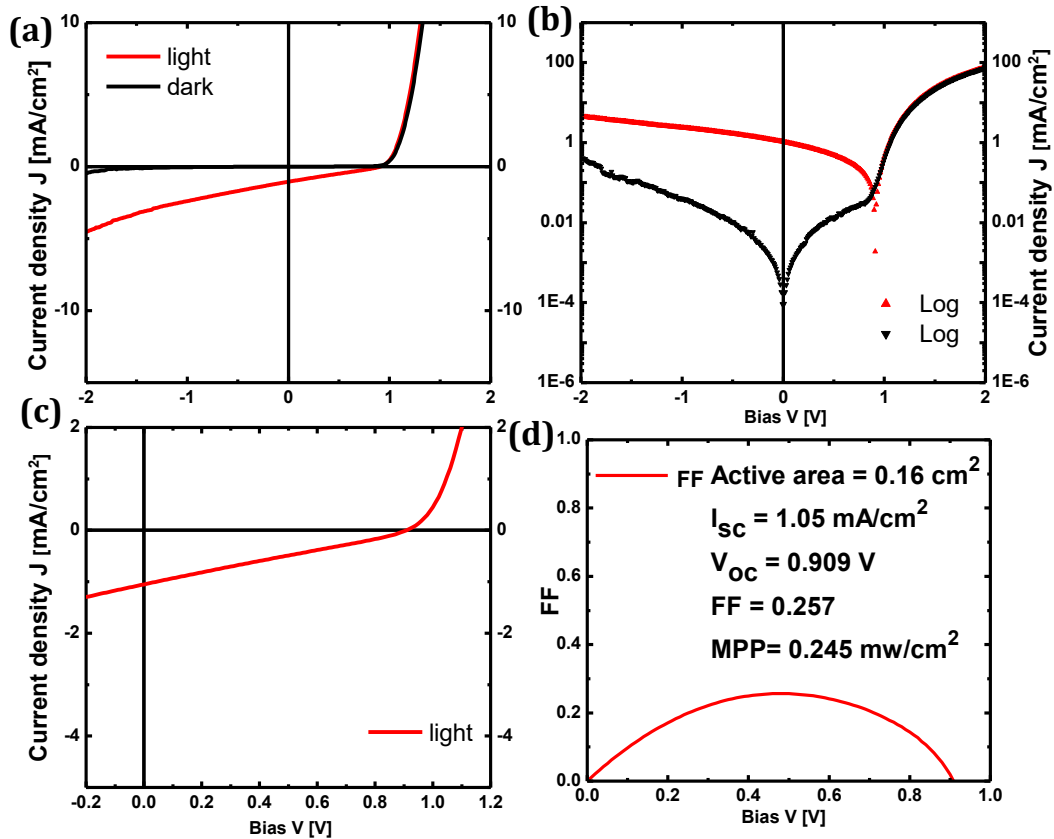


Figure: 2.9 (a) J-V curve of TDPPC₁₀(TPE)₂ : PC₆₁BM in the dark and light. (b) Logarithmic plot of J-V curve of TDPPC₁₀(TPE)₂ : PC₆₁BM in the dark and light. (c) Zoomed portion of J-V curve TDPPC₁₀(TPE)₂ : PC₆₁BM in the light. (d) Fill Factor (FF) Vs Bias V(V) curve.

ination of electron-hole determined by free energy difference between the singlet photoexcited state of the donor material and the charge separated state is given by the equation (1),

$$\Delta G_{cs} = IP_D - EA_A - E_{gD} \quad (1)$$

where, IP_D is the ionization potential of the donor material, EA_A is the electron affinity of the acceptor material, and E_{gD} is the optical band gap of the donor material. The free energy ΔG_{cs} for the TDPPC₁₀(TPE)₂ and TDPPEH(TPE)₂ are equal to -0.51 eV and -0.56 eV respectively and it implies that exciton dissociation is

efficient. But the J_{sc} and FF were moderate which can be due to the suboptimal morphology of active layer. The external quantum efficiency (EQE) is a spectral measurement of the number of electrons extracted out of a solar cell per incident photon. The EQE spectrum of the TDPPC₁₀(TPE)₂ and TDPPEH(TPE)₂ were similar to the absorption spectra of the donor molecules and have the maximum of 0.06 % and 0.08 % at 585 nm respectively. Short circuit current density of TDPPC₁₀(TPE)₂ and TDPPEH(TPE)₂ under AM1.5G conditions from the spectral response were found to be 0.89 mA/cm² and 1.20 mA/cm².

Table 2.4 Device optimization of TDPPEH(TPE)₂ : PC₆₁BM

TDPPEH(TPE) ₂ : PC ₆₁ BM (1:1)	Annea ling temp	V _{oc} (V)	FF	J _{sc} (mA/ cm ²)	MPP (mW/ cm ²)
CHCl ₃	rt	0.79	0.26	1.77	0.37
	rt	0.75	0.26	1.78	0.36
	110 °C	0.54	0.25	1.39	0.19
0.2% DIO/CHCl ₃	rt	0.88	0.25	1.23	0.28
	110 °C	0.95	0.25	1.42	0.35
0.2% o-DCB/CHCl ₃	rt	0.55	0.26	1.42	0.20
	110 °C	0.74	0.25	1.39	0.26
0.2% 1-CN/CHCl ₃	rt	0.42	0.25	1.20	0.13
	110 °C	0.72	0.25	1.36	0.25

*Note: The MPP was estimated from the V_{oc}, FF and J_{sc} obtained from the J-V measurements. J-V characteristics were measured with a Keithley 2400 source meter under ~100 mW/cm² white light illumination from a tungsten-halogen lamp filtered by a Schott GG385 UV filter and a Hoya LB120 daylight filter that provides illumination conditions within ~10 % of 100 mW/cm² AM1.5G for most cells.

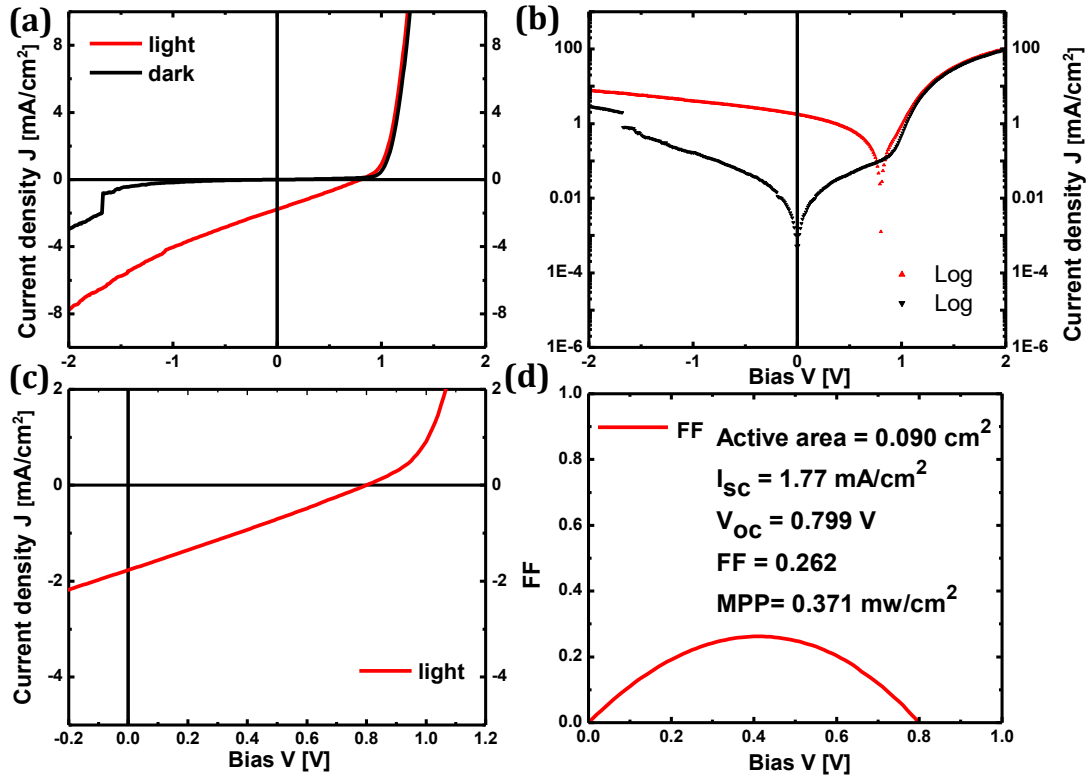


Figure: 2.10 (a) J-V curve of TDPPEH(TPE)₂ : PC₆₁BM in the dark and light. (b) Logarithm plot of J-V curve of TDPPEH(TPE)₂ : PC₆₁BM in the dark and light. (c) Zoomed portion of J-V curve TDPPEH(TPE)₂ : PC₆₁BM in the light. (d) Fill Factor (FF) Vs Bias V (V) curve.

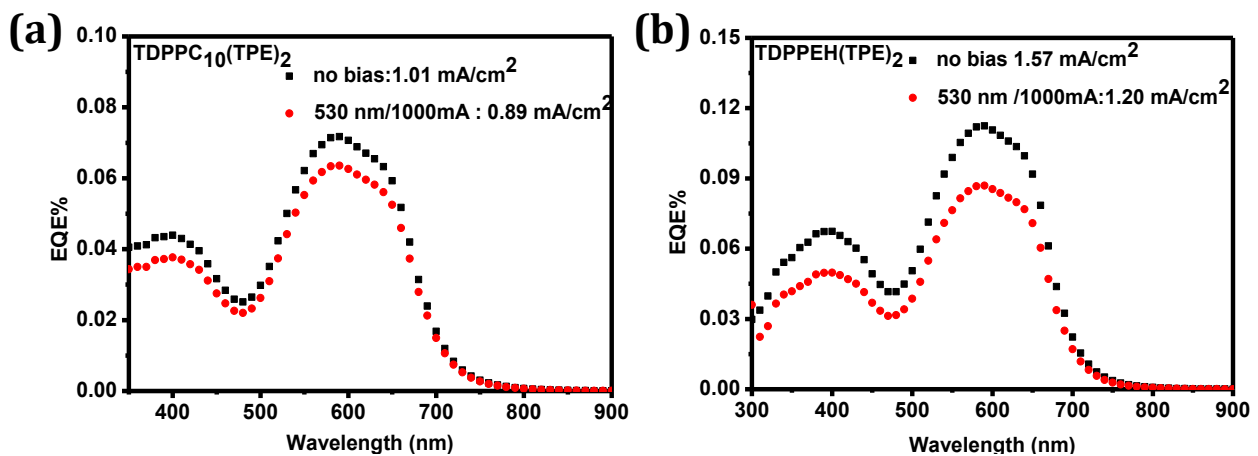


Figure 2.11 EQE of (a) TDPPC₁₀(TPE)₂ and (b) TDPPEH(TPE)₂

Table 2.5 Summary of the best solar cell device performance of TDPPC₁₀(TPE)₂ and TDPPEH(TPE)₂

Donor: Acceptor (1:1)	Spin Coat ing	Thick ness (nm)	J _{sc} (mA /cm ²)	V _{oc} (V)	FF	MPP (mW/ cm ²)	J _{sc} (mA /cm ²) (SR)	PCE (%)
TDPPC ₁₀ (TPE) ₂ : PC ₆₁ BM	1800 rpm	105	1.05	0.90	0.25	0.25	0.89	0.20
TDPPEH (TPE) ₂ : PC ₆₁ BM	1500 rpm	92	1.77	0.79	0.26	0.37	1.20	0.25

Note : J_{sc} (SR) is based on integrating the EQE (measured with 1 sun bias illumination) with the AM1.5G spectrum. The PCE is determined from the EQE integrated J_{sc} (SR).

2.3.6 Morphological studies

In order to study the morphology of the active layer, we repeated the fabrication of the solar cell the (TDPPC₁₀(TPE)₂:PC₆₁BM (1:1)) and obtained an efficiency of 0.10 % with a V_{oc} of 0.86 V, J_{sc} of 0.48 mA/cm² and EQE close to 0.03 % at 585 nm. The ethylhexyl derivative TDPPEH(TPE)₂ with PC₆₁BM in 1:1 ratio achieved an efficiency of 0.25 % with a V_{oc} of 0.89 V and J_{sc} of 1.03 mA/cm² with EQE close to 0.07 % at 585 nm. The J-V characterization and EQE of TDPPC₁₀(TPE)₂ and TDPPEH(TPE)₂ is given in the Figure 1.12 and Figure 1.13 respectively. After the characterization of the solar cell, the glass substrates were dipped into the distilled water. The PEDOT:PSS dissolves in water and the organic layers were collected on the TEM grid. The TEM image of the active layer is given in the Figure 2.14. There is not much contrast on the TEM image of the active layer which indicates absence of phase separated active layer morphology. The amorphous state of the film might be responsible for low J_{sc} and FF.

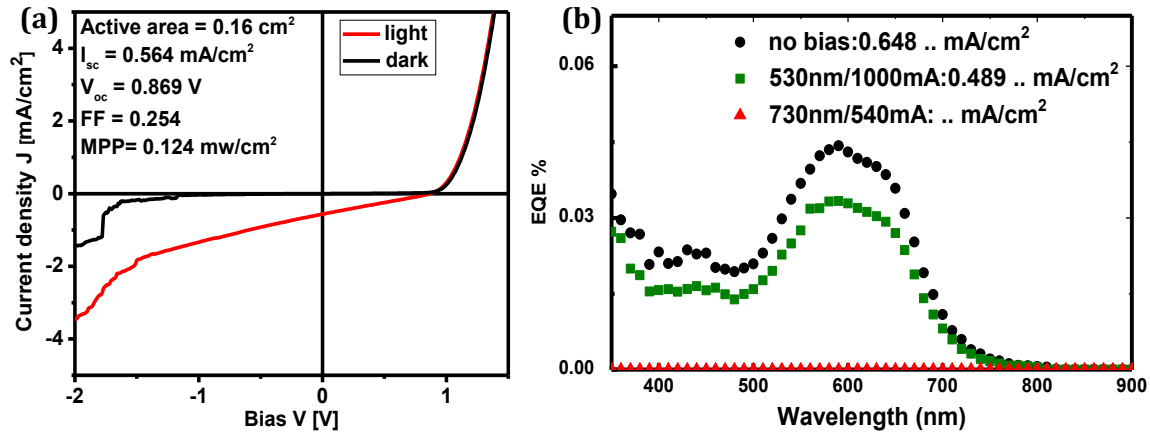


Figure 2.12 (a) J-V curve and (b) EQE of DPPC₁₀(TPE)₂:PC₆₁BM solar cell.

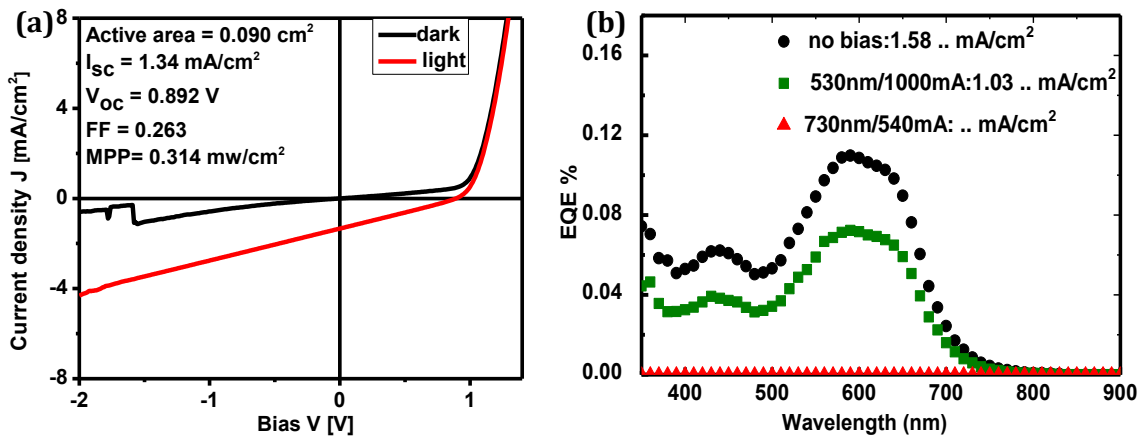


Figure 2.13 (a) J-V curve and (b) EQE of TDPPEH(TPE)₂:PC₆₁BM solar cell.

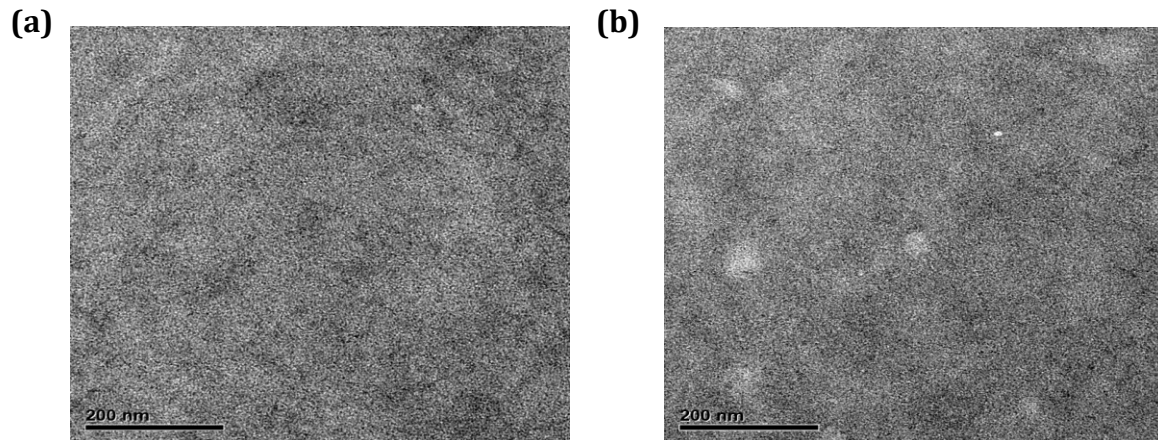


Figure 2.14. TEM Image of the active layer (a) TDPPEH(TPE)₂:PC₆₁BM and (b) TDPPEH(TPE)₂:PC₆₁BM.

2.4 Conclusion

The synthesis of novel donor molecules based on DPP and TPE, investigation of optoelectronic properties and their utility in solar cell application were described. Open circuit voltage of TDPPC₁₀(TPE)₂ and TDPPEH(TPE)₂ were 0.90 V and 0.79 V respectively. Low value of current density 0.89 mA/cm² and 1.2 mA/cm² and fill factor of 0.25 limit the device efficiency to 0.20 % and 0.25 %. The lack of nanoscale phase separation of the photoactive layers is one of the main reasons for low current density as revealed from morphological studies.

2.5 Experimental section

2.5.1 General methods.

Diphenylmethane, 4-bromobenzophenone, *p*-toluenesulfonic acid, Bis(pinacolato) diborane, 2-thiophenecarbonitrile, PdCl₂(dppf)₂, Pd(PPh₃)₄, were purchased from Sigma Aldrich and were used as such. The solvents used were either HPLC grade or freshly distilled before use. All the reactions were carried out under nitrogen atmosphere. ¹H NMR and ¹³C NMR spectra were obtained using a 500 MHz Bruker Avance DPX spectrometer. Differential scanning calorimetry (DSC) was performed using a PerkinElmer Pyris 6 DSC instrument in sealed aluminum pans under nitrogen flow, at a heating/cooling rate of 10 °C/min. Absorption spectra were obtained using a Shimadzu 3101PC UV/Vis-NIR scanning spectrophotometer. Cyclic voltammetry was performed under an inert atmosphere with a scan rate of 0.1 V/s and 0.1 M tetrabutylammoniumhexafluorophosphate in dichloromethane as the electrolyte. A platinum working electrode, a silver counter electrode and a silver

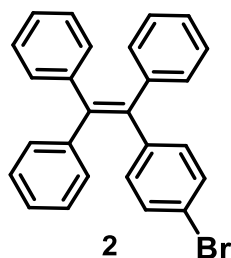
wire coated with silver chloride (Ag/AgCl) quasi-reference electrode were used combined with Fc/Fc⁺ as the internal standard.

2.5.2 Fabrication of bulk heterojunction solar cell

Photovoltaic devices were fabricated by spin coating poly(ethylenedioxythiophene): poly(styrene sulfonate) (PEDOT:PSS) (Clevios P, VP AI 4083) onto pre-cleaned, patterned indium tin oxide (ITO) substrates (14 Ω per square) (Naranjo Substrates). The photoactive layers were deposited by spin coating a chloroform solution containing the TDPPC₁₀(TPE)₂/TDPPEH(TPE)₂ molecule (10 mg/mL), the appropriate amount of PC₆₁BM and the co-solvent (either DIO, o-DCB, 1-CN). For layers that were thermally annealed, the glass substrates with the photoactive layer were placed on a hot plate inside a N₂-filled glove box (< 1 ppm O₂ and < 1 ppm H₂O) at the temperatures and times indicated in the Tables. For cells that were thermal annealed, this was done prior to depositing the metal contacts. To complete the devices, LiF (1 nm) and Al (100 nm) were deposited by vacuum evaporation at $\sim 2 \times 10^{-7}$ mbar as the back electrode. The active area of the cells was 0.09 cm² and 0.16 cm². J-V characteristics were measured under ~ 100 mW/cm² white light from a tungsten-halogen lamp filtered by a Schott GG385 UV filter and a Hoya LB 120 daylight filter, using a Keithley 2400 source meter. Short circuit currents under AM1.5G conditions were estimated from the spectral response and convolution with the solar spectrum. The spectral response was measured under simulated 1 sun operation conditions using bias light from a 532 nm solid state laser (Edmund Optics). Light from a 50 W tungsten halogen lamp (Osram64610) was used as probe

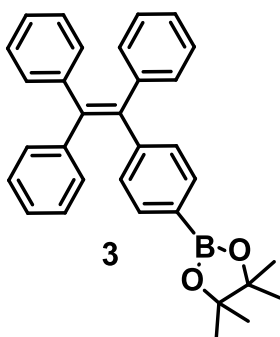
light and modulated with a mechanical chopper before passing the monochromator (Oriel, Cornerstone 130) to select the wavelength. The response was recorded as the voltage over a 50 Ω resistance, using a lock-in amplifier (Stanford Research Systems SR 830). A calibrated Si cell was used as reference. The device was kept behind a quartz window in a nitrogen filled container. The thickness of the active layers in the photovoltaic devices was measured on a Veeco Dektak 150 profilometer.

2.5.3 Experimental procedures



1-(4-Bromophenyl)-1,2,2-triphenylethane (2) : To a solution of diphenylmethane (2.02 g, 12 mmol) in dry THF (50 ml) was added drop wise 1.6 M solution of *n*-butyllithium in hexane (7.5 mL, 12 mmol) at 0 °C under a nitrogen atmosphere. The resultant orange-red solution was stirred for 1 h and then transferred slowly to a solution of 4-bromobenzophenone (2.6 g, 10 mmol) in THF (20 ml) at 0 °C. The reaction mixture was allowed to warm to room temperature and stirred for 6 h. The reaction was quenched by adding an aqueous solution of ammonium chloride. The organic layer was extracted with dichloromethane, and the combined organic layers were washed with a saturated brine solution and dried over anhydrous magnesium sulfate. After filtration and solvent evaporation, the resultant crude alcohol containing excess diphenylmethane was dissolved in ~80 ml

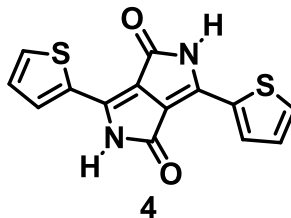
of toluene and a catalytic amount of *p*-toluenesulfonic acid (0.5 g, 2.6 mmol) was added. After heating to reflux for 6 h, the mixture was cooled to room temperature and washed with a saturated brine solution and dried over anhydrous magnesium sulfate. After filtration and solvent evaporation, the residue was purified by silica-gel column chromatography using *n*-hexane as the eluent. White solid of **2** was obtained in 60 % yield (2.5 g). ¹H NMR (500 MHz, CDCl₃, TMS): δ=7.22 (d, *J*=8.5 Hz, 2H), 7.15–7.08 (m, 9H), 7.05–6.99 (m, 8H).



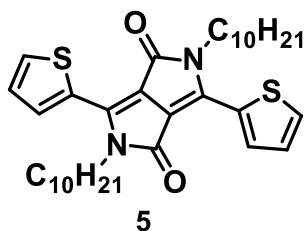
4,4,5,5-tetramethyl-2-(4-(1,2,2-triphenylvinyl)phenyl)-1,3,2-dioxaborolane

(3): 1-(4-Bromophenyl)-1,2,2-triphenylethene (**1**) (0.5 g, 1.2 mmol), Potassium acetate (0.47 g, 4.8 mmol), bis(pinacolato)diborane (0.61 g, 2.4 mmol) and 10 ml of anhydrous dioxane was taken in a three neck round bottom flask. The system was degassed by applying three times freeze-pump-thaw cycles to replace air with argon. Then Pd(dppf)₂Cl₂ was added into it. The reaction was performed at 85 °C for 24 h. After cooling, the mixture was evaporated to dryness and taken up with CH₂Cl₂. The organic layer was washed with H₂O, dried over MgSO₄, filtered and evaporated to dryness. Column chromatography (SiO₂, Hexane/CH₂Cl₂ 95:5) gave compound **3** as a

colorless solid in 68 % yield.¹H NMR (500 MHz, CDCl₃, TMS): δ=7.22 (d, J=8.5 Hz, 2H), 7.15–7.08 (m, 9H), 7.05–6.99 (m, 8H), 1.3(S, 12H).

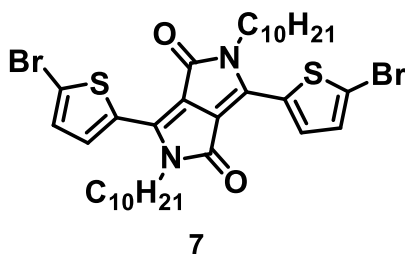


3,6-Di(thiophen-2-yl)pyrrolo[3,4-c]pyrrole-1,4(2H,5H)-dione (4). was synthesized using the similar synthetic procedure as reported previously. Sodium metal (2.42 g, 110 mmol) was added portion-wise to *tert*-amyl alcohol and the solution was stirred overnight at 120 °C. 2-Thiophenecarbonitrile (10 ml, 107 mmol) was then added to the hot alkoxide solution followed by the dropwise addition of a solution of diisopropyl succinate (5 ml, 30 mmol) in 40 mL of *tert*-amyl alcohol. After complete addition of the diethyl succinate solution, the mixture was allowed to reflux overnight. The reaction mixture was then allowed to cool to 60 °C, quenched with 40 mL of acetic acid, and allowed to reflux for an additional hour. The resulting suspension was then filtered and the solid washed with hot methanol and water three times and dried *in vacuo*, affording a dark solid (7.5 g, 84 %).



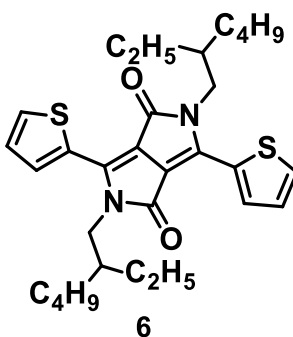
2,5-didecyl-3,6-di(thiophen-2-yl)pyrrolo[3,4-c]pyrrole-1,4(2H,5H)-dione (5)

was synthesized using the similar synthetic procedure as reported previously. A mixture of 3,6-dithiophen-2-ylpyrrolo[3,4-c]pyrrole-1,4-(2H,5H)dione (2.00 g, 6.67 mmol), anhydrous potassium carbonate (3.69 g, 26.7 mmol) and 18-crown-6 (10 mg) were added in anhydrous N,N-dimethylformamide then heated to 100 °C under N₂ for 1 h. After 1 h 1-bromodecane 4 ml was added into it and temperature was increased to 120 °C and the mixture was further stirred for 36 h at same temperature. After the resulting suspension was poured into cold water and extracted with chloroform, the organic phase was washed with brine solution and dried over MgSO₄. The crude product was purified by column chromatography on silica gel, using chloroform/petroleum ether as eluent to afford as a dark red solid (1.35 g, 35 %). ¹H NMR (500 MHz) δ: 8.92 (d, J = 3.0 Hz, 2H), 7.64 (d, J = 5.0 Hz, 2H), 7.28 (t, J = 4.0 Hz, 2H), 4.06 (t, J = 7.5 Hz, 4H), 1.77–1.71 (m, 4H), 1.42–1.25 (m, 28H), 0.89 (t, J = 6.5 Hz, 6H).

**3,6-bis(5-bromothiophen-2-yl)-2,5-didecylpyrrolo[3,4-c]pyrrole-**

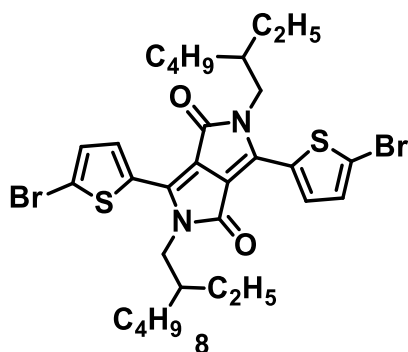
1,4(2H,5H)dione (7) Compound 2 (0.5 g, 0.86 mmol) and N-bromosuccinimide (0.352 g, 1.72 mmol) were dissolved into chloroform (25 mL) in a three neck round flask under argon protection, and then the solution was protected from light and

stirred at room temperature. After 40 h, the mixture was poured into 200 mL of methanol and then filtered. The filter cake was washed with hot methanol twice. After drying in vacuum, the pure product was obtained as a purple-black solid (0.508 g, yield >90 %). $^1\text{H NMR}$ (500 MHz) δ : 8.68 (d, $J = 4.0$ Hz, 2H), 7.24 (d, $J = 4.0$ Hz, 2H), 3.98 (t, $J = 8$ Hz, 4H), 1.74–1.68 (m, 4H), 1.40–1.25 (m, 28H), 0.87 (t, $J = 6.5$ Hz, 6H).



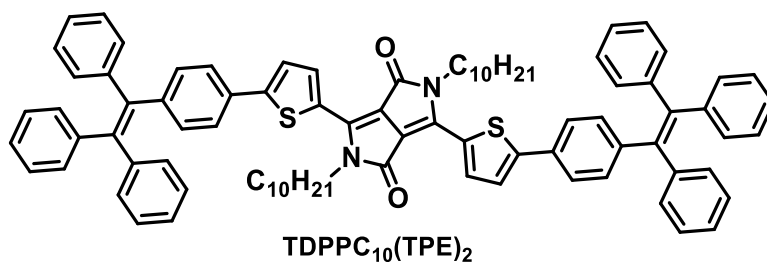
2,5-Bis(2-ethylhexyl)-3,6-di(thiophen-2-yl)pyrrolo[3,4-c]pyrrole-1,4(2H,5H)-dione (6) was synthesized using the similar synthetic procedure as reported previously. A mixture of 3,6-dithiophen-2-ylpyrrolo[3,4-c]pyrrole-1,4-(2H,5H)dione (2.00 g, 6.67 mmol) anhydrous potassium carbonate (3.69 g, 26.7 mmol) and 18-crown-6 (10 mg) were added in anhydrous *N,N*-dimethylformamide then heated to 100 °C under N_2 for 1 h. After 1 h 2-ethylhexyl bromide 4 ml was added into it and temperature was increased to 120 °C and the mixture was further stirred for 36 h at the same temperature. After the resulting suspension was poured into cold water and extracted with chloroform, the organic phase was washed with brine solution and dried over MgSO_4 . The crude product was purified by column chromatography

on silica gel, using chloroform/petroleum ether as eluent to afford as a dark red solid (1.40 g, 40 %). $^1\text{H NMR}$ (500 MHz) δ : 8.87 (d, $J = 3.6$ Hz, 2H), 7.65 (d, $J = 4.5$ Hz, 2H), 7.28 (t, $J = 4.4$ Hz, 2H), 4.07–3.96 (m, 4H), 1.87–1.85 (m, 2H), 1.39–1.22 (m, 16H), 0.89–0.83 (m, 12H).



3,6-bis(5-bromothiophen-2-yl)-2,5-bis(2-ethylhexyl)pyrrolo[3,4-c]pyrrole-

1,4(2H,5H)-dione (8) Compound 2 (0.5 g, 0.86 mmol) and N-bromosuccinimide (0.352 g, 1.72 mmol) were dissolved into chloroform (25 mL) in a three neck round flask under argon protection, and then the solution was protected from light and stirred at room temperature. After 40 h, the mixture was poured into 200 mL of methanol and then filtered. The filter cake was washed with hot methanol twice. After drying in vacuum, the pure product was obtained as a purple-black solid (0.508 g, yield >90 %). $^1\text{H NMR}$ (500 MHz) δ : 8.64 (d, $J = 4.2$ Hz, 2H), 7.22 (d, $J = 4.1$ Hz, 2H), 3.93 (t, $J = 8.5$ Hz, 4H), 1.83 (t, $J = 6.5$, 2H), 1.35–1.25 (t, 16H), 0.90–0.85 (m, 12H).



TDPPC₁₀(TPE)₂ : A 20 mL Schlenk tube was charged with 3,6-bis(5-Bromothiophen-2-yl)-2,5-didecylpyrrolo[3,4-c]pyrrole-1,4(2H,5H)-dione (0.1 g, 1.35 mmol), 4,4,5,5-tetramethyl-2-(4-(1,2,2-triphenylvinyl)phenyl)-1,3,2-dioxaborolane (0.155 g, 3.37), and K₂CO₃ (0.038mg, 2.8 mmol). And Pd(PPh₃)₄ (0.035 g, 0.03 mmol) was transferred to the tube inside the glove box. A mixture of toluene (6 mL)/ ethanol (2 mL)/ H₂O (0.5 mL) was degassed with argon for 0.5 h and the mixture was transferred to the schlenk through cannula. The resulting mixture was stirred at 90 °C for 24 h under argon. Upon cooling to room temperature, the reaction mixture was treated with water, brine solution and extracted with CH₂Cl₂, dried over Na₂SO₄, filtered and the solvent was removed under reduced pressure. The crude product was purified by column chromatography using 75 % chloroform-hexane as eluent to get a dark solid with a yield of 75 %. ¹H NMR (500 MHz) δ: 8.94 (d, J = 4.0 Hz, 2H), 7.43 - 7.39 (m, 6H), 7.16-7.02 (m, 34H), 4.08 (t, J = 7.6 Hz, 4H), 1.77 - 1.72 (m, 4H), 1.43-1.23 (m, 28H), 0.85 (t, J = 6.9Hz, 6H). ¹³C-NMR (100 MHz, CDCl₃) δ:161.3, 149.6, 144.6, 143.4, 143.3, 139.3, 136.6, 132.1, 131.3, 127.9, 127.8, 127.6, 125.3, 31.8, 29.5, 29.2, 26.9, 22.6, 14.1. MALDI-TOF calculated -1240.60 found -1240.62.

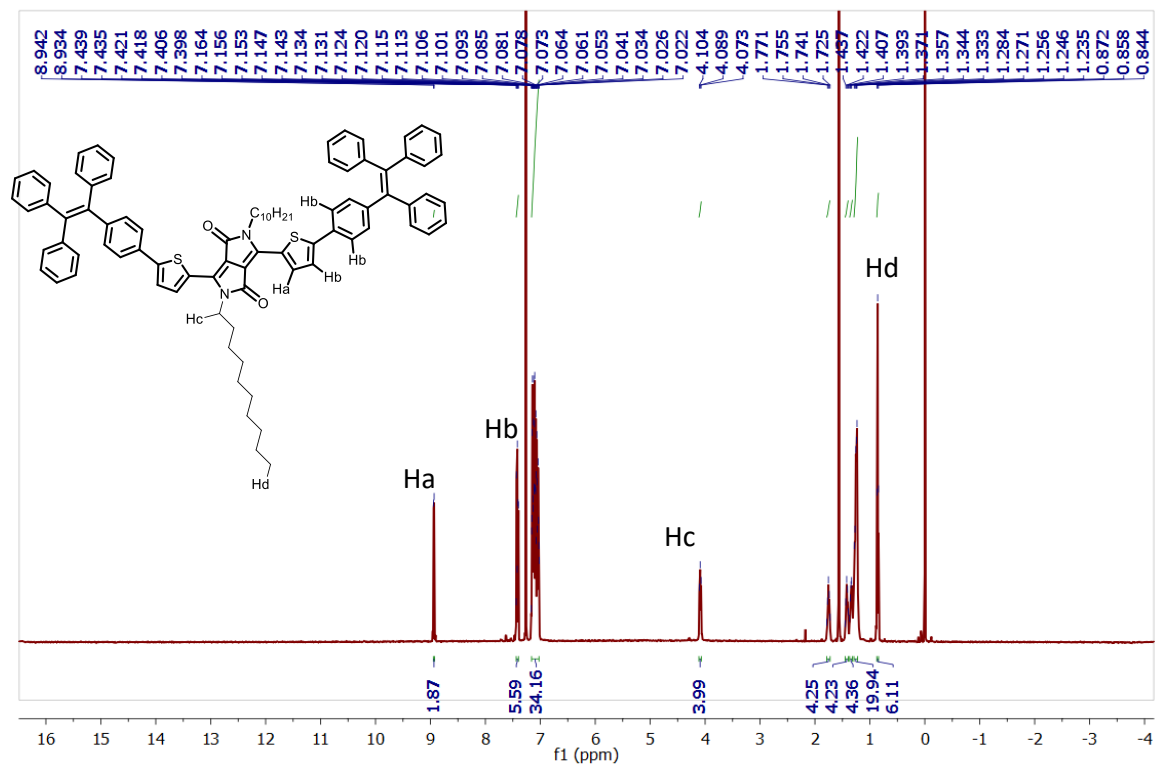


Figure 2.15 NMR spectrum of TDPPC₁₀(TPE)₂

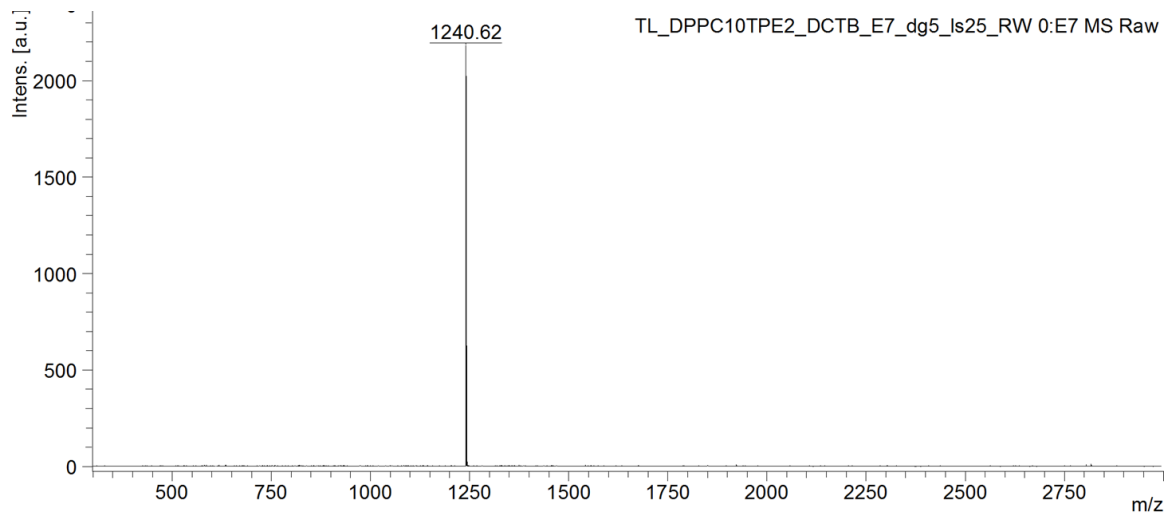
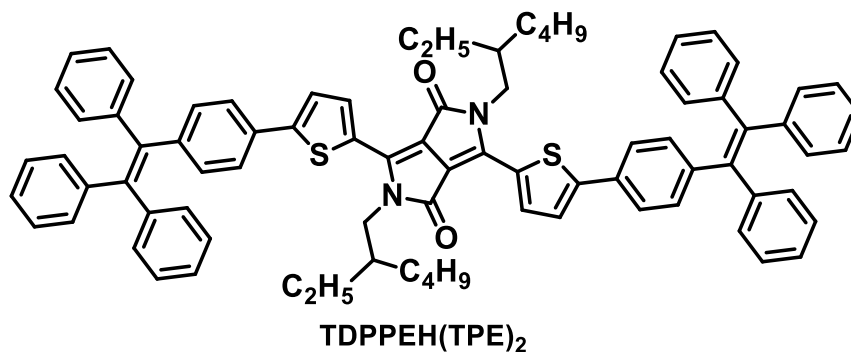
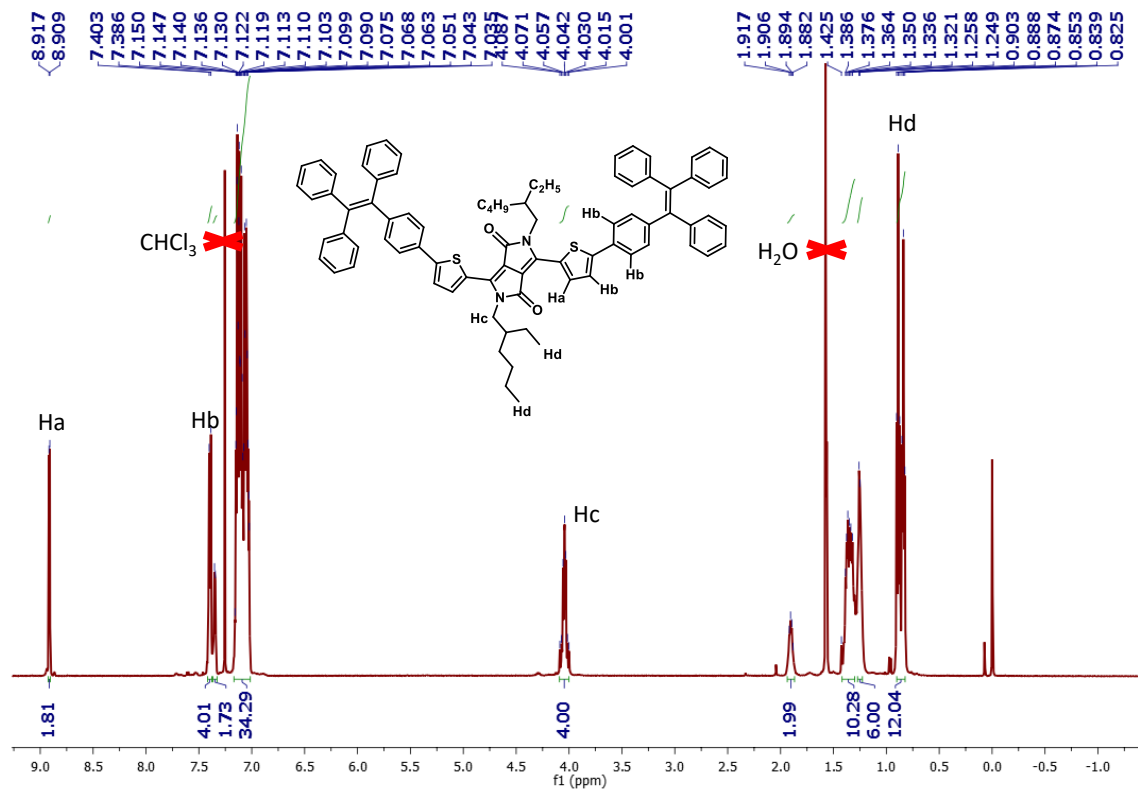
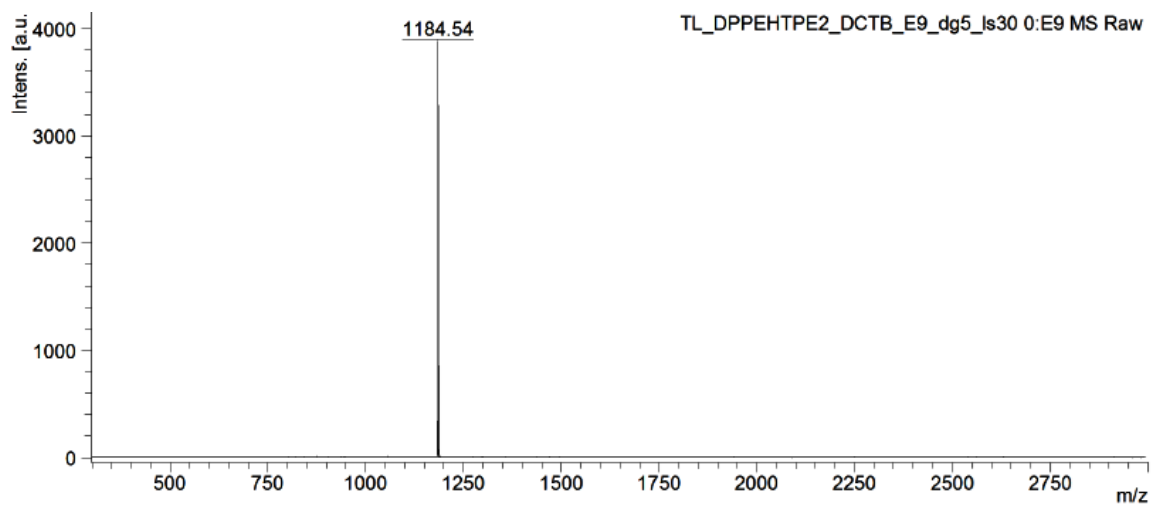


Figure 2.16 MALDI-TOF of TDPPC₁₀(TPE)₂



TDPPEH(TPE)₂ : A 20 mL Schlenk tube was charged with 3,6-bis(5-bromothiophen-2-yl)-2,5-bis(2-ethylhexyl)pyrrolo[3,4-c]pyrrole-1,4(2H,5H)-dione(0.1 g, 1.35 mmol), 4,4,5,5-tetramethyl-2-(4- (1,2,2-triphenylvinyl) phenyl)-1,3,2-dioxaborolane(0.155 g, 3.37 mmol) and K₂CO₃ (0.038 mg , 2.8 mmol). And Pd(PPh₃)₄ (0.035 g, 0.03 mmol), was transferred into the tube inside the glove box. A mixture of toluene (6 mL)/ ethanol (2 mL)/ H₂O (0.5 mL) was degassed with argon for 0.5 h and the mixture was transferred to the schlenk through cannula. The resulting mixture was stirred at 90 °C for 24 h under argon. Upon cooling to room temperature, the reaction mixture was treated with water, brine solution and extracted with CH₂Cl₂, dried over Na₂SO₄, filtered and the solvent was removed under reduced pressure. The crude product was purified by column chromatography 75 % chloroform-hexane as eluent to get dark solid yield of 72 %.¹H NMR (500 MHz) δ: 8.91 (d, J = 4.1 Hz, 2H), 7.40 - 7.38 (m, 6H), 7.14-7.03 (m, 34H), 4.07-4.00 (m, 4H), 1.91-1.88(m, 2H), 1.38-1.25 (m, 16H), 0.90-0.82 (m, 12H).¹³C-NMR (125 MHz, CDCl₃) δ : 161.7, 149.5, 144.4, 143.4, 143.3, 139.7, 136.8, 132.1, 131.3, 127.9, 127.8, 127.6, 125.2, 45.9, 39.1, 30.9, 30.2, 28.5, 23.6, 23.1, 14.0, 10.5 . MALDI-TOF calculated-1184.53 found 1184.54.

Figure 2.17 NMR spectrum of TDPPEH(TPE)₂Figure 2.18 MALDI-TOF spectrum of TDPPEH(TPE)₂

2. 6 References

- (1) Yu, G.; Gao, J.; Hummelen, J. C.; Wudl, F.; Heeger, A. J.; *Science*, **1995**, *270*, 1789-1791.
- (2) Kan, B.; Li, M.; Zhang, Q.; Liu, F.; Wan, X.; Wang, Y.; Ni, W.; Long, G.; Yang, X.; Feng, H.; Zuo, Y.; Zhang, M.; Huang, F.; Cao, Y.; Russell, T. P.; Chen, Y.; *J. Am. Chem. Soc.*, *137*, 3886-3893.
- (3) Zhao, J.; Li, Y.; Yang, G.; Jiang, K.; Lin, H.; Ade, H.; Ma, W.; Yan, H.; *Nat. Energy*, **2016**, *1*, 15027.
- (4) Liu, F.; Gu, Y.; Jung, J. W.; Jo, W. H.; Russell, T. P.; *J. Polym. Sci., Part B: Polym. Phys.*, **2012**, *50*, 1018-1044.
- (5) Henson, Z. B.; Mullen, K.; Bazan, G. C.; *Nat Chem*, **2012**, *4*, 699-704.
- (6) Wakim, S.; Beaupre, S.; Blouin, N.; Aich, B.-R.; Rodman, S.; Gaudiana, R.; Tao, Y.; Leclerc, M.; *J. Mater. Chem.*, **2009**, *19*, 5351-5358.
- (7) Park, J. K.; Jo, J.; Seo, J. H.; Moon, J. S.; Park, Y. D.; Lee, K.; Heeger, A. J.; Bazan, G. C.; *Adv. Mater.*, **2011**, *23*, 2430-2435.
- (8) Osaka, I.; Saito, M.; Mori, H.; Koganezawa, T.; Takimiya, K.; *Adv. Mater.*, **2012**, *24*, 425-430.
- (9) Kim, Y.; Cook, S.; Tuladhar, S. M.; Choulis, S. A.; Nelson, J.; Durrant, J. R.; Bradley, D. D. C.; Giles, M.; McCulloch, I.; Ha, C.-S.; Ree, M.; *Nat. Mater.*, **2006**, *5*, 197-203.
- (10) Kim, Y.; Cook, S.; Kirkpatrick, J.; Nelson, J.; Durrant, J. R.; Bradley, D. D. C.; Giles, M.; Heeney, M.; Hamilton, R.; McCulloch, I.; *J. Phys. Chem. C*, **2007**, *111*, 8137-8141.
- (11) Mao, Z.; Vakhshouri, K.; Jaye, C.; Fischer, D. A.; Fernando, R.; DeLongchamp, D. M.; Gomez, E. D.; Sauv e, G.; *Macromolecules*, **2013**, *46*, 103-112.
- (12) Mishra, A.; B auerle, P.; *Angew. Chem. Int. Ed.*, **2012**, *51*, 2020-2067.
- (13) Walker, B.; Kim, C.; Nguyen, T.-Q.; *Chem. Mater.*, **2011**, *23*, 470-482.
- (14) Lin, Y.; Li, Y.; Zhan, X.; *Chem. Soc. Rev.*, **2012**, *41*, 4245-4272.
- (15) Kim, S.-K.; Oh, S.-Y.; Park, J.-W.; *Thin Solid Films*, **2008**, *517*, 1349-1353.
- (16) Du, X.; Qi, J.; Zhang, Z.; Ma, D.; Wang, Z. Y.; *Chem. Mater.*, **2012**, *24*, 2178-2185.

- (17) Zhu, M.; Yang, C.; *Chem. Soc. Rev.*, **2013**, *42*, 4963-4976.
- (18) Hong, Y.; Lam, J. W. Y.; Tang, B. Z.; *Chem. Commun.*, **2009**, 4332-4353.
- (19) Xu, B.; Chi, Z.; Li, H.; Zhang, X.; Li, X.; Liu, S.; Zhang, Y.; Xu, J.; *J. Phys. Chem. C*, **2011**, *115*, 17574-17581.
- (20) Nie, H.; Huang, J.; Zhao, Z.; Tang, B. Z.: Aggregation-Induced Emission Luminogens (AIEgens) for Non-Doped Organic Light-Emitting Diodes. *Aggregation-Induced Emission: Materials and Applications Volume 2*; American Chemical Society, 2016; Vol. 1227; pp 173-198.
- (21) Tong, H.; Hong, Y.; Dong, Y.; Hau; Lam, J. W. Y.; Li, Z.; Guo, Z.; Guo, Z.; Tang, B. Z.; *Chem. Commun.*, **2006**, 3705-3707.
- (22) Shih, P. I.; Chuang, C. Y.; Chien, C. H.; Diau, E. W. G.; Shu, C. F.; *Adv. Funct. Mater.*, **2007**, *17*, 3141-3146.
- (23) Wan, Q.; Guo, X.; Wang, Z.; Li, W.; Guo, B.; Ma, W.; Zhang, M.; Li, Y.; *Adv. Funct. Mater.*, **2016**, *26*, 6635-6640.
- (24) Liu, Y.; Mu, C.; Jiang, K.; Zhao, J.; Li, Y.; Zhang, L.; Li, Z.; Lai, J.; Hu, H.; Ma, T.; Hu, R.; Yu, D.; Huang, X.; Tang, B.; Yan, H.; *Adv. Mater.*, **2015**, *27*, 1015-1020.
- (25) Rananaware, A.; Gupta, A.; Li, J.; Bilic, A.; Jones, L.; Bhargava, S.; Bhosale, S. V.; *Chem. Commun.*, **2016**, *52*, 8522-8525.
- (26) Misra, R.; Jadhav, T.; Dhokale, B.; Mobin, S. M.; *Chem. Commun.*, **2014**, *50*, 9076-9078.
- (27) Farnum, D. G.; Mehta, G.; Moore, G. G. I.; Siegal, F. P.; *Tetrahedron Lett.*, **1974**, *15*, 2549-2552.
- (28) Hao, Z.; Iqbal, A.; *Chem. Soc. Rev.*, **1997**, *26*, 203-213.
- (29) Zhou, E.; Yamakawa, S.; Tajima, K.; Yang, C.; Hashimoto, K.; *Chem. Mater.*, **2009**, *21*, 4055-4061.
- (30) Chandran, D.; Lee, K.-S.; *Macromol Res.*, **2013**, *21*, 272-283.
- (31) Veldman, D.; Meskers, S. C. J.; Janssen, R. A. J.; *Adv. Funct. Mater.*, **2009**, *19*, 1939-1948.
- (32) Pavlishchuk, V. V.; Addison, A. W.; *Inorganica Chimica Acta*, **2000**, *298*, 97-102.

(33) Bredas, J.-L.; *Mater. Horizons*, **2013**, *1*, 17-19.

Chapter 3

Exploring the Effect of Donor Substituents in Pyridine Capped Diketopyrrolopyrrole Based Small Molecules in Photovoltaics

3.1 Abstract

We describe the synthesis, photophysical, electrochemical, and photovoltaic properties of a series of pyridine capped DPP small molecules having different donor substituents on both ends. Different alkyl groups were employed for solubility reasons. Organic photovoltaic cells with the structure ITO/PEDOT: PSS/PyDPP donors: PC₆₁BM/LiF/Al were fabricated. Pyridine capped DPP with hexyloxy triphenylamine and benzothiophene attached to pyridine capped DPP (PyDPPEH(TPA)₂ and PyDPPEH(BTH)₂) achieved very low efficiency of 0.1 %. The benzofuran and bithiophene having butyloctyl chains PyDPPBO(BF)₂, PyDPPBO(bithio)₂ and hexyldecyl chains PyDPPHD(bithio)₂ on the DPP core show MPP upto 0.87mW/cm², 1.77mW/cm², and 1.87mW/cm² respectively. We replaced MoO₃ with PEDOT: PSS hole transporting layer and fabricated solar cells. With the optimization of total concentration of the donor and acceptor in the ratio of 1:1 we successfully achieved a PCE of 1.56 % for PyDPPHD(bithio)₂.

3.2 Introduction

In the research area of bulk heterojunction organic solar cells, numerous donor and acceptor units have been linked together for constructing small molecules and polymers which meet the basic criteria for achieving higher performance.¹⁻⁷ Among the most efficient building blocks, 2,5-dihydropyrrolo[3,4-c]pyrrole-1,4-dione (DPP) has widely been utilized for constructing D–A type polymers and small molecules which are promising building block for photoactive materials in organic electronics.⁸⁻¹⁰ The electron density of DPP can be altered by utilizing different hetero-aromatic flanking groups and was studied extensively.¹¹⁻¹⁴

In 2013, pyridine capped DPP as an electron-accepting unit with a 2,2-bithiophene donor was used for synthesizing a D–A type copolymer **117** which showed deep HOMO energy level of 5.8 eV. The fabricated BHJ from **117** resulted in higher V_{oc} of over 0.9 V with a PCE of 4.9 %.¹⁵ The same polymer performed a high ambipolar charge transport with a record high electron mobility value of 6.30 cm²/Vs and hole mobility of 2.78 cm²/Vs in OTFT devices.¹⁶ Weiwei Li and co-workers studied a series of pyridine capped DPP polymer conjugated with different aromatic groups having strong electron donating unit dimethoxy-bithiophene **120**, weak electron donating units like benzodithiophene **119** and thiophene **116**. Pyridine bridge DPP polymers **116**, **119** and **120** as electron donors blended with PC₇₁BM as electron acceptor were further applied onto photovoltaic devices, sandwiched between the transparent ITO/PEDOT:PSS front and the reflecting Ca/Al back electrodes. Best performance was obtained for devices spin coated from chloroform

solution with 5 % vol. DIO as additive and the ratio of donor to acceptor was 1: 2. The presence of dimethoxybithiophene provides low V_{oc} of 0.53 V where as the polymer **119**, **116** showed high V_{oc} of 0.86 V and 0.76 V due to their deep HOMO level. The power conversion efficiency of solar cells for the polymers **116**, **119** and **120** were found to be 2.4 %, 2.2 % and 1.4 % respectively.¹⁷ The structure of pyridine capped DPP polymers are given in the Figure 3.1.

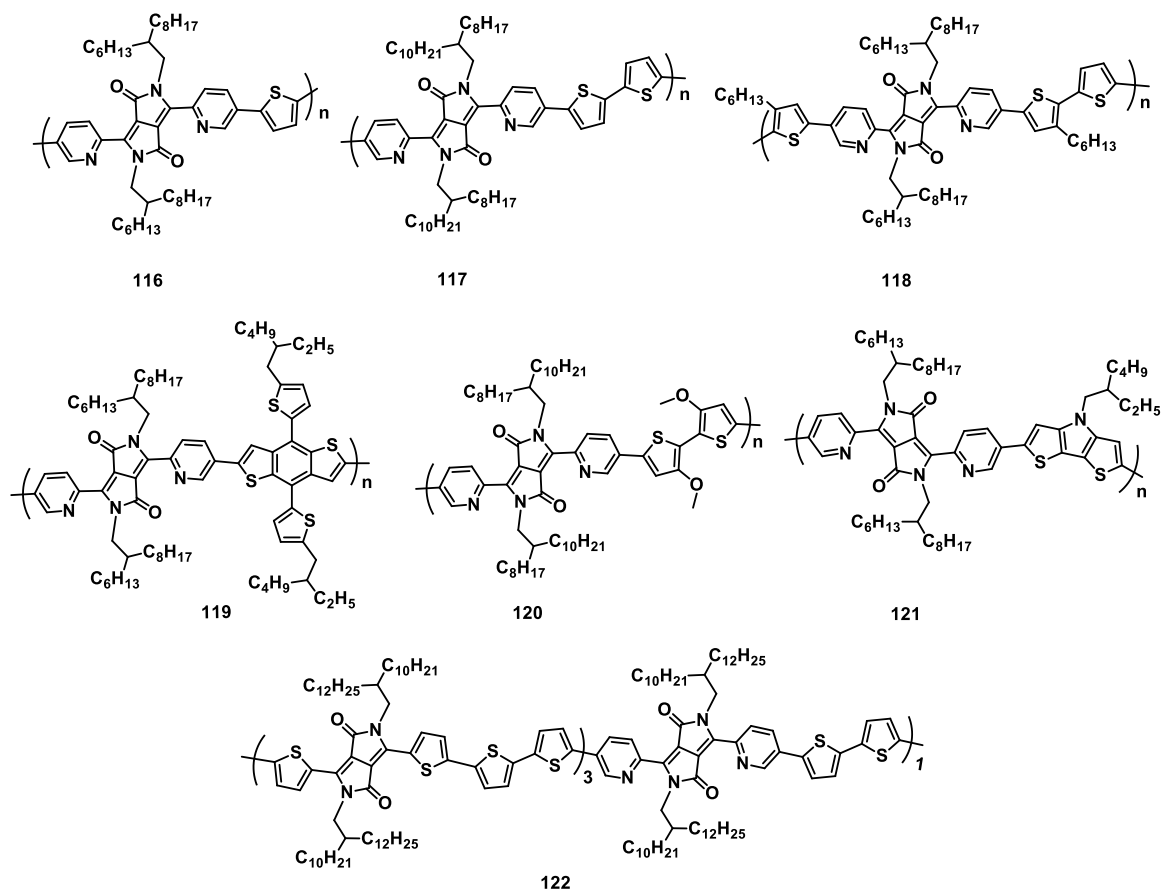


Figure 3.1 Chemical structure based on pyridine capped diketopyrrolopyrrole donor polymers

Janssen and co-workers synthesized a series of pyridine capped DPP polymers with varying donor strength thiophene < bithiophene < terthiophene < dithienopyrrole **116**, **117**, **118**, and **121** respectively. The gap between the LUMOs of the donor polymers and the acceptor (PC₆₁BM/PC₇₁BM) which is defined as Δ LUMO lies between 0.41 to 0.52 eV. Since the strength of the donor units which determines the HOMO level of the polymers and the Δ HOMO (the difference between HOMO of the donor and HOMO of the acceptor) of **116**, **117**, **118** and **121** with PC₆₁BM/PC₇₁BM is found to be 0.43, 0.52, 0.70, and 0.99 eV respectively. The charge generation via excitation of the donor readily produces charges at Δ LUMO = 0.4 eV. In contrast, charges produced via excitation of acceptor PC₆₁BM/PC₇₁BM, only happens when Δ HOMO > 0.7 eV. The PCE of the solar cell with a device structure ITO/MoO₃/ **116** , **117** , **118** & **121** : PC₆₁BM/LiF/Al is found to be 4.61 %, 7.13 %, 5.97 % and 4.87 %.¹⁸ Jo and co-workers synthesized random copolymers **122** composed of electron donating bithiophene and two different electron accepting units' pyridine and thiophene capped DPP in the ratio of 3: 1. The best efficiency obtained from the solar cell device **122** : PC₇₁BM is 8.11 %.¹⁹

Small molecules based on pyridine capped DPP having electronically identical but structurally different molecules from **123** to **126** were synthesized and their photovoltaic properties were studied. The molecule **123** having no alkyl chain on thiophene and hexyl chain substitution at 3, 4, and 5 positions on the thiophene ring were denoted as **124**, **125**, and **126** respectively.

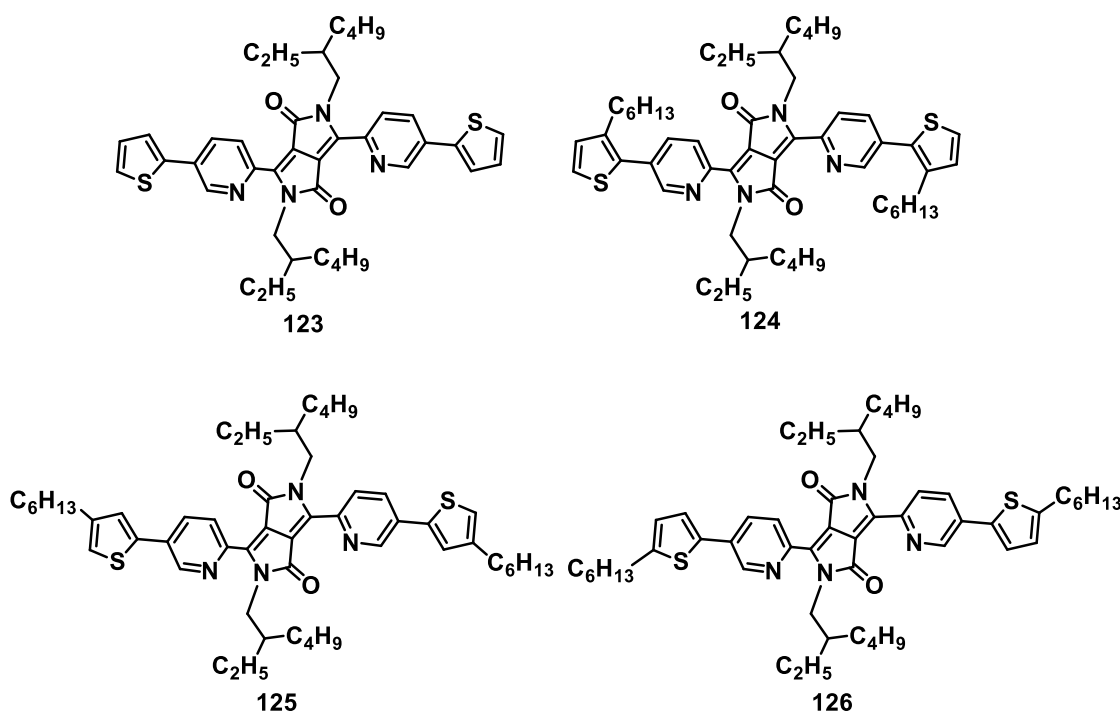


Figure 3.2 Structure of pyridine capped DPP small molecules

The molecule **123** and **124** shows H - aggregates where as **125** and **126** exhibit J-aggregates which is evident from absorption, fluorescence and lifetime measurement. The photovoltaic properties have a prominent impact on the arrangement of molecules in thin film. Thus the active layer treated with CS₂ vapor for the molecules **123** and **124** achieved an efficiency of 0.14 % and 0.23 % where the molecules **125** and **126** exhibits higher efficiency of 1.05 % and 2.60 %.²⁰

Table 3.1 Photovoltaics properties of pyridine capped DPP polymers and small molecules

SL.No	Active Layer (D:A)	Annealing	V _{oc} (V)	J _{sc} (mA/cm ²)	FF	PCE %	Ref
1)	116:PC ₇₁ BM (1:2)	rt	0.79	4.80	0.64	2.4	17
2)	116:PC ₆₁ BM (1:2)	rt	1.00	7.48	0.61	4.61	19
I 3)	116:PC ₇₁ BM (1:2)	rt	0.99	7.00	0.59	4.14	19
4)	117:PC ₇₁ BM (1:2)	rt	0.92	7.96	0.65	4.88	15
5)	117:PC ₆₁ BM (1:2)	rt	0.97	11.34	0.64	7.13	19
6)	117:PC ₇₁ BM (1:2)	rt	0.98	11.38	0.61	6.85	19
7)	118:PC ₆₁ BM (1:2)	rt	0.85	11.10	0.62	5.97	19
8)	118:PC ₇₁ BM (1:2)	rt	0.84	11.24	0.59	5.68	19
9)	119:PC ₇₁ BM (1:2)	rt	0.86	4.70	0.55	2.20	17
10)	120:PC ₇₁ BM (1:2)	rt	0.53	5.00	0.54	1.40	17
11)	121:PC ₆₁ BM (1:2)	rt	0.71	11.68	0.58	4.87	19
12)	121:PC ₇₁ BM (1:2)	rt	0.71	12.61	0.56	5.02	19
10)	122:PC ₇₁ BM (1:2)	rt	0.69	16.44	0.71	8.11	19
11)	123: PC ₇₁ BM (2:1)	rt	0.95	0.74	0.24	0.14	20
12)	124:PC ₇₁ BM (2:1)	rt	0.79	1.16	0.26	0.23	20
N 13)	125:PC ₇₁ BM (2:1)	rt	1.00	5.40	0.48	2.60	20
14)	126:PC ₇₁ BM (2:1)	rt	0.84	3.49	0.36	1.05	20

In this chapter, a series of pyridine capped DPP based small molecules were designed as donor material for organic solar cells. Two kinds of structural variations have been considered, one being changing the donor groups on both ends and the other being varying alkyl chain on the DPP core for solubility. The structures are given in the Figure 3. 3.

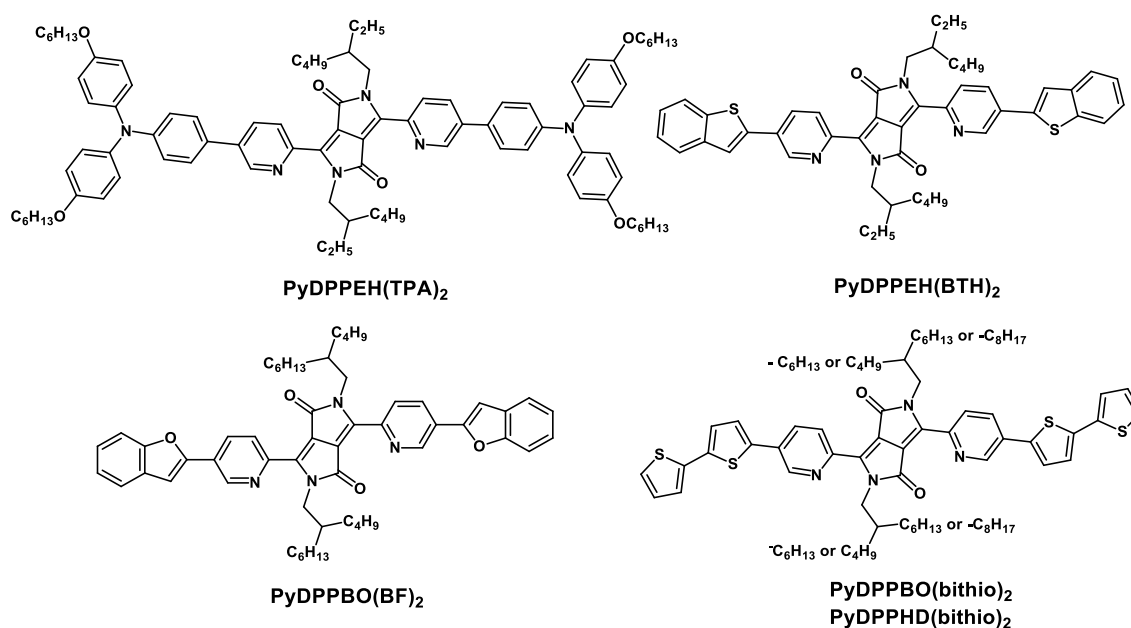
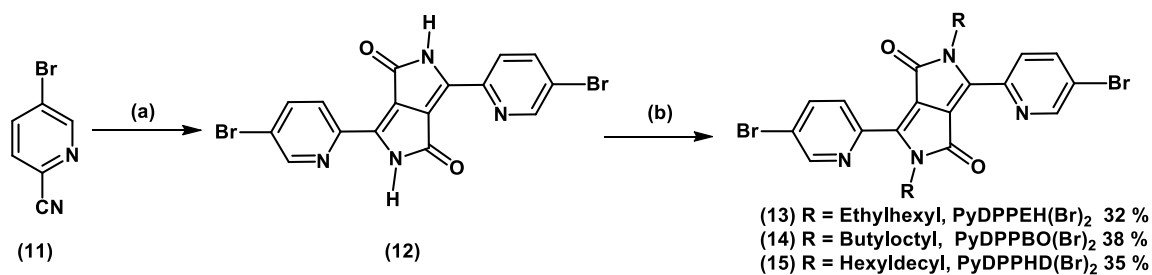


Figure 3. 3 Structures of pyridine capped DPP based small molecules.

3.3 Results and Discussion

3.3.1 Synthesis

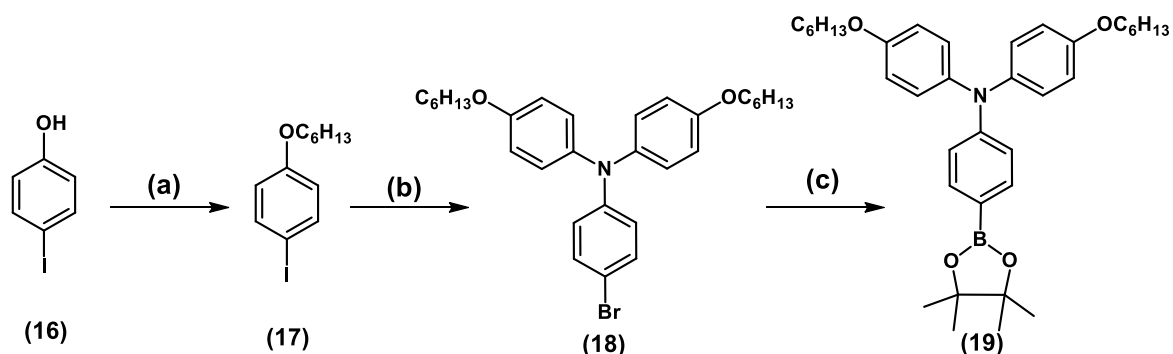
We adopted the literature procedure for the synthesis of pyridine capped DPP **12** from the starting materials 5-bromopyridine carbonitrile **11** and diethyl succinate using a traditional pseudo-Stobbe condensation reaction. Then the pyridine capped DPP core **12** was alkylated with different alkyl chains such as ethylhexyl, butyloctyl, and hexyldecyl using corresponding alkyl bromides in presence of K₂CO₃ in DMF at 110 °C (Scheme 3.1). The reaction provided ethylhexyl, butyloctyl, and hexyldecyl derivatives of **12** in 32 %, 38 %, and 35 % yield respectively.¹⁵ The different alkylated derivatives were denoted as PyDPPEH(Br)₂, PyDPPBO(Br)₂, and PyDPPHD(Br)₂.



Scheme 3.1 Reaction condition (a) Na, tert-amyl alcohol, diethyl succinate, 110 °C, overnight, (b) DMF, K₂CO₃, R-X, 100 °C, 12 h.

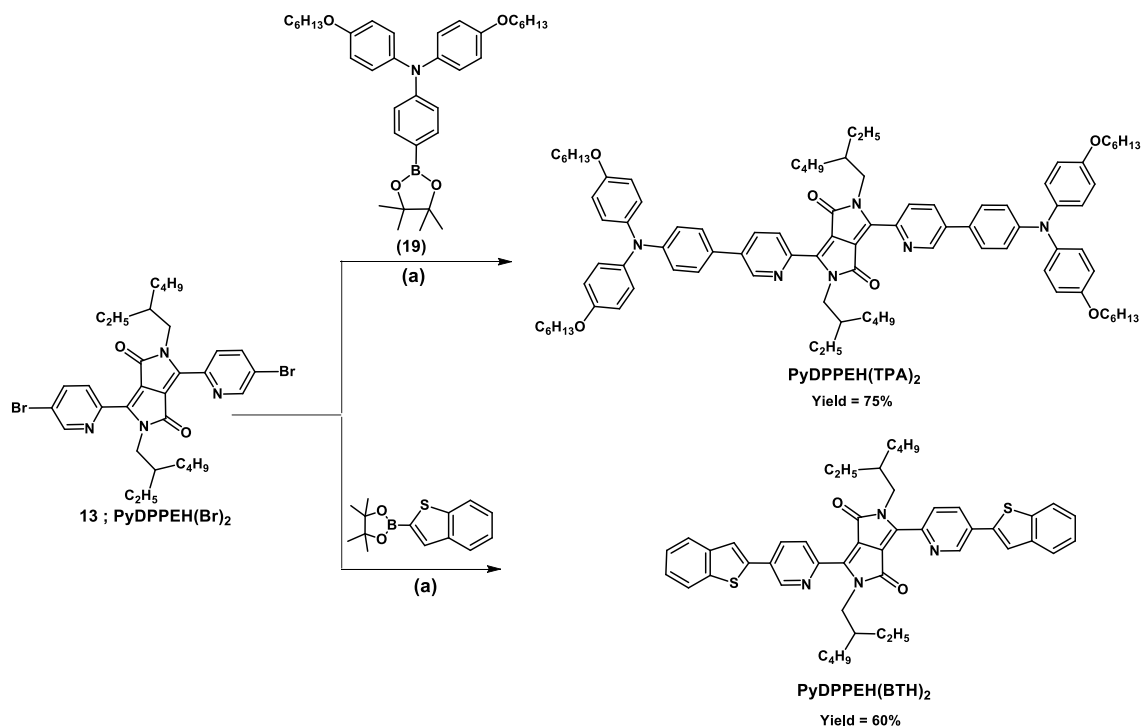
The synthesis of 4,4,5,5-tetramethyl-2-{4-[N,N-bis(4-hexyloxyphenyl)amino]phenyl}-1,3,2-dioxaborolane **19** is given in the Scheme 3.2. The reaction starts with the alkylation of *p*-hydroxyiodobenzene **16** in the presence of hexyl bromide under basic conditions. Then, 4-bromo-N,N-bis(4-(hexyloxy)phenyl)aniline **18** was synthesized by the Ullman reaction condition between the 4-bromoaniline and 1-(hexyloxy)-4-iodobenzene **17**, in the presence of catalytic amount of CuI and 1,10 phenanthroline refluxed in the Dean-Stark apparatus for 36 hours. This reaction yielded 65 % of the product. This is followed by the boronylation of **18** with bis(pinacolato)diboron in the presence of Pd(dppf)₂Cl₂ and potassium acetate in dry dioxane for 24 hours. The final product **19** was obtained in 60 % yield.²¹

The final synthetic step of PyDPPEH(TPA)₂ and PyDPPEH(BTH)₂ is given in the Scheme 3.3. The palladium catalyzed Suzuki-Miyaura coupling of PyDPPEH(Br)₂ and **19**, in the 4 : 1 : 0.5 mixture of toluene : ethanol : water under basic and argon conditions yielded 75 % of PyDPPEH(TPA)₂. In the same way on coupling between 2-(benzo[b]thiophen-2-yl)-4,4,5,5-tetramethyl-1,3,2-dioxaborolane and



Scheme 3.2 Reaction Conditions (a) $\text{C}_6\text{H}_{13}\text{Br}$, K_2CO_3 DMF, 100°C , 90 % (b) 4-bromoaniline, CuI , 1,10 phenanthroline, KOH , Toluene, refluxed, 36 h 65 % (c) Bis(pinacolato)diboron, $\text{Pd}(\text{ddpf})_2\text{Cl}_2$, CH_3COOK , dry Dioxane, 85°C , 24 h 60 %.

$\text{PyDPPEH}(\text{Br})_2$ under similar reaction conditions resulted in 60 % of $\text{PyDPPEH}(\text{BTH})_2$. Following the above conditions for Suzuki-Miyaura coupling,

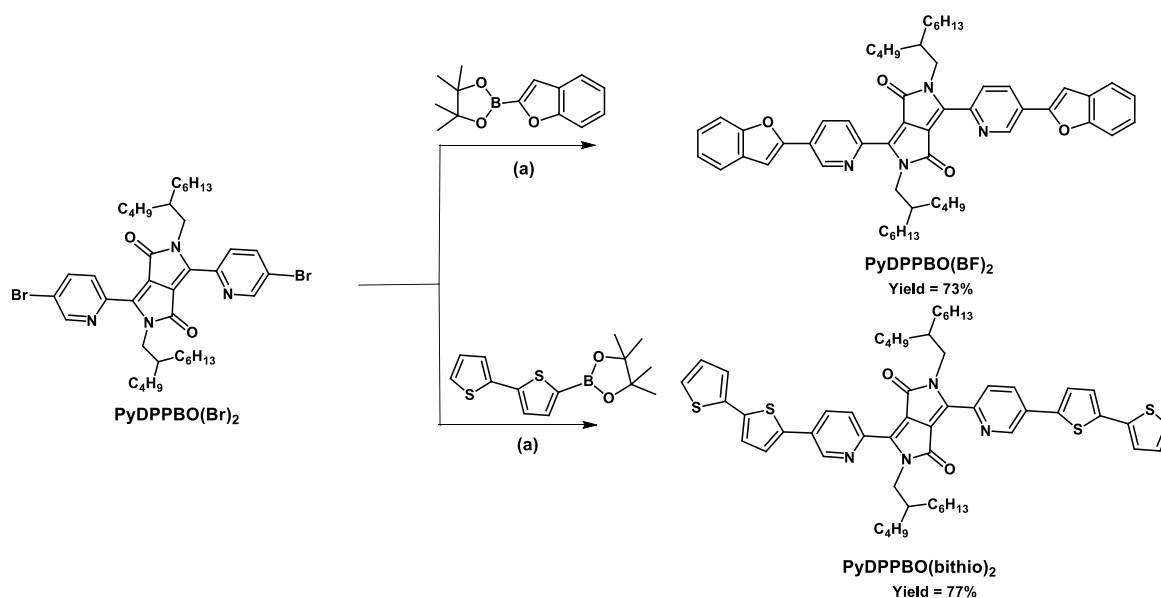


Scheme 3.3 Reaction condition (a) $\text{Pd}(\text{PPh}_3)_4$, K_2CO_3 , Toluene : Ethanol : H_2O , 90°C , 24 h

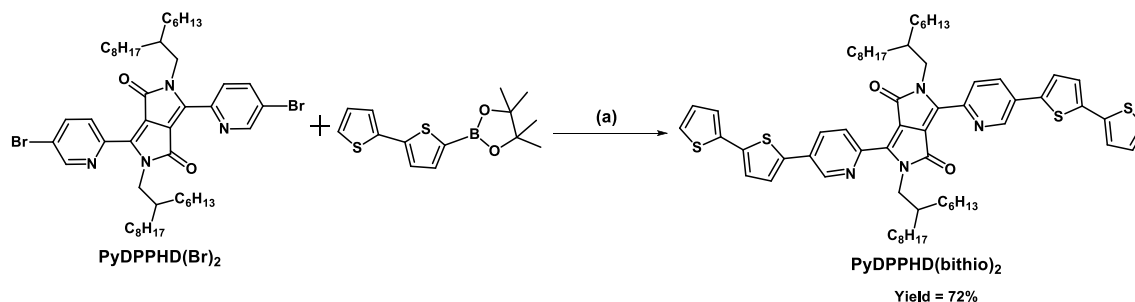
$\text{PyDPPBO}(\text{BF})_2$ and $\text{PyDPPBO}(\text{bithio})_2$ were synthesized from $\text{PyDPPBO}(\text{Br})_2$ and respective boronic esters of benzofuran and bithiophene in 73 % and 77 % yields

(Scheme 3.4). In the similar fashion PyDPPHD(bithio)₂ was synthesized from corresponding PyDPPHD(Br)₂ and boronic ester of bithiophene in 72% yield.

(Scheme 3.5)



Scheme 3.4 Reaction condition (a) Pd(PPh₃)₄, K₂CO₃, Toluene : Ethanol : H₂O, 90 °C, 24 h



Scheme 3.5 Reaction condition (a) Pd(PPh₃)₄, K₂CO₃, Toluene : Ethanol : H₂O, 90 °C, 24 h

3.3.2 Optical properties

The optical properties of pyridine capped DPP small molecules were determined by measuring the absorption in chloroform solution and spin coated thin films (Figure 3.4). The spectral characteristics are summarized in Table 3.2. The spectra represent

the optical transitions between the π and π^* orbitals of the conjugated backbone. The more intense and lowest-energy absorption bands (500–620 nm) are assigned to π - π^* transitions with intramolecular charge transfer character between the electron-rich and electron-deficient moieties, while the weaker high energy bands (350 – 450 nm) are ascribed to localized electronic transitions of the aromatic rings. The absorption spectra of all five compounds shifted bathochromically while going from solution to thin films on quartz substrates. This shift is a consequence of the intermolecular interactions that occur in the solid state and the increased molecular order. The shift is accompanied by the appearance of more-resolved vibronic structure and an enhanced relative intensity of the localized π - π^* absorption bands. The absorption spectrum of the PyDPPEH(TPA)₂ having a broader absorption due to increase in the strength of donor hexyloxytriphenylamine at a maximum of 575 nm, and 630 nm in solution and solid state respectively. The optical band gaps (E_g) in

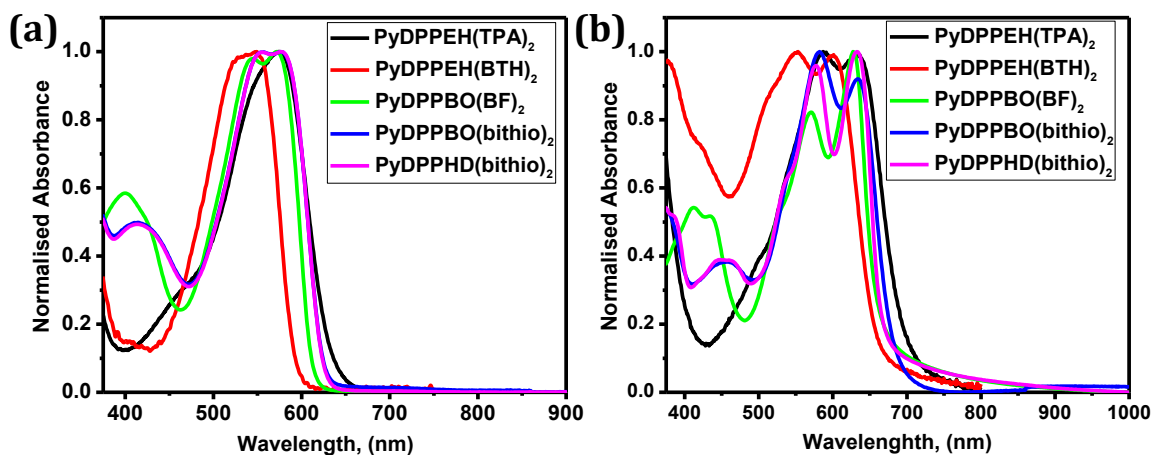


Figure 3.4 Normalized absorption spectra of pyridine DPP small molecules (a) CHCl₃ solution (b) thin film

Table 3.2 Summary of photophysical properties of pyridine capped small molecules

Compound	Absorption			
	λ_{max}^{sol} (nm)	λ_{max}^{film} (nm)	λ_{edge}^{film} (nm)	E_{gap}^{opt} (eV)
PyDPPEH(TPA) ₂	575	630	720	1.72
PyDPPEH(BTH) ₂	550	600	678	1.82
PyDPPBO(BF) ₂	578	627	673	1.84
PyDPPBO(bithio) ₂	578	578, 632	686	1.80
PyDPPHD(bithio) ₂	578	577, 630	686	1.80

the solid state are in the range of 1.72 – 1.84 eV, as determined from the onsets of the absorption at low energy.

3.3.3 Electrochemical Properties

The electrochemical properties of five pyridine capped DPP small molecules were evaluated by cyclic voltammetry in dry dichloromethane solution under inert atmosphere (Figure 3.5 and 3.6). The corresponding redox potentials are summarized in Table 3.3. All five compounds showed two reversible oxidation and one reduction waves. The HOMO and LUMO energy levels were estimated from the onset of the first oxidation and reduction waves, respectively. The first oxidation potential of PyDPPEH(TPA)₂ with respect to Fc/Fc⁺ is +0.22 V, which clearly shows that the oxidation takes place from the hexyloxytriphenylamine donor. The end donor group benzothiophene, benzofuran, and bithiophene attached to the pyridine capped DPP oxidation potential are +0.63 V, +0.65 V, +0.59 V and reduction

potential are -1.30 V, -1.34 V, -1.37 V and hence the four derivatives possess virtually identical HOMO and LUMO energies. Using these redox potentials, the

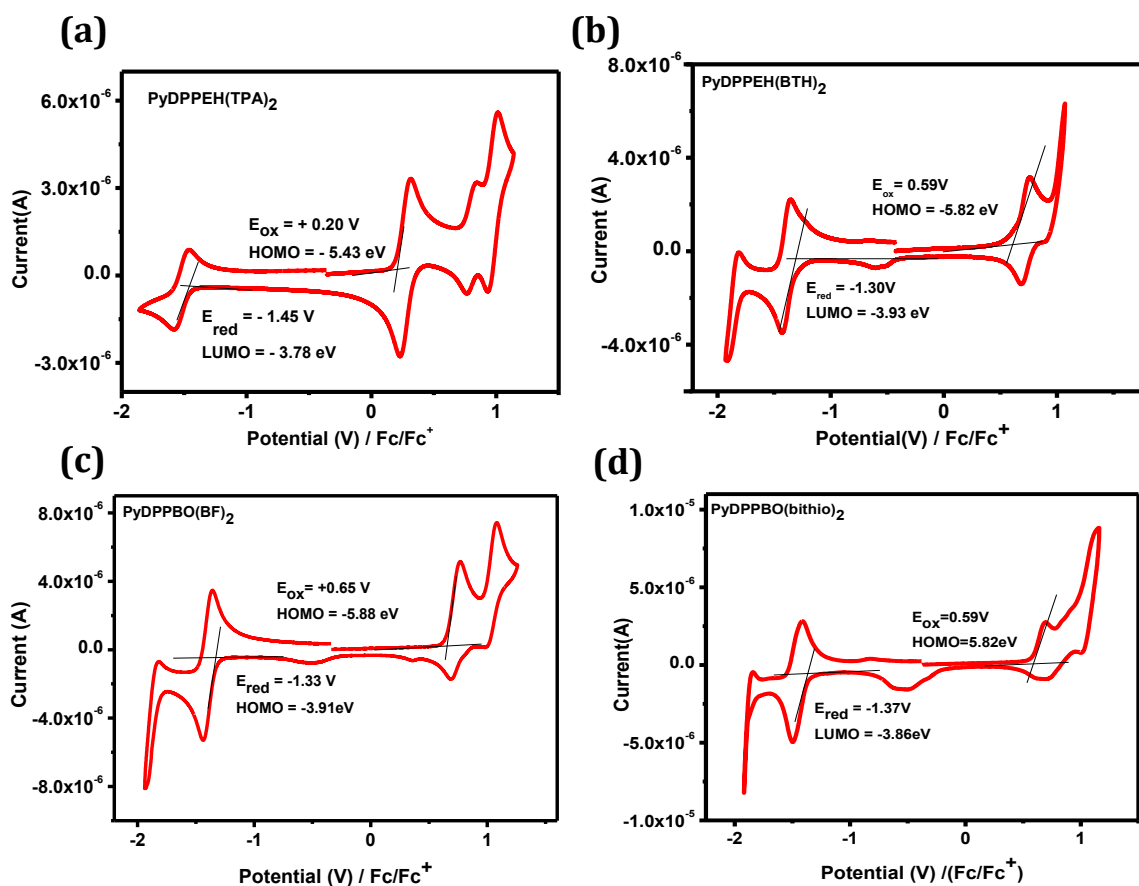


Figure 3.5 Cyclic voltammograms of (a) PyDPPEH(TPA)₂ and (b) PyDPPEH(BTH)₂ (c) PyDPPBO(BF)₂ (d) PyDPPBO(bithio)₂

HOMO and LUMO levels were estimated using equation $E = -5.23 - qE_{\text{redox}}$.²²⁻²⁴ The relatively low-lying HOMO energies are due to the synergistic electron-withdrawing character of the DPP core and the pyridine moieties. The low HOMO level is expected to give a high V_{oc} in photovoltaic devices. There is a good correlation between the optical and the electrochemical gaps, with slightly lower values estimated for the

optical gaps. This could be related to the exciton binding energy which lowers the optical gap relative to the HOMO–LUMO difference, which involves the exchange

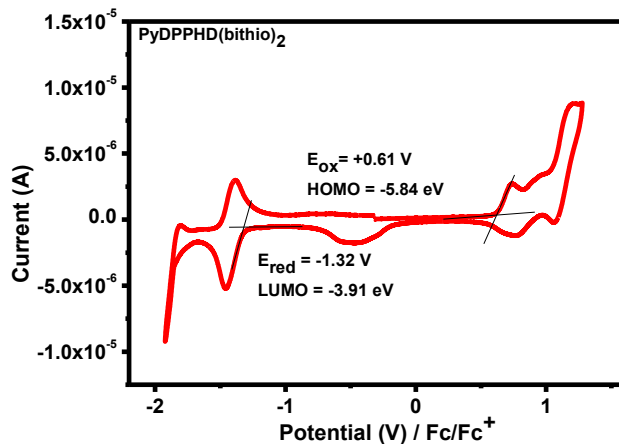


Figure 3.6 Cyclic voltammogram of PyDPPHD(bithio)₂

energy and the difference in solvation energy for ions in solution compared to the neutral molecules.²⁵

3.3.4 Thermal properties

To assess the thermal stability and behavior of the five small molecules based on pyridine capped DPP, all the derivatives were characterized by TGA and DSC. TGA analysis revealed that 5% weight-loss temperatures (T_d) of PyDPPEH(TPA)₂, PyDPPEH(BTH)₂, and PyDPPBO(BF)₂ are 377 °C, 360 °C, and 368 °C respectively. The bithiophene end group small molecules PyDPPBO(bithio)₂ and PyDPPHD(bithio)₂ showed same temperature at 347 °C and profile in the TG analysis. Thus all the five molecules were thermally stable enough for the application of solar cells. The T_d has a sequence of PyDPPEH(TPA)₂ > PyDPPBO(BF)₂ > PyDPPEH(BTH)₂ > PyDPPBO(bithio)₂ suggesting that the triphenylamine and

fused aromatic group have enhanced thermal stability than the aromatic bithiophene.

Table 3.3 Electrochemical properties of pyridine capped DPP small molecules

Compound	Cyclic voltammetry				
	E_{ox}^{sol} (V)	E_{red}^{sol} (V)	HOMO(eV) ^a	LUMO(eV) ^a	E_{gap}^{cv} (eV) ^b
PyDPPEH(TPA) ₂	+0.22	-1.45	-5.0	-3.78	1.22
PyDPPEH(BTH) ₂	+0.63	-1.30	-5.86	-3.93	1.89
PyDPPBO(BF) ₂	+0.65	-1.33	-5.88	-3.91	1.97
PyDPPBO(bithio) ₂	+0.61	-1.34	-5.84	-3.89	1.96
PyDPPHD(bithio) ₂	+0.61	-1.34	-5.84	-3.89	1.93

^a Onset potentials vs. Fc/Fc⁺ converted via: $E = -5.23 - qE_{redox}$. ^b $E_{gap}^{cv} = q(E_{ox} - E_{red})$.

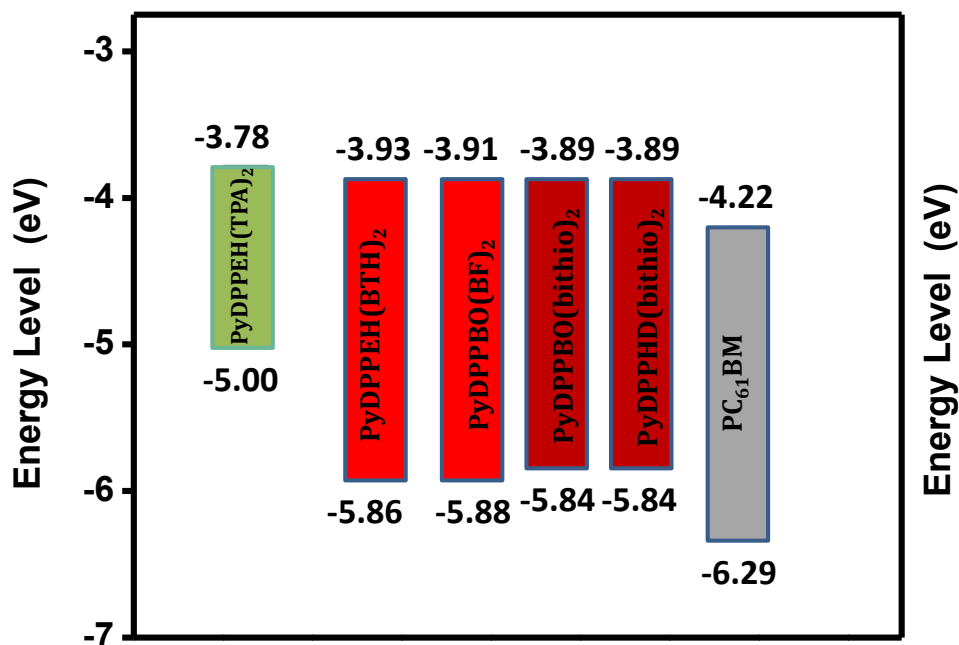


Figure 3.7 Energy level diagram of pyridine capped DPP small molecules

The thermal properties of the pyridine capped DPP small molecules were characterized by DSC measurements. Sharp endothermic peaks corresponding to the melting process were observed. Due to the presence of bithiophene, both PyDPPBO(bithio)₂ and PyDPPHD(bithio)₂ ($T_m = 183$ °C) displayed lower melting temperatures than the PyDPPBO(BF)₂ ($T_m = 202$ °C). PyDPPEH(BTH)₂ and PyDPPEH(TPA)₂ indicate a higher melting temperature of 247 °C and 245 °C and latter doesn't crystallize.

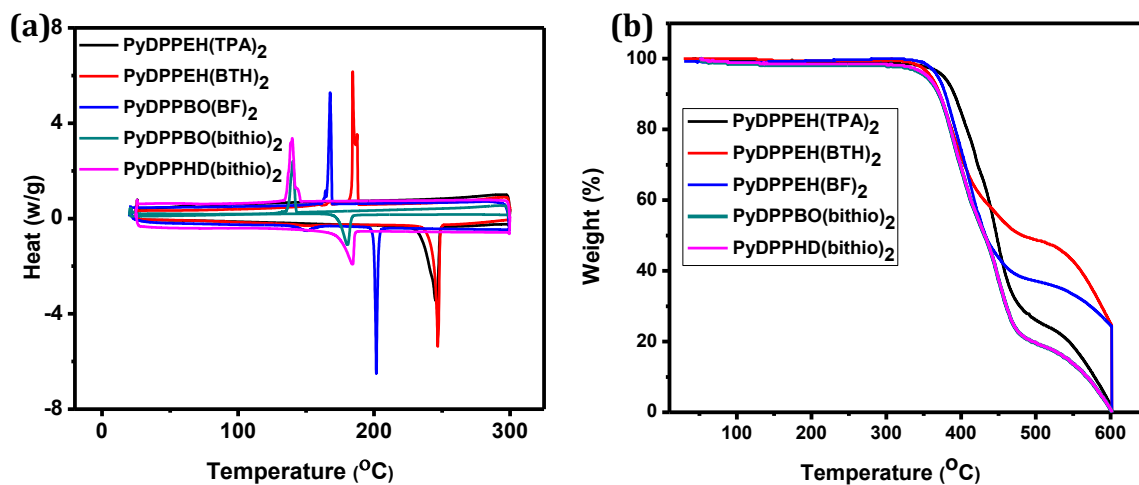


Figure 3.8 (a) DSC and (b) TGA of five pyridine capped DPP derivatives.

3.3.5 Photovoltaic properties

The small molecules were applied in bulk heterojunction solar cells with PC₆₁BM as the acceptor material. The solubility of the five pyridine DPP derivatives in the chlorinated solvents were found to be in the order of PyDPPHD(bithio)₂ > PyDPPBO(bithio)₂ > PyDPPBO(BF)₂ > PyDPPEH(TPA)₂ > PyDPPEH(BTH)₂. The active layers were spin-coated from CHCl₃ solution onto an ITO covered glass substrate covered by a 40 nm film of PEDOT:PSS. LiF (1 nm) and Al (100 nm) were thermally

evaporated as the top electrode. A distinct photovoltaic effect has been observed for each of the five blends. For each blend a 1:1 weight ratio was found to be optimal. Additives like DIO, o-DCB and 1-CN are used for the optimization of solar cell devices.²⁶⁻³⁰ The effects of annealing were studied at 110 °C for 10 minutes. The optimization of solar cell devices for PyDPPEH(TPA)₂:PC₆₁BM in 1:1 ratio with the total concentration of 20 mg/mL is given the Table 3.4. The MPP obtained is only 0.10 mW/cm². The J-V characteristics of the best device PyDPPEH(TPA)₂:PC₆₁BM solar cell is given in the Figure 3.9.

Table 3.4 Characteristics of PyDPPEH(TPA)₂:PC₆₁BM devices under 100 mW/cm² white light illumination

PyDPPEH(TPA) ₂ : PCBM (1:1)	Annealing	V _{oc} (V)	Fill Factor	J _{sc} (mA/cm ²)	MPP (mW/cm ²)
CHCl ₃	rt	0.76	0.26	0.51	0.10
	110 °C	0.34	0.23	0.07	0.01
0.2% DIO/CHCl ₃	rt	0.79	0.26	0.44	0.09
	110 °C	Leakage current			
0.2% O-DCB/CHCl ₃	rt	0.79	0.27	0.44	0.10
	110 °C	Leakage current			
0.2% 1-CN/CHCl ₃	rt	0.80	0.27	0.44	0.10
	110 °C	0.44	0.24	0.10	0.01

*Note: The MPP was estimated from the V_{oc}, FF and J_{sc} obtained from the J-V measurements. J-V characteristics were measured with a Keithley 2400 source meter under ~100 mW/cm² white light illumination from a tungsten-halogen lamp filtered by a Schott GG385 UV filter and a Hoya LB120 daylight filter that provides illumination conditions within ~10 % of 100 mW/cm² AM1.5G for most cells.

The solubility of PyDPPEH(BTH)₂ in chloroform, chlorobenzene and tetrachloroethylene is found to be ~ 7 mg/mL, ~ 5 mg/mL, and ~ 13 mg/mL respectively. Since the PyDPPEH(BTH)₂ have very low solubility and the spin coating of active layer in the CHCl₃ solution was done by the hot process at 60 °C. The total concentration of 20 mg/mL and 10 mg/mL in 1:1 ratio of PyDPPEH(BTH)₂ : PC₆₁BM were used for the active layer preparation. The details were summarized in the Table 3.5. The best efficiency obtained was 0.10 %, and J-V curve and EQE spectra are given in the Figure 3.10.

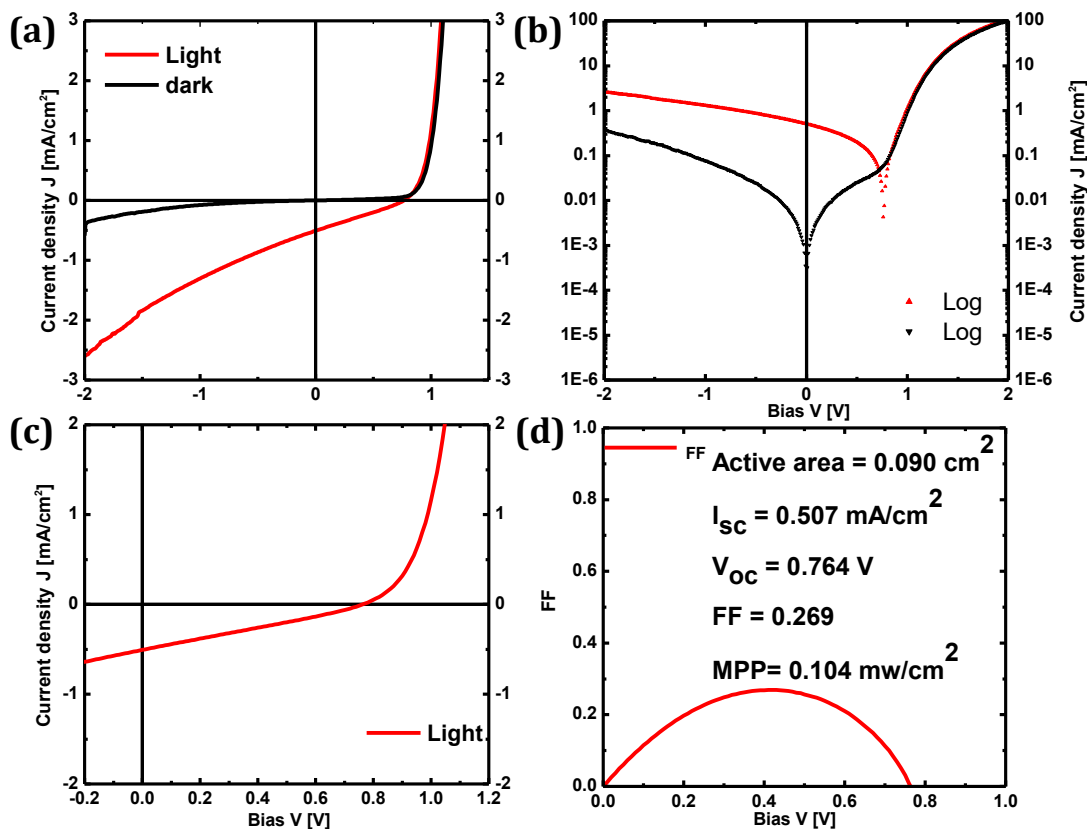


Figure 3.9 (a) J-V curve of PyDPPEH(TPA)₂ : PC₆₁BM in the dark and light. (b) Logarithmic plot of J-V curve of PyDPPEH(TPA)₂ : PC₆₁BM in the dark and light. (c) Zoomed portion of J-V curve PyDPPEH(TPA)₂ : PC₆₁BM in the light. (d) Fill Factor (FF) Vs Bias V (V) curve.

The pyridine analog of (DPP(TBFu)₂) having benzofuran on both ends of the pyridine capped DPP with butyloctyl chain coded PyDPPBO(BF)₂ were applied in the bulk heterojunction solar cells.³¹ The donor PyDPPBO(BF)₂ is higher solubility in CHCl₃ than the PyDPPEH(TPA)₂ and PyDPPEH(BTH)₂. The device optimization of PyDPPBO(BF)₂ is given in the Table 3.6. The best MPP obtained for PyDPPBO(BF)₂ :

Table 3.5 Characteristics of PyDPPEH(BTH)₂:PC₆₁BM (1:1) devices under 100mW/cm² white light illumination

Concentration mg/mL	Spin Coating (rpm)	Thickness (nm)	J _{sc} (mA/ cm ²)	V _{oc} (V)	FF	MPP (mA/ cm ²)	J _{sc} (mA/ cm ²) (SR)	PCE (%)
20	1500	83	0.43	0.49	0.25	0.05	0.39	0.04
10	700	66	0.87	0.49	0.26	0.11	0.84	0.10

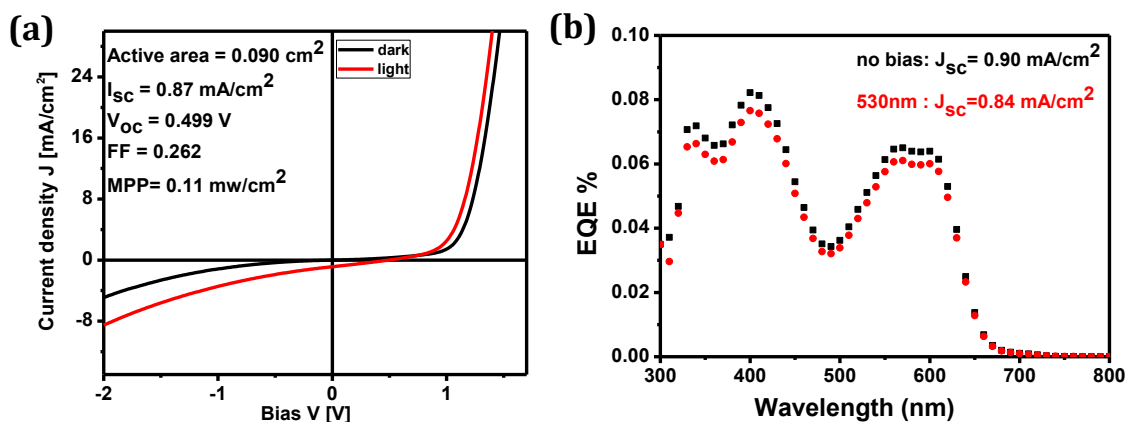


Figure 3.10 (a) Representative J-V curve for PyDPPEH(BTH)₂ : PC₆₁BM solar cell in dark (black) and under simulated A M 1.5G conditions (red). (b) EQE spectra of PyDPPEH(BTH)₂ : PC₆₁BM solar cell under low monochromatic light intensity and with 1 Sun equivalent light bias illumination. The numbers in the panels represent the J_{sc} that is obtained with convoluting the EQE with the solar A M 1.5G spectrum.

PC₆₁BM is 0.87 mW/cm² with J_{sc} 2.18 mA/cm², V_{oc} 0.85 V and FF 0.46 in the presence 0.2 % DIO in CHCl₃ solution. The J-V characterization of the solar cell device is given in the Figure 3.11.

The details of the solar cell device optimization of PyDPPBO(bithio)₂ and PyDPPHD(bithio)₂ are given in the Table 3.7 and 3.8 respectively. The optimized blend ratio of PyDPPBO(bithio)₂ : PC₆₁BM was 1:1, the active layer spin coated at 1500 rpm in CHCl₃ solution, maintained a thickness of 96 nm. In pure CHCl₃ solution, the MPP of 0.64 mW/cm² was obtained, with J_{sc} 3.43 mA/cm², V_{oc} 0.64 V, and FF 0.27. But the addition of 0.2 % DIO improved the MPP of 1.71 mW/cm² with a J_{sc} 5.32 mA/cm², V_{oc} of 0.78 V, and FF of 0.41.

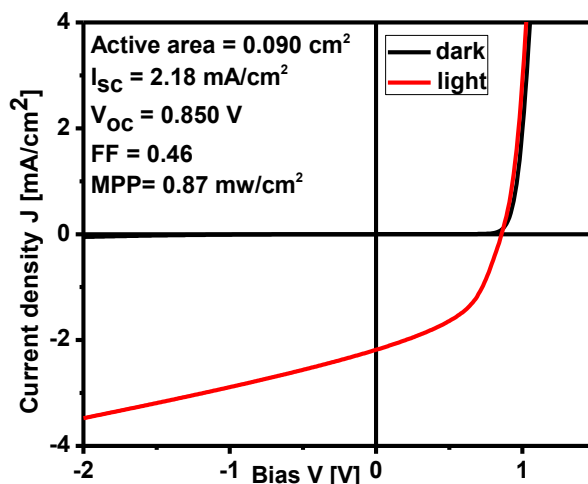


Figure 3.11 Representative J-V curve for PyDPPBO(BF)₂ : PC₆₁BM solar cell in dark (black) and under simulated A M 1.5G conditions (red).

The PyDPPHD(bithio)₂ : PC₆₁BM (1:1) blend solution was spin coated at 1800 rpm and the thickness of the active layer was maintained at 92 nm. In CHCl₃ solution, MPP was found to be 0.64mW/cm². Further optimization using a small

Table 3.6 Characteristics of PyDPPBO(BF)₂ : PC₆₁BM devices under 100mW/cm² white light illumination

Material	Solvent	Annea ling	J _{sc} (mA /cm ²)	V _{oc} (V)	FF	MPP (mW/ cm ²)
PyDPPBO(BF) ₂ :PCBM (1:1) Thickness = 101nm (1800 rpm)	CHCl ₃	rt	0.81	0.63	0.33	0.17
	CHCl ₃	110 °C	0.87	0.65	0.37	0.22
	0.2% DIO	rt	2.18	0.85	0.46	0.87
	0.2% DIO	110 °C	0.98	0.67	0.36	0.24
	0.2% o-DCB	rt	0.98	0.51	0.25	0.06
	0.2% o-DCB	110 °C	1.07	0.63	0.35	0.24
	0.2% 1-CN	rt	0.39	0.62	0.25	0.06
	0.2% 1-CN	110 °C	1.01	0.64	0.37	0.24

Table 3.7 Characteristics of PyDPPBO(bithio)₂ : PC₆₁BM devices under 100mW/cm² white light illumination

Material	solvent	Annea ling	J _{sc} (mA /cm ²)	V _{oc} (V)	FF	MPP (mW/ cm ²)
PyDPPBO(bithio) ₂ :PCBM (1:1) Thickness = 96nm	CHCl ₃	rt	2.96	0.64	0.29	0.57
	CHCl ₃	110°C	0.83	0.46	0.29	0.11
	0.2% DIO	rt	5.32	0.78	0.41	1.71
	0.2% DIO	110°C	4.23	0.63	0.37	1.00
	0.2% o-DCB	rt	2.81	0.67	0.28	0.54
	0.2% o-DCB	110°C	0.97	0.52	0.28	0.14
	0.2% 1-CN	rt	2.81	0.54	0.28	0.44
	0.2% 1-CN	110°C	1.10	0.28	0.28	0.13

amount of additive like DIO, *o*-DCB and 1-CN to manipulate the morphology during the film casting process.³² The addition of 0.2 % DIO and 0.2 % 1-CN increases the MPP to 1.77 mW/cm² and 1.86 mW/cm² respectively. The J-V characterization of the

best device for PyDPPBO(bithio)₂ : PC₆₁BM and PyDPPHD(bithio)₂ : PC₆₁BM are given in the Figure 3.12.

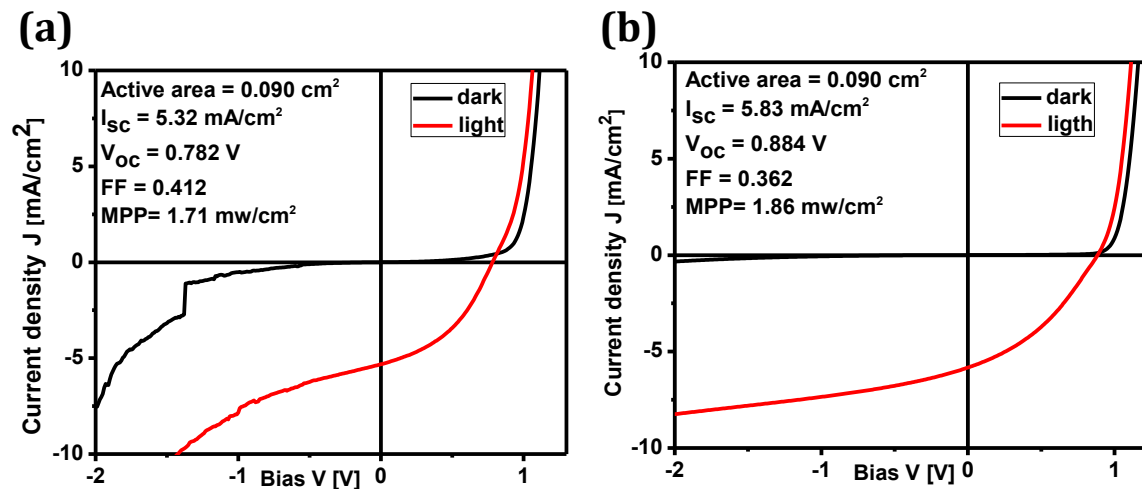


Figure 3.12 Representative J-V curve for (a) PyDPPBO(bithio)₂ : PC₆₁BM (1:1) 0.2 % DIO in CHCl₃ solution and (b) PyDPPHD(bithio)₂ : PC₆₁BM (1:1) 0.2 % 1-CN in CHCl₃ solution. Solar cell device in dark (black) and under simulated A M 1.5G conditions (red).

In order to study the effect of DIO volume fractions in CHCl₃ for PyDPPHD(bithio)₂ : PC₆₁BM device. We used 0.1, 0.2, 0.3, 0.4, 0.5, 1, 5, 2 % and found that 0.2 % shows

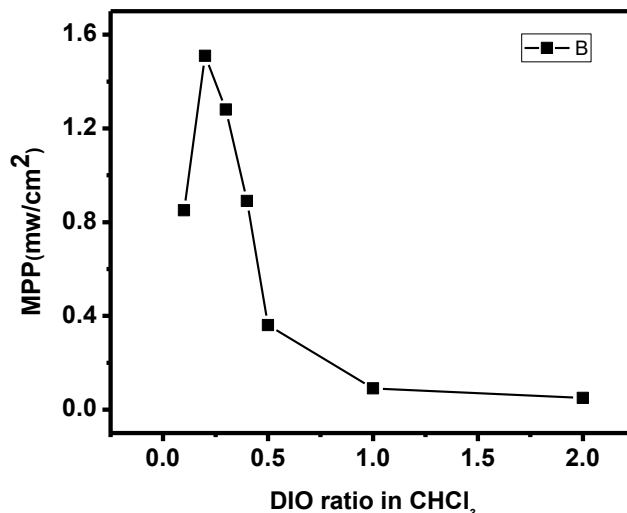


Figure 3.13 Plot of variation of DIO ratio in CHCl₃, PyDPPHD(bithio)₂ : PC₆₁BM (1:1)

the best performance. The device performance is summarized in Table 3.9, J-V characterization, and EQE is given in the Figure 3.14.

Table 3.8 Characteristics of PyDPPHD(bithio)₂: PC₆₁BM devices under 100mW/cm² white light illumination

Material	Solvent	Annea ling	J _{sc} (mA /cm ²)	V _{oc} (V)	FF	MPP (mW/cm ²)
PyDPPHD(bithio) ₂ : PCBM(1:1) Thickness = 92nm	CHCl ₃	rt	3.43	0.67	0.27	0.64
	CHCl ₃	110°C	2.70	0.68	0.38	0.70
	0.2% DIO	rt	5.31	0.88	0.37	1.77
	0.2% DIO	110°C	3.27	0.72	0.38	0.91
	0.2% o-DCB	rt	3.83	0.80	0.30	0.93
	0.2% o-DCB	110°C	3.40	0.72	0.39	0.97
	0.2% 1-CN	rt	5.83	0.88	0.36	1.86
	0.2% 1-CN	110°C	3.43	0.67	0.35	0.80

Table 3.9 Variation of DIO ratio in CHCl₃ PyDPPHD(bithio)₂: PC₆₁BM (1:1)

Percentage of DIO	J _{sc} (mA/cm ²)	V _{oc} (V)	FF	MPP (mW/ cm ²)
0.1%	3.78	0.75	0.29	0.85
0.2%	4.58	0.85	0.38	1.51
0.3%	4.13	0.80	0.38	1.28
0.4%	2.75	0.82	0.39	0.89
0.5%	1.70	0.87	0.42	0.62
1.0 %	0.38	0.72	0.31	0.08
2.0%	0.27	0.63	0.32	0.05

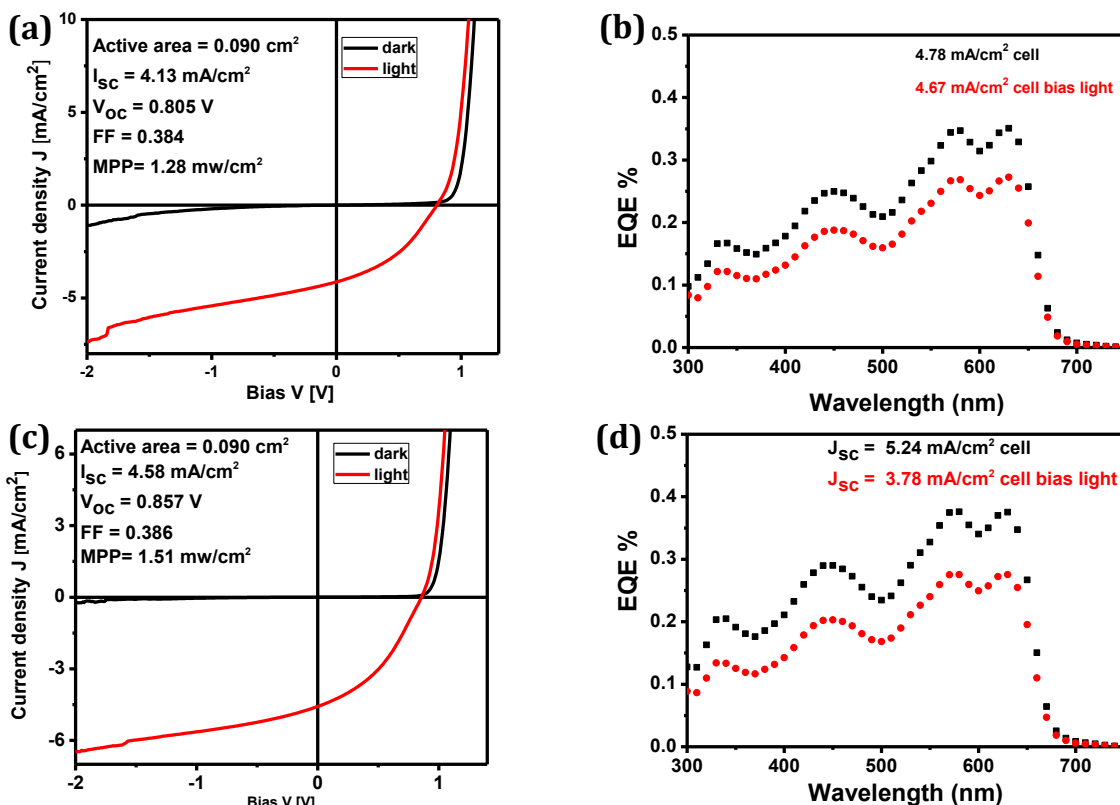


Figure 3.14 (a) and (c) Representative J-V curve for PyDPPHD(bithio)₂: PC₆₁BM active layer spin casted in 0.3 % and 0.2 % DIO additive in CHCl₃ respectively. Dark (black) and under simulated A M 1.5G conditions (red). (b) and (d) EQE spectra of PyDPPEH(bithio)₂: PC₆₁BM active layer spin casted in 0.3 % and 0.2 % DIO additive in CHCl₃ respectively. (Black) solar cell under low monochromatic light intensity and (red) with 1 sun equivalent light bias illumination. The numbers in the panels represent the J_{sc} that is obtained with convoluting the EQE with the solar AM 1.5G spectrum.

3.3.5.1. Effect of MoO₃ hole transporting layer and total concentration

The conventional PEDOT: PSS hole transporting layer produces S-shaped J-V characteristics for the active layer containing aromatic amines such as pyridine and thiazole.^{17,33-34} And the use of 10 nm MoO₃ solves this problem. Apart from that it also has other advantage like increasing the shelf-life of devices. In the device, the total concentration of donor and acceptor plays an important role in the

performance of the solar cells. Thus we maintained the thickness of the active layer between 90-100 nm by varying the total concentration and spin speed. The pyridine capped DPP molecules PyDPPBO(BF)₂, PyDPPBO(bithio)₂, and PyDPPHD(bithio)₂ were subjected to study the effect of total concentration on MoO₃ layer. The details of concentration depended studies of PyDPPBO(BF)₂ : PC₆₁BM (1:1) solar cell device from 12 mg/mL to 36 mg/mL is given in the Table 3.10. The best performance obtained for PyDPPBO(BF)₂ :PC₆₁BM solar cell with 20 mg/mL with a J_{sc} of 0.94 mA/cm², V_{oc} of 1.04 V, FF of 0.33 and a PCE of 0.33 %. J-V characterization and EQE for PyDPPBO(BF)₂:PC₆₁BM solar cell is given in the Figure 3.15. The optimum concentration for PyDPPBO(bithio)₂ and PyDPPHD(bithio)₂ is 30 mg/mL and 12 mg/mL respectively. The details are given in the Table 3.11 and 3.12. The PCE for PyDPPBO(bithio)₂ :PC₆₁BM solar cell is 1.07 % and J-V curve and EQE is given in the Figure 3.16. The best efficiency obtained among five small molecules is PyDPPHD(bithio)₂ with a PCE of 1.56 %. J-V curve and EQE is given in the Figure 3.17. More than 1.0% PCE value are obtained for the PyDPPHD(bithio)₂ : PC₆₁BM device with a concentration of 12 mg/mL, 16 mg/mL, and 36 mg/mL. Thus we studied the effect of additives in the device performance; spin coated in CHCl₃ solution with a concentration of 12 mg/mL and 36 mg/mL. The results are summarized in the Table 3.13 and 3.14. The performance of PyDPPHD(bithio)₂ : PC₆₁BM solar cell devices was detrimental in the presence of additives.

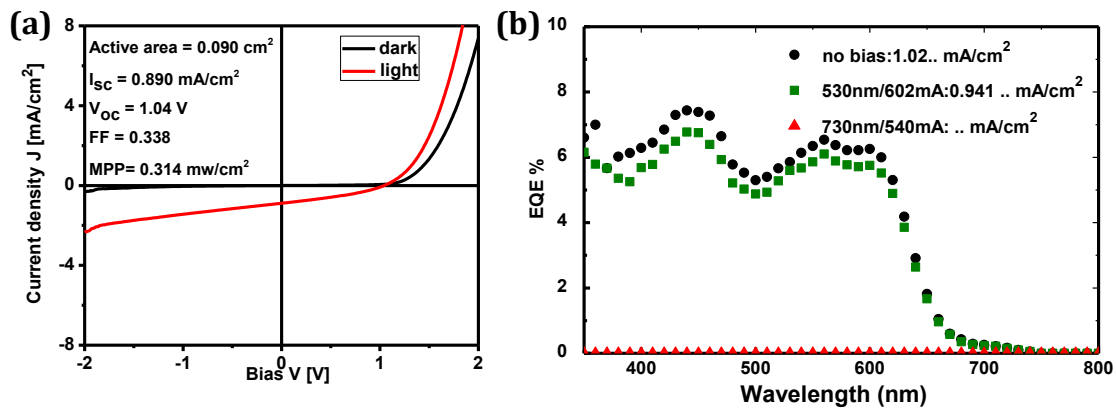


Figure 3.15 (a) Representative J-V curve for PyDPPBO(BF)₂ : PC₆₁BM solar cell in dark (black) and under simulated A M 1.5G conditions (red). (b) EQE spectra of PyDPPBO(BF)₂ : PC₆₁BM solar cell under low monochromatic light intensity and with 1 sun equivalent light bias illumination. The numbers in the panels represent the J_{sc} that is obtained with convoluting the EQE with the solar A M 1.5G spectrum.

Table 3.10 Characteristics of PyDPPBO(BF)₂:PC₆₁BM devices on MoO₃ hole transporting layer under 100mW/cm² white light illumination

Concentration (mg/mL)	Spin coating (rpm)	Thickness (nm)	J_{sc} (mA/cm ²)	V_{oc} (V)	FF	MPP (mW/cm ²)	J_{sc} (mA/cm ²) (SR)	PCE (%)
12	500	90	0.59	0.91	0.25	0.13	0.47	0.10
16	1100	92	0.90	0.99	0.32	0.29	0.94	0.30
20	1200	97	0.89	1.04	0.33	0.31	0.94	0.33
24	2200	122	1.01	0.93	0.30	0.32	0.64	0.18
30	2900	100	0.69	0.97	0.27	0.19	0.63	0.16
36	3550	98	0.73	1.09	0.30	0.23	0.68	0.22

Table 3.11 Characteristics of PyDPPBO(bithio)₂: PC₆₁BM devices on MoO₃ hole transporting layer under 100mW/cm² white light illumination

Concentration (mg/mL)	Spin coating (rpm)	Thickness (nm)	J _{sc} (mA/cm ²)	V _{oc} (V)	FF	MPP (mW/cm ²)	J _{sc} (mA/cm ²) (SR)	PCE (%)
16	1000	100	2.81	0.83	0.30	0.71	2.95	0.74
20	1500	107	3.09	0.89	0.30	0.85	3.21	0.88
24	2000	92	2.94	0.92	0.30	0.82	3.10	0.86
30	4000	97	3.39	0.95	0.30	0.98	3.70	1.07
36	4300	83	2.37	0.77	0.29	0.54	2.07	0.46

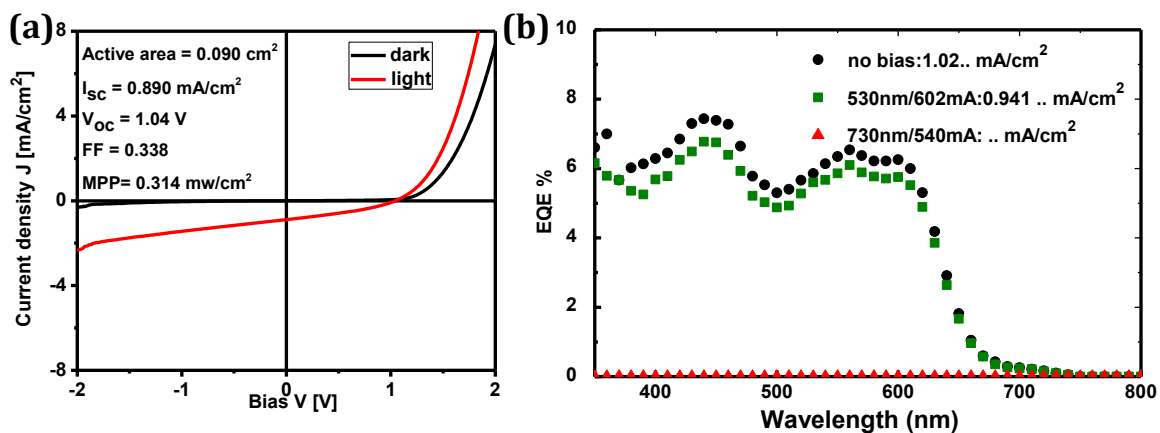
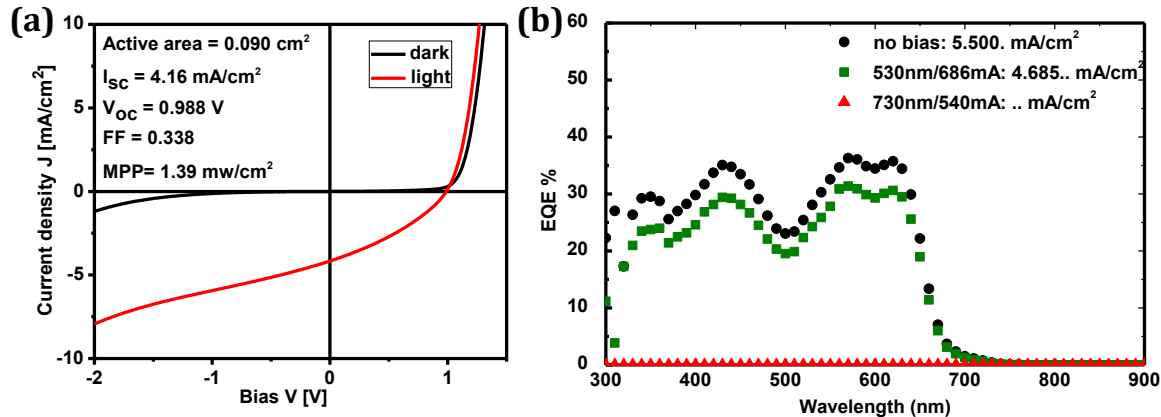


Figure 3.16 (a) Representative J-V curve for PyDPPBO(bithio)₂: PC₆₁BM solar cell in dark (black) and under simulated A M 1.5G conditions (red). (b) EQE spectra of PyDPPBO(bithio)₂: PC₆₁BM solar cell under low monochromatic light intensity and with 1 sun equivalent light bias illumination. The numbers in the panels represent the J_{sc} that is obtained with convoluting the EQE with the solar AM 1.5G spectrum.

Table 3.12 Characteristics of PyDPPHD(bithio)₂: PC₆₁BM devices on MoO₃ hole transporting layer under 100 mW/cm² white light illumination

Concentration (mg/mL)	Spin Coating (rpm)	Thickness (nm)	J _{sc} (mA/cm ²)	V _{oc} (V)	FF	MPP (mW/cm ²)	J _{sc} (mA/cm ²) (SR)	PCE (%)
12	600	92	4.16	0.98	0.33	1.39	4.68	1.56
16	800	95	3.84	0.95	0.31	1.15	4.07	1.22
20	900	91	2.70	0.91	0.27	0.68	0.92	0.23
24	1300	100	2.95	0.87	0.27	0.71	2.26	0.54
30	3300	95	2.96	0.98	0.28	0.82	1.43	0.40
36	6580	97	4.03	0.92	0.32	1.19	4.24	1.25

**Figure 3.17** (a) Representative J-V curve for PyDPPHD(bithio)₂: PC₆₁BM solar cell in dark (black) and under simulated AM 1.5G conditions (red). (b) EQE spectra of PyDPPHD(bithio)₂: PC₆₁BM solar cell under low monochromatic light intensity and with 1 sun equivalent light bias illumination. The numbers in the panels represent the J_{sc} that is obtained with convoluting the EQE with the solar AM 1.5G spectrum.**Table 3.13** PyDPPHD(bithio)₂: PCBM(1:1) conc : 12 mg/mL : Area of the cell 0.0900cm²

Additives (0.2%)	Spin Coating (rpm)	Thickness (nm)	J _{sc} (mA/cm ²)	V _{oc} (V)	FF	MPP (mW/cm ²)	J _{sc} (mA/cm ²) (SR)	PCE (%)
DIO	400	80	1.59	0.93	0.39	0.59	1.55	0.57
o-DCB	550	90	2.84	0.80	0.38	0.88	2.85	0.87

Table 3.14 PyDPPHD(bithio)₂: PCBM(1:1) conc : 36 mg/mL : Area of the cell 0.0900cm²

Additives (0.2%)	Spin coating (rpm)	Thickness (nm)	J _{sc} (mA/cm ²)	V _{oc} (V)	FF	MPP (mW/cm ²)	J _{sc} (mA/cm ²) (SR)	PCE (%)
DIO	6500	98	4.59	0.80	0.35	1.30	4.39	1.24
o-DCB	6500	95	3.42	0.92	0.31	0.98	3.43	0.98
1-CN	6500	95	3.40	0.87	0.31	0.93	3.28	0.90

3.3.6 Morphological studies

We repeated the solar cell device fabrication for understanding the morphology of the active layer for two pyridine capped DPP derivatives PyDPPEH(TPA)₂ and PyDPPHD(bithio)₂. Organic solar cells were fabricated by sandwiching a bulk heterojunction of the PyDPPEH(TPA)₂ : PC₆₁BM (1:1) between ITO/PEDOT:PSS on bottom and LiF/Al on top contact. The J-V characterization and EQE are given in the Figure 3.18. The PCE of 0.019 % with a J_{sc} = 0.12 mA/cm², V_{oc} = 0.71 V and FF 0.24. In the case of PyDPPHD(bithio)₂ instead of PEDOT:PSS hole transporting layer MoO₃ is used. The details of the solar cell on pattern ITO glass substrate with two different area having 0.09 cm² (A1 and A2) and 0.16 cm² (B1 and B2) is given in the Table 3.15. The best efficiency obtained for PyDPPHD(bithio)₂ : PC₆₁BM (1:1) with a total

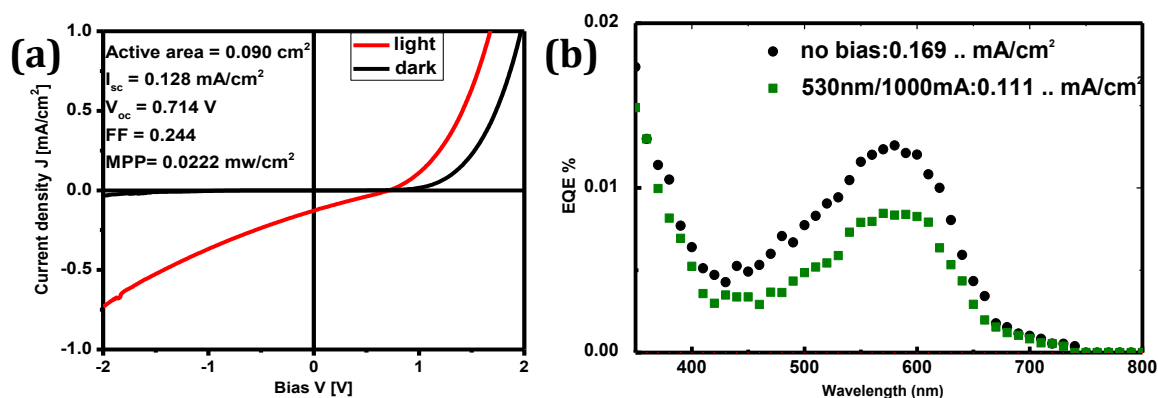


Figure 3.18 (a) Representative J-V curve for PyDPPEH(TPA)₂ : PC₆₁BM solar cell in dark (black) and under simulated A M 1.5G conditions (red). (b) EQE spectra of PyDPPEH(TPA)₂ : PC₆₁BM solar cell under low monochromatic light intensity and with 1 Sun equivalent light bias illumination. The numbers in the panels represent the J_{sc} that is obtained with convoluting the EQE with the solar A M 1.5G spectrum.

Table 3.15 PyDPPHD(bithio)₂: PCBM(1:1) conc : 12 mg/mL : Area of the cell 0.0900 cm² (A1 and A2) and (B1 and B2) 0.16 cm²

Cell	J _{sc} (mA /cm ²)	V _{oc} (V)	FF	MPP (mW/cm ²)	J _{sc} (mA /cm ²) (SR)	PCE (%)
A1	4.04	1.010	0.314	1.29	4.32	1.37
B1	3.94	0.891	0.317	1.11	4.06	1.14
A2	4.25	0.993	0.332	1.44	4.48	1.47
B2	4.09	1.010	0.328	1.36	4.71	1.56

concentration of 12 mg/mL in CHCl₃ is 1.56 %. The J-V characterization and EQE of PyDPPHD(bithio)₂ : PC₆₁BM solar cell is given in the Figure 3.19. The TEM image of the active layer PyDPPEH(TPA)₂ : PC₆₁BM and PyDPPHD(bithio)₂ : PC₆₁BM solar cells are given in the Figure 3.20.

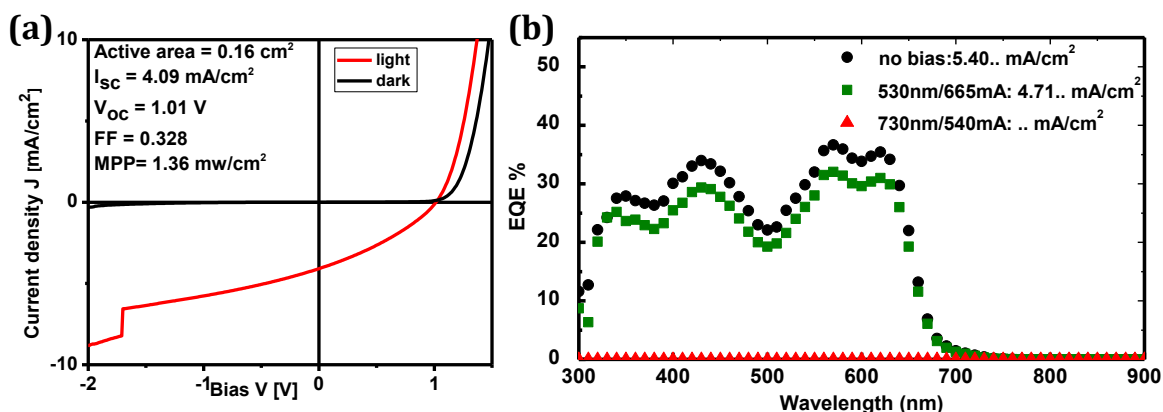


Figure 3.19 (a) Representative J-V curve for PyDPPHD(bithio)₂ : PC₆₁BM solar cell in dark (black) and under simulated A M 1.5G conditions (red). (b) EQE spectra of PyDPPHD (bithio)₂ : PC₆₁BM solar cell under low monochromatic light intensity and with 1 sun equivalent light bias illumination. The numbers in the panels represent the J_{sc} that is obtained with convoluting the EQE with the solar A M 1.5G spectrum.

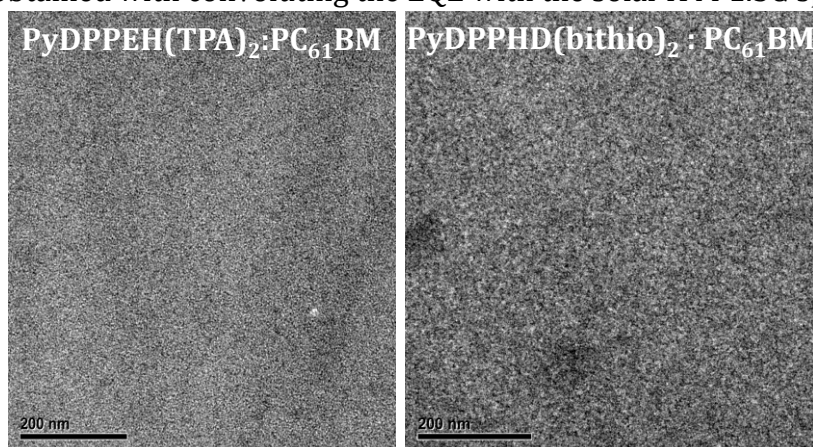


Figure 3.20 TEM images of active layers comprised of PyDPPEH(TPA)₂ : PC₆₁BM and good soluble PyDPPHD(bithiohexyl)₂ : PC₆₁BM (EH = 2-ethylhexyl, HD = 2-hexyldecyl).

From these two TEM images, there are no pronounced phase separation and also no crystallized domains (fringes) were observed. But comparing the morphology of the active layer of both derivatives, mixing of donor and acceptor was more profound in the PyDPPEH(TPA)₂ : PC₆₁BM layer.

3.4 Conclusion

In the third chapter, we explored the effect of donor substituents in the pyridine capped DPP in the BHJ solar cell with PC₆₁BM as an acceptor. A series of five pyridine capped DPP based small molecules have been synthesized. The 2-ethylhexyl derivatives of pyridine capped DPP with donor triphenylamine (PyDPPEH(TPA)₂) and benzothiophene (PyDPPEH(BTH)₂) are less soluble and very difficult to get high quality thin films with the PC₆₁BM acceptor and the efficiency are only 0.1 %. The best MPP obtained for solar cell device with the active layer PyDPPBO(BF)₂ : PC₆₁BM and PyDPPBO(bithio)₂ : PC₆₁BM spin coated in the presence of 0.2 % DIO in CHCl₃ solution is 0.87 mW/cm² and 1.71 mW/cm² respectively. Among the five small molecules, the solar cell based on PyDPPHD(bithio)₂:PC₆₁BM blend exhibits the best PCE. The PCE of 1.25 % with a V_{oc} of 0.85 V, J_{sc} of 3.78 mA/cm², and a FF of 0.38 was obtained with PEDOT: PSS as a hole transporting layer. At the same time, a PCE of 1.56 % with a V_{oc} of 0.98 V, a J_{sc} of 4.68 mA/cm² and a FF of 0.33 was achieved by using MoO₃ as the hole transporting layer for the solar cell based on PyDPPHD(bithio)₂:PC₆₁BM blend.

3.5 Experimental section

3.5.1 General methods

4-Iodophenol, *p*-bromoaniline, 5-bromo-2-pyridinecarbonitrile, Bis(pinacolato) diborane, PdCl₂(dppf)₂, Pd(PPh₃)₄, were purchased from Sigma Aldrich and were

used as such. Solvent used were either HPLC grade or freshly distilled before use. All the reactions were carried out under nitrogen atmosphere. ^1H NMR and ^{13}C NMR spectra were obtained using a 500 MHz Bruker Avance DPX spectrometer and also with varian mercury 400MHz spectrometer using the deuterated solvents CDCl_3 and tetramethylsilane (TMS) as the internal standard. DSC was performed using a PerkinElmer Pyris 6 DSC instrument in sealed aluminum pans under nitrogen flow, at a heating/cooling rate of $5\text{ }^\circ\text{C}/\text{min}$. Absorption spectra were obtained using a Shimadzu 3101PC UV/Vis-NIR scanning spectrophotometer. Cyclic voltammetry was performed under an inert atmosphere with a scan rate of $0.1\text{ V}/\text{s}$ and 0.1 M tetrabutylammoniumhexafluorophosphate in dichloromethane as the electrolyte. A platinum working electrode, a silver counter electrode and a silver wire coated with silver chloride (Ag/AgCl) quasi-reference electrode were used combined with Fc/Fc⁺ as the internal standard.

3.5.2 Fabrication of bulk heterojunction solar cell

Photovoltaic devices with an active area of 0.09 and 0.16 cm^2 were fabricated by spin coating poly(ethylenedioxythiophene):poly(styrenesulfonate) (PEDOT:PSS) at 3000 rpm for 60 sec on pre-cleaned, patterned indium tin oxide (ITO) glass substrates ($14\text{ }\Omega$ per square) (Naranjo Substrates). In case of pyridine capped DPP the hole transporting layer of MoO_3 was also used. MoO_3 of 10 nm was thermally evaporated under high vacuum ($\sim 3 \times 10^{-7}\text{ mbar}$). Commercially available PEDOT:PSS was obtained from Clevios P, VP Al4083 and PC₆₁BM (99 %) was obtained from Solenne BV. The photoactive layers were deposited by spin coating a

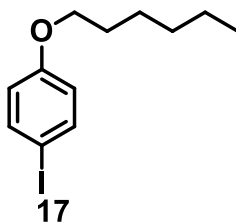
chloroform solution containing the pyridine capped DPP small molecule (10 mg/ml), the appropriate amount of PC₆₁BM and the co-solvent DIO, o-DCB, or 1-CN. The Thickness of the photoactive layer was maintained at 90 nm -100 nm by adjusting the speed (rpm) of spin coating. For layers that were thermally annealed, the glass substrates with the photoactive layer were placed on a hot plate inside an N₂-filled glovebox (< 1 ppm O₂ and < 1 ppm H₂O) at 110 °C for 10 minutes. For cells that were thermal annealed, this was done prior to depositing the metal contacts. The back electrode consisted of LiF (1 nm) with Al (100 nm). LiF and Al were deposited by evaporation under high vacuum ($\sim 3 \times 10^{-7}$ mbar).

J-V characteristics were measured with a Keithley 2400 source meter under ~ 100 mW/cm² white light illumination from a tungsten-halogen lamp filtered by a Schott GG385 UV filter and a Hoya LB120 daylight filter that provides illumination conditions within ~ 10 % of 100 mW cm⁻² AM1.5G for most cells. The MPP was estimated from the V_{oc}, FF, and J_{sc} obtained from the J-V measurements.

Short-circuit currents under AM1.5G conditions were determined by convoluting the spectral response with the solar spectrum. Spectral response measurements were conducted under 1 sun operating conditions by using a 530 nm high power LED (Thorlabs) for bias illumination. The device was kept in a nitrogen filled box behind a quartz window and irradiated with modulated monochromatic light, from a 50 W tungsten-halogen lamp (Philips focusline) and monochromator (Oriel, Cornerstone 130) with the use of a mechanical chopper. The response was recorded as a voltage over a 50 Ω resistor using a lock-in amplifier (Stanford Research Systems SR830). A

calibrated silicon cell was used as reference. The estimated PCE were determined by combining V_{oc} and FF from the obtained J-V measurements together with J_{sc} values obtained during spectral response measurements. The thicknesses of the active layers of the photovoltaic devices were measured on a Veeco Dektak 150 profilometer. TEM was performed on a Tecnai G2 Sphera TEM (FEI) operated at 20 kV.

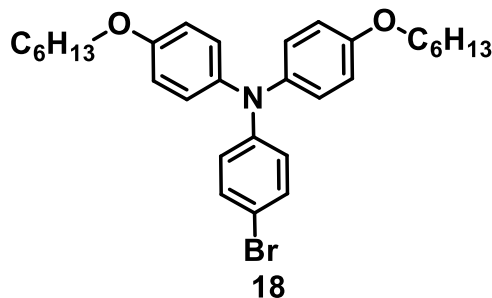
3.5.3 Experimental procedures



1-n-Hexyloxy-4-iodobenzene (**17**)

4-Iodophenol (10.0 g, 45.5 mmol), 1-bromohexane (6.45 mL, 46.0 mmol), K_2CO_3 (18.5 g, 134 mmol), and DMF (100 mL) were placed in a one-neck 300 mL flask equipped with a reflux condenser and a magnetic stir bar. The mixture was kept stirring at 110 °C for overnight, and was poured into aqueous NaOH (1 M, 1200 mL). The resulting suspension was stirred for 30 min and was extracted four times with n-hexane (100 mL×4). The organic mixture was dried over anhydrous magnesium sulfate. After filtration, the solvent was removed by rotary evaporation. The residue was purified by column chromatography using n-hexane as the eluent to afford compound (**17**) as a transparent oil (12.45 g, 90 %) 1H NMR ($CDCl_3$, 500 MHz) δ 7.55-7.54(d, 2H, $J = 9.00$ Hz), 6.69-6.67 (d, 2H, $J = 9.00$ Hz), 3.93-3.90 (t, 2H, $J = 6.50$

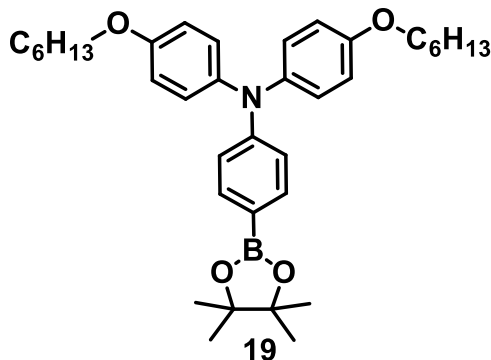
Hz), 1.79-1.76 (m, 2H), 1.45-1.44 (m, 2H), 1.34-1.36(m, 4H), 0.92-0.90 (t, 3H, $J = 7.00$ Hz). ^{13}C NMR (CDCl_3 , 125 MHz) δ 158.98, 138.09, 116.91, 82.36, 68.09, 31.53, 29.09, 25.65, 22.56, 14.00.



N,N-bis(4-hexyloxyphenyl)-4-bromoaniline (18)

To a stirred solution of 1-n-Hexyloxy-4-iodobenzene (5.2 g, 17.23 mmol), p-bromoaniline (1 g, 5.7 mmol), and 1,10-phenanthroline (0.11 g, 0.57 mmol) in toluene (50 mL) at 100 °C were added potassium hydroxide (5.1 g, 90 mmol) and cuprous chloride (108 mg, 0.57 mmol) under argon. The reaction mixture was refluxed in Dean-Stark apparatus for 24 h and then water (100 mL) was added. The crude product was extracted into dichloromethane, and the organic layer was washed with water and dried over anhydrous sodium sulfate. After removing solvent under reduced pressure, the residue was purified by column chromatography using ethyl acetate/hexane(v/v = 1/50) as eluent to yield as a white powder (1.9 g, 65 %). ^1H NMR (CDCl_3 , 500 MHz, ppm) δ 7.21-7.17 (m, 2H), 7.08-7.06 (d, $J = 9.00$ Hz, 4H), 6.98-6.97 (d, $J = 8.00$ Hz 2H) 6.90-6.83 (m, 4H), 3.97-3.94 (t, $J = 6.50$ Hz, 4H), 1.83-1.78 (m, 4H), 1.52-1.49 (m, 4H), 1.40-1.38 (m, 8H), 0.97-0.94 (t, $J = 6.50$ Hz, 6H). ^{13}C NMR

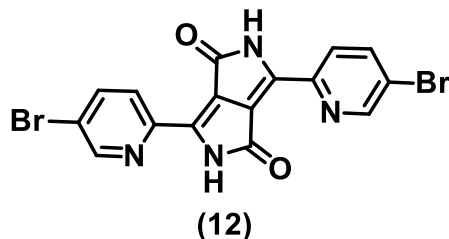
(CDCl₃, 125 MHz, ppm) δ 155.21, 148.78, 140.90, 128.83, 126.34, 120.75, 120.35, 115.13, 68.16, 31.58, 29.30, 25.74, 22.59, 14.03



4,4,5,5-tetramethyl-2-{4-[N,N-bis(4-hexyloxyphenyl)amino]phenyl}-1,3,2-dioxaborolane (19)

A mixture of N,N-bis(4-hexyloxyphenyl)-4-bromoaniline (1.0 g, 1.9 mmol), 4,4,4',4',5,5,5',5'-octamethyl-2,2'-bi(1,3,2-dioxaborolane) (0.96 g, 3.8 mmol), potassium acetate (1.1 g, 11.4 mmol), and Pd(dppf)Cl₂ (0.139 g, 0.19 mmol) in anhydrous dioxane (25 mL) was stirred at 85 °C under argon for 48 h and then water (20 mL) was added. The crude product was extracted into ethyl acetate, washed with water, and dried over anhydrous sodium sulfate. After removing solvent under reduced pressure, the residue was purified by column chromatography using hexane/ dichloromethane (v/v = 2/1) as eluent to obtain as a white powder (0.65 g, 60 % yield). ¹H NMR (CDCl₃, 500 MHz, ppm) δ 7.72-7.70 (d, J = 8.50 Hz, 2H), 7.15-7.13 (d, J = 9.00 Hz, 4H), 6.98-6.96 (d, J = 8.50 Hz, 2H), 6.91-6.89 (d, J = 8.50 Hz, 4H), 4.01-3.99 (t, J = 6.50 Hz, 4H), 1.87-1.84 (m, 4H), 1.57-1.54 (m, 4H), 1.45-1.42 (m, 8H), 1.41 (s, 12H), 1.02-0.99 (t, J = 7.00 Hz, 6H). ¹³C NMR (CDCl₃,

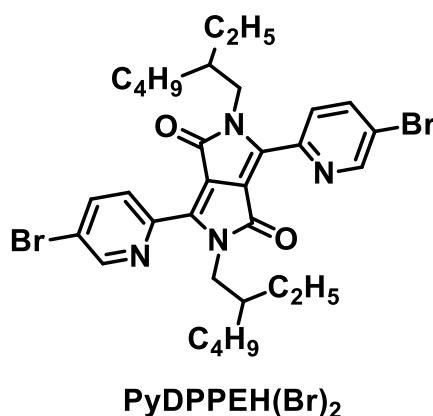
125 MHz, ppm) δ 155.69, 151.33, 140.09, 135.66, 126.97, 118.42, 115.14, 83.17, 68.03, 31.51, 29.23, 25.68, 24.75, 22.52, 13.96.



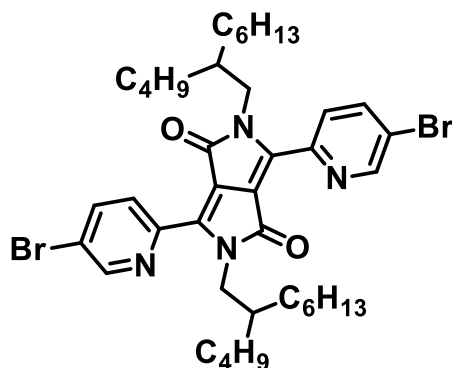
Synthesis of 3,6-bis(5-bromopyridin-2-yl)pyrrolo[3,4-c]pyrrole-1,4(2H,5H)-dione (12) : In a dry 250 mL round bottom flask, 150 mL of *t*-amyl alcohol was added to a mixture of sodium pieces (1.0 g, 43.4 mmol) and 10 mg of FeCl₃. After fully dissolving sodium by heating the solution at 90 °C for 3 h, 5-bromo-2-pyridinecarbonitrile (6 g, 32.7 mmol) and diethyl succinate (1.91 g, 11 mmol) were rapidly added to the solution, and then the solution was refluxed for 1 h. The solution was then cooled to room temperature, and then the solution was poured into 200 mL of cold MeOH. After the precipitates were filtered, which is intermediate of 3,6-bis(5-bromopyridin-2-yl)pyrrolo[3,4- c]pyrrole-1,4-(2H,5H)-dione, the dark red solid. 4.4 g (Yield 90 %).

General alkylation procedure of DPP cores: In a three-necked, oven-dried 250 mL round-bottom flask, 3,6-bis(5-bromopyridin-2-yl)pyrrolo[3,4-c]pyrrole-1,4(2H,5H)-dione (3.00 g, 10.0 mmol) and anhydrous K₂CO₃ (4.15 g, 30.0 mmol) were dissolved in 100 mL of anhydrous *N,N*-dimethylformamide (DMF) and heated to 110 °C under argon for 30 minutes. Branched alkyl chain bromide (25.0 mmol) was then added dropwise, and the reaction mixture was further stirred and refluxed

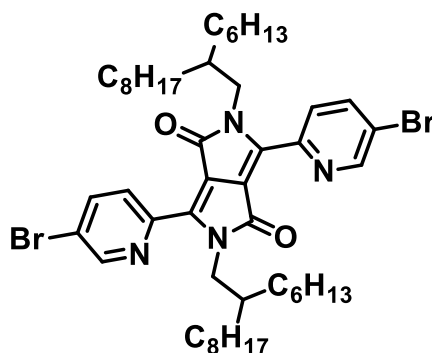
for 2 h. The reaction mixture was allowed to cool down to room temperature; after that it was poured into 400 mL of distilled water, and the resulting suspension was stirred at room temperature for 1 h. The solid was collected by vacuum filtration, washed with several portions of distilled water, washed with methanol, and then air-dried. Further the crude solid was purified by column chromatography using dichloromethane as an eluent yielding pure product as a dark red solid.



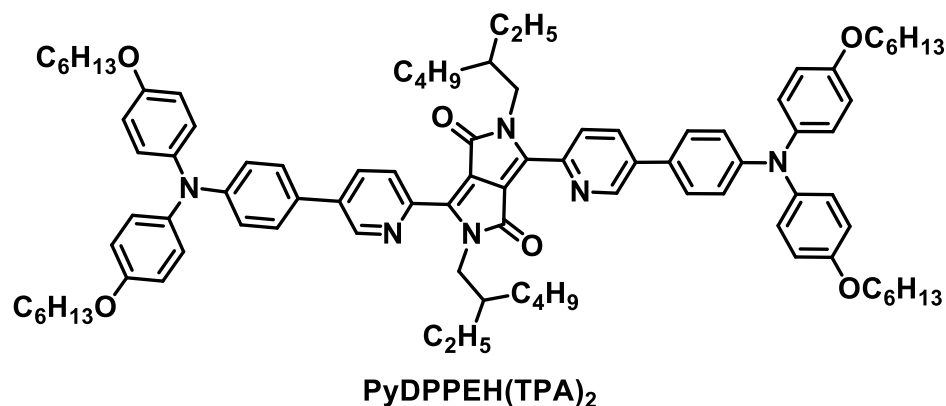
3,6-bis(5-bromopyridin-2-yl)-2,5-bis(2-ethylhexyl)pyrrolo[3,4-c]pyrrole-1,4(2H,5H)-dione(PyDPPEH(Br)₂) following the general procedure (1.5 g, 32 % yield). ¹H NMR (500 MHz, CDCl₃, δ): 8.94 (d, J = 9 Hz, 2H), 8.75 (s, 2H), 8.02 (d, J=8.5, 2H), 4.33-4.2 (m, 4H), 1.57 (d, J=9.5Hz, 2H), 1.29-1.20(m, 16H), 0.82(t, J = 7Hz, 12H) ¹³C NMR (100 MHz, CDCl₃) δ 162.5, 150.0, 146.0, 144.9, 139.7, 128.4, 122.6, 111.4, 46.0, 39.7, 30.5, 28.5, 23.8, 23.0, 14.0, 10.7.

PyDPPBO(Br)₂

3,6-bis(5-bromopyridin-2-yl)-2,5-bis(2-butyl-octyl)pyrrolo[3,4-c]pyrrole-1,4(2H,5H)-dione(PyDPPBO(Br)₂) following the general procedure (1.9 g, 38 % yield). ¹H NMR (400 MHz, CDCl₃, δ): 8.91 (d, J = 8.8 Hz, 2H), 8.74 (d, J=2Hz, 2H), 8.01 (dd, J=8.8, J = 2.4, 2H), 4.28 (d, J = 7.6, 4H), 1.58 (broad s, 2H), 1.32-1.19(m, 32H), 0.88-0.82(m, 12H)

PyDPPHD(Br)₂

3,6-bis(5-bromopyridin-2-yl)-2,5-bis(2-hexyl-decyl)pyrrolo[3,4-c]pyrrole-1,4(2H,5H)-dione(PyDPPHD(Br)₂) following the general procedure (2.0 g, 35 % yield). ¹H NMR (400 MHz, CDCl₃, δ): 8.91 (d, J = 8.8 Hz, 2H), 8.74 (d, J=2 Hz, 2H), 8.01 (dd, J=8.8 Hz, J = 2.4 Hz, 2H), 4.28 (d, J = 7.6 Hz, 4H), 1.58 (broad s, 2H), 1.32-1.19(m, 58H), 0.88-0.82(m, 12H) MALDI-TOF calculated- 894.40; found -896.42



3,6-bis(5-(4-(bis(4-(hexyloxy)phenyl)amino)phenyl)pyridin-2-yl)-2,5-bis(2-ethylhexyl)pyrrolo[3,4-c]pyrrole-1,4(2H,5H)-dione (PyDPPEH(TPA)₂)

A 50 mL Schlenk tube was filled with 4,4,5,5-tetramethyl-2-{4-[N,N-bis(4-hexyloxyphenyl)amino]phenyl}-1,3,2dioxaborolane (0.212 g, 0.371 mmol), PyDPPEH(Br)₂ (0.1 g, 0.148 mmol), and K₂CO₃ (0.081 g, 0.592 mmol), and Pd(PPh₃)₄ (0.017 g, 10 mol %) catalyst was transferred from Glove box. A mixture of toluene, ethanol and water in the ratio of 4:1:0.5 was purged with argon gas for 20 minutes to deoxygenate. Then the solvent was cannulated or transferred to the Schlenk tube. The tube was sealed and heated at 90 °C for 18 hours. The crude reaction mixture was allowed to cool to room temperature after which the organic layer was washed with water and brine, dried over anhydrous MgSO₄, filtered, and the solvent evaporated under reduced pressure. The crude product was preadsorbed onto silica gel and chromatographed to give PyDPPEH(TPA)₂ as a dark brown solid (yield: 75 %). ¹H NMR (400 MHz, CDCl₃, δ): 9.05 (d, J = 8.4 Hz, 2H), 8.9 (s, 2H), 8.04(d, J=8.4 Hz, 2H), 7.50 (d, J=8.8Hz, 4H), 7.12 (d, J=8.8Hz, 8Hz), 7.02(d, J= 8.8Hz, 4H), 6.88(d, J=8.8, 8Hz) 4.47-4.36 (m, 4H), 3.97 (t, J = 6.4Hz, 8H) 1.84 - 1.77 (m, 8H), 1.53-1.45 (m,

8H) 1.38-1.37(m, 18H), 1.31-1.22(m, 18H), 0.94 (t, J=6.8Hz, 12H) 0.87-0.83(m, 12H)

^{13}C NMR (100 MHz, CDCl_3) δ 206.9, 162.9, 156.0, 149.5, 146.5, 145.4, 145.3, 139.9, 136.9, 133.5, 127.7, 127.5, 127.4, 127.1, 119.8, 115.4, 111.0, 68.2, 45.8, 39.6, 31.6, 30.9, 30.5, 29.3, 28.6, 25.7, 23.9, 23.0, 22.6, 14.1, 10.7. MALDI-TOF calculated- 1400.92; found -1401.92

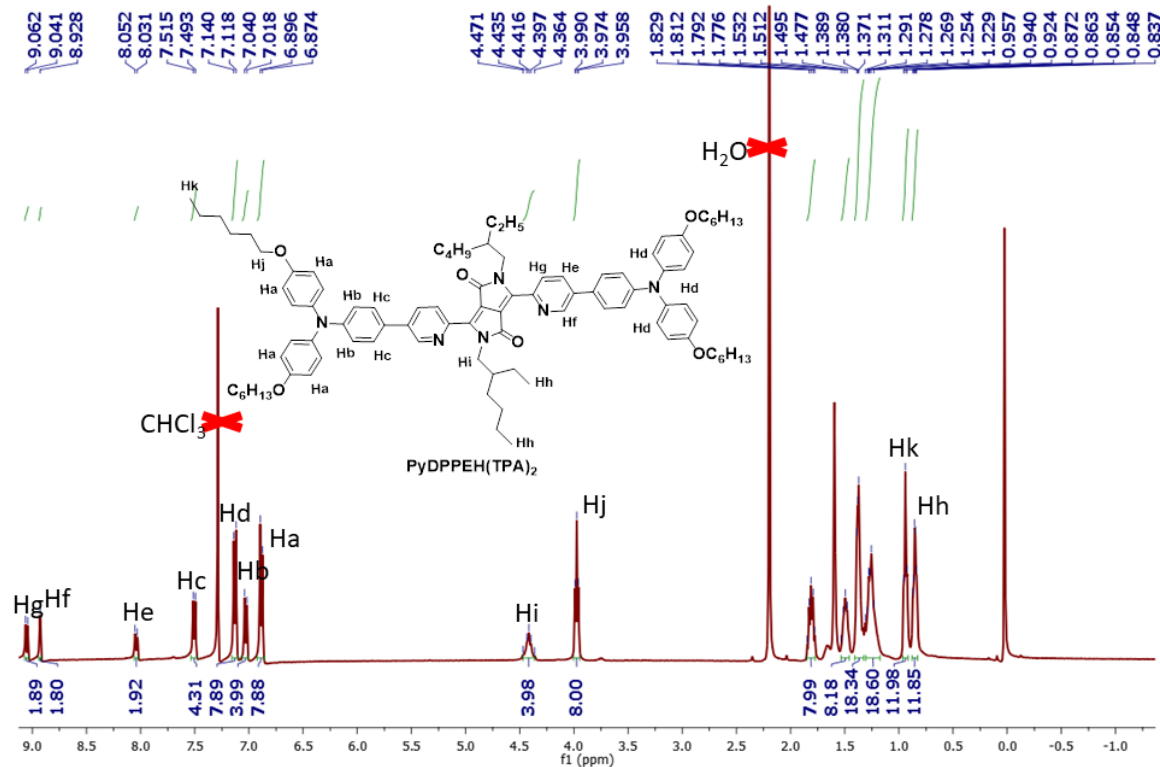


Figure 3.21 NMR Spectrum of PyDPPEH(TPA) $_2$

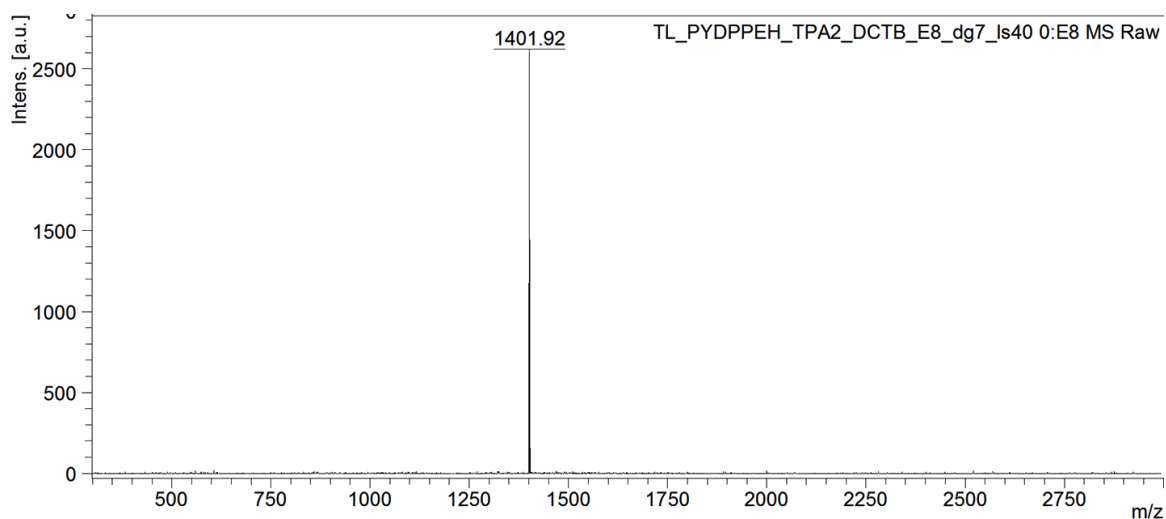
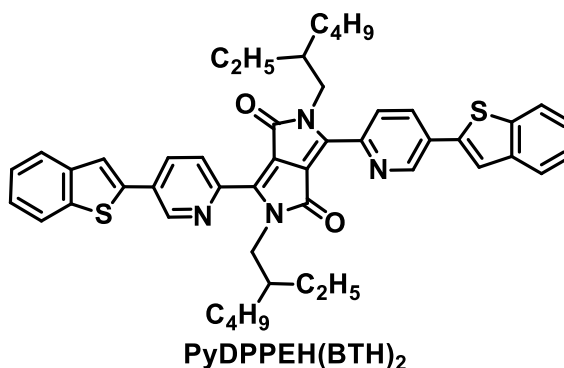


Figure 3.22 MALDI-TOF spectrum of PyDPPEH(TPA)₂



3,6-bis(5-(benzo[b]thiophen-2-yl)pyridin-2-yl)-2,5-bis(2-ethylhexyl)pyrrolo[3,4-c]pyrrole-1,4(2H,5H)-dione (PyDPPEH(BTH)₂)

(PyDPPEH(BTH)₂) was synthesized according to the same procedure as described above (0.122 g, 70 % yield) but by using 2-(benzo[b]thiophen-2-yl)-4,4,5,5-tetramethyl-1,3,2-dioxaborolane (0.1 g, 0.562 mmol), PyDPPEH(Br)₂ (0.15 g, 0.225 mmol), and K₂CO₃ (0.077 g, 0.562 mmol), and Pd(PPh₃)₄ (0.025 g, 10 mol%) ¹H NMR (500 MHz, CDCl₃, δ): 9.12 (d, J = 8.5 Hz, 2H), 9.06(d, J = 2 Hz, 2H), 8.17(dd, J = 8.4 Hz, J = 2.5Hz, 2H), 7.89 - 7.84 (m, 5H) 7.42 - 7.37 (m, 5H), 4.45-4.36 (m, 4H), 1.66 (t, J =

6Hz, 2H) 1.33 - 1.23 (m, 16H), 0.88-0.84 (m, 12H) ^{13}C NMR (125 MHz, CDCl_3) δ 162.7, 146.8, 146.3, 145.1, 140.3, 140.0, 139.6, 133.8, 131.1, 127.5, 125.4, 125.0, 124.1, 122.4, 121.8, 111.6, 100.0, 46.1, 39.7, 30.5, 28.6, 23.9, 23.0, 14.1, 10.8. MALDI TOF calculated- 778.34; found - 778.35.

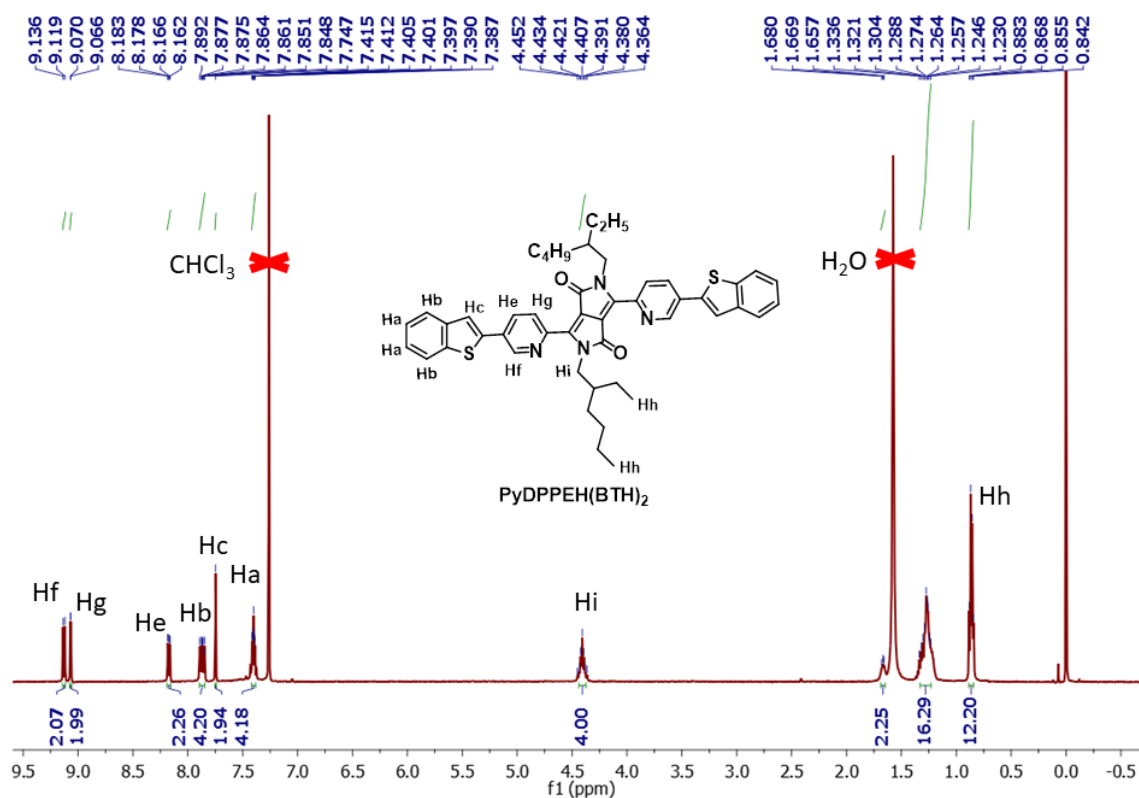


Figure 3.23 NMR spectrum of PyDPPEH(BTH) $_2$

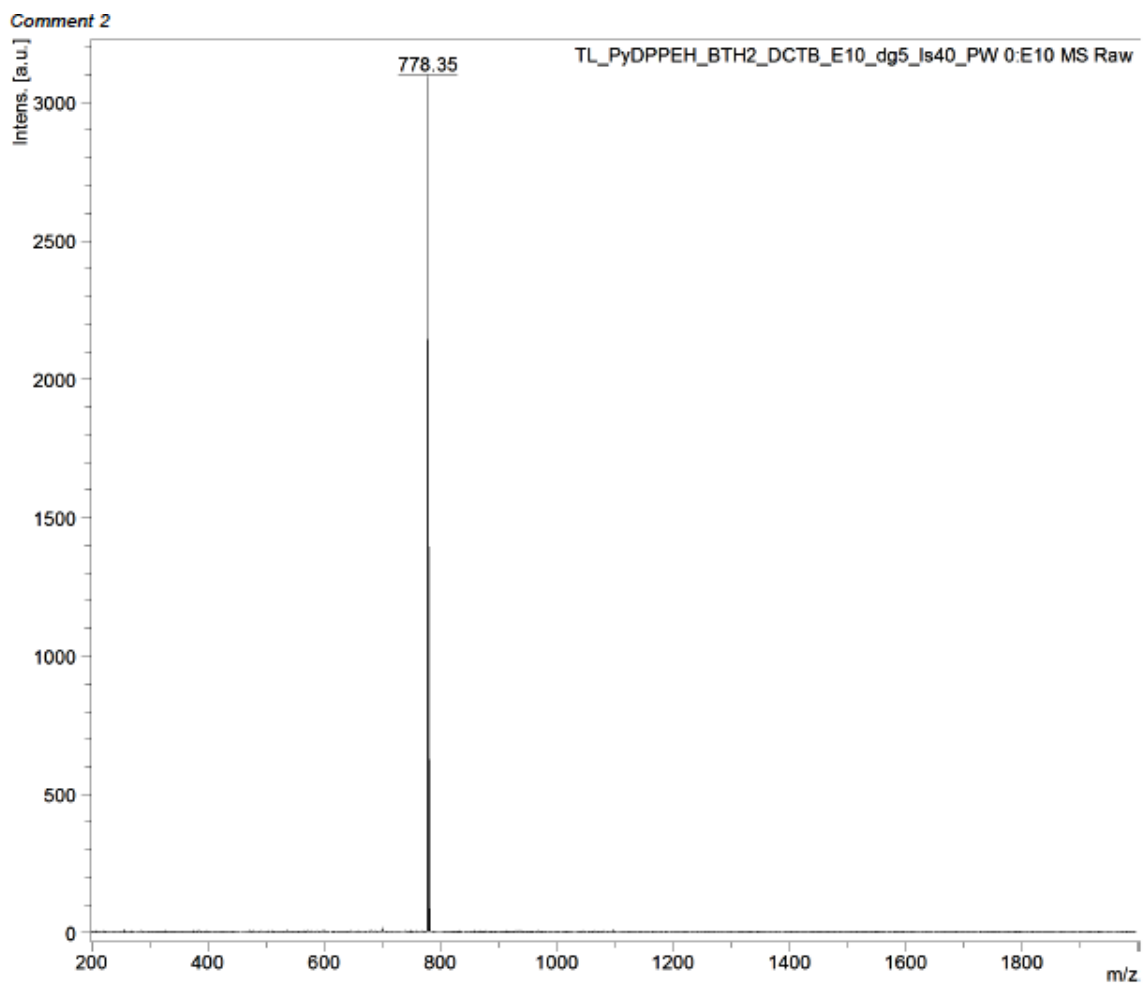
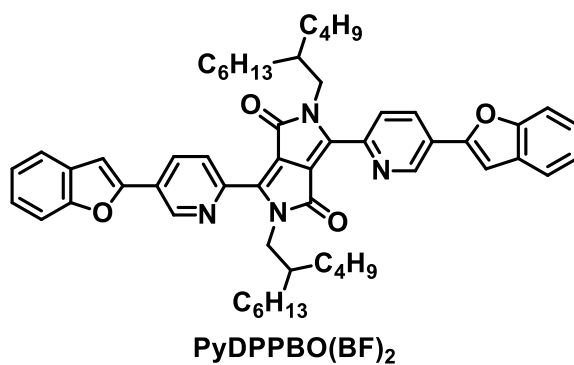


Figure 3.24 MALDI TOF spectrum of PyDPPEH(BTH)₂



3,6-bis(5-(benzofuran-2-yl)pyridin-2-yl)-2,5-bis(2-butyl-1-octylamino)pyrrolo[3,4-c]pyrrole-1,4(2H,5H)-dione (PyDPPBO(BF)₂)

(PyDPPBO(BF)₂) was synthesized according to the same procedure as described above (0.137 g, 73 % yield), but by using 2-(benzofuran-2-yl)-4,4,5,5-tetramethyl-1,3,2-dioxaborolane (0.139 g, 0.573 mmol), PyDPPBO(Br)₂ (0.15 g, 0.191 mmol), and K₂CO₃ (0.079 g, 0.573 mmol), and Pd(PPh₃)₄ (0.022 g, 10 mol %) ¹H NMR (400 MHz, CDCl₃, δ): 9.19 (dd, J = 2 Hz, J = 0.4 Hz, 2H), 9.12 (dd, J = 8.4 Hz, J = 0.8 Hz, 2H), 8.28 (dd, J = 8.4, J = 2 Hz, 2H), 7.65 (d, J = 7.6 Hz, 2H) 7.39-7.34 (m, 2H), 7.30-7.26 (m, 2H), 7.26-7.24 (m, 2H), 4.40 (d, J = 8 Hz, 4H), 1.54 (brs 2H) 1.24 - 1.20 (m, 32H), 0.85-0.80 (m, 12H) ¹³C NMR (100 MHz, CDCl₃) δ 162.7, 155.4, 152.5, 146.9, 145.3, 145.2, 132.2, 128.6, 127.3, 127.0, 125.6, 123.5, 121.4, 111.7, 111.4, 104.4, 46.4, 38.2, 31.8, 31.4, 31.1, 29.7, 28.6, 26.3, 23.0, 22.6, 14.1. MALDI TOF calculated- 858.51; found - 858.53.

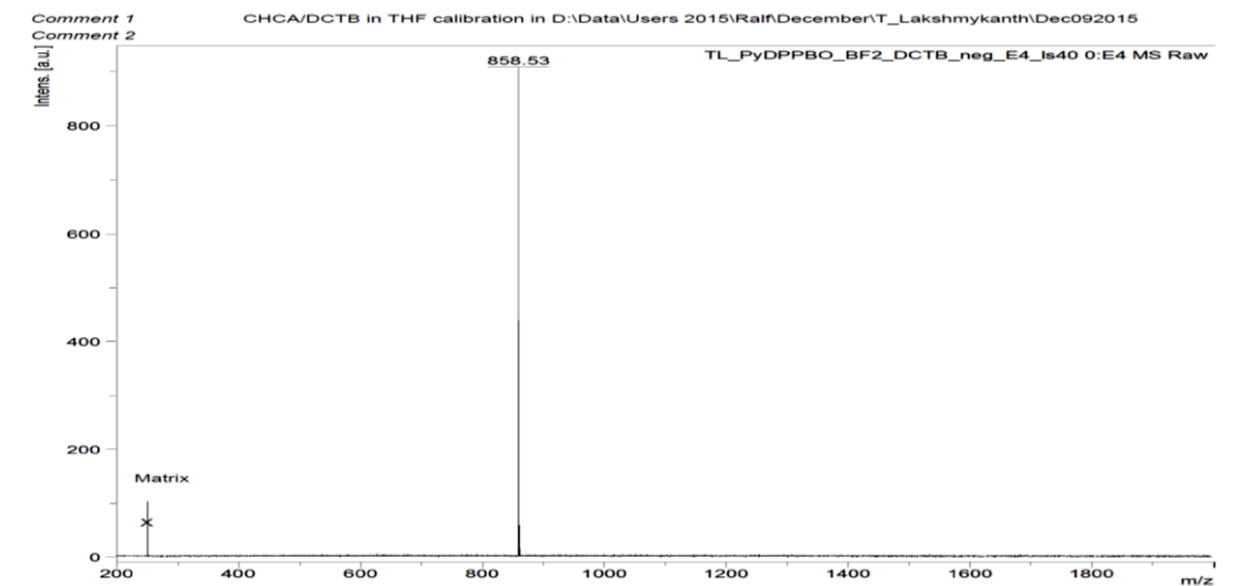
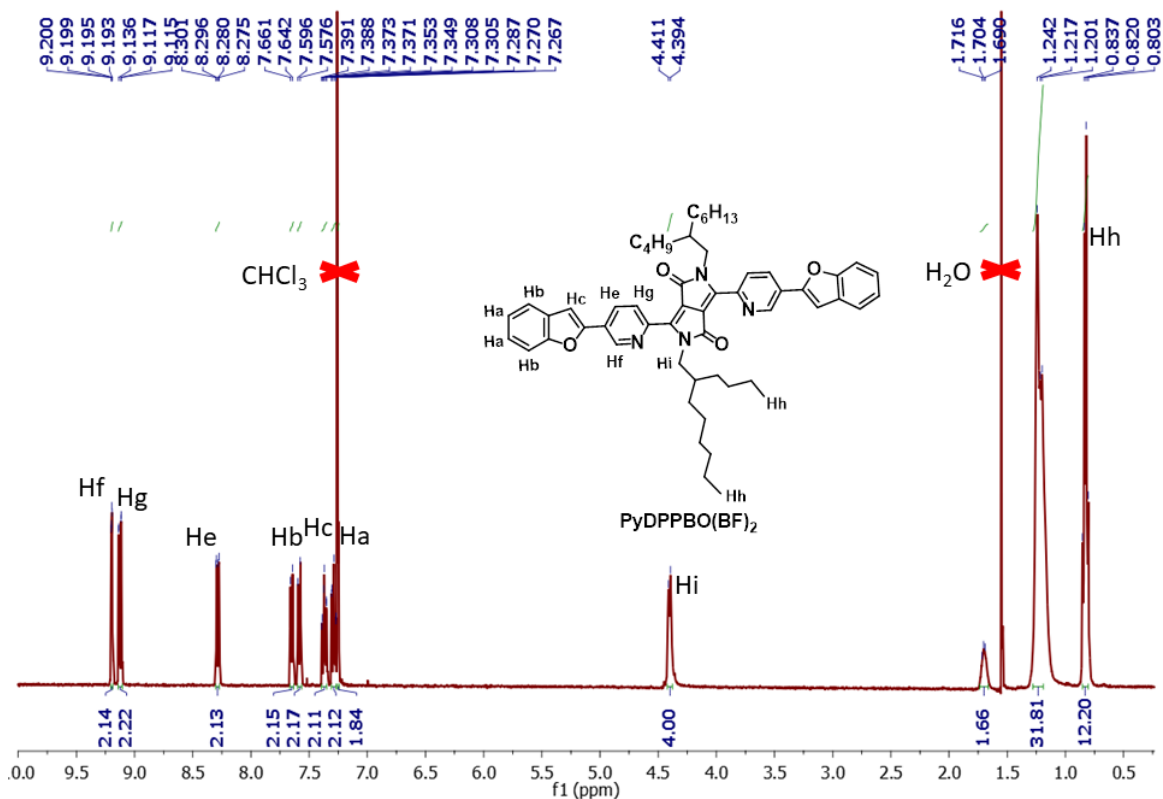
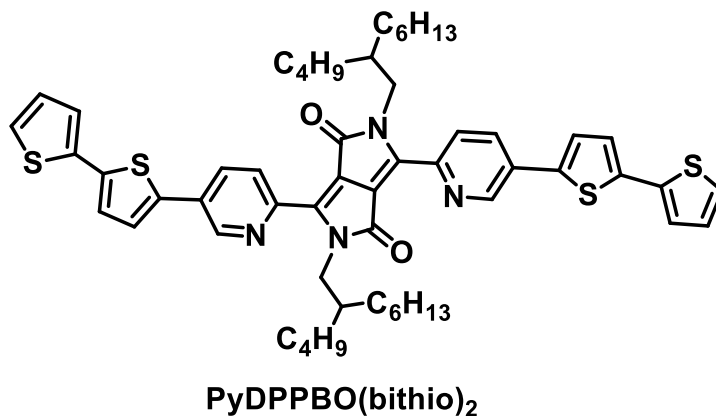


Figure 3.25 MALDI TOF spectrum of PyDPPBO(BF)₂

Figure 3.26 NMR spectrum of $\text{PyDPPBO}(\text{BF}_2)_2$ 

**3,6-bis(5-([2,2'-bithiophen]-5-yl)pyridin-2-yl)-2,5-bis(2-butyl-octyl)pyrrolo
[3,4-c]pyrrole-1,4(2H,5H)-dione ($\text{PyDPPBO}(\text{bithio})_2$)**

($\text{PyDPPBO}(\text{bithio})_2$) was synthesized according to the same procedure as described above (0.093 g, 77% yield), but by using 2-([2,2'-bithiophen]-5-yl)-4,4,5,5-

tetramethyl-1,3,2-dioxaborolane (0.11 g, 0.382 mmol), PyDPPBO(Br)₂ (0.10 g, 0.127 mmol), and K₂CO₃ (0.052 mg, 0.382 mmol), and Pd(PPh₃)₄ (0.014 g, 10 mol%) ¹H NMR (400 MHz, CDCl₃, δ): 9.06 (dd, J = 8.4 Hz, J = 0.8 Hz 2H), 8.94 (dd, J = 8.4, J = 0.4 Hz, 2H), 8.03 (dd, J = 8.4 Hz, J = 0.8 Hz, 2H), 7.41 (d J=3.6Hz, 2H) 7.29-7.26 (m, 2H), 7.22 (d, J = 4 Hz, 2H), 7.07-7.05 (m, 2H), 4.38 (d, J = 8Hz, 4H), 1.70 (brs 2H) 1.23 - 1.18 (m, 32H), 0.85-0.81 (m, 12H) ¹³C NMR (100 MHz, CDCl₃) δ 162.7, 146.1, 145.4, 145.0, 139.3, 138.4, 136.7, 132.6, 130.7, 128.0, 127.5, 126.0, 125.2, 125.0, 124.4, 111.4, 53.4, 46.3, 38.1, 31.8, 31.5, 31.2, 30.9, 29.7, 28.6, 26.4, 23.0, 22.6, 14.1 MALDI TOF calculated- 954.41 found -954.42

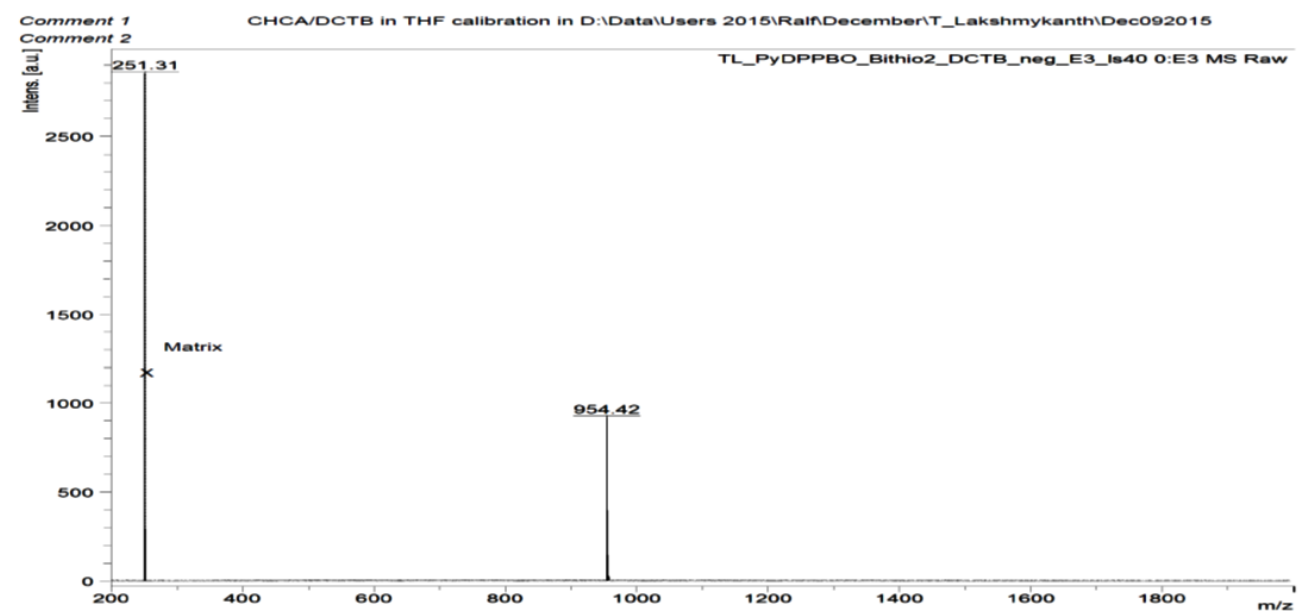


Figure 3.27 MALDI TOF spectrum of PyDPPBO(bithio)₂

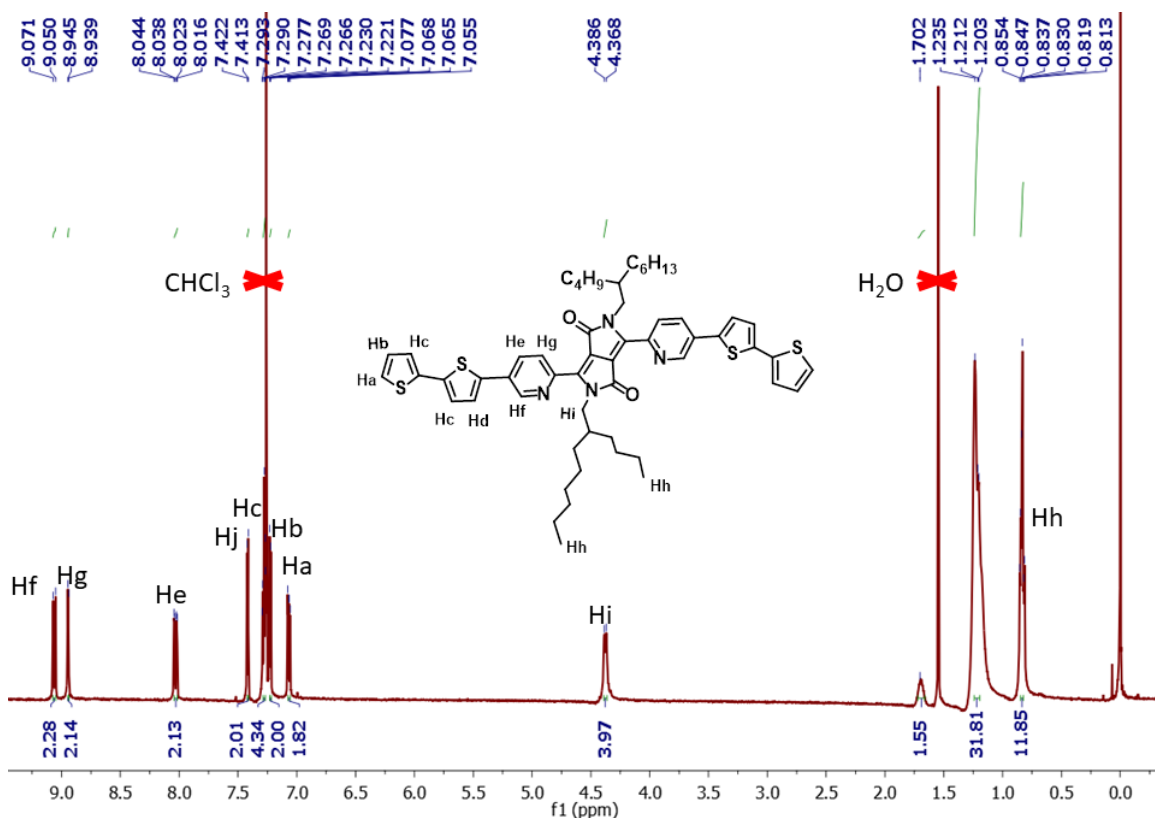
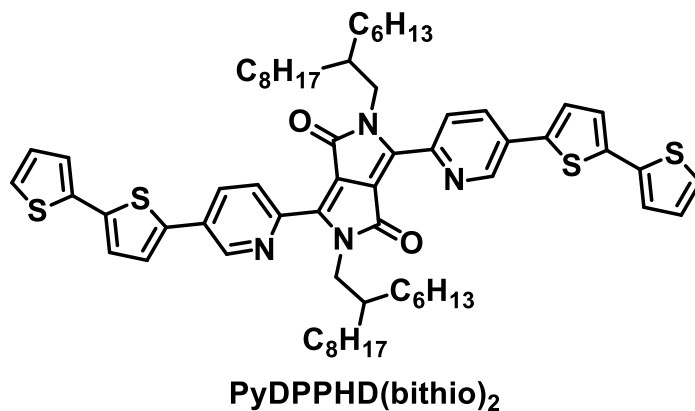


Figure 3.28 NMR spectrum of PyDPPBO(bithio)₂



3,6-bis(5-([2,2'-bithiophen]-5-yl)pyridin-2-yl)-2,5-bis(2-hexyldecyl)pyrrolo[3,4-c]pyrrole-1,4(2H,5H)-dione (PyDPPHD(bithio)₂)

(PyDPPHD(bithio)₂) was synthesized according to the same procedure as described above (0.085 g, 72% yield), but by using 2-([2,2'-bithiophen]-5-yl)-4,4,5,5-

tetramethyl-1,3,2-dioxaborolane (0.098 g, 0.335 mmol), PyDPPHD(Br)₂ (0.1 g, 0.11 mmol), K₂CO₃ (0.046 g, 0.335 mmol), and Pd(PPh₃)₄ (0.012 g, 10 mol %) ¹H NMR (400 MHz, CDCl₃, δ): 9.06 (dd, J = 8.4 Hz, J = 0.8 2H), 8.93 (dd, J = 2.4 Hz, J = 0.4 Hz, 2H), 8.01 (dd, J = 8.4, J = 2.4 Hz, 2H), 7.40 (d J = 4Hz, 2H) 7.28-7.26 (m, 4H), 7.21 (d, J = 4Hz, 2H), 4.37 (d, J = 7.6Hz, 4H), 1.70 (brs 2H) 1.23 - 1.20 (m, 48H), 0.85-0.81 (m, 12H) ¹³C NMR (100 MHz, CDCl₃) δ 162.7, 146.1, 145.4, 145.0, 139.3, 138.3, 136.7, 132.5, 130.7, 128.0, 127.5, 125.9, 125.2, 124.9, 124.4, 111.4, 46.3, 38.2, 31.9, 31.8, 31.5, 30.0, 29.7, 29.6, 29.3, 26.4, 22.6, 14.1, MALDI TOF calculated- 1068.55; found - 1066.59.

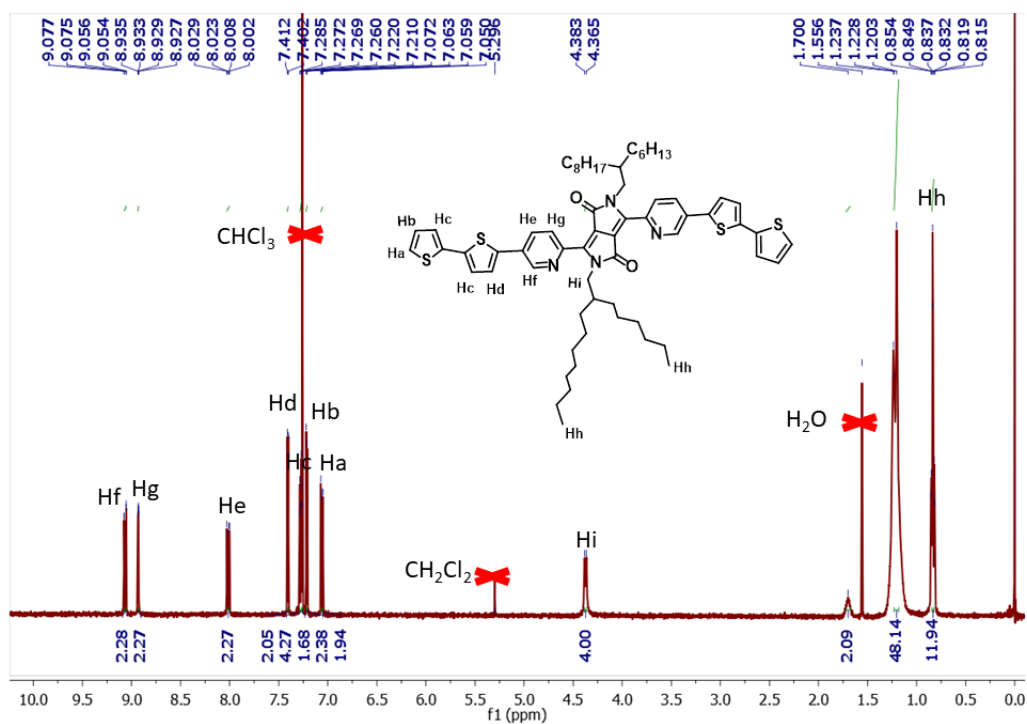


Figure 3.29 NMR Spectrum of PyDPPHD(bithio)₂

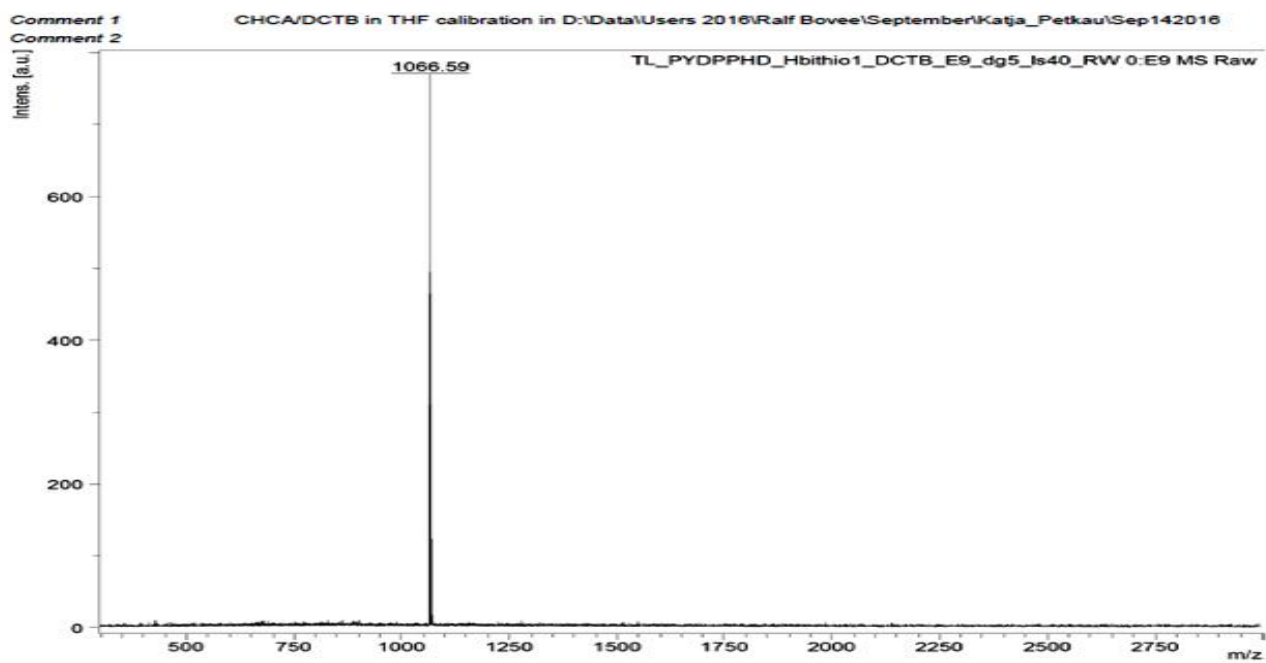


Figure 3.30 MALDI TOF spectrum of PyDPPHD(bithio)₂

3.6 References

- (1) Peet, J.; Kim, J. Y.; Coates, N. E.; Ma, W. L.; Moses, D.; Heeger, A. J.; Bazan, G. C.; *Nat. Mater.*, **2007**, *6*, 497.
- (2) Yao, Y.; Hou, J.; Xu, Z.; Li, G.; Yang, Y.; *Adv. Funct. Mater.*, **2008**, *18*, 1783-1789.
- (3) Park, S. H.; Roy, A.; Beaupré, S.; Cho, S.; Coates, N.; Moon, J. S.; Moses, D.; Leclerc, M.; Lee, K.; Heeger, A. J.; *Nat. Photonics*, **2009**, *3*, 297.
- (4) Huang, F.; Chen, K.-S.; Yip, H.-L.; Hau, S. K.; Acton, O.; Zhang, Y.; Luo, J.; Jen, A. K. Y.; *J. Am. Chem. Soc.*, **2009**, *131*, 13886-13887.
- (5) Kan, B.; Li, M.; Zhang, Q.; Liu, F.; Wan, X.; Wang, Y.; Ni, W.; Long, G.; Yang, X.; Feng, H.; Zuo, Y.; Zhang, M.; Huang, F.; Cao, Y.; Russell, T. P.; Chen, Y.; *J. Am. Chem. Soc.*, **2015**, *137*, 3886-3893.
- (6) Ke, G.; Lisheng, L.; Tianqi, L.; Liangang, X.; Yuan, H.; Fei, H.; Junbiao, P.; Yong, C.; Feng, L.; Thomas, P. R.; René, A. J. J.; Xiaobin, P.; *J. Am. Chem. Soc.*, **2008**, *137*, 7282-7285.
- (7) Zhao, J.; Li, Y.; Yang, G.; Jiang, K.; Lin, H.; Ade, H.; Ma, W.; Yan, H.; *Nat. Energy*, **2016**, *1*, 15027.
- (8) Sonar, P.; Singh, S. P.; Li, Y.; Ooi, Z.-E.; Ha, T.-j.; Wong, I.; Soh, M. S.; Dodabalapur, A.; *Energy Environ. Sci.*, **2011**, *4*, 2288-2296.
- (9) Dou, L.; You, J.; Yang, J.; Chen, C.-C.; He, Y.; Murase, S.; Moriarty, T.; Emery, K.; Li, G.; Yang, Y.; *Nat. Photonics*, **2012**, *6*, 180.
- (10) Hendriks, K. H.; Heintges, G. H. L.; Gevaerts, V. S.; Wienk, M. M.; Janssen, R. A. J.; *Angew. Chem. Int. Ed.*, **2013**, *52*, 8341-8344.
- (11) Ashraf, R.; Meager, I.; Nikolka, M.; Kirkus, M.; Planells, M.; Schroeder, B.; Holliday, S.; Hurhangee, M.; Nielsen, C.; Siringhaus, H.; McCulloch, I.; *J. Am. Chem. Soc.*, **2015**, *137*, 1314-1321.
- (12) Bronstein, H.; Chen, Z.; Ashraf, R.; Zhang, W.; Du, J.; Durrant, J.; Tuladhar, P.; Song, K.; Watkins, S.; Geerts, Y.; Wienk, M.; Janssen, R.; Anthopoulos, T.; Siringhaus, H.; Heeney, M.; McCulloch, I.; *J. Am. Chem. Soc.*, **2011**, *133*, 3272-3275.

- (13) Meager, I.; Ashraf, R.; Mollinger, S.; Schroeder, B.; Bronstein, H.; Beatrup, D.; Vezie, M.; Kirchartz, T.; Salleo, A.; Nelson, J.; McCulloch, I.; *J. Am. Chem. Soc.*, **2013**, *135*, 11537-11540.
- (14) Hendriks, K.; Li, W.; Wienk, M.; Janssen, R.; *J. Am. Chem. Soc.*, **2014**, *136*, 12130-12136.
- (15) Jung, J.; Liu, F.; Russell, T. P.; Jo, W.; *Chem. Commun. (Cambridge, U. K.)*, **2013**, *49*, 8495-8497.
- (16) Sun, B.; Hong, W.; Yan, Z.; Aziz, H.; Li, Y.; *Adv. Mater. (Weinheim, Ger.)*, **2014**, *26*, 2636-2642.
- (17) Zhang, X.; Xiao, C.; Zhang, A.; Yang, F.; Dong, H.; Wang, Z.; Zhan, X.; Li, W.; Hu, W.; *Polym. Chem.*, **2015**, *6*, 4775-4783.
- (18) Hendriks, K. H.; Wijpkema, A. S. G.; van Franeker, J. J.; Wienk, M. M.; Janssen, R. A. J.; *J. Am. Chem. Soc.*, **2016**, *138*, 10026-10031.
- (19) Lee, J.; Ahn, H.; Jo, W.; *Macromolecules*, **2015**, *48*, 7836-7842.
- (20) Más-Montoya, M.; Janssen, R. A. J.; *Adv. Funct. Mater.*, **2017**, *27*, 1605779.
- (21) Cai, L.; Moehl, T.; Moon, S.-J.; Decoppet, J.-D.; Humphry-Baker, R.; Xue, Z.; Bin, L.; Zakeeruddin, S. M.; Grätzel, M.; *Org. Lett.*, **2014**, *16*, 106-109.
- (22) Cardona, C. M.; Li, W.; Kaifer, A. E.; Stockdale, D.; Bazan, G. C.; *Adv. Mater. (Weinheim, Ger.)*, **2011**, *23*, 2367-2371.
- (23) Veldman, D.; Meskers, S. C. J.; Janssen, R. A. J.; *Adv. Funct. Mater.*, **2009**, *19*, 1939-1948.
- (24) Pavlishchuk, V. V.; Addison, A. W.; *Inorg. Chim. Acta*, **2000**, *298*, 97-102.
- (25) Bredas, J.-L.; *Mater. Horizons*, **2013**, *1*, 17-19.
- (26) Machui, F.; Maisch, P.; Burgués-Ceballos, I.; Langner, S.; Krantz, J.; Ameri, T.; Brabec, C. J.; *ChemPhysChem*, **2015**, *16*, 1275-1280.
- (27) Lee, J. K.; Ma, W. L.; Brabec, C. J.; Yuen, J.; Moon, J. S.; Kim, J. Y.; Lee, K.; Bazan, G. C.; Heeger, A. J.; *J. Am. Chem. Soc.*, **2008**, *130*, 3619-3623.
- (28) Buss, F.; Schmidt-Hansberg, B.; Sanyal, M.; Munuera, C.; Scharfer, P.; Schabel, W.; Barrena, E.; *Macromolecules*, **2016**, *49*, 4867-4874.

- (29) Kawano, K.; Sakai, J.; Yahiro, M.; Adachi, C.; *Sol. Energy Mater. Sol. Cells*, **2009**, *93*, 514-518.
- (30) Chen, F.-C.; Tseng, H.-C.; Ko, C.-J.; *Appl. Phys. Lett.*, **2008**, *92*, 103316.
- (31) Yuan, Z.; Xuan-Dung, D.; Chunki, K.; Thuc-Quyen, N.; *Adv. Energy Mater.*, **2011**, *1*, 610-617.
- (32) Hongyu, W.; Feng, L.; Laju, B.; Jun, G.; Cheng, W.; Wei, W.; Thomas, P. R.; *Adv. Mater. (Weinheim, Ger.)*, **2013**, *25*, 6519-6525.
- (33) Li, W.; Hendriks, K. H.; Furlan, A.; Wienk, M. M.; Janssen, R. A. J.; *J. Am. Chem. Soc.*, **2015**, *137*, 2231-2234.
- (34) Sakthivel, P.; Kranthiraja, K.; Saravanan, C.; Gunasekar, K.; Kim, H. I.; Shin, W. S.; Jeong, J.-E.; Woo, H. Y.; Jin, S.-H.; *J. Mater. Chem. A*, **2014**, *2*, 6916-6921.

Chapter 4

D-A-D and D-A-D-A-D Small Molecules Based on Pyridine capped Diketopyrrolopyrrole for Bulk Heterojunction Solar Cell

4.1 Abstract

In the present chapter, we report the design and synthesis of two D-A-D type molecules (PyDPPBO(bithiohexyl)₂, and PyDPPHD(bithiohexyl)₂) and one D-A-D-A-D type molecule (DTP(PyDPPHD(bithiohexyl)₂) for use as active material in BHJ solar cells. The D-A-D molecules have a pyridine-capped DPP as acceptor core and two bithiophene units as donors and they differ only in the nature of the alkyl chains on the DPP. The D-A-D-A-D molecule has a dithienopyrrole (DTP) as central donor core which is attached to two pyridine-capped DPP carrying bithiophene donor groups. The D-A-D molecules have optical band gap of 1.76 eV whereas the D-A-D-A-D molecule displayed a relatively narrow optical band gap of 1.56 eV. The HOMO energy levels are deeper for both D-A-D (~-5.80 eV) and D-A-D-A-D (-5.44 eV) systems. The photovoltaic properties of these small molecules blended with PC₆₁BM as electron acceptor were investigated in detail. Among these, PyDPPBO(bithiohexyl)₂ : PC₆₁BM device exhibited the best PCE of 1.36% with V_{oc} = 0.88 V, J_{sc} = 3.37 mA/cm² with FF = 0.43.

4.2 Introduction

In the area of bulk heterojunction solar cell research, the active layer comprises donor polymers/small molecules along with acceptor fullerene derivatives. A small change in the chemical structure of polymers/small molecules like functional group replacements, variation in length and position of aromatic groups and alkyl chains, and replacement of elements to a greater extent results in the change in properties like molecular weight, solubility, photo electrochemical properties, film state morphology of pristine and blend with acceptor etc. These properties have a profound influence on the performance of the device, which gives an opportunity for the researchers to explore different aspects of OPVs. In addition to this, it makes it difficult to predict the efficiency of organic solar cell.¹⁻⁶ This is the reason why researchers explore small variations in the chemical structure. Thus, analogy of thiophene in the class of DPP, such as thienothiophene, selenophene, furan, thiazole, and pyridine were applied as bridges for DPP polymers for the application of organic solar cell.⁷⁻¹⁶ In the case of small molecules, DPP other than thiophene capped DPP systems are less investigated.¹⁷ We designed two mono pyridine capped DPP having butyloctyl and hexyldecyl chains, with 5-hexyl-2,2'-bithiophene on both sides of the DPP and bis-pyridine capped DPP with dithieno[3,2-*b*:2',3'-*d*]pyrrole as centre core along with 5-hexyl-2,2'-bithiophene as end group. The chemical structures of the molecules are given in the Figure 4.1.

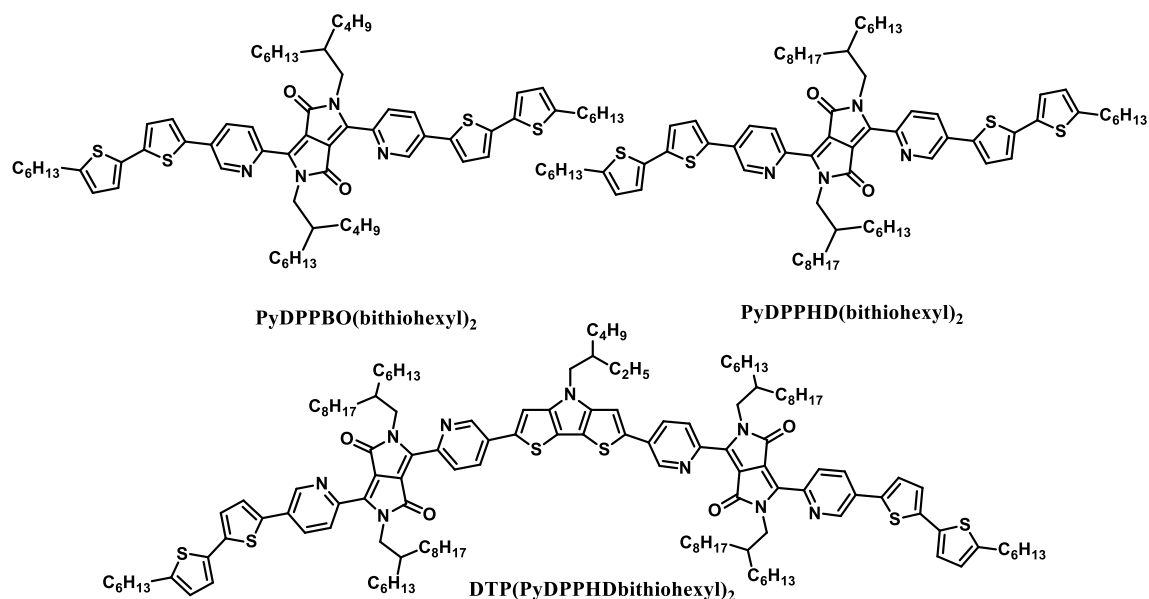


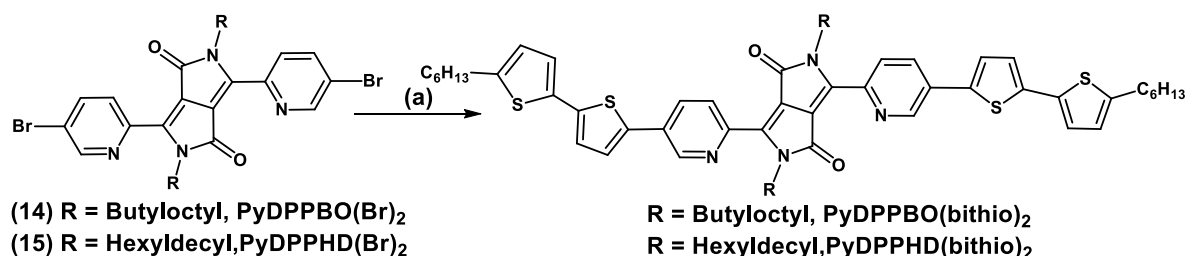
Figure 4.1 Chemical structure of mono and bis pyridine capped DPP molecules

4.3 Results and discussion

4.3.1 Synthesis

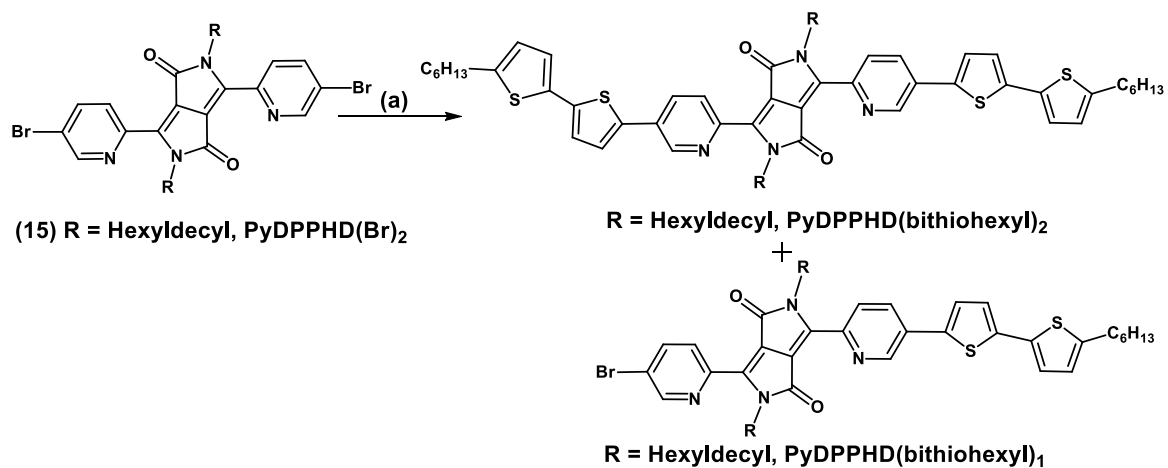
The synthesis of starting material PyDPPBO(Br)₂ (**14**) and PyDPPHD(Br)₂ (**15**) were carried out according to a previously reported procedure, using a traditional pseudo-Stobbe condensation reaction between 5-bromo-2-pyridinecarbonitrile and diethyl succinate to yield the pyridine DPP core, followed by its alkylation employing 2-butyloctyl bromide and 2-hexyldecyl bromide under basic conditions.¹⁸ As shown in Scheme 4.1, among the three small molecules, PyDPPBO(bithiohexyl)₂ and PyDPPHD(bithiohexyl)₂ were synthesized using a double Suzuki–Miyaura cross-coupling reaction between the alkylated dibromo pyridine–DPP derivative and the 2-(5'-hexyl-[2,2'-bithiophen]-5-yl)-4,4,5,5-tetramethyl-1,3,2-dioxaborolane yielding

the desired bithiophene attached with pyridine DPP compounds, bearing a hexyl chains at 5th positions of the end thiophene ring.¹⁹

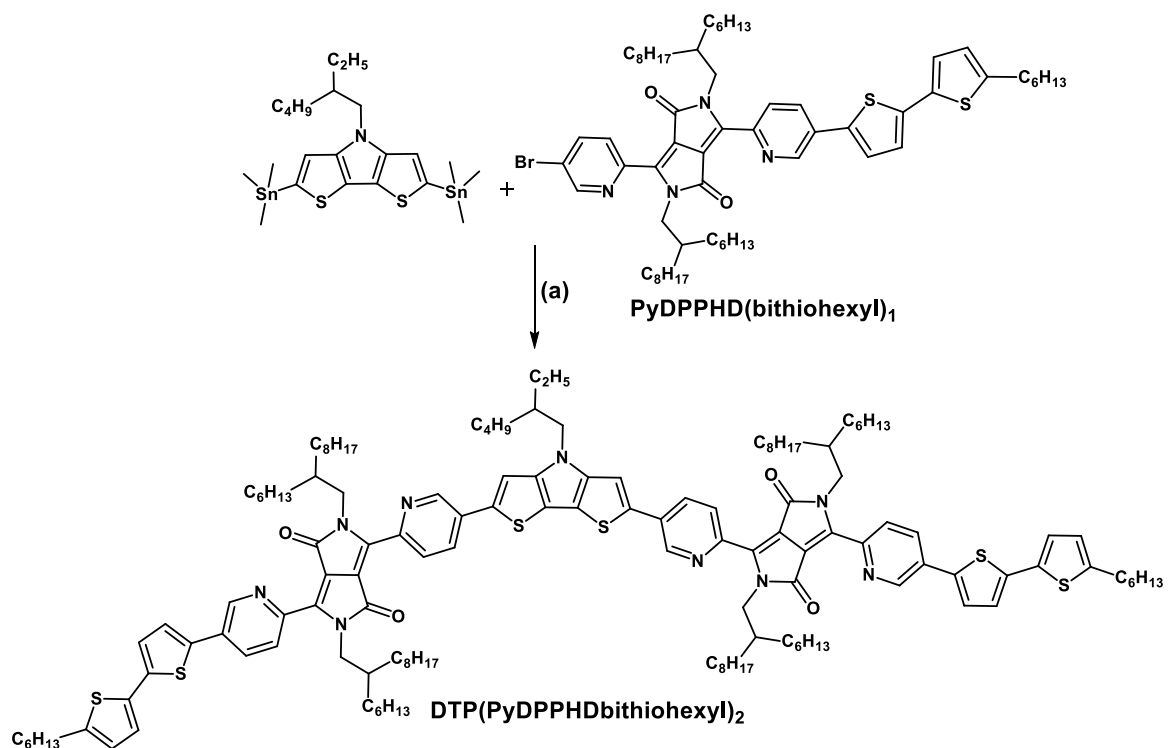


Scheme 4.1 Reaction condition (a) 2-(5'-hexyl-[2,2'-bithiophen]-5-yl)-4,4,5,5-tetramethyl-1,3,2-dioxaborolane, Pd(PPh₃)₄, K₂CO₃, Toluene : ethanol : H₂O, 90 °C, 24h

Synthesis of bis pyridine capped DPP having a central core of dithiopyrrole donor having two pyridine capped DPP with an end group of 5-hexyl-2,2'-bithiophene, DTP(PyDPPHD(bithiohexyl))₂ was successfully carried out by a two-step Suzuki–Miyaura cross coupling and Stille reactions. PyDPPHD(bithiohexyl)₁ synthesized from PyDPPHD(Br)₂ and 1 equivalent of 2-(5'-hexyl-[2,2'-bithiophen]-5-yl)-4,4,5,5-tetramethyl-1,3,2-dioxaborolane resulted in a mixture of 25 % mono substituted product PyDPPHD(bithiohexyl)₁ and 10 % di-substituted PyDPPHD(bithiohexyl)₂. This was followed by Stille reaction between 4-(2-ethylhexyl)-2,6-bis(trimethylstannyl)-4Hdithieno[3,2-*b*:2',3'-*d*]pyrrole and PyDPPHD(bithiohexyl)₁ in dry toluene using Pd(PPh₃)₄ resulting in 55 % of DTP(PyDPPHD(bithiohexyl))₂.²⁰ The details of the reaction are given in the Scheme 4.2 and Scheme 4.3 respectively.



Scheme 4.2 Reaction condition (a) 2-(5'-hexyl-[2,2'-bithiophen]-5-yl)-4,4,5,5-tetramethyl-1,3,2-dioxaborolane, Pd(PPh₃)₄, K₂CO₃, Toluene : ethanol : H₂O, 90 °C, 24 h



Scheme 4.3 Reaction condition (a) Pd(PPh₃)₄, K₂CO₃, Toluene, 90 °C, 24 h

4.3.2 Optical properties

The UV–visible absorption spectra of three small molecules in CHCl_3 solutions and in thin films are shown in Figure 4.2. The corresponding optical data are summarized in Table 4.1. In CHCl_3 solution the two small molecules having same chromophore PyDPPBO(bithiohexyl)₂ and PyDPPHD(bithiohexyl)₂ with different alkyl chains showed similar absorption range. The mono pyridine capped DPP exhibits, two absorption peaks at (λ_{max}) 350 nm and 573 nm can be assigned to the π – π^* absorption of the molecule and ICT transition from electron-donating units (thiophene) to electron-accepting unit DPP. Moreover, from Figure 4.2c, it is seen that third molecule, bis pyridine capped DPP with central core dithieno[3,2-*b*:2',3'-*d*]pyrrole group, resulted in a red shift of (λ_{max}) at 650 nm indicating the effect of electron donating units in the molecular energy levels. Compared to the absorption in dilute CHCl_3 solutions, broadening and structured absorption peaks with red shifted absorption edge in the films (for both PyDPPBO(bithiohexyl)₂ and PyDPPHD(bithiohexyl)₂ 55 nm; and (DTP(PyDPPHD(bithiohexyl)₂), 70 nm), which may be caused by the existence of π – π stacking of the molecules in the dense solid state. As the absorption edges of the mono pyridine DPP small molecule at 702 nm, and that of bis pyridine DPP at 776 nm. The optical band gaps (E_g) are calculated as 1.76 eV for PyDPPBO(bithiohexyl)₂ and PyDPPHD(bithiohexyl)₂ and 1.56 eV for DTP(PyDPPHD(bithiohexyl)₂) respectively. Each small molecule exhibited a broad absorption range and a relatively low band gap, which would be in favor of light-harvesting when used as the active-layer materials in OPVs.

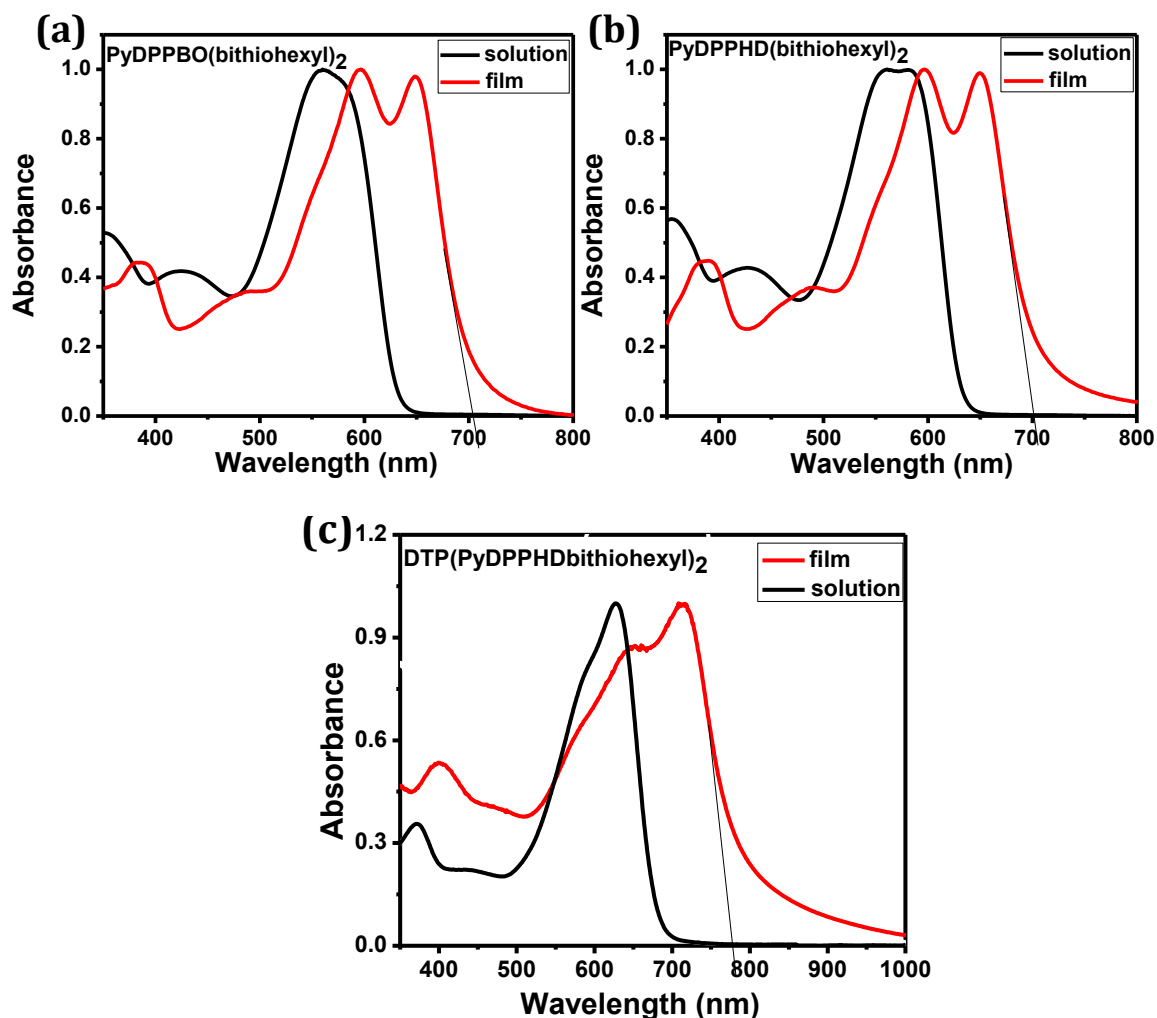


Figure 4.2 Absorption spectra of (a) PyDPPBO(bithiohexyl)₂ (b) PyDPPHD(bithiohexyl)₂ (c) DTP(PyDPPHDbithiohexyl)₂

4.3.3 Electrochemical properties

The redox properties of the three molecular materials were determined by cyclic voltammetry in CH₂Cl₂ solutions of 0.1 M tetrabutylammonium hexafluorophosphate (TBAPF₆) using a three electrode setup equipped with a platinum disc working electrode, silver counter electrode and a silver electrode coated with silver chloride (Ag/AgCl) as quasi reference electrode in combination

with Fc/Fc⁺ as internal standard. The data are summarized in Table 4.1 and shown in Figure 4.3. Both of the two small molecules PyDPPBO(bithiohexyl)₂ and PyDPPHD(bithiohexyl)₂ undergo a quasi-reversible multiple electron oxidation originating from the successive oxidation of the chromophore. The onset potential of PyDPPBO(bithiohexyl)₂ and PyDPPHD(bithiohexyl)₂ with respect to Fc/Fc⁺ redox couple is found to be nearly same value as +0.57/+0.56 V for the oxidation and -1.35/-1.37 V for reduction. The electron rich central group dithieno[3,2-*b*:2',3'-*d*]pyrrole central unit in the bis pyridine capped DPP is capable of removing electrons with a first oxidation potential of +0.21 V with respect to Fc/Fc⁺ where as the reduction potential as nearly same as the mono pyridine capped DPP (-1.37 V). The HOMO and LUMO energy level were estimated from the onset of the first oxidation and reduction waves, respectively. Using these redox potentials the HOMO and LUMO levels were estimated using $E = -5.23 - qE_{\text{redox}}$.²¹⁻²² The presence of dithieno[3,2-*b*:2',3'-*d*]pyrrole in the bis pyridine DPP small molecule is well reflected in the rise in HOMO energy level of 0.36 eV with respect to mono pyridine capped DPP. The LUMO energy levels are dominated by the acceptor units in the molecular structure. The nature of pyridine capped DPP are not much affected by the strength of donor and LUMO energy level lie between -3.86 eV and -3.88 eV. The difference between the LUMO of the donors and LUMO of the PC₆₁BM, $\Delta\text{LUMO} = 0.36 \text{ eV} - 0.34 \text{ eV}$. Comparing the HOMO energy levels of three small molecules, the mono pyridine DPP PyDPPHD(bithiohexyl)₂ shows a 5.78 eV, where as the HOMO energy level of bis pyridine DPP DTP(PyDPPHD(bithiohexyl)₂) rises to -5.44 eV. Thus the ΔHOMO ,

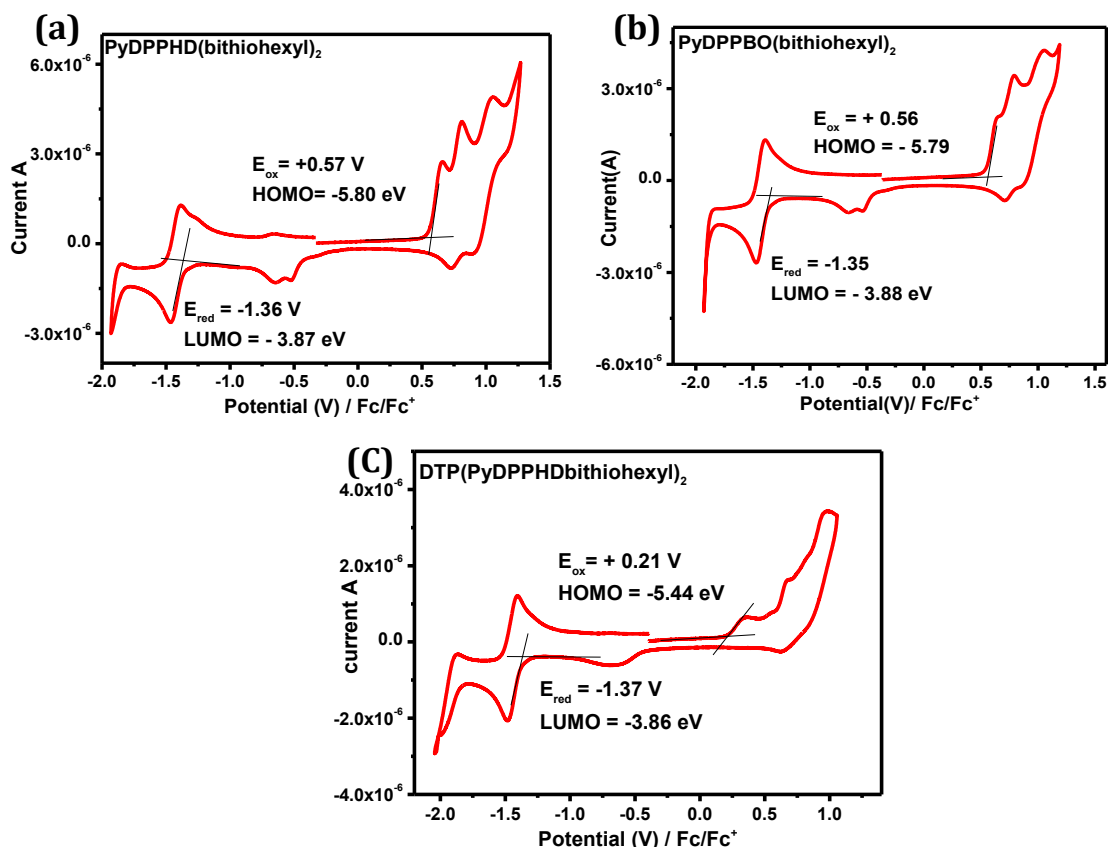


Figure 4.3 Cyclic voltammetry of (a) PyDPPBO(bithiohexyl)₂ (b) PyDPPHD(bithiohexyl)₂ (c) DTP(PyDPPHD(bithiohexyl)₂) DPP resulted in the deep HOMO level of -5.80 eV for PyDPPBO(bithiohexyl)₂, and –

Table 4.1 Summary of photophysical and electrochemical studies

Compound	Absorption				Cyclic voltammetry				
	λ_{max}^{sol} (nm)	λ_{max}^{film} (nm)	λ_{edge}^{film} (nm)	E_{gap}^{opt} (eV)	E_{ox}^{sol} (V)	E_{red}^{sol} (V)	HOMO (eV)	LUMO (eV)	E_{gap}^{cv} (eV)
PyDPPBO (bithiohexyl) ₂	573	595, 647	702	1.76	+0.57	-1.35	-5.80	-3.87	1.93
PyDPPHD (bithiohexyl) ₂	573	596, 648	702	1.76	+0.56	-1.36	-5.78	-3.88	1.90
DTP(PyDPPHD bithiohexyl) ₂	627	652, 712	776	1.59	+0.21	-1.37	-5.44	-3.86	1.58

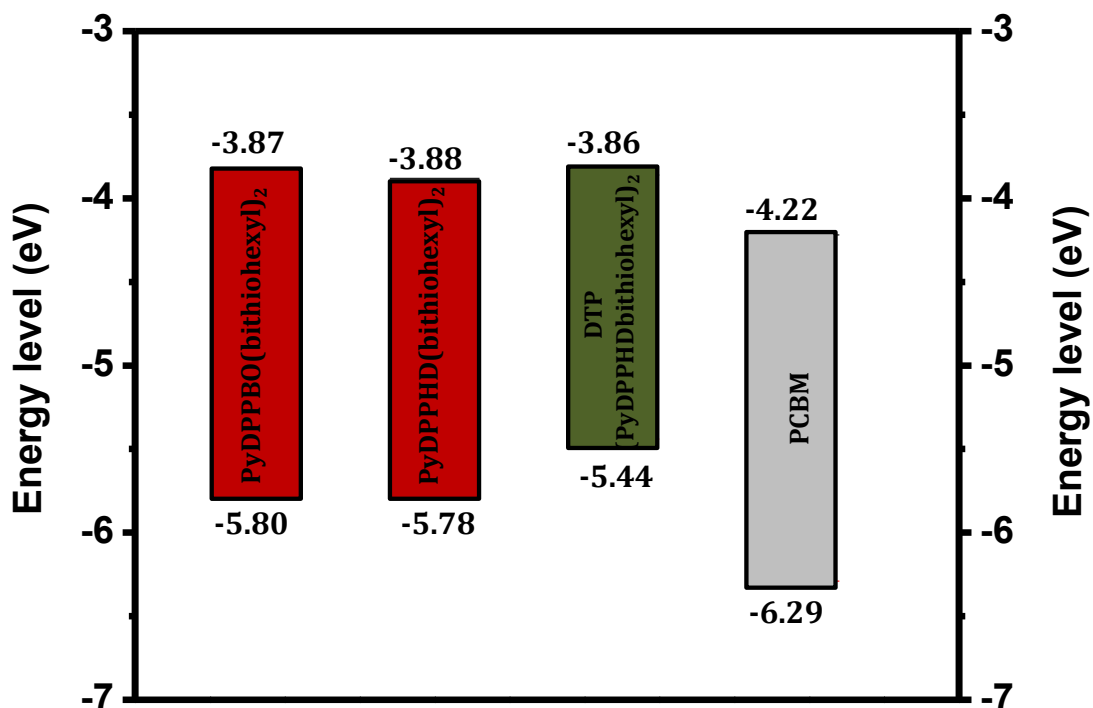


Figure 4.4 Energy level diagram mono and bis pyridine DPP molecules.

the difference between the HOMO of the donor and the HOMO of the PC₆₁BM for the mono pyridine DPP is 0.49 eV - 0.51 eV and that of bis pyridine capped DPP is 0.85 eV. This large difference of Δ HOMO resulted in higher percentage of EQE for the device fabricated with DTP(PyDPPHD(bithiohexyl)₂): PC₆₁BM in the region below 400 nm.⁷

4.3.4 Photovoltaic properties

Solar cells were fabricated using three small molecule donors each mixing with PC₆₁BM as an electron acceptor in the regular configuration of ITO/MoO₃/active layer/ LiF/Al. Since the small molecules are pyridine capped DPP, instead of the conventional PEDOT: PSS bottom contact, a 10 nm MoO₃ on ITO was used as the hole

extraction layer to prevent S-shaped J-V characteristics. The observation of S-shaped J-V characteristics was reported for solar cells with active layers containing aromatic amines such as pyridine and thiazole on PEDOT: PSS.^{13,23-24} MoO₃ hole transporting layer solves this problem. The processing conditions of small molecule/PC₆₁BM active layers were carefully optimized in terms of total concentration in 1:1 weight ratio, and layer thickness is maintained between 90-100 nm. The details of influence of donor/acceptor concentration on device performance for PyDPPBO(bithiohexyl)₂: PC₆₁BM, and PyDPPHD(bithiohexyl)₂: PC₆₁BM are summarized in the Table 4.2 and Table 4.3. respectively. The solubility of PyDPPBO(bithiohexyl)₂ ~ 11 mg/mL in CHCl₃. When we increase the concentration of PyDPPBO(bithiohexyl)₂: PC₆₁BM (1:1) from 12 to 36 mg/mL, the PCE varies from 0.21 % to a maximum value of 1.36 %. It is found that at 20 mg/mL devices exhibit much better photovoltaic performance than other total concentrations, with the highest PCE of 1.36 % with a J_{sc} of 11.4 mA/cm², V_{oc} of 0.88 V and FF of 0.43. The J-V characterization and EQE spectra of PyDPPBO(bithiohexyl)₂: PC₆₁BM best device are shown in the Figure 4.5. But the more soluble PyDPPHD(bithiohexyl)₂ (~13 mg/mL) shows inferior performance in the solar cell devices. The best efficiency obtained for the total concentration of 36 mg/mL in 1:1 donor-acceptor ratio is 0.52 %. The J-V characterization and EQE spectra of PyDPPHD(bithiohexyl)₂: PC₆₁BM best device is given in the Figure 4.6. The concentration dependence in the

Table 4.2 Device optimization of PyDPPBO(bithiohexyl)₂: PC₆₁BM

Concent ration (mg/mL)	Spin coating (rpm)	Thick ness (nm)	J_{sc} (mA/ cm ²)	V_{oc} (V)	FF	MPP (mW/ cm ²)	J_{sc} (mA/ cm ²) (SR)	PCE (%)
12	400	107	1.36	0.59	0.30	0.25	1.20	0.21
16	1000	99	1.47	0.82	0.32	0.47	1.39	0.45
20	1300	90	3.37	0.88	0.43	1.30	3.60	1.36
24	1900	92	1.50	0.83	0.40	0.50	1.36	0.45
30	3100	100	3.10	0.87	0.39	1.08	2.91	0.98
36	3800	112	2.32	0.85	0.38	0.75	2.25	0.72

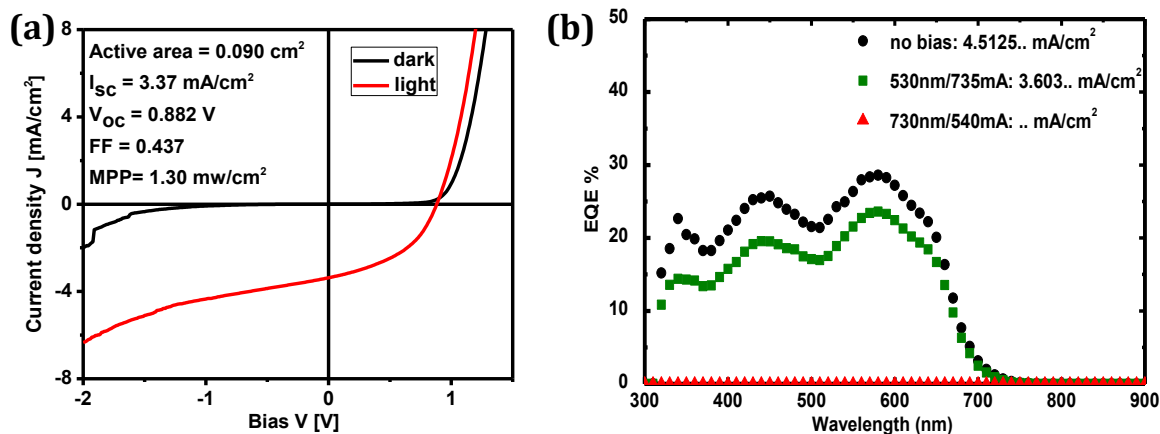


Figure: 4.5 (a) Representative J-V curves for PyDPPBO(bithiohexyl)₂ : PC₆₁BM solar cells in dark (black) and under simulated AM 1.5G conditions (red). (b) EQE spectra of PyDPPBO(bithiohexyl)₂ : PC₆₁BM solar cell under low monochromatic light intensity and with 1 Sun equivalent light bias illumination. The numbers in the panels represent the J_{sc} that is obtained with convoluting the EQE with the solar A M 1.5G spectrum.

performance of solar cell devices for PyDPPHD(bithiohexyl)₂ is less pronounced than the PyDPPBO(bithiohexyl)₂. The two mono-pyridine capped DPP molecules possess identical optical absorption bands and energy levels, but their solubility is very different and hence there is a difference in their photovoltaics properties. The J-

V characterization and the EQE of the best device are given in the Figure 4.6. The solubility of bis pyridine capped DPP is comparatively lower and the solvent CHCl_3 can dissolve only 3.5 mg/mL. Hence hot process at 60 °C is performed for the device fabrication of the solar cell. Solution and pipettes were heated to 60 °C for hot spin coating. Due to its low solubility a fixed concentration of 12 mg/mL was used for the hot process. The optimization of solar cell device and effect of additives and temperature is summarized in the Table 4.4. The best efficiency obtained for $\text{DTP}(\text{PyDPPHDbithiohexyl})_2$ is 0.67 % with a J_{sc} of 1.31 mA/cm^2 , V_{oc} of 0.80 V and FF of 0.59. The J-V characterization and the EQE of the $\text{DTP}(\text{PyDPPHDbithiohexyl})_2$: PC_{61}BM best device are given in the Figure 4.7. The effect of additives and temperature is detrimental in the performance of the solar cell devices for all three small molecules discussed in this chapter.

Table 4.3 Device optimization of $\text{PyDPPHD}(\text{bithiohexyl})_2$: PC_{61}BM

Concentration (mg/mL)	Spin coating (rpm)	Thickness (nm)	J_{sc} (mA/cm^2)	V_{oc} (V)	FF	MPP (mW/cm^2)	$J_{sc}(\text{mA}/\text{cm}^2)$ (SR)	PCE (%)
10	400	90	1.67	0.62	0.32	0.34	-	-
14	600	112	1.90	0.67	0.32	0.42	-	-
18	1000	96	2.19	0.67	0.32	0.40	-	-
22	1300	93	1.65	0.50	0.33	0.28	-	-
30	2820	96	2.33	0.52	0.42	0.52	-	-
36	3800	95	2.35	0.56	0.38	0.51	2.45	0.52

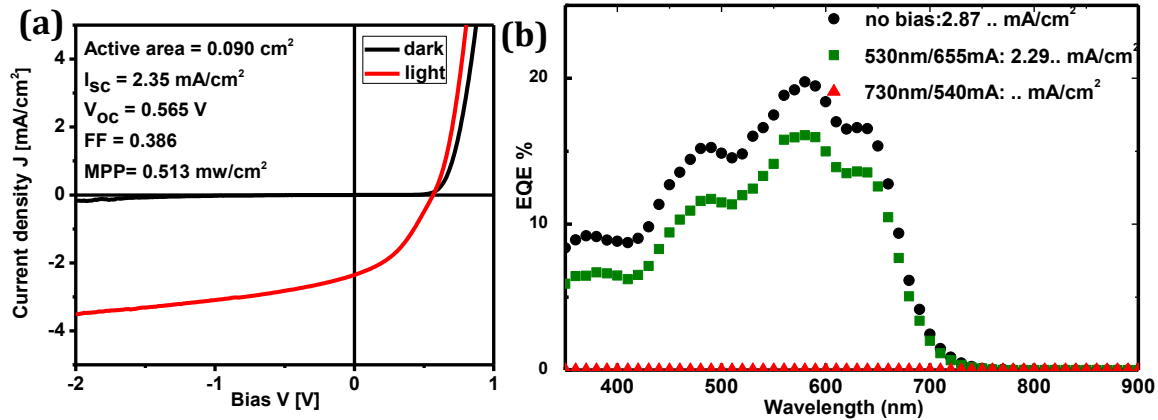


Figure 4.6 (a) Representative J-V curve for PyDPPHD(bithiohexyl)₂ : PC₆₁BM solar cell in dark (black) and under simulated A M 1.5G conditions (red). (b) EQE spectra of PyDPPHD(bithiohexyl)₂ : PC₆₁BM solar cell under low monochromatic light intensity and with 1 Sun equivalent light bias illumination. The numbers in the panels represent the J_{sc} that is obtained with convoluting the EQE with the solar A M 1.5G spectrum.

Table 4.4 Device optimization of DTP(PyDPPHD(bithiohexyl)₂ : PC₆₁BM

Spin coating (rpm)	Thickness (nm)	J _{sc} (mA/cm ²)	V _{oc} (V)	FF	MPP (mW/cm ²)	J _{sc} (mA/cm ²) (SR)	PCE (%)
800	110 nm	1.31	0.80	0.59	0.62	1.42	0.67
1000	91 nm ^b	1.29	0.75	0.43	0.42	1.35	0.44
1000	83 nm	1.34	0.79	0.59	0.63	1.41	0.66
1000	85 nm	1.53	0.64	0.45	0.44	1.70	0.49
900	103 nm ^a	1.06	0.56	0.30	0.18	0.94	0.15
1000	90 nm ^{a,b}	2.35	0.56	0.38	0.51	2.45	0.52
1000	99 nm ^a	0.67	0.70	0.36	0.17	0.63	0.15

a = 0.2% DIO, b = annealing at 110 °C for 10 minute

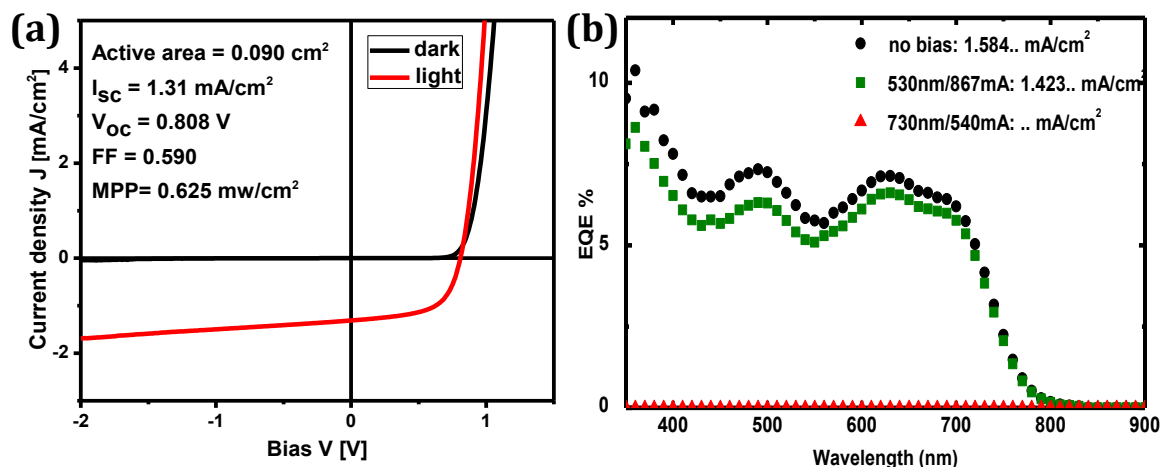


Figure: 4.7 (a) Representative J-V curve for DTP (PyDPPHDbithiohexyl)₂ : PC₆₁BM solar cell in dark (black) and under simulated A M 1.5G conditions (red). (b) EQE spectra of DTP(PyDPPHDbithiohexyl)₂ : PC₆₁BM solar cell under low monochromatic light intensity and with 1 sun equivalent light bias illumination. The numbers in the panels represent the J_{sc} that is obtained with convoluting the EQE with the solar A M 1.5G spectrum.

4.3.5 Morphological studies

To study the morphology of the active layer of the best performing solar cells, we fabricated solar cells using the same conditions with the device structure (ITO)/MoO₃/PyDPPBO(bithiohexyl)₂:PC₆₁BM/LiF/Al. The J-V curve and EQE are given in Figure 4.8 and the TEM image of the active layer of the solar cell is given in the Figure 4.9. Losses in the current density J_{sc} is mainly related to the coarse demixing of the PyDPPBO(bithiohexyl)₂:PC₆₁BM blend as evidenced by TEM. Similarly the morphology of the active layer for the DTP(PyDPPHDbithiohexyl)₂:PC₆₁BM solar cell device was also investigated by TEM. The best fabrication condition is repeated, and the J-V characterization and EQE of the solar cell is shown in Figure 4.10. The thin film blends processed, formed large phase separated domains as indicated by the black circular regions in the image which corresponds to the PC₆₁BM aggregates.

These results are quite similar to that found with DPP based polymer/PC₆₁BM blends casted from chloroform.²⁵⁻²⁶

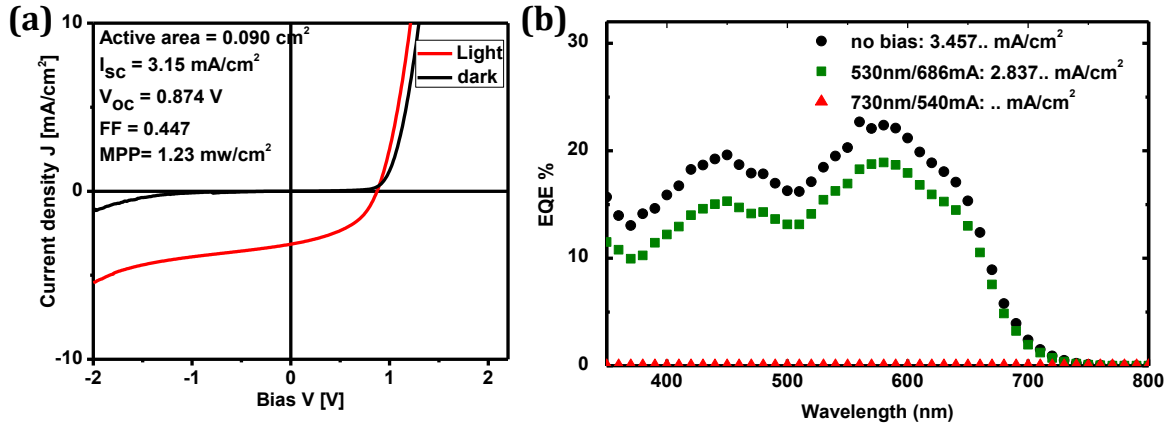


Figure 4.8 (a) Representative J-V curve for PyDPPBO(bithiohexyl)₂ : PC₆₁BM solar cell in dark (black) and under simulated A M 1.5G conditions (green). (b) EQE spectra of PyDPPBO(bithiohexyl)₂ : PC₆₁BM solar cell under low monochromatic light intensity and with 1 Sun equivalent light bias illumination. The numbers in the panels represent the J_{sc} that is obtained with convoluting the EQE with the solar A M 1.5G spectrum.

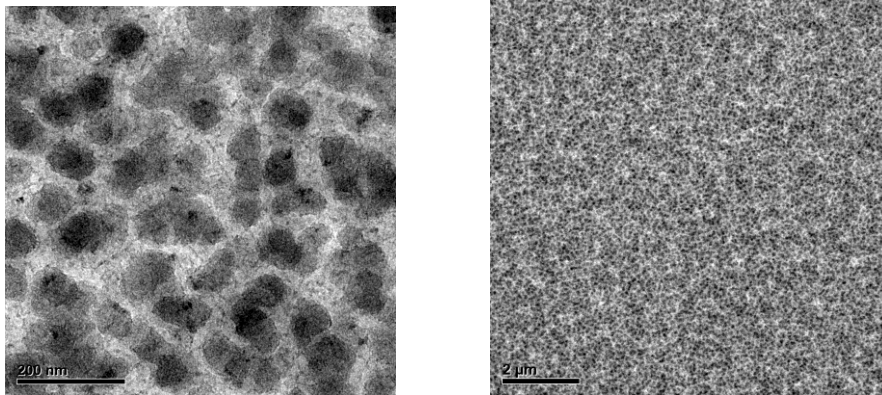


Figure 4.9 TEM images of PyDPPBO(bithiohexyl)₂ : PC₆₁BM solar cell

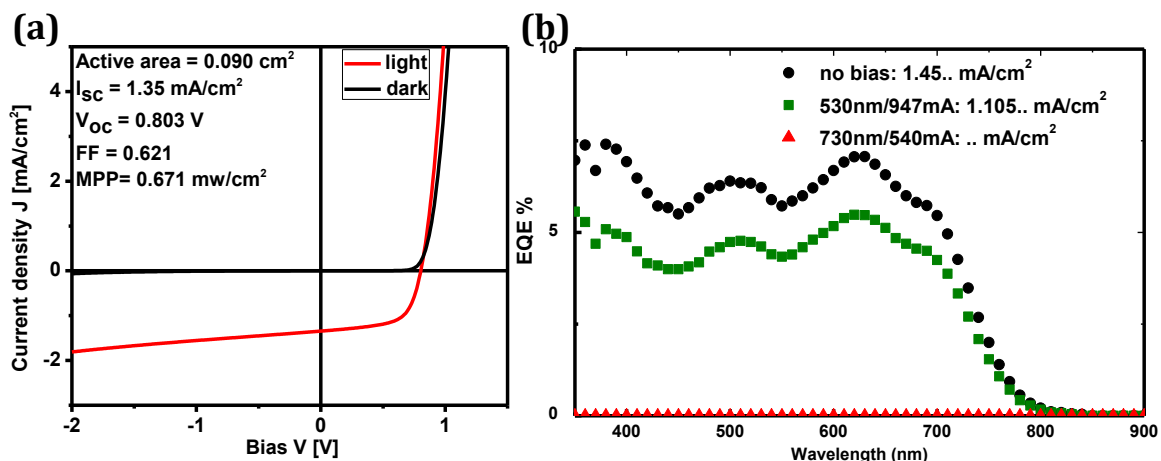


Figure 4.10 (a) Representative J-V curve for DTP(PyDPPHDbithiohexyl)₂ : PC₆₁BM solar cell in dark (black) and under simulated A M 1.5G conditions (red). (b) EQE spectra of DTP(PyDPPHDbithiohexyl)₂ : PC₆₁BM solar cell under low monochromatic light intensity and with 1 Sun equivalent light bias illumination. The numbers in the panels represent the J_{sc} that is obtained with convoluting the EQE with the solar A M 1.5G spectrum.

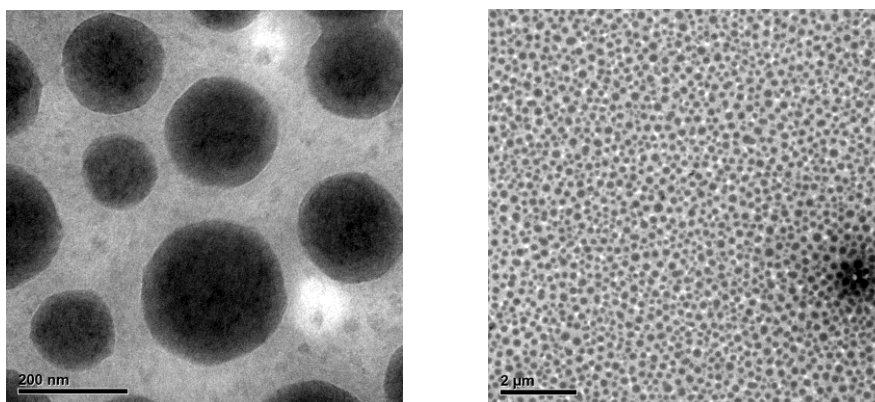


Figure 4.11 Tem images of DTP(PyDPPHDbithiohexyl)₂ : PC₆₁BM solar cell

In these coarse phase separated morphologies only a small amount of the photo generated excitons reach the donor acceptor interface and, hence, the current that can be extracted is low resulting in poor device performances.

4.4 Conclusion

Mono and bis pyridine capped DPP with 5'-hexyl-2,2'-bithiophene on end groups and dithienopyrrole as the central core were synthesized and characterized in detail. PyDPPBO(bithiohexyl)₂ /PyDPPHD(bithiohexyl)₂ and DTP(PyDPPHD(bithiohexyl)₂) have optical band gaps of 1.76 eV and 1.56 eV respectively. The PCE of PyDPPBO(bithiohexyl)₂ with butyloctyl chain is 1.36 % where as for PyDPPHD(bithiohexyl)₂ with hexyldecyl chain is 0.52 %. Bis pyridine capped DPP DTP(PyDPPHD(bithiohexyl)₂) showed a PCE up to 0.67 % with $V_{oc} = 0.80$ V, $J_{sc} = 1.42$ mA/cm², and FF of 0.59.

4.5. Experimental section

4.5.1. General methods

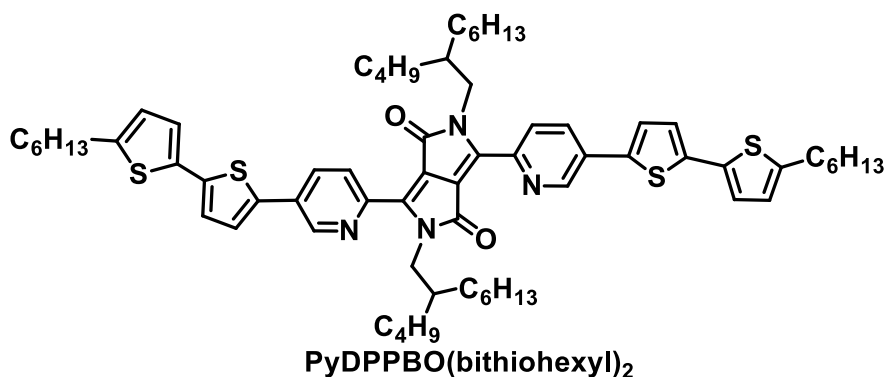
5'-Hexyl-2,2'-bithiophene-5-boronic acid pinacol ester, Pd(PPh₃)₄, were purchased from Sigma Aldrich and were used as such. 4-(2-ethylhexyl)-2,6-bis(trimethylstannyl)-4*H*-dithieno[3,2-*b*:2',3'-*d*]pyrrole was purchased from SunaTech and used as received. Solvent used were either HPLC grade or freshly distilled before use. All the reactions were carried out under nitrogen atmosphere. ¹H NMR and ¹³C NMR spectra were obtained using a 400 MHz Bruker Avance DPX spectrometer. Absorption spectra were obtained using a Shimadzu 3101PC UV/Vis-NIR scanning spectrophotometer. Cyclic voltammetry was performed under an inert atmosphere with a scan rate of 0.1 V/s and 0.1 M tetrabutylammonium hexafluorophosphate in dichloromethane as the electrolyte. A platinum working electrode, a silver counter electrode and a silver wire coated with silver chloride

(Ag/AgCl) quasi-reference electrode were used combined with Fc/Fc⁺ as the internal standard.

4.5.2 Fabrication of bulk heterojunction solar cell

The procedure for device fabrication is similar as chapter 3 (page no : 121)

4.5.3. Experimental procedures



PyDPPBO(bithiohexyl)₂ : A 50 mL Schlenk tube was filled with 5'-Hexyl-2,2'-bithiophene-5-boronic acid pinacol ester (0.24 g, 0.635 mmol), and PyDPPBO(Br)₂ (0.20 g, 0.254 mmol) and K₂CO₃ (0.087 g, 0.635 mmol), and Pd(PPh₃)₄ (0.029 g, 10 % mol) catalyst was transferred from glove box. A mixture of toluene, ethanol and water in the ratio of 4:1:0.5 was purged with argon gas for 20 minutes to deoxygenate. Then the solvent was cannulated or transferred to the schlenk tube. The tube was sealed and heated at 90 °C for 18 h. The crude reaction mixture was allowed to cool to room temperature after which the organic layer was washed with water and brine, dried over anhydrous MgSO₄, filtered, and the solvent evaporated under reduced pressure. The crude product was preadsorbed onto silica gel and chromatographed to give PyDPPBO(bithiohexyl)₂ as a dark brown solid (yield: 70 %). ¹H NMR (400 MHz, CDCl₃, δ): 9.05 (d, J = 8.4 Hz, 2H), 8.92 (d, J = 2.4Hz, 2H), 8.01

(dd, $J = 8.4$ Hz, $J = 2.4$ Hz, 2H), 7.39 (d, $J = 3.6$ Hz, 2H), 7.13 (d, $J = 4$ Hz, 2H), 7.07 (d, $J = 3.6$, 2H), 6.72 (d, $J = 3.6$ Hz, 2H), 4.37 (d, $J = 6.8$ Hz, 4H), 2.81 (t, $J = 7.6$ Hz, 4H), 1.73-1.66 (m, 6H), 1.41 - 1.20 (m, 40H), 0.90 (t, $J = 6.8$, 6H), 0.85 - 0.81 (m, 12H). ^{13}C NMR (100 MHz, CDCl_3) δ 162.7, 162.5, 150.0, 146.6, 146.5, 146.2, 145.9, 145.8, 145.7, 145.3, 145.3, 145.0, 144.1, 139.9, 139.6, 137.6, 134.0, 132.4, 131.0, 130.8, 128.3, 127.6, 127.5, 126.0, 125.9, 125.0, 124.1, 122.3, 111.6, 111.3, 111.0, 46.4, 46.3, 46.2, 38.1, 31.8, 31.5, 31.4, 31.2, 31.1, 30.2, 29.7, 28.7, 28.6, 26.4, 23.0, 22.6, 22.58 14.1, 14.0, -0.00. MALDI TOF : calculated- 1122.59, found- 1122.60

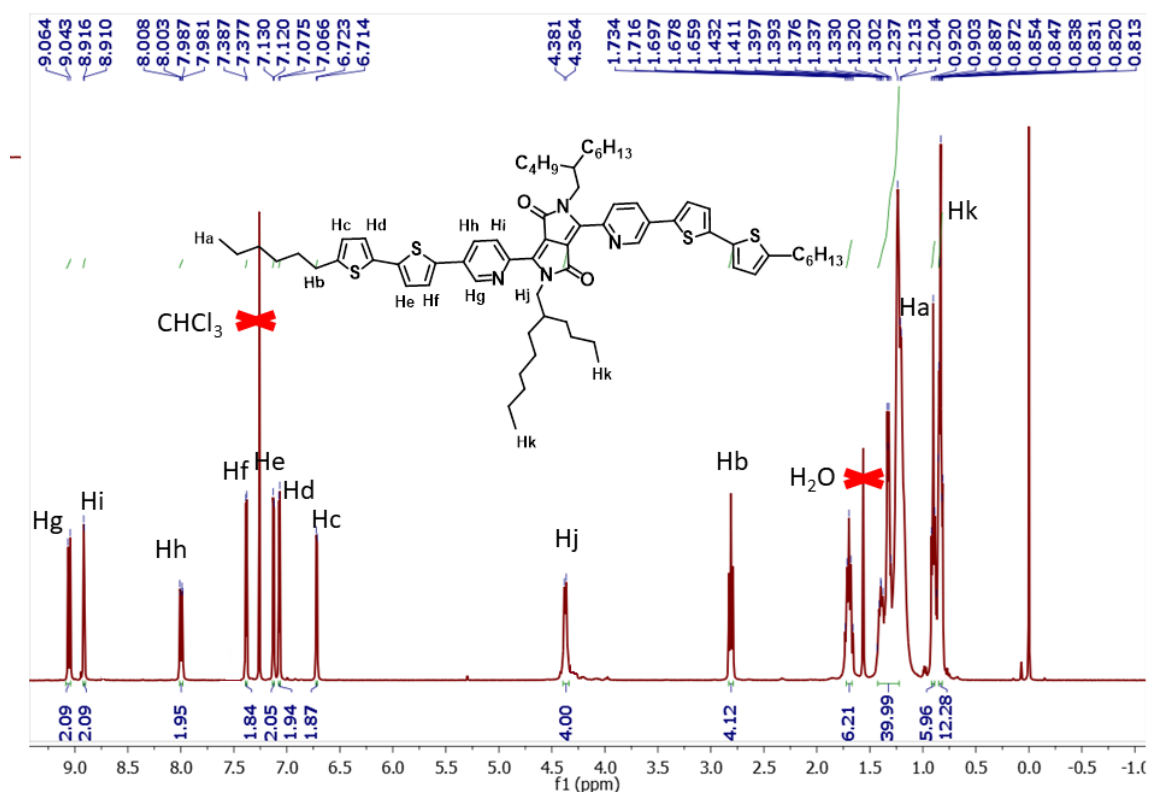


Figure 4.12 NMR Spectrum of PyDPPBO(bithiohexyl) $_2$

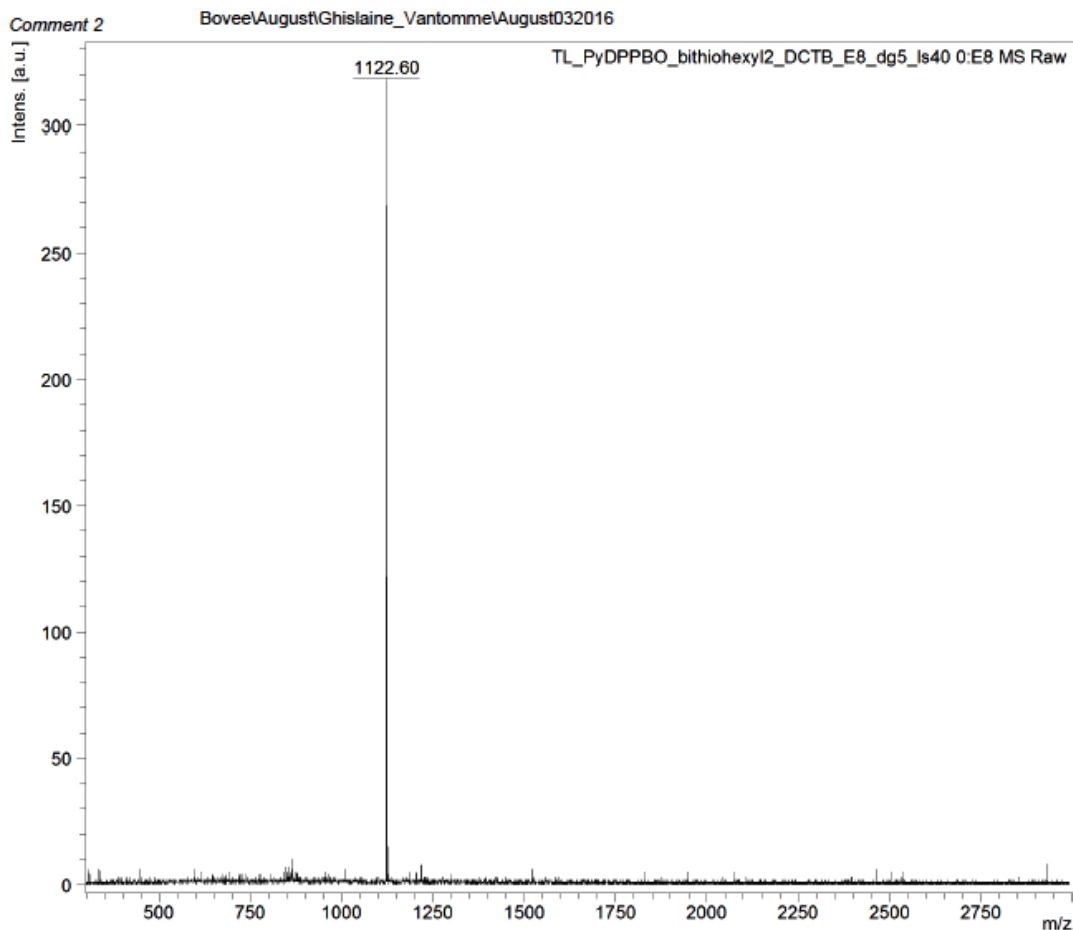
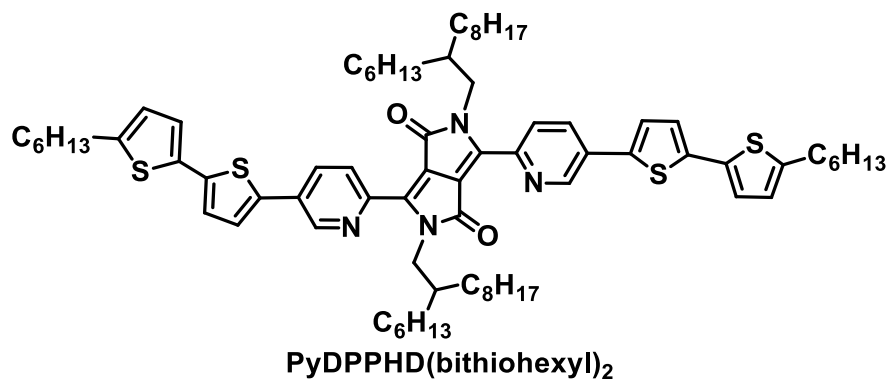


Figure 4.13 MALDI TOF spectrum of PyDPPBO(bithiohexyl)₂



PyDPPHD(bithiohexyl)₂ : A 50 mL Schlenk tube was filled with 5'-Hexyl-2,2'-bithiophene-5-boronic acid pinacol ester (0.157 g , 0.418 mmol), PyDPPHD(Br)₂ (0.15 g, 0.167 mmol), K₂CO₃ (0.057 g, 0.418 mmol), and Pd(PPh₃)₄ (0.02 g, 10 % mol)

catalyst was transferred from glove box. A mixture of toluene, ethanol and water in the ratio of 4 : 1: 0.5 was purged with argon gas for 20 minutes to deoxygenate. Then the solvent was cannulated or transferred to the schlenk tube. The tube was sealed and heated at 90 °C for 18 h. The crude reaction mixture was allowed to cool to room temperature after which the organic layer was washed with water and brine, dried over anhydrous MgSO₄, filtered, and the solvent evaporated under reduced pressure. The crude product was preadsorbed onto silica gel and chromatographed to give PyDPPHD(bithiohexyl)₂ as a dark brown solid (yield: 70 %).¹H NMR (400 MHz, CDCl₃, δ): 9.05 (d, J = 8.4 Hz, 2H), 8.92 (d, J = 2.4Hz, 2H), 8.00 (dd, J= 8.4 Hz, J= 2.4 Hz , 2H), 7.38 (d, J= 3.6 Hz, 2H), 7.13 (d, J = 3.6Hz, 2H), 7.07 (d, J = 3.6Hz, 2H), 6.72 (d, J = 3.6 Hz, 2H), 4.37 (d, J= 7.2 Hz, 4H), 2.81 (t, J= 7.6Hz, 4H), 1.73-1.66 (m, 8H), 1.54 (s, 2H), 1.41-1.20 (m, 56H), 0.90 (t, J = 6.8, 6H),0.85 - 0.81 (m, 12H). ¹³C NMR (100 MHz, CDCl₃) δ 162.7, 146.5, 145.9, 145.2, 144.9, 139.9, 137.6, 134.0, 132.3, 130.8, 127.5, 125.9, 125.0, 124.1, 111.3, 46.3, 38.2, 31.9, 31.8, 31.5, 30.2, 29.6, 29.3, 28.7, 26.4, 22.7, 22.5, 14.1. MS (MALDI): calculated: 1234.72 found:1234.74

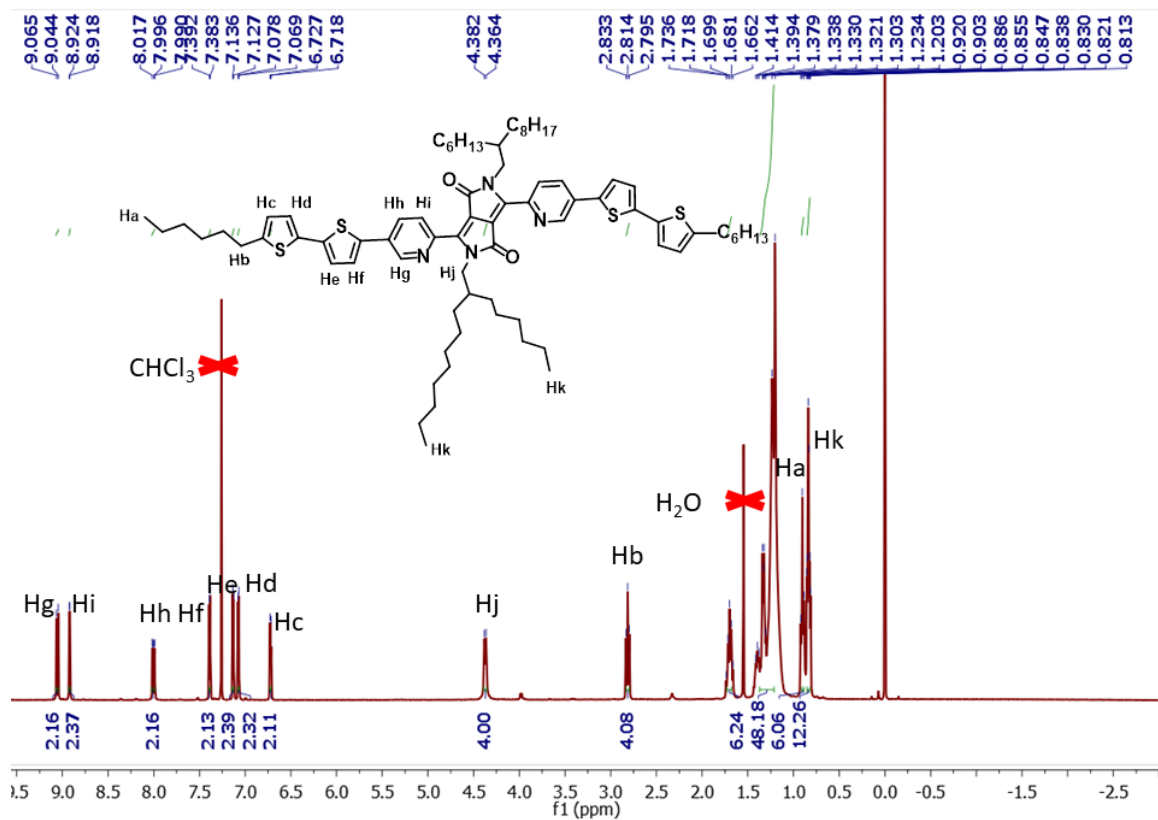


Figure 4.14 NMR Spectrum of PyDPPHD(bithiohexyl)₂

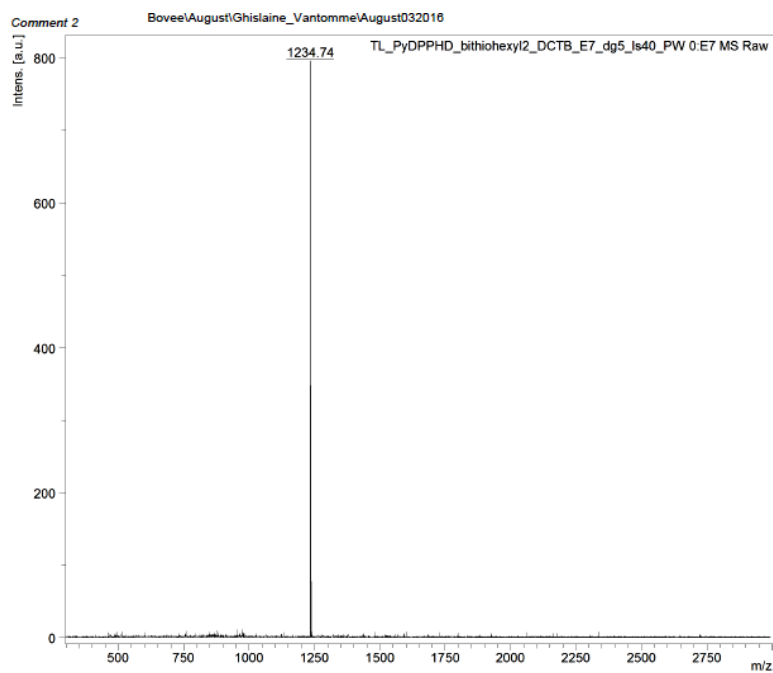
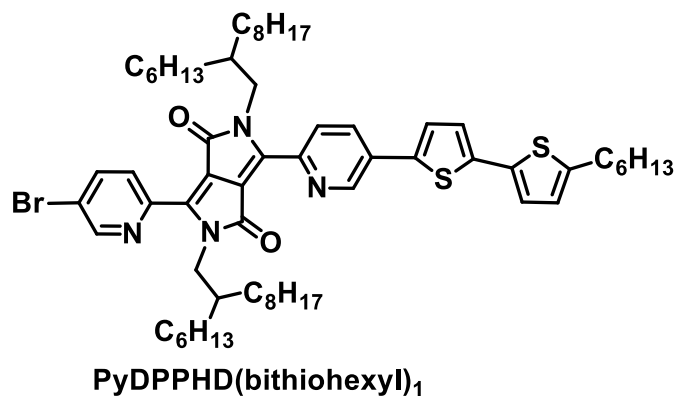


Figure 4.15 MALDI TOF spectrum of PyDPPHD(bithiohexyl)₂



PyDPPHD(bithiohexyl)₁ : A 50 mL schlenk tube was filled with 5'-Hexyl-2,2'-bithiophene-5-boronic acid pinacol ester (0.062 g, 0.167 mmol), and PyDPPHD(Br)₂ (0.15 g, 0.167 mmol) and K₂CO₃ (0.023 g, 0.167 mmol), Pd(PPh₃)₄ (0.02 g, 10 % mol) catalyst was transferred from glove box. A mixture of toluene, ethanol and water in the ratio of 4 : 1 : 0.5 was purged with argon gas for 20 minutes to deoxygenate. Then the solvent was cannulated or transferred to the schlenk tube. The tube was sealed and heated at 90 °C for 18 h. The crude reaction mixture was allowed to cool to room temperature after which the organic layer was washed with water and brine, dried over anhydrous MgSO₄, filtered, and the solvent evaporated under reduced pressure. The crude product was preadsorbed onto silica gel and chromatographed to give PyDPPHD(bithiohexyl)₁ as a dark brown solid (yield: 25 %).¹H NMR (400 MHz, CDCl₃, δ): 9.04 (d, J = 8.8 Hz, 1H), 8.94-8.92 (m, 2H), 8.73 (d, J = 2Hz, 1H), 8.02-7.98 (m, 2H), 7.39 (d, J = 3.6 Hz, 1H), 7.13 (d, J = 4 Hz, 1H), 7.07 (d, J = 3.6 Hz, 1H), 6.72 (d, J = 3.6 Hz, 1H), 4.35 (d, J = 7.2 Hz, 2H), 4.30 (d, J = 7.2 Hz, 2H), 2.81 (t, J = 7.6 Hz, 2H), 1.73-1.66 (m, 4H), 1.41-1.32 (m, 54H), 0.90-0.81 (m, 15H). ¹³C NMR (101 MHz, CDCl₃) δ 162.7, 162.4, 150.0, 146.6, 146.2, 145.8, 145.7, 145.3, 144.1, 140.1, 139.6, 137.5, 134.0, 132.4, 131.1, 128.3, 127.6, 126.0, 125.0, 124.2,

122.3, 111.7, 111.0, 46.4, 46.2, 38.2, 38.1, 31.9, 31.9, 31.8, 31.8, 31.5, 31.4, 30.2, 30.0,
29.7, 29.6, 29.5, 29.3, 28.7, 26.4, 22.6, 22.5, 14.1, 14.0. calculated: 1064.56 found:
1066.59

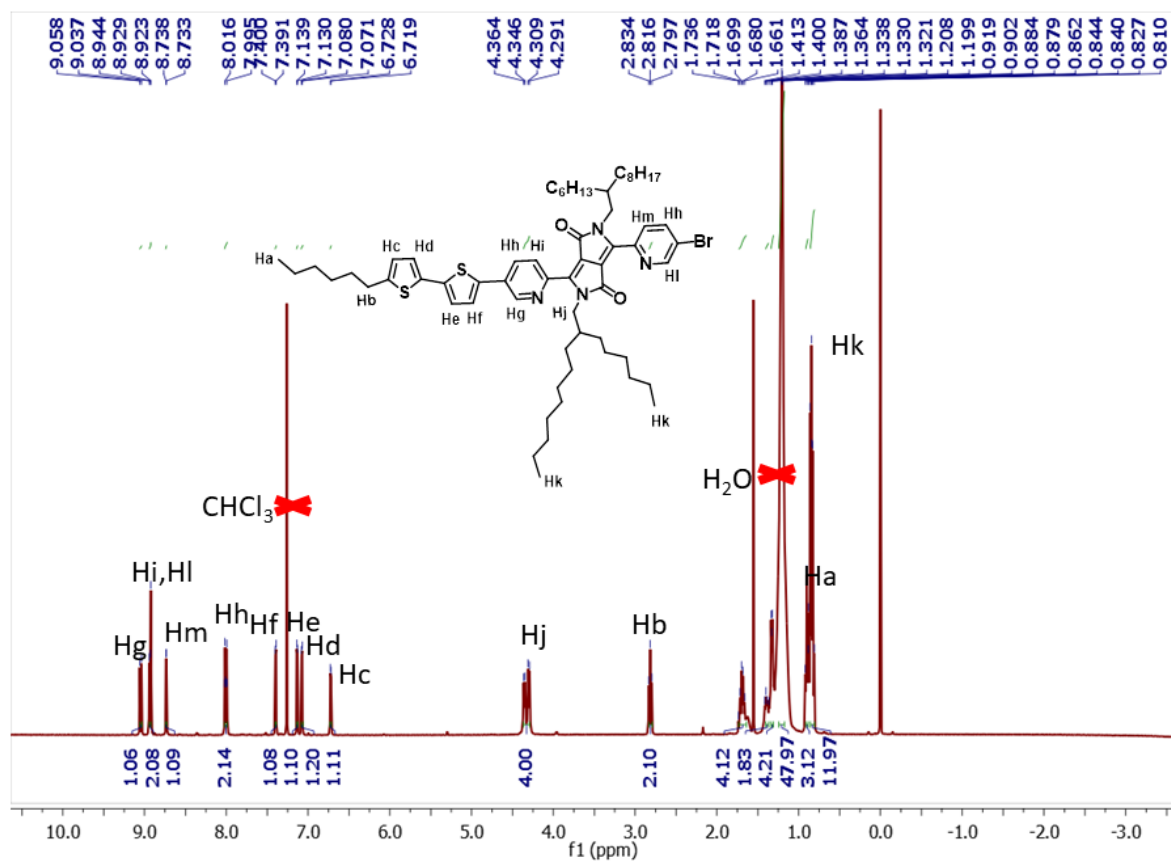


Figure 4.16 NMR Spectrum of PyDPPHD(bithiohexyl)₁

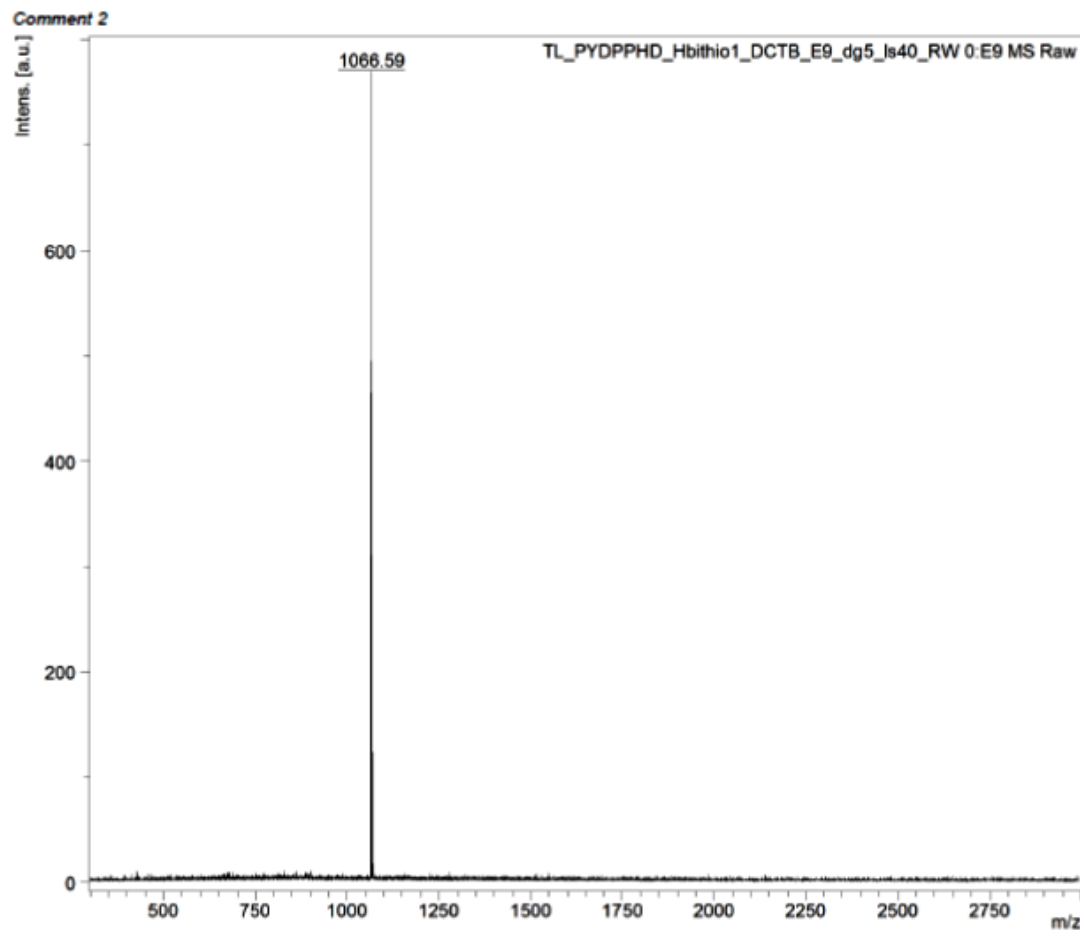
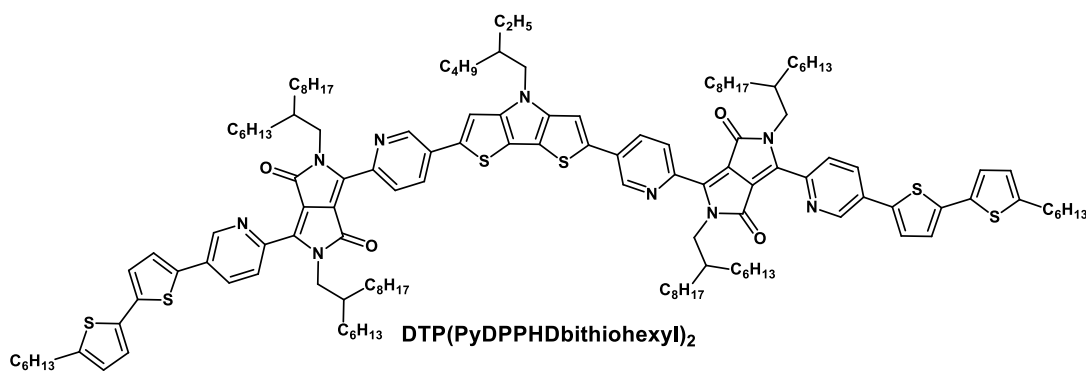


Figure 4.17 MALDI TOF Spectrum of PyDPPHD(bithiohexyl)₁



DTP(PyDPPHDbithiohexyl)₂ : A 50 mL Schlenk tube was filled with 4-(2-ethylhexyl)-2,6-bis(trimethylstannyl)-4*H*dithieno[3,2-*b*:2',3'-*d*]pyrrole (0.043 g, 0.068 mmol), and PyDPPHD(bithiohexyl)₁ (0.144 g, 0.135 mmol) Pd(PPh₃)₄ (0.0155

10 % mol) catalyst was transferred from glove box. A mixture of toluene was purged with argon gas for 20 minutes to deoxygenate. Then the solvent was cannulated or transferred to the schlenk tube. The tube was sealed and heated at 90 °C for 18 h. The crude reaction mixture was allowed to cool to room temperature after which the organic layer was washed with water and brine, dried over anhydrous MgSO₄, filtered, and the solvent evaporated under reduced pressure. The crude product was preadsorbed onto silica gel and chromatographed to give DTP(PyDPPHDbithiohexyl)₂ as a dark brown solid (yield : 55 %). ¹H NMR (400 MHz, CDCl₃, δ): 9.06-9.03 (m, 4H), 8.82 (d, J = 1.2 Hz, 4H), 7.88 (d, J = 8.4 Hz, 4H), 7.32 (d, J = 4 Hz, 2H), 7.03 (dd, J = 12.4 Hz, J = 3.6 Hz, 4H), 6.66 (d, J = 3.2 Hz, 2H), 4.38 (brs, 8H), 4.22-4.10 (m, 2H), 2.75 (t, J = 7.6 Hz, 4H), 1.76 (brs, 4H), 1.69-1.62 (m, 4H), 1.32-1.25 (m, 117H), 1.00-0.82 (m, 36H). calculated: 2260.38 found: 2262.39.

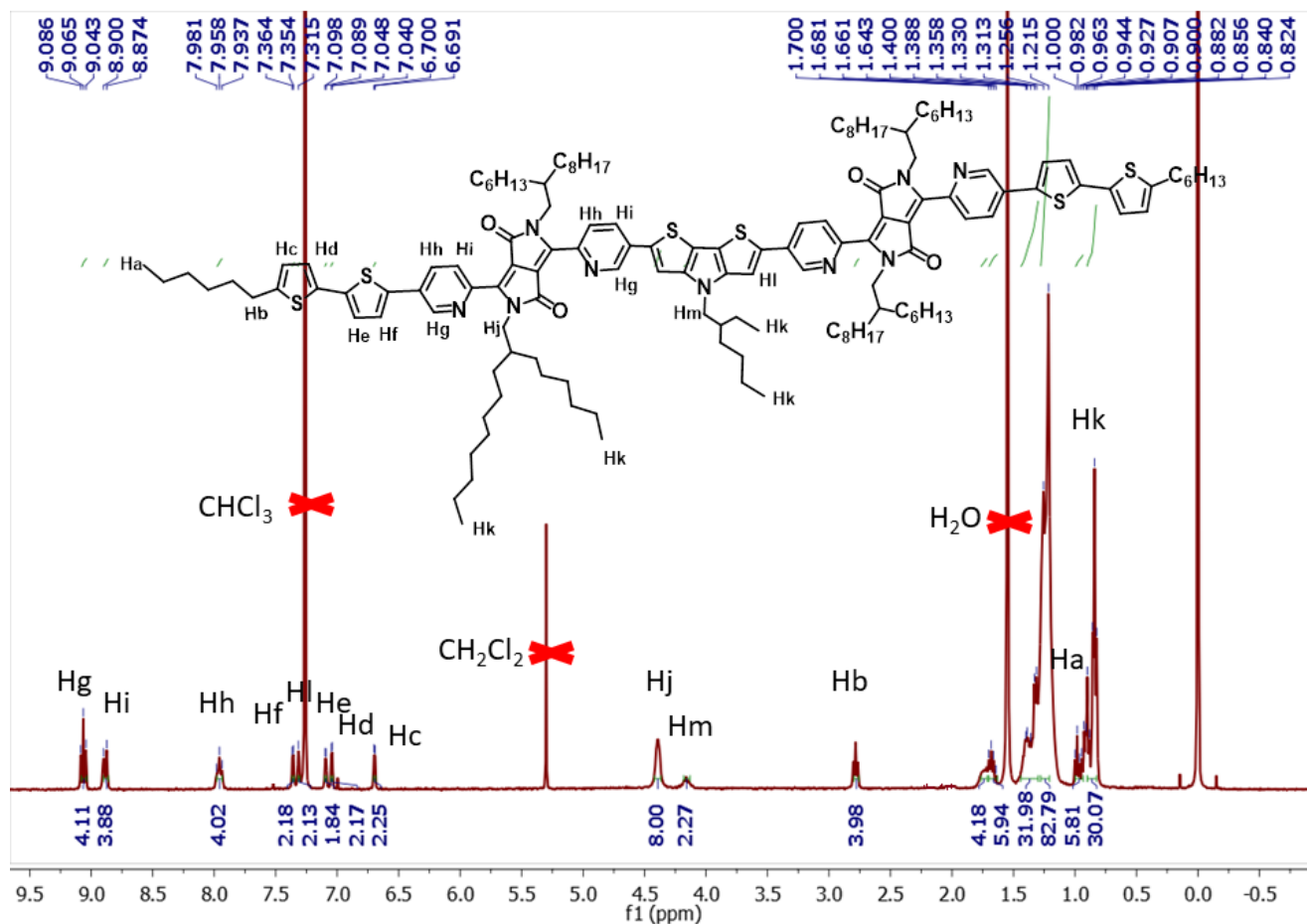


Figure 4.18 NMR Spectrum of $\text{DTP}(\text{PyDPPHDbithiohexyl})_2$

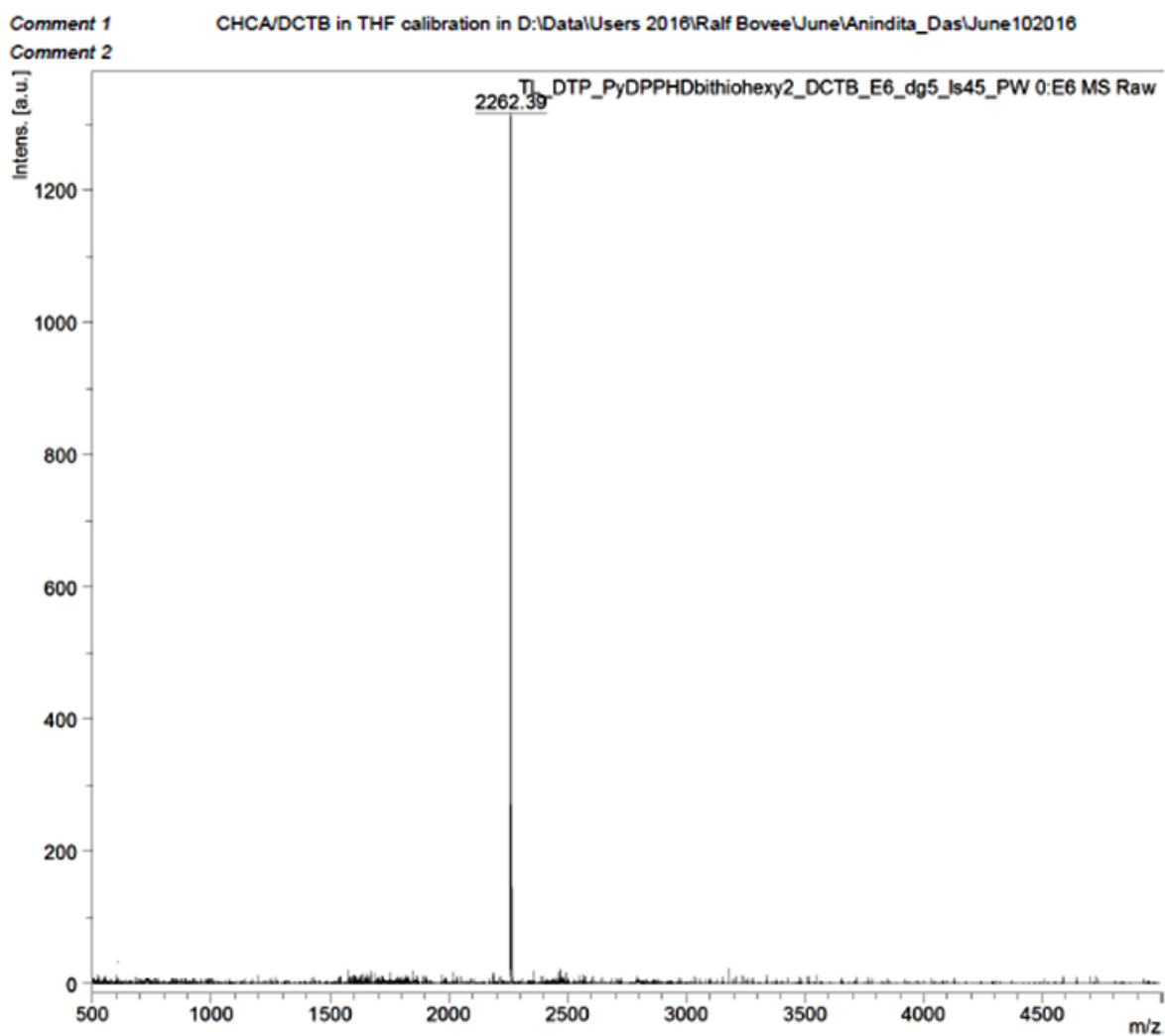


Figure 4.19 MALDI-TOF Spectrum of DTP(PyDPPHDbithiohexyl)₂

4.6 References

- (1) Li, S.; He, Z.; Yu, J.; Chen, S. a.; Zhong, A.; Tang, R.; Wu, H.; Qin, J.; Li, Z.; *J. Mater. Chem.*, **2012**, *22*, 12523-12531.
- (2) Takacs, C. J.; Sun, Y.; Welch, G. C.; Perez, L. A.; Liu, X.; Wen, W.; Bazan, G. C.; Heeger, A. J.; *J. Am. Chem. Soc.*, **2012**, *134*, 16597-16606.
- (3) Zerdan, R. B.; Shewmon, N. T.; Zhu, Y.; Mudrick, J. P.; Chesney, K. J.; Xue, J.; Castellano, R. K.; *Adv. Funct. Mater.*, **2014**, *24*, 5993-6004.
- (4) Meager, I.; Ashraf, R.; Mollinger, S.; Schroeder, B.; Bronstein, H.; Beatrup, D.; Vezie, M.; Kirchartz, T.; Salleo, A.; Nelson, J.; McCulloch, I.; *J. Am. Chem. Soc.*, **2013**, *135*, 11537-11540.
- (5) Warnan, J.; Cabanetos, C.; Labban, A. E.; Hansen, M. R.; Tassone, C.; Toney, M. F.; Beaujuge, P. M.; *Adv. Mater.*, **2014**, *26*, 4357-4362.
- (6) Lindgren, L. J.; Zhang, F.; Andersson, M.; Barrau, S.; Hellström, S.; Mammo, W.; Perzon, E.; Inganäs, O.; Andersson, M. R.; *Chem. Mater.*, **2009**, *21*, 3491-3502.
- (7) Hendriks, K. H.; Wijpkema, A. S. G.; van Franeker, J. J.; Wienk, M. M.; Janssen, R. A. J.; *J. Am. Chem. Soc.*, **2016**, *138*, 10026-10031.
- (8) Hendriks, K.; Li, W.; Wienk, M.; Janssen, R.; *J. Am. Chem. Soc.*, **2014**, *136*, 12130-12136.
- (9) Ashraf, R.; Meager, I.; Nikolka, M.; Kirkus, M.; Planells, M.; Schroeder, B.; Holliday, S.; Hurhangee, M.; Nielsen, C.; Siringhaus, H.; McCulloch, I.; *J. Am. Chem. Soc.*, **2015**, *137*, 1314-1321.
- (10) Bronstein, H.; Chen, Z.; Ashraf, R.; Zhang, W.; Du, J.; Durrant, J.; Tuladhar, P.; Song, K.; Watkins, S.; Geerts, Y.; Wienk, M.; Janssen, R.; Anthopoulos, T.; Siringhaus, H.; Heeney, M.; McCulloch, I.; *J. Am. Chem. Soc.*, **2011**, *133*, 3272-3275.
- (11) Dou, L.; Chang, W.-H.; Gao, J.; Chen, C.-C.; You, J.; Yang, Y.; *Adv. Mater.*, **2013**, *25*, 825-831.
- (12) Woo, C. H.; Beaujuge, P. M.; Holcombe, T. W.; Lee, O. P.; Fréchet, J. M. J.; *J. Am. Chem. Soc.*, **2010**, *132*, 15547-15549.

- (13) Li, W.; Hendriks, K. H.; Furlan, A.; Wienk, M. M.; Janssen, R. A. J.; *J. Am. Chem. Soc.*, **2015**, *137*, 2231-2234.
- (14) Lee, J.; Ahn, H.; Jo, W.; *Macromolecules*, **2015**, *48*, 7836-7842.
- (15) Yiu, A. T.; Beaujuge, P. M.; Lee, O. P.; Woo, C. H.; Toney, M. F.; Fréchet, J. M. J.; *J. Am. Chem. Soc.*, **2012**, *134*, 2180-2185.
- (16) Carsten, B.; Szarko, J. M.; Lu, L.; Son, H. J.; He, F.; Botros, Y. Y.; Chen, L. X.; Yu, L.; *Macromolecules*, **2012**, *45*, 6390-6395.
- (17) Más-Montoya, M.; Janssen, R. A. J.; *Adv. Funct. Mater.*, **2017**, *27*, 1605779.
- (18) Jung, J.; Liu, F.; Russell, T. P.; Jo, W.; *Chem. Commun.*, **2013**, *49*, 8495-8497.
- (19) Misra, R.; Jadhav, T.; Dhokale, B.; Mobin, S. M.; *Chem. Commun.*, **2014**, *50*, 9076-9078.
- (20) Wang, Q.; van Franeker, J. J.; Bruijnaers, B. J.; Wienk, M. M.; Janssen, R. A. J.; *J. Mater. Chem. A*, **2016**, *4*, 10532-10541.
- (21) Veldman, D.; Meskers, S. C. J.; Janssen, R. A. J.; *Adv. Funct. Mater.*, **2009**, *19*, 1939-1948.
- (22) Cardona, C. M.; Li, W.; Kaifer, A. E.; Stockdale, D.; Bazan, G. C.; *Adv. Mater.*, **2011**, *23*, 2367-2371.
- (23) Zhang, X.; Xiao, C.; Zhang, A.; Yang, F.; Dong, H.; Wang, Z.; Zhan, X.; Li, W.; Hu, W.; *Polymer Chemistry*, **2015**, *6*, 4775-4783.
- (24) Sakthivel, P.; Kranthiraja, K.; Saravanan, C.; Gunasekar, K.; Kim, H. I.; Shin, W. S.; Jeong, J.-E.; Woo, H. Y.; Jin, S.-H.; *J. Mater. Chem. A*, **2014**, *2*, 6916-6921.
- (25) Liu, F.; Gu, Y.; Wang, C.; Zhao, W.; Chen, D.; Briseno, A. L.; Russell, T. P.; *Adv. Mater.*, **2012**, *24*, 3947-3951.
- (26) Bijleveld, J. C.; Gevaerts, V. S.; Di Nuzzo, D.; Turbiez, M.; Mathijssen, S. G. J.; de Leeuw, D. M.; Wienk, M. M.; Janssen, R. A. J.; *Adv. Mater.*, **2010**, *22*, E242-E246.

List of Publications

- 1) A detailed evaluation of charge recombination dynamics in dye solar cells based on starburst triphenylamine derivatives. M. V. Vinayak, M. Yoosuf, S. C. Pradhan, T. M. Lakshmykanth, S. Soman and K. R. Gopidas, *Sustainable Energy Fuels*, **2018**, 2, 303-314.
- 2) Solution process small molecule bulk heterojunction solar cell based on tetraphenylethylene attached to diketopyrrolopyrrole. T. M. Lakshmykanth, K. R. Gopidas* Proceedings of the international workshop on Advanced functional materials and devices. January **2017** ISBN No. 978-93-81402-38-2. page 72.
- 3) Effect of recombination and binding properties on the performance of dye sensitized solar cells based on propeller shaped triphenylamine dyes with multiple binding groups. M.V.Vinayak, T. M. Lakshmykanth. M. Yoosuf, S. Soman, K. R. Gopidas. *Solar energy* **2016** 124 227-241.

Posters and Oral Presentations Presented at National Conferences:

- 1) Solution process small molecule bulk heterojunction solar cell based on tetraphenylethylene attached to diketopyrrolopyrrole. T. M. Lakshmykanth, K. R. Gopidas*, PP, IWAFMD2017 held at Tirunelveli in January 2017.

Curriculum Vitae

Lakshmykanth T.M. was born on 4th July 1985, in Pothanur, India. He obtained his bachelor degree in chemistry from Govt College Chittur affiliated to the University of Calicut, in 2006. He did his Master of Science in chemistry from Bharathiyar University, Coimbatore in 2008. He joined as a project fellow at IISER, Trivandrum, in Computational chemistry with Dr. Ayan Datta. He qualified CSIR (JRF) and entered for the Ph. D. programme in Photosciences and Photonics section of National Institute for Interdisciplinary Science and Technology (CSIR) in March 2010, under the guidance of Dr. K.R.Gopidas. His research interest is in the area of dye-sensitized solar cell and bulk heterojunction solar cell. He worked in the solution process small molecule bulk heterojunction solar cell at Eindhoven Technical University, Netherlands from October 2015 to September 2016 for completing his Ph.D. work. The results of his research are described in this thesis.